PHOTOTRANSFORMATION OF POLLUTANTS USING LUTETIUM AND ZINC PHTHALOCYANINES ANCHORED ON ELECTROSPUN POLYMER FIBERS

A thesis submitted in fulfillment of the requirement for the degree of

DOCTOR OF PHILOSOPHY

OF

RHODES UNIVERSITY

By

RUPHINO ZUGLE

JULY 2012

DEDICATION

This work is dedicated to the glory of God; his amazing grace has led to the production of this work. The work is also dedicated to:

My wife

Mrs Ernestina L. Zugle

My Daughter

Miss Rhoda Nuo-ire Zugle

My son

Mr Rudolf Mwin-tire Zugle

Acknowledgement

It is with heart-felt gratitude that I wish to express my profound appreciation to individuals and groups who have facilitated the production of this piece of work.

I first of all thank Professor Tebello Nyokong for accepting me into her research laboratory and also taking on the task of directing the research to its final production.

My gratitude also goes to Professor Victor Patrick Yao Gadzekpo, President, Central University College, Accra, Ghana, my mentor, who facilitated my being admitted into the programme together with Professor James Darkwa of University of Johannesburg, South Africa. Professor Darkwa, I am very grateful to have enjoyed the fruits of your extensive network of friends.

My appreciation also goes to Nelson Torto in whose laboratory I started the basics of electrospinning. The role of all staff of the Department of Chemistry, Rhodes University is acknowledged, especially members of S22 research group both students and support staff. Staff of the Department of Textile, Gent University, Belgium is also acknowledged.

I also thank the management of University of Cape Coast for granting me a study leave.

A special thanks goes to my wife, Mrs Ernestina L. Zugle, for the able manner with which she ran the family in my absence. Thanks for making it possible for me to

have the peace of mind to do this research. My cousin and the wife, Mr and Mrs Yangtul, thanks for all the assistance to my family during my absence.

Last but not the least; I thank Mr Schalk Van Niekerk, my landlord, for his fatherly assistance during my stay in South Africa. My co-tenant, Mr Braam Snyder, thanks for the happy moments we shared in Grahamstown, South Africa.

Finally, praise to the Almighty for bringing all these people into my life.

Abstract

Novel lanthanide phthalocyanines containing dysprosium, erbium and lutetium as central metals were synthesized using phthalonitrile:metal salt ratio of 4:1 or lower phthalonitrile content as well as using unmetallated phthalocyanine. They were characterized using various spectroscopic and elemental analyses. Dysprosium bis-phthalocyanine was obtained while monomers were obtained for erbium and lutetium phthalocyanines. The open-shell dysprosium bis-phthalocyanine and the monomeric complex of the open-shell erbium were neither fluorescent nor showed the ability to generate singlet oxygen. The triplet states of all the lutetium phthalocyanines were found to be populated with high triplet quantum yields and corresponding high singlet oxygen quantum yields. The fluorescence quantum yields of the lutetium phthalocyanines were however found to be very low.

The lutetium phthalocyanines together with unsubstituted zinc phthalocyanine and its derivatives were successfully incorporated into electrospun polymer fibers either by covalent linkage or sorption forces. Spectral characteristics of the functionalized electrospun polymer fibers indicated that the phthalocyanines were bound and their integrity maintained within the fiber matrices. Most importantly the fluorescence and photoactivity of the phthalocyanines were equally maintained within the electrospun fibers.

The functionalized electrospun polymer fibers especially those containing the zinc phthalocyanines could qualitatively detect nitrogen dioxide, a known environmental air pollutant. Also all the functionalized electrospun polystyrene and polysulfone fibers containing lutetium and zinc phthalocyanines could be applied for the

photoconversion of 4-chlorophenol, 4-nitrophenol and methyl orange. Those of polystyrene could be re-used. Polyacrylic acid and polyurethane functionalized electrospun fibers were found not to be suitable for photocatalytic applications in aqueous medium. 4-Chlorophenol was found to be more susceptible to photodegradation while methyl orange very difficult to degrade.

TABLE OF CONTENTS

Chapter 2

Chapter 4

Chapter 6

List of symbols

K_{ads}	-	Adsorption coefficient
k_a	-	Apparent reaction rate constant
ΔA_s	-	Changes in the singlet state absorbances
ΔA_T	-	Changes in the triplet state absorbances
$^1O_2(^1\Sigma^-_g)$	-	Excited short-lived singlet oxygen
T_1	-	First excited triplet excited state
Φ_F	-	Fluorescence quantum yield
τ_F	-	Fluorescence lifetime
$t_{1/2}$	-	Half-life
hv	-	Light
ε	-	Molar extinction coefficient
T_n	-	nth triplet state
α	-	Non-peripheral position
k_{obs}	-	Observed rate constant
β	-	Peripheral position
PC	-	Personal computer
Φ_p	-	Photobleaching quantum yield
RA	-	Relative amplitude
T_2	-	Second excited triplet state
S_1	-	Singlet excited state

S_0	-	Singlet ground state
$O_2(^1\Delta_g)$	-	Singlet molecular oxygen
Φ_Δ	-	Singlet oxygen quantum yield
ε_S	-	Singlet state molar extinction
t	-	Time
τ_T	-	Triplet lifetime
Φ_T	-	Triplet quantum yield
ε_T	-	Triplet state molar extinction coefficient

List of Abbreviations

A	-	Absorption
Ac	-	Acetate
AA	-	Acetic acid
acac	-	Acetylacetate
ADMA	-	Tetrasodium α,α–(anthracene-9,10-diyl) dimethyl malonate
AOD	-	Advanced oxidation process
AFM	-	Atomic Force Microscopy
BET	-	Brunauer, Emmett and Teller
4-CP	-	4-Chlorophenol
DMSO-d_6	-	Deuterated dimethylsulfoxide
D_2O	-	Deuterated water
DBU	-	1,8-Diazabicyclo[5.4.0]undec-7-ene
DCM	-	Dichloromethane
DCP	-	2,4-Dichlorophenol
DCC	-	Dicyclohexylcarbodiimide
DPBF	-	3-Diphenylisobenzofuran
DSC	-	Differential scanning calorimetry
DMAE	-	N,N-dimethylaminoethanol
DMF	-	*N,N*-dimethylformamide
DMSO	-	Dimethylsufoxide
FA	-	Formic acid

F	-	Fluorescence
GC	-	Gas chromatography
fod	-	6,6,7,7,8,8,8-Heptafluoro-2,2-dimethyloctane-3,5-dionate
HPTCP	-	6,6,7,7,8,8,8-heptafluoro-2,2-dimethyloctane-3,5-dionate
HOMO	-	Highest occupied molecular orbital
HPLC	-	High performance liquid chromatography
IR	-	Infrared
IC	-	Internal conversion
ISC	-	Intersystem crossing
Ln	-	Lanthanide metal
I	-	Light intensity
LACO	-	Linear combination of atomic orbitals
LUMO	-	Lowest unoccupied molecular orbital
MCM-41	-	Mesoporous molecular sieve
MO	-	Methyl orange
(MCP)-PMT	-	Monochromator photomultiplier
4-NP	-	4-Nitrophenol
PCP	-	Pentachlorophenol
P	-	Phosphorescence
PDT	-	Photodynamic therapy
PMT	-	Photomultipiler tube

PAA	-	Polyacrylic acid
PS	-	Polystyrene
PSU	-	Polysulfone
PUR	-	Polyurethane
PVA	-	Poly(vinyl alcohol)
^{1}H NMR	-	Proton nuclear magnetic resonance spectroscopy
q	-	Quinolinato
$Pc^{\cdot+}$	-	Radical species of phthalocyanine
SEM	-	Scanning electron microscopy
TA	-	Tetraamino
TCP	-	Tetracarboxyphenoxy
THF	-	Tetrahydrofuran
TmPy	-	Tetra-N-methylpyridiloxy
TP	-	Tetraphenoxy
TN	-	Tetranitro
TPy	-	Tetrapyridiloxy
TSPc	-	Tetrasulphonated phthalocyanine
TCSPC	-	Time correlated single photon counting
TEM	-	Transmission electron microscopy
TCP	-	2,4,6-Trichlorophenol
btfa	-	4,4,4-Trifluoro-1-phenylbutane-1,3-dionate
^{3}Pc*	-	Triplet state of phthalocyanine

VR	-	Rotovibrational relaxation
V_R	-	Volume of sample
XRD	-	X-ray diffraction

LIST OF FIGURES

Chapter 3

LIST OF SCHEMES

LIST OF TABLES

Chapter 4

Chapter 5

Chapter 1

Introduction: Background and literature survey

1.1. Background on phthalocyanines

1.1.1. Structure and general applications

Phthalocyanines (Pcs) are the tetraaza tetrabenzo analogues of the naturally occurring porphyrins. Pcs form an important class of macrocyclic compounds which do not occur in nature [1, 2].

The phthalocyanines were accidentally discovered in the early 1900's and subsequent studies confirmed their structure, Fig. 1.1 [3-12]. Pcs are blue-green conjugated 18π-electron aromatic macrocyclic compounds. Almost all metals including the actinides and lanthanides as well as some non-metals can be introduced into the cavity of the Pc ring (**1**), Fig. 1.1b, to form metallophthalocyanines (**2**, MPc). A wide variety of substituents can be attached to the outer hydrocarbon moiety of the molecule at positions designated α, (non-peripheral) and β (peripheral), Fig 1.1b.

Phthalocyanines are characterized by high chemical and thermal stability. In recent years phthalocyanines have been used as redox catalysts, photocatalysts, semiconductors and photoconductors. They are also applied in gas sensing devices, medicine, solar energy conversion, dye transfer photography as well as non-linear optical systems. This demonstrates the versatility of this class of molecules [13-15].

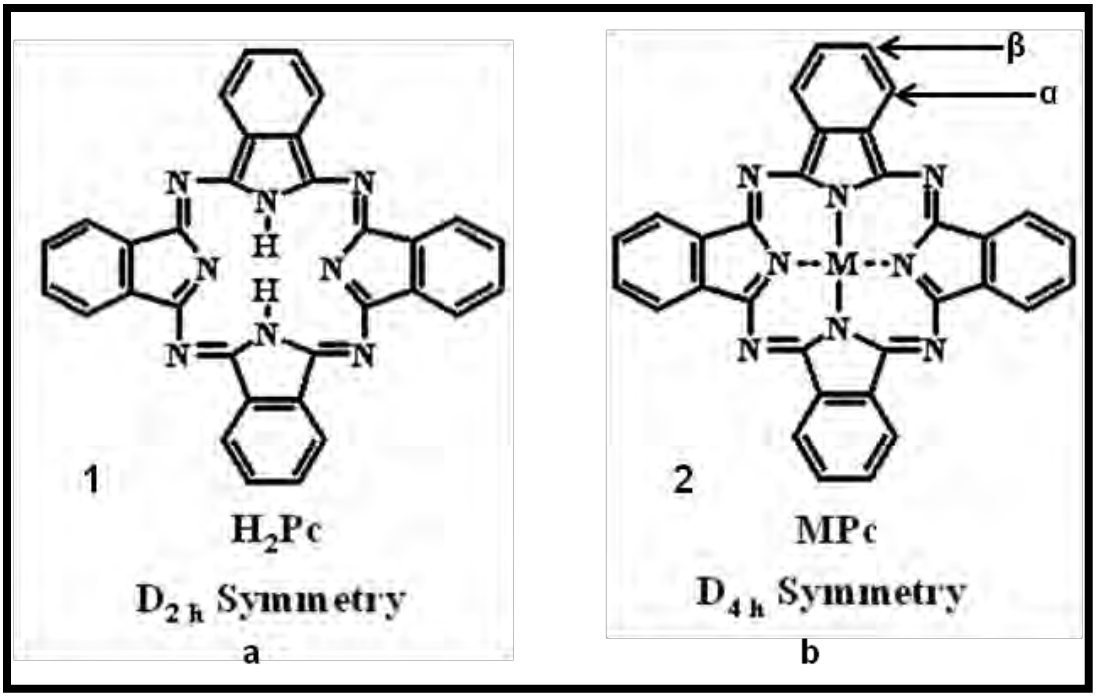

Figure 1.1: The molecular structures of (a) unmetallated (H_2Pc) and (b) metallated (MPc) phthalocyanines.

In recent years, compounds of lanthanide ions (Ln^{3+}) with organic ligands have found wide applications in areas such as fluorescence materials [16, 17], electroluminescence [18] and as fluorescence probes and labels in a variety of biological systems [19-21]. Interest in lanthanide phthalocyanines in particular has been as a result of possible coordination of more than one phthalocyanine macrocyclic unit per metal atom forming dimers or trimers [$LnPc_2$ or Ln_2Pc_3, Ln = lanthanide metal] and are often referred to as the sandwinch-type phthalocyanine complexes [22, 23]. Lanthanide phthalocyanines have pronounced electrochromic and chemochromic properties, hence are attractive for sensor development [24]. The first lanthanide bis-phthalocyanines were obtained by

Kirin *et al.*, in 1965 [25] and it was later observed that the colour of lutetium bis-phthalocyanine thin films changes under applied electric potential [26] and changes in pH [27] which finally led to the use of lanthanide phthalocyanines in electrochromism.

Lanthanide bis-phthalocyanines have also been applied as photocatalyst [28]. However, very little attempt has been made in the synthesis and application of their monomeric counterparts.

1.1.2. Synthesis

1.1.2.1. General synthetic pathways for peripherally and non-peripherally substituted phthalocyanines

The synthesis of phthalocyanines in general can be achieved by cyclotetramerization of phthalonitriles precursors in the presence of a metal salt (for MPcs) and a catalyst. Metallophthalocyanines can also be obtained by the use of phthalimides, phthalic acids and other precursors such as phthalic anhydrides (**3-8**) in the absence of a metal for unmetallated Pc and in the presence of a metal for the metallated counterparts, Scheme 1.1 [29, 30].

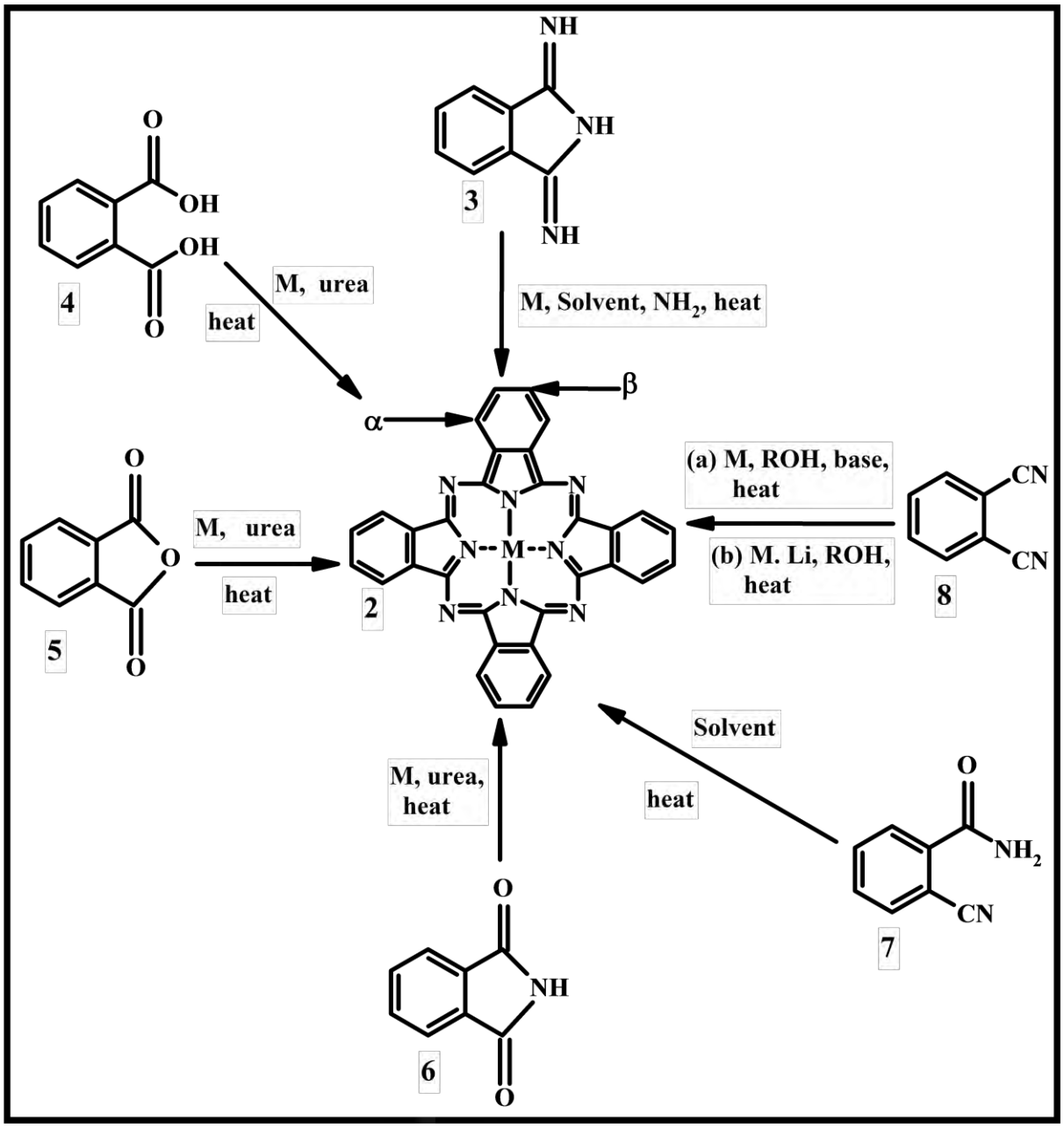

Scheme 1.1: Synthetic routes of metallophthalocyanines from different precursors.

Introduction of a substituent(s) into either the peripheral (β) or non-peripheral (α) positions of the phthalocyanine is usually done using base catalyzed nucleophilic aromatic substitution reaction of the starting 3-nitrophthalonitrile or 4-

nitrophthalonitrile precursors (**9**, **11**), Scheme 1.2 [31-34]. The products are referred to as mono-substituted phthalonitriles (**10**, **12**).

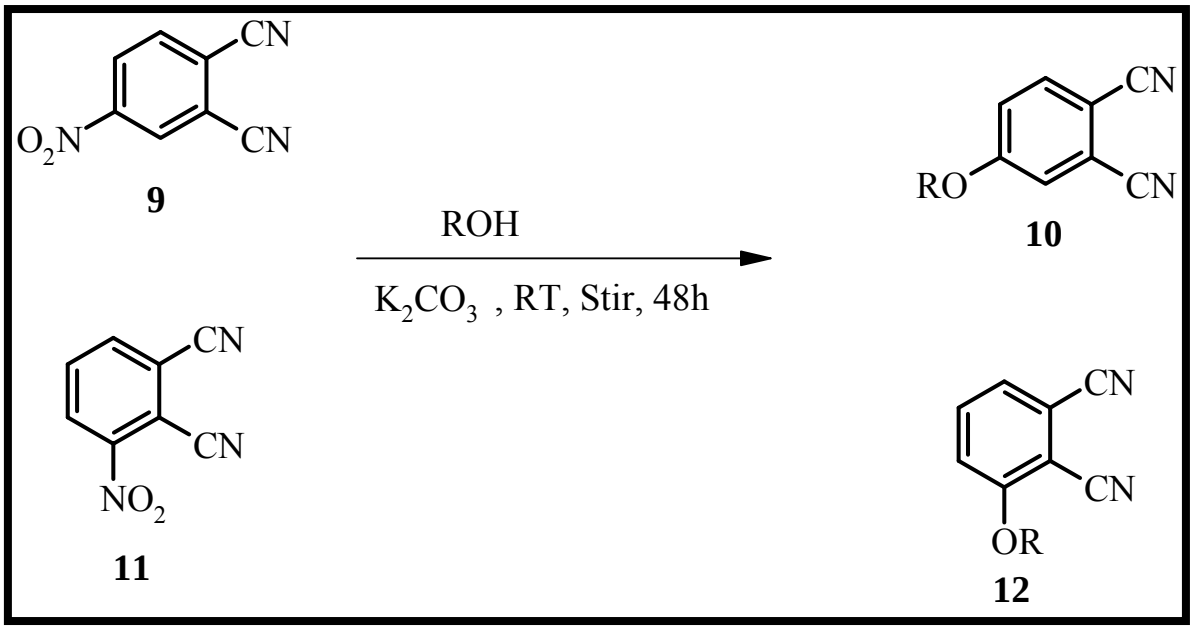

Scheme 1.2: Substitution reaction of nitro for alkoxy group on either at the peripheral or non-peripheral positions of the nitro phthalonitrile.

1(4),8(11),15(18),22(25)-Tetra-substituted (non-peripheral position) phthalocyanines are synthesized from 3-substituted phthalonitriles while 2(3),9(10),16(17),23(24)-tetra-substituted (peripheral position) phthalocyanines are synthesized from the 4-substituted analogues. Various reaction conditions have been described.

The cyclotetramerization reaction could be done at a high temperature in the presence of a metal salt and a basic solvent such as N,N-dimethylaminoethanol (DMAE). Alternatively, a milder and efficient cyclotetramerization can be achieved using high

boiling alcoholic solvents such as pentanol in the presence of a basic catalyst such as 1,8-diazabicyclo[5.4.0]undec-7-ene (DBU) or cyclohexylamine [35].

Also the cyclotetramerization reaction involving the mono-substituted phthalonitrile could first be done to form a metallophthalocyanine containing a labile metal such as lithium or sodium. The labile metal is then replaced within the phthalocyanine cavity with the desired metal [36].

The synthesis of tetra-substituted metallophthalocyanines with substituents either on the peripheral position or non-peripheral position normally lead to a mixture of products made up of four structural isomers. The four probable isomers are designated by their molecular symmetry as C_{4h}, C_{2v}, C_s, and D_{2h}. Separation of the mixture to obtain the individual isomers is difficult and time consuming [37] and can only be achieved by specifically designed high performance liquid chromatographic (HPLC) column. For the peripherally tetra-substituted phthalocyanines the isomers always occur in an expected statistical ratio of 12.5% C_{4h}, 25% C_{2v}, 50% C_s, 12.5% D_{2h} [38, 39]. However for the non-peripherally tetrasubsituted phthalocyanines, the composition depends on the central metal ion and the structure of the peripheral substituent.

Bulky substituents are often selected for the advantage of enhancing solubility of the phthalocyanines in common organic solvents as well as reducing aggregation.

1.1.2.2. Synthesis of lanthanide phthalocyanines

In this thesis, monomeric lanthanide phthalocyanines tetrasubstituted with amino, carboxyphenoxy, phenoxy, and pyridiloxy groups were synthesized. 4-Phenoxyphthalonitrile (**10a**), 4-carboxyphenoxyphthalonitrile (**10b**), 4-pyridiloxyphthalonitrile (**10c**) [31-33] as well as 3-phenoxyphthalonitrile (**13**) were used as the synthetic precursors [34].

Various synthetic strategies have been devoted to producing lanthanide phthalocyanines. Some of these include direct conventional chemical synthesis in which classic template reactions using precursors such as phthalonitrile [40] and diiminoisoindoline [1] are employed. The reactions occur generally in high boiling point non-aqueous solvents. Methods involving direct electrochemical synthesis [41] and microwave synthesis [42] have been reported.

The lanthanide phthalocyanines obtained by direct conventional chemical methods usually contain one or two macrocycles per metal atom [43-45]. The ratio of the starting metal to phthalonitrile as well as other reaction conditions are paramount in deciding the type and amount of phthalocyanine formed, whether monomeric or oligomeric in a particular reaction mixture [22]. According to Sokolova *et al*. [22], for phthalonitrile: metal salt ratio of 6:1, a maximum yield of about 80-90% of the Ln_2Pc_3 is obtained. Kalashnikova *et al*. [23], used phthalonitrile-metal ratio of 8:1 and obtained the monomeric, dimeric, trimeric and even the unsubstituented phthalocyanines. These two works jointly suggest that higher oligomeric forms of lanthanide phthalocyanines can

be obtained if the initial phthalonitrile content is increased. Conversely then, it might be reasonable to suggest that the monomeric lanthanide phthalocyanines will be expected to be the major reaction products if the starting phthalonitrile – metal ratio is set to 4:1 or lower phthalonitrile content, as typical of phthalocyanines in general.

Apart from the initial phthalonitrile-metal ratio in deciding the type of product for lanthanide phthalocyanines, it has also been established that the particular lanthanide metal also determines the type of phthalocyanine complex formed, whether monomeric or oligomeric. Thus it has been reported [43, 44, 45] that the heaviest lanthanides form phthalocyanine complexes with lower phthalocyanine units per lanthanide ion while the lighter lanthanides form complexes with higher number of phthalocyanine units with lanthanum and neodymium being predominant in this.

Thus combining the two scenarios; low initial phthalonitrile ratio and the use of the heavier lanthanide metal ions, for instance lutetium, could result in the monomer as the major product. However, it has been maintained that it is impossible to avoid the formation of mixed phthalocyanines [43, 44, 46].

Nemykin *et al*. [47, 48] have reported on the synthesis of a series of monomeric unsubstituted or tetra-tert-butyl-2,3-substituted lanthanide naphthalocyanines, Table 1.1. The success of the preparation of monomers as the major products was based on the use of dimethylsulfoxide (which stabilizes the monophthalocyanine by coordination) and the use of excess of the lanthanide salt. Other reported lanthanide

monophthalocyanine are also listed in Table 1.1, [49-52]. It therefore seems that not much conscious effort has been made at synthesizing monomers of the lanthanide phthalocyanines. They are only reported as by-products during the synthesis of their oligomeric counterparts. Substituents such as phenoxy and pyridiloxy on monomeric lanthanide phthalocyanines have not been reported though they could enhance the solubility of the phthalocyanine.

Sub Aim of the work:

This work therefore, in part, is aimed at synthesizing and characterizing monomeric phthalocyanine complexes of the lanthanides (erbium and lutetium) substituted with phenoxy, carboxyphenoxy, pyrilidiloxy and amino groups. For dysprosium, a dimer was formed. Applications of these monomeric lanthanide phthalocyanines will be compared with those of zinc Pc complexes especially the unsubstituted zinc phthalocyanine with the view of drawing parallels between metallophthalocyanines of the d-block metals and those of the f-block.

Table 1.1: Some monomeric lanthanide phthalocyanines reported.

Lanthanide ion	Substituent(s)	Axial ligand	Ref.
Lu	Tetra-tert-2,3-naphthyl	Dipivaloylmethanato	47
Lu	Tetra-tert-2,3-naphthyl	Acetylacetate	47
Lu	Tetra-tert-2,3-naphthyl	Acetate	47
Lu	Tetra-tert-2,3-naphthyl	Chloride	47
Tm	Tetra-tert-2,3-naphthyl	Acetate	47
Er	Tetra-tert-2,3-naphthyl	Acetate	47
Ho	Tetra-tert-2,3-naphthyl	Acetate	47
Tb	Tetra-tert-2,3-naphthyl	Acetate	47
Gd	Tetra-tert-2,3-naphthyl	Acetate	47
Eu	Tetra-tert-2,3-naphthyl	Acetate	47
Eu	Tetra-tert-2,3-naphthyl	Chloride	47
Sm	Tetra-tert-2,3-naphthyl	Acetate	47
Nd	Tetra-tert-2,3-naphthyl	Chloride	47
Pr	Tetra-tert-2,3-naphthyl	Acetate	47
Sm	H	Fod	48
Eu	H	Fod	48
Gd	H	Fod	48

Lu	**H**	**Btfa**	**48**
Lu	**H**	**Acetate**	**49**
Nd	**H**	**Acetate**	**49**
Er	**n-Pentoxy/ tert-butyl**	**Acetylacetate**	**50**
Eu	**H**	**Acetylacetate/ Oxyquinoline**	**51**
Lu	**HPTCP**	**Acetate**	**52**

HPTCP = hexaphenoxycyclotriphophazenyl

fod = 6,6,7,7,8,8,8-heptafluoro-2,2-dimethyloctane-3,5-dionate

btfa = 4,4,4-trifluoro-1-phenylbutane-1,3-dionate

1.1.3. Absorption spectra

1.1.3.1. Origins of spectra and general spectral properties

The electronic absorption spectra of phthalocyanine and its metal complexes have been studied extensively in the gas phase, in solution and in the solid state [53-56]. Their extended π-systems, molecular symmetry and packing in the solid state have made them very attractive for theoretical investigations [57-61].

The basic model that is widely used to explain the origin of the characteristic bands of phthalocyanines is the Gouterman's four-obital model. The model is based on linear combination of atomic orbitals (LCAO) [62]. In this model optical spectra are interpreted in terms of electronic transitions between the highest occupied molecular

orbitals (HOMO) and the lowest unoccupied molecular orbitals (LUMO), Fig. 1.2. In phthalocyanines, the a_{2u} is much lower in energy than a_{1u}, Fig 1.2, as opposed to porphyrins where they are closer together and a_{2u} is above a_{1u}. The degeneracy of the LUMOs (e_g) is maintained in metallophalocyanines because of their high symmetry, D_{4h}. In the case of unmetallated phthalocyaines, D_{2h}, the low symmetry results in a breakdown of the degeneracy of the e_g orbitals resulting in additional spectral features of the phthalocyanine. Thus if the symmetry of a metallophthalocyanine is quite altered from the D_{4h} geometry, changes in the optical spectral features will be expected. Large metals which do not fit in exactly in the phthalocyanine cavity protrude out and lower the symmetry to C_{4v}. For instance zinc metallophthalocyanine is domed shaped [63, 64], while those of lead assumes shuttlecock shape [65].

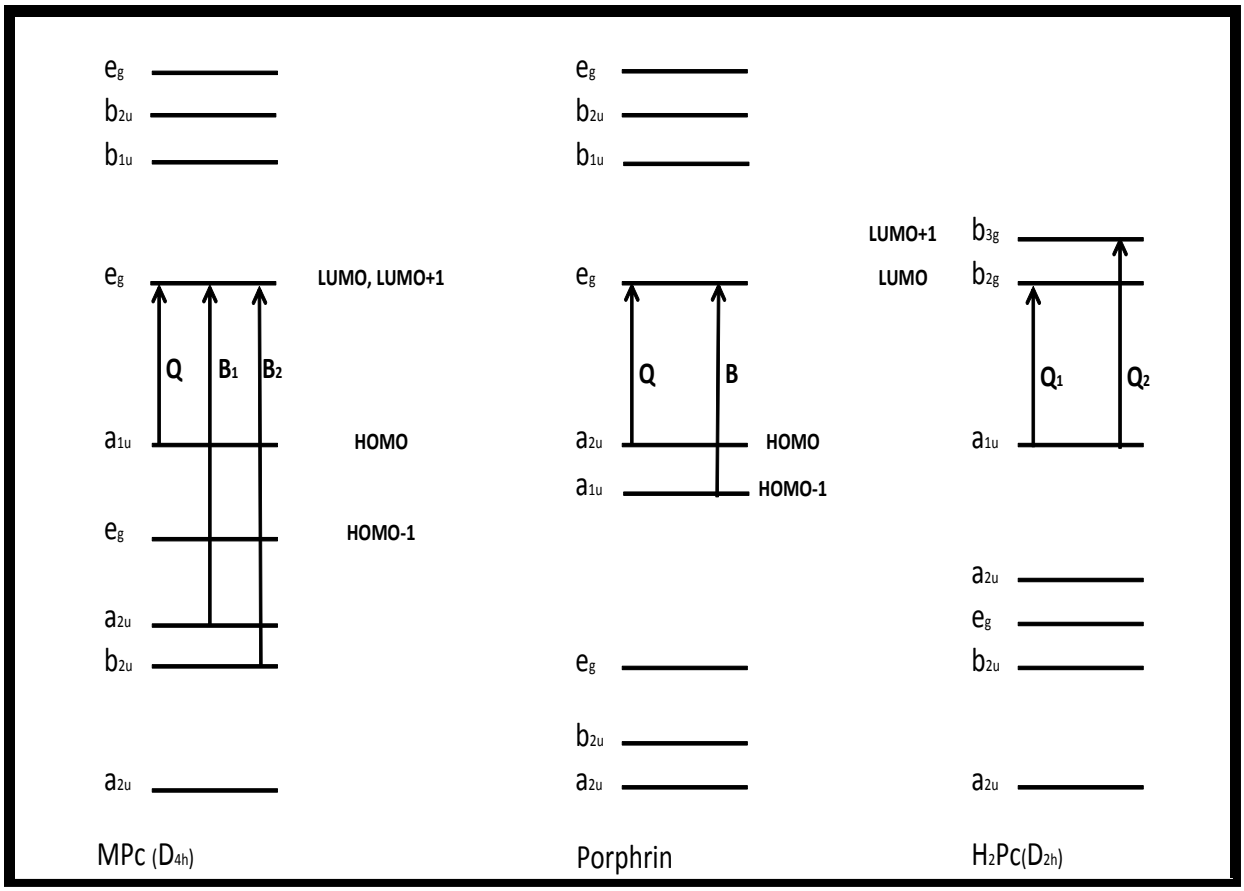

Figure 1.2: Electronic energy orbital diagram showing the origin of the two major absorption bands in phthalocyanines and porphyrins.

In practice, the electronic spectra of phthalocyanines can be categorized into two main band regions which arise from the π-π* transitions originating from their delocalized 18π electron system, Fig. 1.3. The spectra usually consist of an intense band in the near-IR referred to as the Q band. The band is characterized by high molar absorptivity than any other band within the spectrum and it is the one that is responsible for the overall color of the phthalocyanine molecule [66, 67]. The Q band originates from transition from a_{1u} of the HOMO to the e_g of the LUMO. As indicated earlier, for metallophthalocyanines with high symmetry, D_{4h}, the Q band is a single band,

Fig. 1.3a.

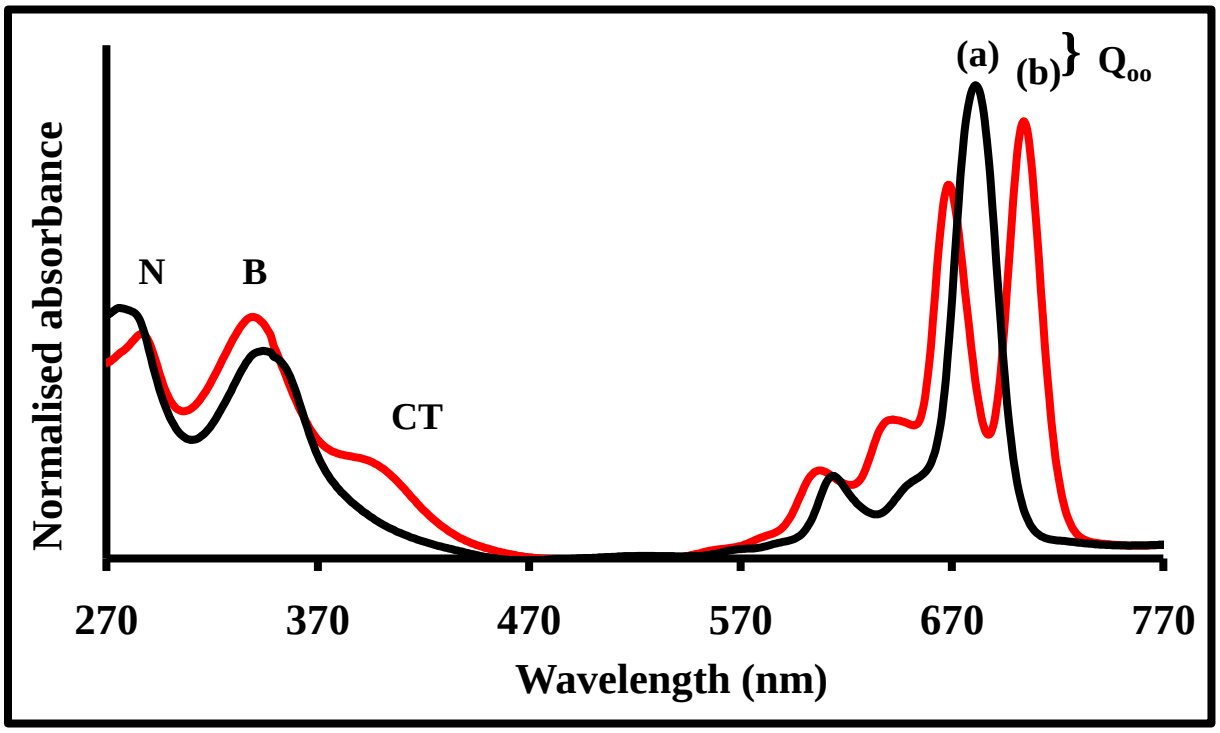

Figure 1.3: Ground state electronic absorption spectra of (a) metallated and (b) unmetallated phthalocyanines.

However for the unmetallated phthalocyanine, the lower symmetry, D_{2h}, results in a split in the Q-band, Fig. 1.3b. If the symmetry of the metallophthalocyanine is lowered by the introduction of large metals, the split in the Q band is also observed.

The optical spectra of phthalocyanines also contain a second band towards the ultra-violet portion of the spectrum referred to as the Soret or B band. This band originates from a transition from the a_{2u} of the HOMO to the e_g of the LUMO with only one band expected. However, the Gouterman's model has been modified to cater for two Soret bands B_1 and B_2.

Depending on the solvent in which the spectra are run additional bands; N, L and C may be observed.

Just like any conjugated aromatic π-system, the electronic properties of phthalocyanines can be modified by extension of the conjugation through fusion of additional benzene rings at the periphery of the macrocycle [68] or construction of conjugated oligomers [69]. Most phthalocyanines exhibit the Q band around 680 nm. This band will usually shift towards the near IR region up to 1000 nm and beyond on extension of conjugation [70]. The exciton interaction in non-conjugated dimers [69, 71-73] and in phthalocyanine aggregates [74-76] as well as their solid crystals [77] also induces shifts in the electronic absorption bands depending on the arrangement of the macrocycles.

Also the spectral features of the phthalocyanines could be changed by introducing electron withdrawing or donating substituents on the ring as well as changing the central coordinating atom.

1.1.3.2. Spectra of lanthanide phthalocyanines

In general, the lanthanide bis-phthalocyanines can exist in two forms depending on the medium. In a non-basic medium, the dimer contains a radical and is usually referred to as 'the Green form'. By adding alkalis such as potassium hydroxide or sodium methoxide, the corresponding reduced form, usually called 'the Blue form' is obtained [78-81].

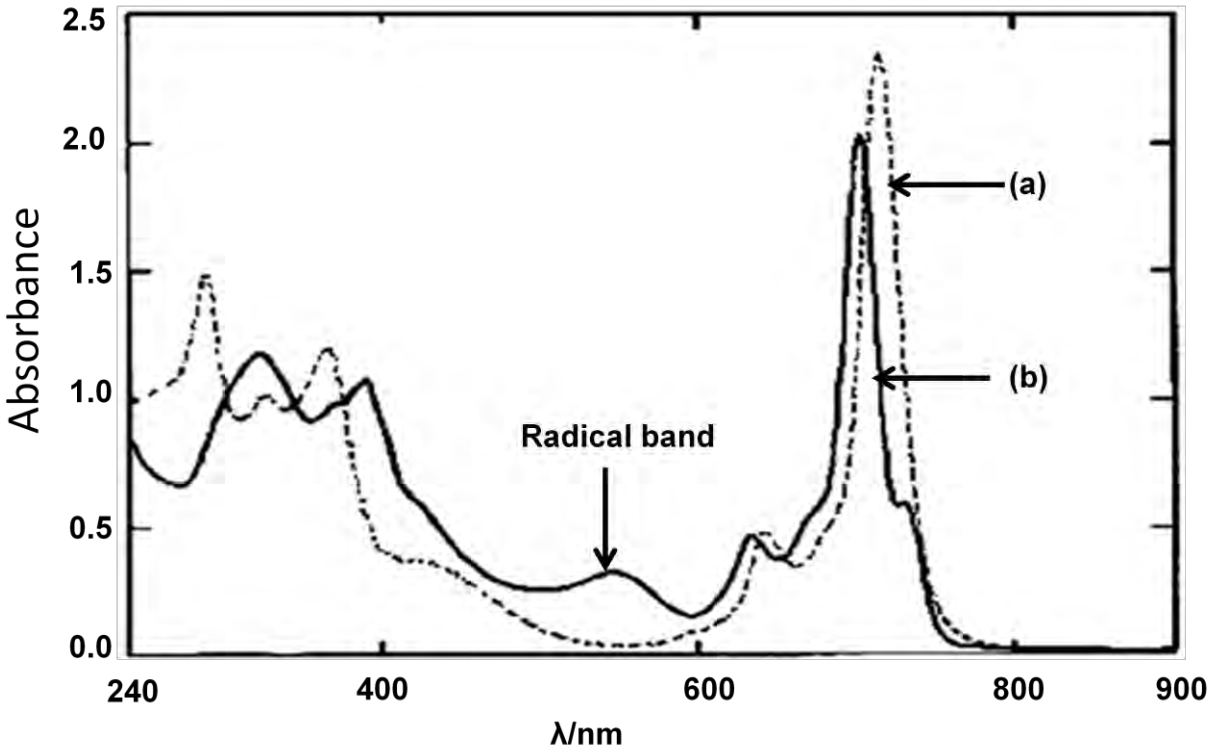

Figure 1.4: UV-visible spectra of (a) the blue form (b) the green form of lutetium bis-phthalocyanine in chloroform [82].

The absorption spectra of the green form of the lanthanide bis-phthalocyanines which usually contain a radical have additional spectral bands compared to the blue counterpart, Fig. 1.4 [82]. Apart from the typical Soret (B) and Q-bands found in a phthalocyanine, there is usually a medium intensity peak around 500 nm, Fig. 1.4 (b), referred to as the radical peak, a weak near-IR peak around 900 nm and a broad absorption comprising one or two peaks in the 1100-1800 nm region.

However the electronic absorption spectra of the monomeric lanthanide phthalocyanines have similar features as the normal monomeric phthalocyanine absorption spectra. A monomeric unsubstituted lutetium phthalocyanine with an

acetate axial ligand has been reported to have a split Q band with maxima as 626 (intense) and 712 (weak) nm in dichloromethane [49].

1.1.4. Photophysical and photochemical processes

Absorption of light by materials at their molecular level produces physical and chemical changes [83]. Photochemistry focuses on the chemistry involved as a material is impacted by photons, whereas photophysics deals with physical changes that result from the impact of photons. Phthalocyanines are able to absorb visible light of the appropriate wavelengths resulting in interesting physical processes such as fluorescence [84] as well as being able to effect chemical transformation of compounds such as organic substrates [85].

1.1.4.1. Jablonski diagram

The origin of photophysical processes is illustrated by the Jablonski diagram, Fig. 1.5 [86-89].

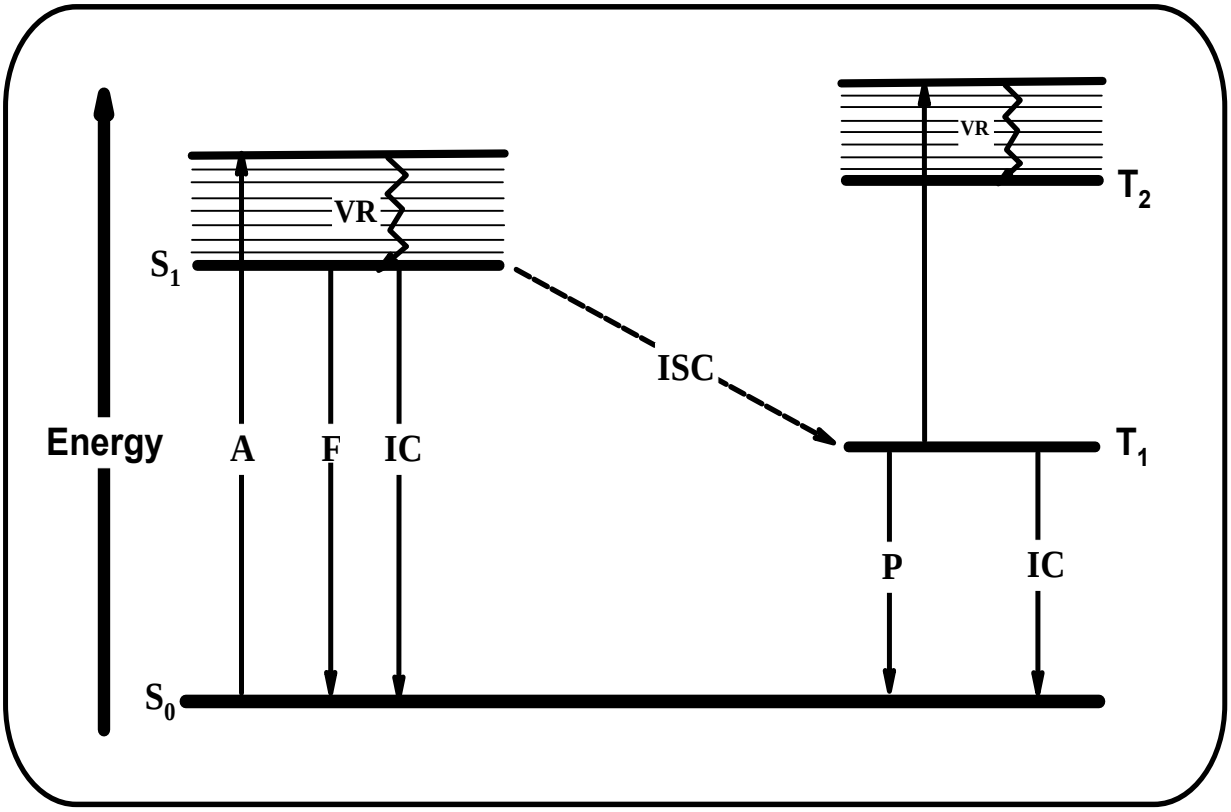

Figure 1.5: Jablonski diagram displaying transitions of a molecule from its lower ground state energy to its higher excited state energy following irradiation with light; A = absorption, VR = rotovibrational relaxation, ISC = intersystem crossing, F = fluorescence, IC = internal conversion, P = phosphorescence, S_0 = singlet ground state, S_1 = singlet excited state and T_1 = first excited triplet excited state, T_2 = second excited triplet state.

The interaction of light with phthalocyanines and the subsequent physical and chemical processes have been widely researched particularly because these complexes have very high molar absorptivity in the visible region [66, 67]. Phthalocyanines containing large diamagnetic metals are known to enhance intersystem crossing of the singlet excited state to the triplet state, generating singlet oxygen. Singlet oxygen is implicated in several photochemical processes such as photodynamic therapy [90] and has also been applied in the photochemical transformation of various analytes [85, 91]. Lanthanide phthalocyanines contain large metals and are expected to show interesting photophysical and photochemical properties.

Sub aim:

Lanthanide phthalocyanines are to be embedded in electrospun polymer fibers and used for the detection and phototransformation of environmental pollutants.

1.1.4.2. Equations usually employed for triplet state studies: triplet quantum yield (Φ_T) and triplet lifetime(τ_T)

The triplet quantum yield of a photosensitizer refers to the fraction of the excited singlet state molecules that can undergo intersystem crossing to the triplet state. Experimentally, the triplet state parameters (Φ_T, τ_T) of phthalocyanines are determined using laser flash photolysis. This involves rapid introduction of pulse of laser light into a sample solution of the phthalocyanine. A time-resolved absorption signal is obtained if the triplet state of the phthalocyanine is populated. The signal originates from a

transition from T_1 to T_2 or higher states, Fig. 1.5, and information on Φ_T and τ_T may be obtained.

The triplet quantum yield of a phthalocyanine may be determined by a comparative method, Equation 1.1, using a standard. Most often for phthalocyanines, the standard is unsubstituted zinc phthalocyanine.

$$\Phi_T = \Phi_T^{Std} \frac{\Delta A_T \varepsilon_T^{Std}}{\Delta A_T^{Std} \varepsilon_T} \quad (1.1)$$

where ΔA_T and ΔA_T^{Std} are the changes in the triplet state absorbances of the sample and the standard, respectively. ε_T and ε_T^{std} are the triplet state molar extinction coefficients for the sample and the standard, respectively. Φ_T^{std} is the triplet quantum yield of the standard in the particular solvent.

The molar extinction coefficient of the triplet state, ε_T is determined from Equation 1.2 [92]:

$$\varepsilon_T = \varepsilon_S \frac{\Delta A_T}{\Delta A_S} \quad (1.2)$$

where ΔA_T and ΔA_S are the changes in the triplet state and singlet state absorptions respectively. ε_S is the singlet state molar extinction coefficient.

1.1.4.3. Fluorescence quantum yield (Φ_F) and fluorescence lifetime (τ_F)

Fluorescence quantum yields (Φ_F) of the phthalocyanines may be determined by the comparative method [93], Equation 1.3:

$$\Phi_F = \Phi_F^{Std} \frac{F\, A_{Std}\, n^2}{F_{Std}\, A\, n_{Std}^2} \qquad (1.3)$$

where F and F_{Std} are the areas under the fluorescence emission curves of sample and the standard, respectively. A and A_{Std} are the respective absorbances of the sample and standard at the excitation wavelength. Unsubstituted zinc phthalocyanine is usually employed as the standard.

For the lanthanide phthalocyanines especially those containing lutetium which is a large diamagnetic metal, intersystem crossing to the triplet states of the MPcs is expected. Correspondingly low fluorescence and high triplet quantum yields are expected. Dysprosium and erbium phthalocyanines are expected to have their triplet states being populated but with a very short lifetimes because of their paramagnetic nature.

Fluorescence lifetimes are usually of the order of nanoseconds (10^{-9} s). Several techniques are available for the determination of fluorescence lifetimes [94-96]. In this work however, time–correlated single photon counting technique (TCSPC) is used [97, 98].

1.1.4.4. Singlet oxygen quantum yield (Φ_Δ)

Singlet oxygen ($O_2(^1\Delta_g)$) is known to play a key role in many photo-induced oxidative processes in biological as well as in chemical systems. Singlet oxygen is believed to be the initial agent in the photodynamic therapy of cancer (PDT) [90, 99-102] and it participates in many photochemical processes such as photo-oxidation of sulfides [103], thiols [104], phenols [105] and other organic compounds [106-108]. Singlet oxygen is generated by energy transfer from the triplet excited state of the phthalocyanine (a photosensitizer) to ground state triplet oxygen O_2 ($^3\Sigma_g^-$). Singlet oxygen lies 0.98 eV in energy above the corresponding triplet ground state, thus the energy difference between T_1 and S_0 of the phthalocyanine should be above this value to enable the generation of singlet oxygen. The $T_1 \rightarrow S_0$ energy gap of most phthalocyanine complexes containing diamagnetic metals is above 0.98 eV and thus they are capable of generating singlet oxygen [109]. For applications of the phthalocyanine in any phototransformation reaction, it is important to determine singlet oxygen quantum yield (Φ_Δ), which is a measure of the efficiency of singlet oxygen generation of the phthalocyanine within the applied environment.

Experimentally, singlet oxygen quantum yields of phthalocyanines can be determined using optical or chemical methods.

The optical method involves the time-resolved phosphorescence decay of singlet oxygen at 1270 nm [110]. The dynamic course of $O_2(^1\Delta_g)$ concentration [$O_2(^1\Delta_g)$] can be

clearly monitored and recorded, following Equation 1.4 as theoretically described in literature [111].

$$I(t) = B\frac{\tau_D}{\tau_T - \tau_D}[e^{-t/\tau_T} - e^{-t/\tau_D}] \quad (1.4)$$

where, I(t) is the phosphorescence intensity of $O_2(^1\Delta_g)$ at time *t*, τ_D is the lifetime of $O_2(^1\Delta_g)$ phosphorescence decay, τ_T is the triplet state lifetime of standard or sample and B is a coefficient involved in sensitizer concentration and singlet oxygen quantum yield.

The singlet oxygen quantum yield, Φ_Δ, of the phthalocyanine is then determined by a comparative method using Equation 1.5:

$$\Phi_\Delta = \Phi_\Delta^{Std} \cdot \frac{B \cdot A^{Std}}{B^{Std} \cdot A} \quad (1.5)$$

where Φ_Δ^{Std} is the singlet oxygen quantum yield for the standard usually unsubstituted zinc phthalocyanine. B and B^{Std} refer to coefficient for the sample and standard respectively and; A and A^{Std} to the absorbances of the sample and standard respectively at the excitation wavelength.

The chemical method requires a suitable singlet oxygen sensitive compound (quencher) that can react quickly with the singlet oxygen in a 1:1 ratio without side reactions. It is expected that the decomposition product of the quencher should neither react with the singlet oxygen nor interfere with the monitoring process. The chemical method does not require extensive and expensive instrumentation. The experiment is usually carried out by irradiating a sample solution containing the phthalocyanine, oxygen and the

quencher. The degradation of the quencher is usually monitored spectrocoscopically [112, 113]. The most common chemical quencher in organic solvents is 1,3-diphenylisobenzofuran (DPBF). However, other furans as well as derivatives of anthracene, guanine and bilirubin have been used [112, 114, 115]. In water, the commonly used chemical quencher is anthracene-9,10-bis-methylmalonate (ADMA).

The singlet oxygen quantum yield of the phthalocyanine can be determined using a comparative method based on Equation 1.6. Unsubstituted zinc phthalocyanine is often used as standard.

$$\Phi_{\Delta} = \Phi_{\Delta}^{std} \cdot \frac{R^{Sample} \cdot I^{std}}{R^{std} \cdot I^{Sample}} \qquad (1.6)$$

where Φ_{Δ}^{std} is the singlet oxygen quantum yield for the standard, R^{sample} and R^{Std} are the photobleaching rates of the quencher in the presence of sample and standard respectively, while I^{Sample} and I^{std} are the respective rates of light absorption by sample and standard.

Alternatively, an absolute methods based on Equation 1.7 can be used.

$$\Phi_{quenc\ her} = \frac{(C_0 - C_t)V_R}{I_{abs}.t} \qquad (1.7)$$

where C_0 and C_t are the concentrations of the chemical quencher prior to and after irradiation, respectively; V_R is the solution volume; t is the irradiation time per cycle and I_{abs} is defined by Equation 1.8:

$$I_{abs} = \frac{\alpha.A.I}{N_A} \qquad (1.8)$$

where $\alpha = 1 - 10^{-A(\lambda)}$, $A(\lambda)$ is the absorbance of the sensitizer at the irradiation wavelength, A is the irradiated area, I is the intensity of light expressed as photons cm^{-2} s^{-1}) and N_A is Avogadro's constant. The singlet oxygen quantum yields Φ_Δ can then be calculated using equation 1.9 [116].

$$\frac{1}{\Phi_{quenc\ her}} = \frac{1}{\Phi_\Delta} + \frac{1}{\Phi_\Delta}.\frac{k_d}{k_a}.\frac{1}{[quenc\ her]} \qquad (1.9)$$

where k_d is the decay constant of singlet oxygen in respective solvent and k_a is the rate constant of the reaction of the quencher with $O_2(^1\Delta_g)$. The intercept obtained from the plot of $1/\Phi_{quencher}$ versus 1/[quencher] gives $1/\Phi_\Delta$.

1.1.4.5. Photobleaching quantum yield (Φ_p)

The stability of a phthalocyanine is of paramount importance for any application involving the generation of the singlet oxygen. While generation of singlet oxygen by phthalocyanine is essential in its applications in PDT and photoconversions of both organic as well as inorganic substrates, singlet oxygen has the tendency of oxidizing the phthalocyanine itself. This leads to decomposition of the phthalocyanine to low molecular weight compounds such as phthalimide and the efficiency of singlet oxygen production is reduced. This process is referred to as photobleaching.

Photobleaching quantum yield (Φ_p) refers to the fraction of phthalocyanines molecules decomposed per quanta of light absorbed.

The determination of the photobleaching quantum yield of a phthalocyanine is done by monitoring the intensity of its Q-band absorption upon irradiation. The quantum yield (Φ_p) is calculated from Equation 1.7, where the change in the concentration of the phthalocyanine replaces that of the quencher.

The phthalocyanine complexes of the f-block metals are expected to show interesting photophysical and photochemical properties. Apart from lanthanum and lutetium, the rest of the lanthanides are paramagnetic in all their normal oxidation states. La(III) and Lu(III) are diamagnetic and because of their large size, their phthalocyanine complexes are expected to show enhanced singlet oxygen production since their excited singlet state can easily undergo intersystem crossing to the triplet state due to the heavy atom effect [117]. This will result in corresponding low fluorescence quantum yields. For the phthalocyanine complexes of the other lanthanides, singlet oxygen production is not expected due to very short triplet lifetimes (τ_T). Table 1.2 shows the spectral, photophysical and photochemical properties of some lanthanide phthalocyanines. As can be seen on Table 1.2, the studies of the photophysical and photochemical properties of lanthanide phthalocyanines are limited and hence are part of the aims of this thesis.

Table 1.2: Spectral, photophysical and photochemical properties of some lanthanide phthalocyanines.

MPc	Type	λ_{abs}Q-band/nm	λ_{em}/nm	Φ_F (τ_F/ns)	Φ_T (τ_T)	Φ_Δ	Ref
[(acac)Er{Pc(β-$OC_5H_{11})_4$}]	monomer	675	700-710	--	--	--	50
[(acac)Er{Pc(β-$C_4H_9)_4$}]	monomer	670	700-710	--	--	--	50
Er{ Pc(β-$OC_5H_{11})_4\}_2$	Dimer	678	700-710	--	--	--	50
Er{Pc(β-$C_4H_9)_4\}_2$	Dimer	675	700-710	--	--	--	50
Eu(acac)Pc	monomer	670	697	--	--	--	51
Eu(q)Pc	monomer	679	696				51
[(Ac)Lu{Pc(β-HPTCP)$_4$}]	monomer	680	690	0.01(0.07)	--	0.66	52
Lu{Pc(HPCP)$_4\}_2$	Dimer	665	703	0.03(0.03)	--	0.10	52

HPTCP = hexaphenoxycyclotriphophazenyl, q = quinolinato, acac = ethylacetate

Most applications of phthalocyanines such as photodynamic therapy [90] and homogeneous catalysis [85] usually occur in solution. However, some applications of phthalocyanines are preferable in their solid state as in read-write compact disc [118] or when the phthalocyanine is incorporated into solid support systems. Such support systems offer comparably better advantages such as ease of recovery of the phthalocyanine during photocatalysis. In this work, lutetium and zinc phthalocyanines (the later for comparison) are supported on electrospun polymer fibers and applied for the detection and/or phototransformation of environmental analytes.

1.2. Phthalocyanines on polymer support systems

1.2.1. General

The evolution of polymer composite technology is opening up prospects for creating materials made from synthetic phthalocyanines which are supported on a polymer matrix [119-121]. Attaching the phthalocyanine in a polymer support offers many advantages which do not exist when unattached phthalocyanines are used. They include cooperative reactions in polymer chains, separation of active sites, the possibility of specific binding of different substrates on active sites, increasing the stability of the tetrapyrole component and decrease in its toxicity with respect to biological media [121, 122]. Phthalocyanines-containing polymers are obtained by covalent, ionic or coordinate binding of the Pc with the polymer. Two groups of modified polymer matrices containing physically attached and chemically bound phthalocyanines can therefore be distinguished [123]. Systems in which the phthalocyanine is primarily bound to the support by sorption forces constitute the group of physically supported phthalocyanines. Phthalocyanines can also be incorporated inside the polymer matrix during synthesis of the polymer or formation of thin films, fibers and composites [124].

Natural and synthetic macromolecular substances of different structures are used as polymer supports. Polysaccharides and proteins are most often used among the biopolymers. Synthetic polymeric materials are however more convenient supports since their properties, composition and structure can be purposefully altered with

respect to subsequent binding to phthalocyanines. Of the synthetic polymer supports, polyethelene glycol, polyesters, polyacrylates, acrylate copolymers among others are commonly used [125-129].

Various applications of these phthalocyanine bound polymers have been reported. These include the use of metallophthalocyanine containing chlorine or phosphorus bound to polymers as fireproofing materials [130, 131]. Phthalocyanine containing polymer materials have also been applied in biological systems and medicine [119, 132]. Another application of phthalocyanine containing polymers is in optics and electronics [133, 134].

The use of phthalocyanine-containing polymers in solving environmental problems is an ongoing exciting challenge. As functional molecules in chemical sensors, phthalocyanines when incorporated on polymer supports can be used in the detection of toxic gases such as nitrogen oxides, carbon monoxide and sulfur oxides as well as hydrazine, phosphine, methane and other gases [135]. It has been reported that cobalt (II) and copper(II) bis-(3,4-dicarboxybenzoyl)phthalocyanines, covalently bound to linear polystyrene showed high sensitivity to nitrogen dioxide gas as well as responding to chloroform and perchloroethylene [136]. Also cobalt(II) tetracarboxyphthalocyanine, covalently bound to polyvinylamine has been shown to have high stability and exhibits catalytic activity in the oxidation of mercaptoethanol [137]. In another report [138], iron(III) phthalocyanine complex covalently bound to copolymer consisting of N-acrylo-β-alanine(aminoethylene)amide, N-

acryloylpyrrolidone and N,N-bis-(methacyloyl)-1,2-diaminoethane has been shown to be catalytically active towards the oxidation of 2,4,6-trichlorophenol and 3,5-di-tert-butylcatenol.

In particular, Amanbaeva [137], suggested that if the phthalocyanine-containing polymer is made porous, it could be used as a catalyst in the treatment of industrial petroleum products and wastewater to remove sulfur. Such porosity of the functionalized polymer could be achieved by electrospinning the polymer into fibers as is the case in this work. Thus this work focuses on the use of electrospun polymer fibers from polyacrylic acid, polystyrene, polysulfone and polyurethane, functionalized with metallophthalocyanines for photocatalytic conversions. This is due to the fact that electrospun polymer fibers are characterized by large surface area to volume ratio and high porosity that can allow effective interaction between the embedded phthalocyanine molecules and light or with reactant species such as gas molecules.

1.2.2. Electrospun polymer fibers

1.2.2.1. Basics of electrospinning

Among the techniques used to form polymeric fibers, such as drawing, template synthesis, phase separation and self-assembly, electrospinning is quite a promising technique in forming fibers, in the sense that it is simple, convenient, reproducible process and generally versatile technique for generating fibers with diameters that range from several micrometers to tens of nanometers [139, 140]. By changing the

process parameters, such as solution concentration and molecular weight of the polymer [141], fibers of different diameters can be prepared to meet the requirements of various applications.

In the process of electrospinning, fibers are generated through an electrically charged jet of polymer solution. The fundamental principle of electrospinning is similar to electrospraying.

The principal variables that govern the quality of polymer fibers or determine whether electrospinning will occur at all are the average molecular weight of the polymer, the nature of the solvent, and the magnitude of the electric field used to induce the electrospinning process. Usually, for the process to be feasible, a polymer of adequate average molecular weight should be dissolved in a solvent having suitable conductivity, surface tension, and vapor pressure. The concentration of the polymer solution should be moderately high to facilitate its flow during the electrospinning process.

Experimentally, the apparatus for electrospinning consist of three basic components, Fig. 1.6 as described by Carlberg B. *et al*. [142]:

(a) A container, usually a syringe for the polymer solution

(b) A high voltage source

(c) Conductive collector plate where the fiber mat is deposited.

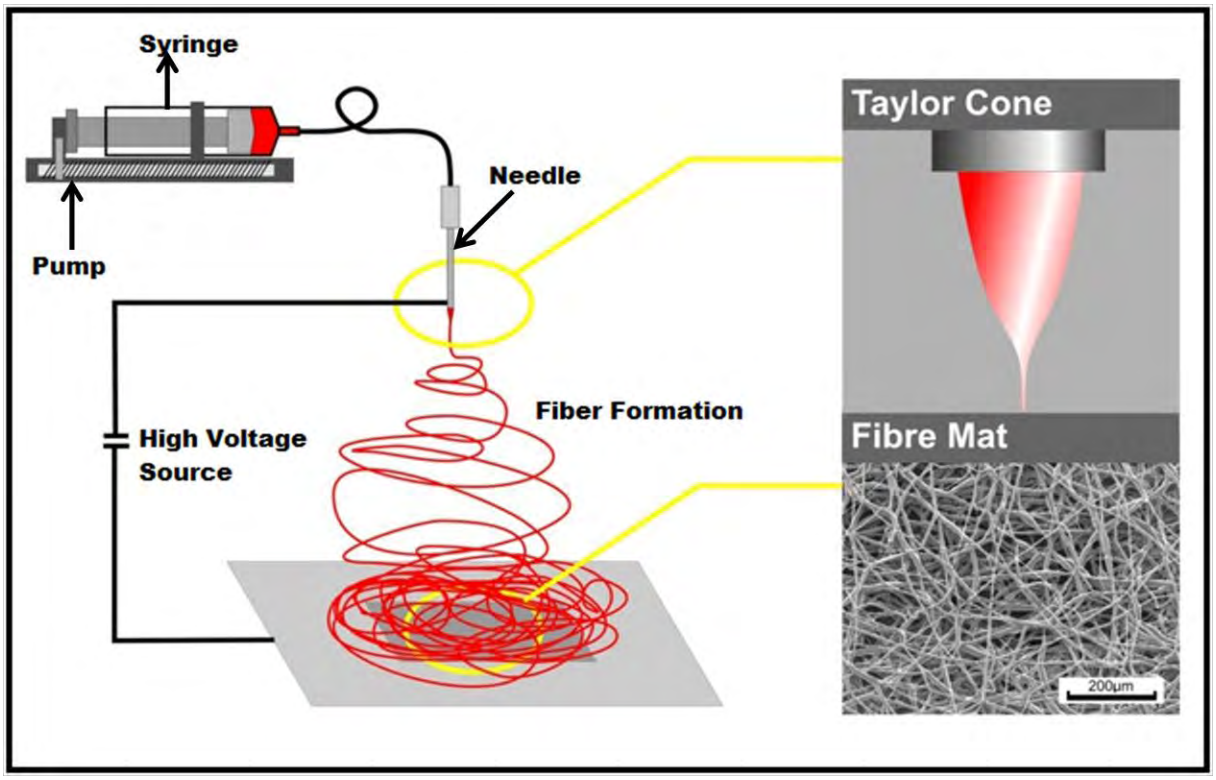

Figure 1.6: Schematic diagram of an electrospinning setup [142].

The process begins with polymer solution being gradually pumped out of the syringe through the needle to form a drop of solution at the tip of the needle. The drop is charged by applying a high voltage on the needle. When the applied voltage is gradually increased, the Coulombic forces will counteract the surface tension that tends to hold the drop in a spherical shape thus distorting it into the so-called Taylor cone. When the electric field surpasses a certain threshold value, a charged fluid jet is ejected from the tip of the Taylor cone in the form of fiber toward the collector plate and is collected as unwoven fiber mat.

1.2.2.2. Factors affecting the morphology of electrospun polymer fibers

It has been reported that the morphology of the electrospun fibers is influenced by a large number of different parameters. However these parameters can be broadly classified into three main categories: solution properties, processing conditions and ambient conditions [143].

The concentration of the polymer solution should allow adequate chain entanglement, continuous and uniform electrospun fibers under the applied electric field. The concentration of polymer in solution often determines whether it can be electrospun at all and generally has a dominant effect on the fiber diameter, as well as fiber morphology [144]. High concentrations generally yield fibers of large average diameters but the quantitative relationship between the concentrations of the solution and the average fiber diameters appears to be variable depending on the polymer used. At extremely low polymer concentrations, fibers do not usually form and the solution simply sputters.

Environmental factors such as humidity and temperature affect the quality of the fibers formed. The rate of drying of the polymer jet is determined by the surrounding conditions and will determine whether the fibers will be fused or not in the fiber mat.

The process parameters include tip to collector distance, flow or pump rate and the voltage applied. All these affect the quality of the fibers obtained differently. A good blend of all these factors usually leads to fibers for the desired application.

1.2.2.3. Characterization of electrospun polymer fibers

In principle there are a large number of different characterization techniques that can be used for electrospun fibers. However, four common characterization methods for fiber mats that are relevant to this work will be discussed, although only microscopic and X-Ray diffraction techniques were used.

(a) Mat porosity and pore size distribution

The interstitial porosity of an electrospun fiber mat is referred to as the fractional void space contained within it. It is the pore size distribution and is three-dimensional geometry that determines the key properties such as filtration or permeability to gases of the fiber mats. Various techniques are available for the determination of the porosity of fiber mats. These include Brunauer, Emmett and Teller (BET) surface area, Mercury Intrusion Porosimetry, Liquid Extrusion Porosimetry and Capillary Flow Porosimetry.

(b) Diameters and pore size

Microscopic imaging is routinely used in the initial characterization of electrospun fiber mats. Although optical microscopy has sometimes been used to assess fiber diameter distributions in electrospun fiber mats, it is electron microscopy that is extensively used for the purpose.

Scanning electron microscopy (SEM) and transmission electron microscopy (TEM) techniques are both particularly useful in understanding and quantifying fiber morphology. Both techniques essentially yield two-dimensional representations of electrospun fibers and pores. Only the surface of the fiber can be observed in an image

of the mat. Fig. 1.7 shows a SEM image of electrospun fiber mat of poly(methyl methacrylate) (PMMA) [145].

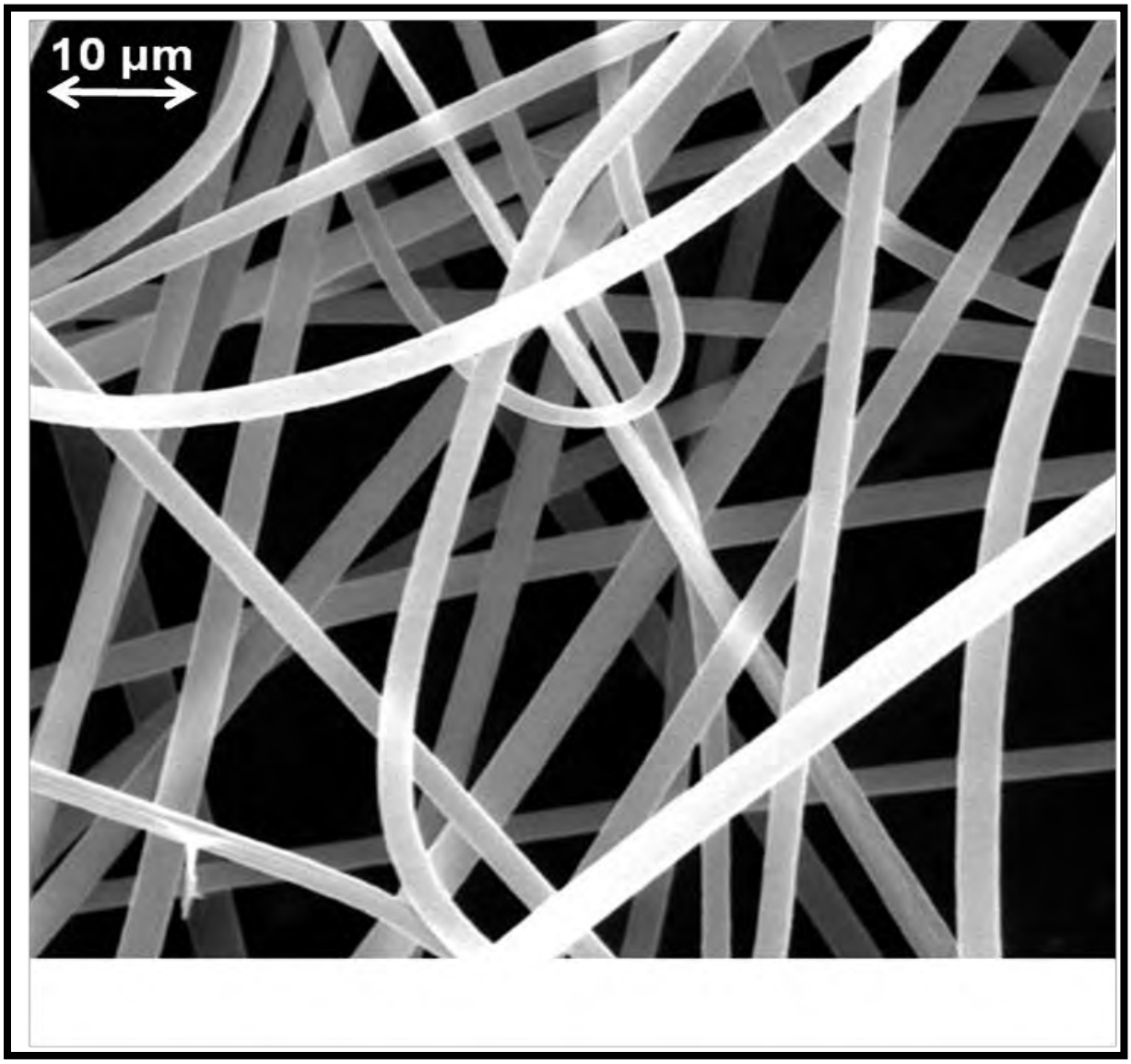

Figure 1.7: Scanning electron microscopy (SEM) image of electrospun PMMA fiber mat [145].

The periodic variation of morphological features on the surface of the fiber as well as occurrence of beads is an important feature of fibers that is usually characterized. Atomic Force Microscopy (AFM) has been used extensively for this. Various authors have reported AFM images of fibers of different polymers. Demir *et al*. [146] have reported the AFM image of electrospun fibers of polyurethane, while Morozov *et al*. [147] have studied the occurrence of beads in electrospun fibers of poly(ethylene dioxide) using the same technique.

(c) Mechanical properties of fiber mat (Modulus, Tensile strength and Elongation)

The techniques available to measure the mechanical properties of films and textile materials in most instances can be applied with some modification to electrospun fiber mats. The most common of such technique is tensile property measurement using the same general experimental technique used for film or woven textile samples. Electrospun polymer fiber mats usually contain randomly aligned single fibers. Various authours have described cutting them into some shapes (rectangular or bumbbell-shape) [148, 149] and using a universal testing machine to obtain the tensile properties. Wang *et al*. [150] for instance, successfully measured the mechanical properties of 100 mm thick poly(vinyl alcohol) (PVA) electrospun fiber mats. This is feasible with the thicker electrospun fiber mat samples.

Factors unrelated to the chemical nature of the polymer used in electrospinning affect the tensile properties of the fiber mats. Electrospun fibers of the same polymer obtained from different solvents often display very different mechanical properties. This is due to

the morphology of the electrospun fibers being affected by the different rates of evaporation of solvent and consequently different kinetics of development of the relevant phase morphologies, giving rise to different degrees of fusion of the individual fibers, existence of imperfections and branching of fibers.

(d) Crystallinity of electrospun fibers

The crystallinity or the molecular orientation within electrospun fibers is usually determined using differential scanning calorimetric (DSC) technique [151, 152]. It is a comparative method in which differences in the thermal capacity of metal sample pan containing the electrospun fiber and reference metal pan without any sample is used to generate a DSC curve. The sample pan containing the electrospun fiber is expected to have higher thermal capacity than the reference pan. Thus more thermal energy is required to raise the temperature of the sample by the same amount as for the reference. In the DSC measurement, this is translated into differences in electric power required which is then monitored as a function of temperature to yield the thermal data on the electrospun fiber.

Events such as first and second-order transitions, chemical reactions, or solvent evaporation can generally be readily observed as distinctive patterns in DSC curve. With electrospun fiber samples, the significant thermal event anticipated is the melting of the crystalline fraction, an endothermic process. Loss of residual solvent from the electrospun fiber mat may also take place and will constitute an endothermic event. These thermal data are particularly useful for the polymer fiber containing a functional

molecule such as phthalocyanines [130, 131]. X-ray diffraction technique (XRD) can also be used to give a fair idea of the crystalline nature of the fiber, though information on phase transitions and the lost of residual solvent cannot be obtained as with DSC technique.

Functionalization of electrospun fibers through the integration of functional molecules into polymer fiber core, are often desirable in fields such as biosensor technology, tissue engineering, drug delivery, heterogeneous catalysis and nanoelectronics. Incorporation of phthalocyanines into electrospun polymer fibers has been reported with the properties of the phthalocyanine still maintained within the fiber matrix [153-157]. Such functionalized electrospun polymer fibers are promising fabric materials for various applications. Table 1.3 shows some typical applications of phthalocyanine functionalized electrospun fibers.

Table 1.3: Electrospun fibers functionalized with phthalocyanines and their applications.

Phthalocyanine	Polymer	Application	Ref.
Copper(II) tetraamino-Phthalocyanine	Poly(ethylene oxide)	for optoelectronic devices (expected)	153
Zinc phthalocyanine	Polyurethane	Antibacterial activity, photooxidation of iodide	154
Cobalt tetraamino-phthalocyanine	Cellulose fiber	Photoconversion of Reactive Red X-3B	155
Iron tetranitro-phthalocyanine	TiO2/ Poly(vinylpyrrolidone)	Photoconversion of methyl orange	156
HOAlPc$(SO_3H)_4$ ZnPc$(OC_2H_4N^+CH_3)_4$	Polyurethane	Gram-positive bacteria	157

Sub Aim:

As Table 1.3 shows, electrospun polymer fibers incorporating lanthanide phthalocyanines have not been reported, hence the aims of this thesis.

1.3. Phthalocyanines as photocatalysts and gas sensors.

There has been growing interest in the use of dyes such as phthalocyanines in photosensitized catalytic applications for some industrial by-products [85] and environmental pollutants [158]. This is due in part to the fact that currently, emphasis is being placed on advanced oxidation processes (AOPs) [159] for environmental remediation and in particular for water treatment. Photochemical oxidation using molecular oxygen is one of the most important methodologies, since it does not liberate any additional pollutants. Singlet oxygen is a particularly good candidate for these applications. It is a very reactive species, as can be seen from its applications in areas such as photodynamic therapy [90]. As already stated, phthalocyanines have been shown to be highly effective photosensitizers capable of producing singlet oxygen with high quantum yields [160]. Phthalocyanines are particularly very promising sensitizers since their maximum light absorption occurs in the visible portion of the electromagnetic spectrum, which constitutes a larger portion of the spectrum and thus more available than the ultra-violet portion required by other sensitizers [161, 162].

Two mechanisms of the photocatalytic behavior of phthalocyanines are described: Type I mechanism, also referred to as free radical mechanism and Type II, which involves the generation of singlet oxygen [163-166]. In both cases the reaction is principally initiated by the triplet excited state of the phthalocyanine.

In Type I, Scheme 1.3, the triplet state of the phthalocyanine ($^3Pc^*$) transfers an electron to ground state molecular oxygen resulting in the formation of radicals ($Pc^{\cdot+}$ and $^3O_2^{\cdot-}$). In a series of subsequent intermediate reactions (Scheme 1.3), the oxygen radical is transformed into hydroxyl radicals, hydroxide ions and other reactive species. All these reactive species are then able to effect the phototransformation of the substrate.

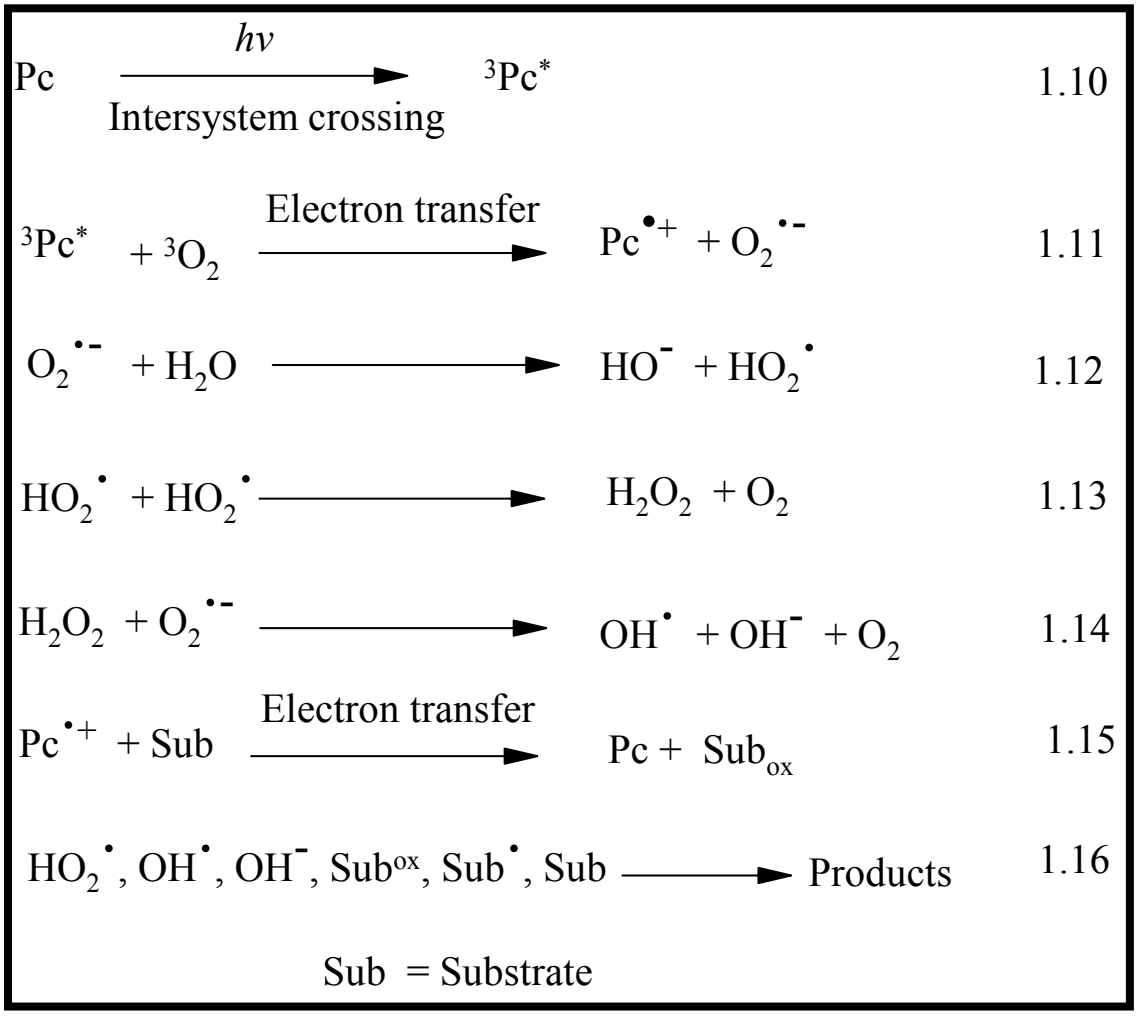

Scheme 1.3: Type I reaction mechanism by free radical production.

In Type II mechanism, Scheme 1.4, singlet oxygen is generated from the ground state molecular oxygen by energy transfer from the triplet excited stated of the phthalocyanine. It is the singlet oxygen that is responsible for the transformation of the analyte.

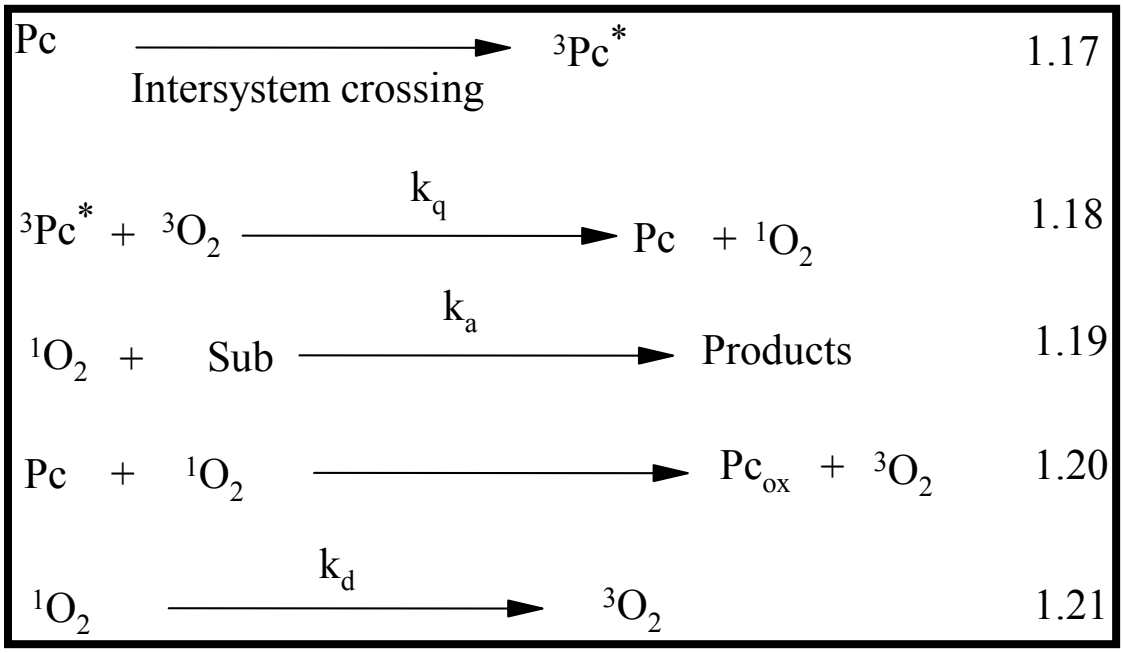

Scheme 1.4: Type II reaction mechanism by singlet oxygen generation.

In order to facilitate recovery of the phthalocyanine from the sample matrix during photocatalysis, various solid support systems have been used to anchor the phthalocyanine, Table 1.4. As indicated in the table, such support systems have been applied in the photoconversion of various analytes such as phenols and dyes using phthalocyanines [167-175], but not electrospun fibers.

Table 1.4: Phthalocyanines on various supports and analytes photocatalyzed.

Complex	Support	Species photocatalyzed	Ref.
CoPcs	MCM-41 (Mesoporous molecular sieve)	2,4-DCP	167
ZnPcs, AlPcs, GePcs, SiPcs, SnPcs	Amberlite	4-CP, 2,4-DCP, 2,4,6-TCP, PCP	168
ZnPc	Polydivinylbenzene	2,4-DCP	169
H_2Pc	Al_2O_3/TiO_2	Sulfite ion	170
FePc	Silica/Zeolite Y	Phenol sulfur heterocycles	158
NiPc, CoPc, FePc, TiPc, CuPc, SiPc, ZnPc, AlPc	Al_2O_3	Peroxo- substances	171
MnPcs	$TiO_2@SiO_2$	Rhodamine B o-phenyldiammine	172
$HoPc_2$	TiO_2 (Nano-microcrystalline)	4-NP	173

CoPc	**TiO_2** **WO_2**	**Sulphite ion** **Thiosulphite ion**	**174**
$Ln(TSPc)_2$ **Ln = Sm, Eu, Dy, Ho**	**SiO_2 gel**	**Promising photocatalyst**	**175**

TSPc = tetrasulphonated phthalocyanine DCP = 2,4-dichlorophenol TCP =2,4,6-trichlorophenol PCP = pentachlorophenol

Although electrospun polymer fibers are promising support systems for phthalocyanines they have not been used for phototransformation of phenols [154-156]. Moreover, to the best of the candidate's knowledge, lanthanide phthalocyanines have not been functionalized on polymer fibers for catalytic application though the use of lanthanide phthalocyanine as catalyst in solution has been reported [28]. Due to the large size of the central metal, the corresponding phthalocyanines are expected to be efficient photocatalysts. This work reports for the first time, the use of lanthanide phthalocyanines on electrospun polymer fibers for the phototransformation of pollutants. Lutetium phthalocyanines are either mixed with polymers or covalently linked to them. ZnPc derivatives are used for comparison.

The structures of all phthalocyanines used in this work are shown Fig. 1.8 and those of the polymers are in Fig. 1.9.

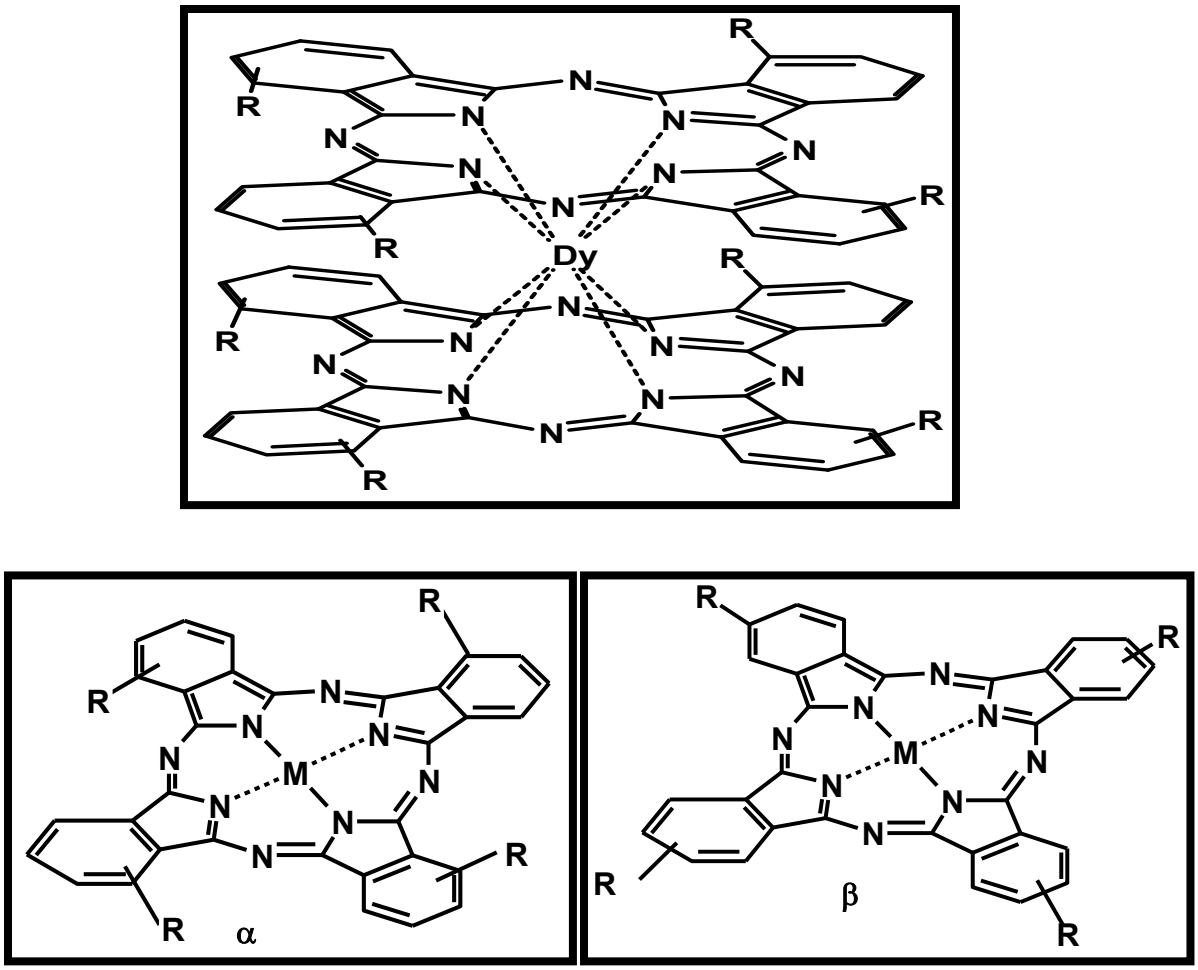

Figure 1.8: Structures of all the phthalocyanines in this work. Substituents are shown in Table 1.5.

Table 1.5: Key to structures in Figure 1.8 (b).

Abbreviation of complex	R =	Position	Axial ligand	Complex number
AcLuTPPc $^{\alpha}$	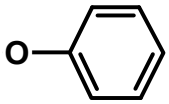	**α**	**Acetate**	**14**
$DyPc_2$	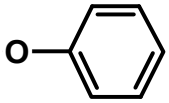	**α**	**-----**	**15**
H_2TPPc $^{\alpha}$	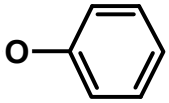	**α**	**-----**	**16**
ClErTPPc $^{\alpha}$	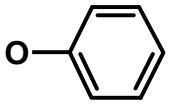	**α**	**Chloride**	**17**
AcLuTPPc$^{\beta}$	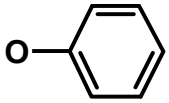	**β**	**Acetate**	**18a**
AcLuTCPPc$^{\beta}$	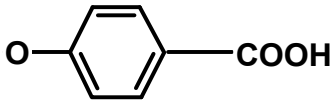	**β**	**Acetate**	**18b**
AcLuTPyPc$^{\beta}$	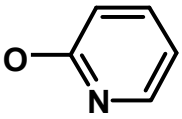	**β**	**Acetate**	**18c**
AcLuTmPyPc$^{\beta}$	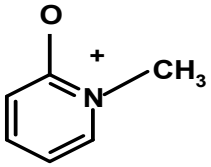	**β**	**Acetate**	**19**

AcLuTNPc$^{\beta}$	**NO_2**	**β**	**Acetate**	**20**
AcLuTAPc$^{\beta}$	**NH_2**	**β**	**Acetate**	**21**
ZnTAPc$^{\beta}$	**NH_2**	**β**	**--**	**22**
ZnTPyPc$^{\beta}$	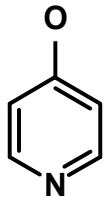	**β**	**--**	**23**
ZnTmPyPc$^{\beta}$	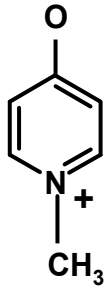	**β**	**--**	**24**

TCP = tetracarboxyphenoxy, TN = Tetranitro, TP = tetraphenoxy, TA = tetraamino, TPy = tetrapyridiloxy and TmPy = tetra-N-methylpyridiloxy, α = non-peripheral β = peripheral positions

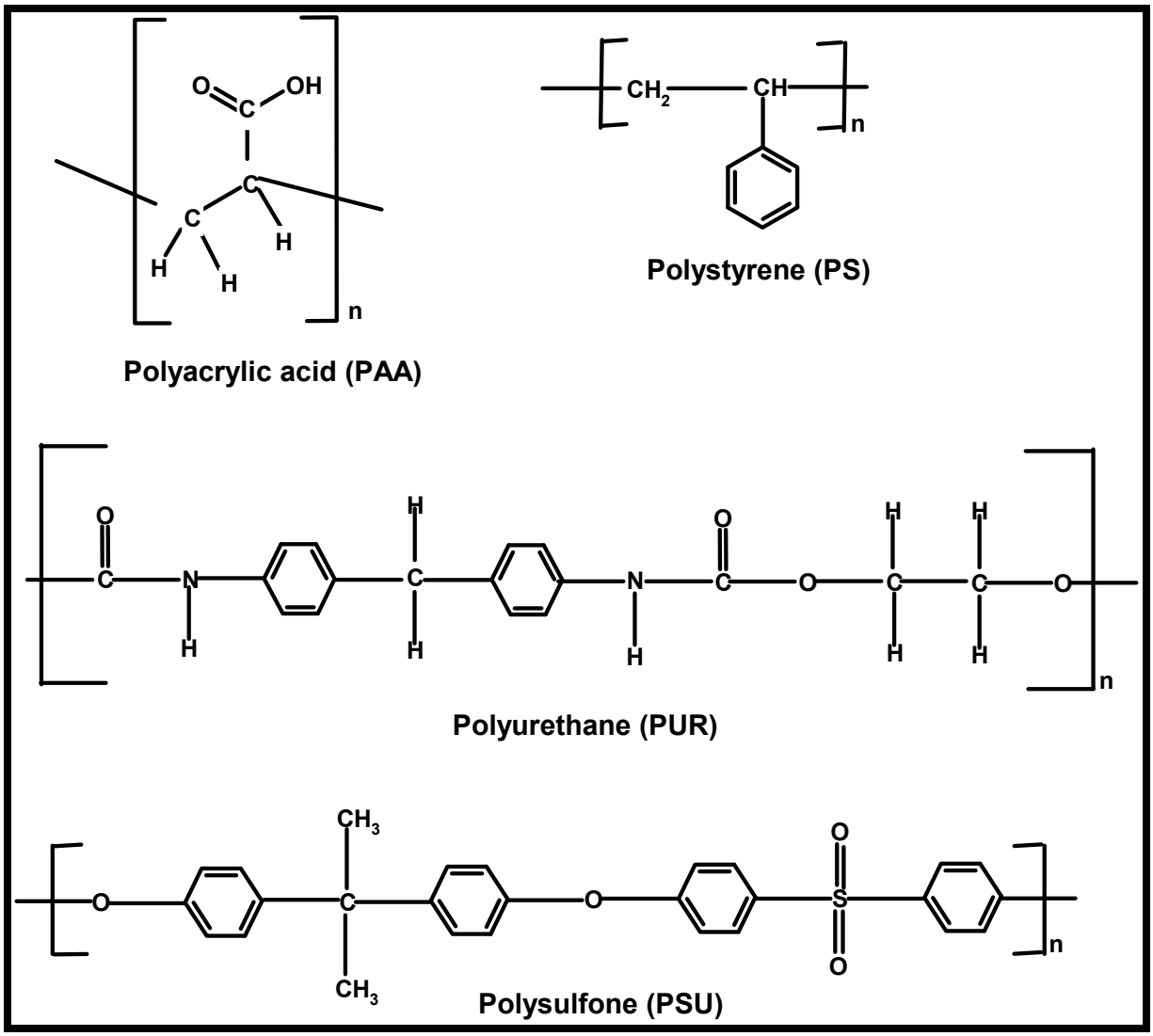

Figure 1.9: Structure of all polymers used in this work.

Polystyrene (PS) and polysulfone (PSU) polymers were chosen for this work because of their extensive aromatic systems. This will allow for π-π electronic interaction between the aromatic systems of the phthalocyanine and the polymers, hence preventing leaching of the former from the latter during application. The carboxylic acid functional group of polyacryclic acid allows a covalent amide bond formation with lutetium and

zinc tetraaminophthalocyanines (21, 22), while the choice of polyurethane is governed by the presence of secondary amine groups that can also form an amide bond with the carboxylic acid functional groups of lutetium tetracarboxyphenoxy phthalocyanines (18b). Phenoxy substituent was used to enhance solubility of the Pcs for easier solvent compartibility with the polymer required for formation of the functionalized electrospun fibers.

Some of the phthalocyanine functionalized electrospun polymer fibers discussed above will also be used for gas sensing. Detection of toxic and flammable gases is a subject of growing importance in both domestic and industrial environments. For local monitoring, devices that are smaller, cheaper and more sensitive than analytical instruments are currently being used for atmospheric measurements. The well known gas sensors are semiconducting metal oxide sensors made of ZnO, SnO_2 and WO_3 [176] which respond based on changes in conductivity. However these sensors are highly energy consuming, sensitive to humidity and therefore not attractive as gas or fire detectors. Alternatively phthalocyanines have been used in gas sensing as indicated in Table 1.6.

Table 1.6: Phthalocyanines on various supports and gas sensed.

Phthalocyanine	Support system	Gas	Ref
CoPc	Polystyrene polymer	NO_2, $CHCl_3$, perchloroethylene	[135]
CuPc	Thin film	NO_2	[177]
Crown ether substituted H_2Pc	Thin film	NO_2	[178]
PbPc	Thin film	NO_2	[179]
PbPc	Thin film	Cl_2	[180]
Tetrasulphonated CuPc	Thin film	NO_2, N_2O_4	[181]
$(NR_3)_2FePc$	Nanostructure matrix	NO_2	[182]

As indicated in Table 1.6, the application of phthalocyanines in gas sensing has been limited to the use of thin films employing the semiconductor properties of the phthalocyanine [177-181]. Few cases involving the use of the optical properties of the phthalocyanine are reported [182].

This work reports for the first time the use of phthalocyanines on electrospun fibers for qualitative optical detection of nitrogen dioxide gas ($NO_{2(g)}$).

1.4. Background on environmental pollutants studied in this work

Nitrogen dioxide, chlorophenols and azo dyes are used as examples for the application of phthalocyanines incorporated in electrospun fibers. They represent air and water pollutants which are commonly encountered.

1.4.1. Oxides of nitrogen (nitroxides)

Nitrogen oxides (NO_x) are among the most toxic gaseous pollutants and are major components of outdoor air pollutants which directly affect humans [183]. Nitrogen oxides play an important role in the generation of photochemical smog and photochemical oxidants such as ozone and peroxyacetyl nitrate [184]. In particular, the concentration of $NO_{2(g)}$ has been found to increase spontaneously on the onset of fire and this is independent of the material involved in the burning [185]. Therefore, NO_2 in the gas phase is an early indicator of heat developed. Various methods have been reported for the detection of nitrogen dioxide including the use of organometallic compounds [186]. Phthalocyanines containing metal ions such as Fe(II) or Fe(III) can bind gaseous ligands such as NO_2 and hence can be used as gas sensors [187].

The general low solubility of phthalocyanines in common solvents make it imperative for the use of appropriate solid support systems in which the phthalocyanine is quite dispersed. Thus in order to develop sensors based on phthalocyanines for the detection of $NO_{2(g)}$, the following gas permeable supports among others have been suggested: tin modified mesoporous silica [188], tin dioxide (SnO_2) [189], gas-permeable liquid core waveguides [190] and porous silicon [191].

However, the use of phthalocyanines anchored on electrospun polymer fibers for the detection of gases particularly nitrogen dioxide has not been explored though there are numerous advantages associated with their use. Electrospun fibers are generally very porous that will allow permeation of gas molecules. Thus in this work lutetium and zinc phthalocyanines functionalized on various electrospun polymer fibers are applied for the detection of NO_2 gas.

1.4.2. Phenols

Phenols and phenolic compounds are ubiquitous pollutants which are introduced into the natural water resources from the effluents of a variety of chemical industries such as phenol manufacturing, pharmaceuticals, paint, dyeing, textile, wood, petrochemical and pulp mills [192-194]. As a result, aquatic organisms including fish are subjected to these pollutants [195]. Phenol and its derivatives are capable of inducing genotoxic, carcinogenic, immunotoxic, and physiological effects [196, 197] and have a high bioaccumulation rate along the food chain due to their lipophilicity. Thus phenol pollution represents a threat against natural environment and also to human health [198].

Increasing research activities have been devoted to development of various treatment methods for removing or destroying phenolic compounds including biodegradable processes [199-201], photocatalytic oxidation [84, 202], electrochemical oxidation [203, 204] and adsorption [205, 206] among others. Photocatalytic oxidation of phenolic compounds using semiconductors such as TiO_2 [207, 208] or photo-assisted Fenton

reaction [209] have been reported and are receiving attention because of the potential use of sunlight. However these two photocatalytic methods require high energy which is in the less available ultra-violet portion of the electromagnetic radiation. Removal of these phenolic compounds using environmentally friendly processes involving hydrogen peroxide or molecular oxygen as oxidant and water as solvent has been encouraged. The use of phthalocyanines in activating the oxygen for such photocatalytic processes is gaining ground because phthalocyanines absorb in the much more abundant visible portion of the electromagnetic spectrum. Aluminum and zinc phthalocyanines have been reported to catalyze such photocatalytic conversions [210-212]. However, very few cases involving the use of lanthanide phthalocyanines as catalyst have been reported [28]. Thus this work also reports of the use of lanthanide phthalocyanines anchored on electrospun polymer fibers in the photocatalytic oxidation of phenolic compounds. The use of phthalocyanines on electrospun polymer fibers is reported for the first time for phenolic transformation.

1.4.3. Azo dyes

Different types of dyes are used in industries such as textiles, paint, ink, plastics and cosmetics. However about a half of the total global production are classified as azo compounds that have characteristic –N=N- as a chromophore in their molecular structure. The azo bond determines the colour of the dye and is the most reactive usually undergoing oxidation leading to a fading of the color of its solution [213]. Complete degradation of azo dye is difficult due to their complex structure [214]. Apart

from given aesthetic problems, azo dyes are reported to show biotoxicity as well as possible mutagenic and carcinogenic effects [215]. Azo dyes are resistant to aerobic bacterial degradation [216]. On the other hand, anaerobic bacteria reduce the azo linkage to produce potentially carcinogenic aromatic amines [217].

Various chemical and physical processes such as chemical precipitation, coagulation and electrocoagulation [218] as well as adsorption on activated charcoal have been applied in the removal of azo dyes from the environment. However, these methods are not destructive but only transfer the dye from one phase to another requiring yet a different kind of treatment [219, 220]. In recent years an alternative to these conventional methods is the AOPs discussed above based on the generation of very reactive species such as hydroxyl radicals and singlet oxygen that oxidize a broad range of organic pollutants. Inorganic photosensitizers such as ZnO have been applied particularly in the conversion of azo dye [221]. The use of electrospun polymer fibers functionalized with phthalocyanines offer promising heterogeneous catalytic mimetic systems for the photoconversion of azo dyestuff. However, very few cases have been reported [155]. This work further explores the use of electrospun polymer fibers functionalized with phthalocyanines for the conversion of methyl orange, a typical azo dye.

1.5. Summary of aims of thesis

The aims of this thesis are as follows:

1. Syntheses and characterization of a variety of novel monomeric lutetium phthalocyanines with alkoxy and amino substituents at both peripheral and non-peripheral positions.
2. Syntheses and characterization of novel dysprosium and erbium phthalocyanines with phenoxy substituent at non-peripheral position.
3. Studies of the photophysical and photochemical properties of the phthalocyanine complexes in solution.
4. Anchoring these complexes on electrospun polymer fibers through:
   (a) Physisorption.
   (b) Covalent linked.
   (c) Ionic interactions.
5. Characterization of these functional fibers using spectroscopic (FT-IR, Raman, XRD) and microscopic (SEM) techniques.
6. Investigation of the fluorescence and photoactivity of the embedded lutetium phthalocyanines within the functionalized fibers, using zinc phthalocyanines including the un-substituted phthalocyanine for comparison.
7. Investigation of the suitability of each polymer fiber containing lutetium and zinc phthalocyanines as gas sensing fabric material for the detection of nitrogen dioxide.

8. Investigation of the suitability of each polymer fiber containing lutetium and zinc phthalocyanines for the photodegradation of 4-chlorophenol, 4-nitrophenol and methyl orange in aqueous media.
9. Compare the relative ease of photodegradation of 4-chlorophenol, 4-nitrophenol and methyl orange.
10. Assess the re-usability of each polymer fiber in the photocatalytic process.

Chapter 2

2. Experimental

2.1 Materials

2.1.1 Solvents

Dichloromethane (DCM), diethyl ether, N, N- dimethylformamide (DMF), dimethylsulfoxide (DMSO), ethanol, formamide, glacial acetic acid, n-hexane, methanol, tetrahydrofuran (THF), 1-pentanol and quinoline were purchased from SAARCHEM. Acetic acid (AA) (99.8%) and formic acid (FA) (98-100%) were from Sigma Aldrich. Ultra-pure water was obtained from (Milli-Q water system, Millipore Corp., Bedford, MA, USA). Phosphate buffer solutions were prepared using reagent grade potassium dihydrogen orthophosphate (ACE) and dipotassium phosphate (PAL chemicals).

2.1.2 Synthesis reagents

Ammonia (25%), anthracene-9,10-bis-methylmalonate (ADMA), deuterated dimethylsulfoxide (DMSO-d_6), dimethyl sulphate, 1,8-diazabicyclo[5.4.0] undec-7-ene (DBU), dicyclohexylcarbodiimide (DCC) (99%), 3-diphenylisobenzofuran (DPBF), dysprosium(III) acetate, erbium(III) chloride, 4-hydroxybenzoic acid, lutetium(III) acetate, metallic copper, phenol, potassium carbonate, nitric acid (55%), potassium nitrate and sodium azide (99%) were from Sigma Aldrich. Deuterated water (D_2O), silica gel 60PF_{254} and 3-nitrophthalic acid were purchased from Merck. Sodium sulphite nanohydrate ($Na_2S{\cdot}9H_2O$) and thionyl chloride were purchased from SAARCHEM.

2.1.3 Polymers for electrospinning

Polyacrylic acid (PAA) (average molecular weight = 450,000 g/mol), polystyrene (PS) (average molecular weight = 192,000 g/mol), polysulfone (PSU) (average molecular weight = 22,000 g/mol) and polyurethane (PUR) (average molecular weight = 5000 g/mol, specific gravity 1.14) were from Sigma Aldrich. Polyamide 4.6 (P.A 4.6) (average molecular weight = 80,000 g/mol and polyamide 6.9 (P.A 6.9) (average molecular weight = 60,000 g/mol) were obtained from DSM and Scientific Polymer Products respectively.

2.1.4 Photocatalysis analytes and products

4-Chlorophenol (4-CP) (99%) and tert-butanol (99%) were from Fluka. Hydroquinone was from May and Baker. Benzoquinone, methyl orange (MO), 4-nitrocatechol and 4-nitrophenol (4-NP) were from Sigma Aldrich.

2.1.5 Previously synthesized phthalocyanines and their precursors

4-Nitrophthalonitrile (**9**), 4-phenoxyphthalonitrile (**10a**), 4-carboxyphenoxyphthalonitrile (**10b**), 4-pyridiloxyphthalonitrile (**10c**) [31-33], 3-nitrophthalonitrile (**11**), 3-phenoxyphthalonitrile (**13**) [34], 1(4), 8(11), 15(18), 22(25)-tetraphenoxyphthalocyanine H_2TPPc^{α} (**16**) [222], zinc(II) 2(3), 9(10), 16(17), 23(24)-tetraaminophthalocyanine $ZnTAPc^{\beta}$ (**22**) [223], zinc(II) 2(3), 9(10), 16(17), 23(24)-(tetra-4-pyridyloxy)]-phthalocyanine $ZnTPyPc^{\beta}$ (**23**) and zinc(II) 2(3), 9(10), 16(17), 23(24)-

tetrakis[4-(N-methylpyridyloxy)]-phthalocyanine ZnTmPyPc$^{\beta}$ (**24**) [224], were synthesized according to literature procedures. Zinc phthalocyanine (ZnPc) was purchased from Sigma Aldrich.

2.2 Instrumentation

(a) Elemental analyses for CHNS were done using a Vario-Elementar Microcube ELIII Series.

(b) Mass spectral data for the characterization of phthalocyanines were collected with a Bruker AutoFLEX III Smartbeam TOF/TOF mass spectrometer. The instrument was operated in the positive ion mode using an m/z range of 400-3000 amu. The voltage of the ion sources were set at 19 and 16.7 kV for ion sources 1 and 2 respectively, while the lens was set at 8.50 kV. The reflector 1 and 2 voltages were set at 21 and 9.7 kV respectively. The spectra were acquired using α-cyano-4-hydroxycinnamic acid as the MALDI matrix and a 354 nm nitrogen laser as ionizing source.

(c) Ground state electronic absorption spectra were recorded on either Cary 500 UV/Vis/ NIR or Shimadzu UV-2550 UV/Vis spectrophotometer. Quartz cells of 1 cm pathlengths were employed. The absorbance of the phthalocyanine in the fiber was measured by placing the modified fiber directly on a glass plate.

(d) Infrared (IR) spectra were recorded using either Perkin-Elmer Fourier transform–IR (100 FT-IR) or Perkin-Elmer Fourier transform-IR (2000 FT-IR) spectrophotometer.

(e) Proton-nuclear magnetic resonance spectra (^{1}H-NMR) were recorded in deuterated solvent (DMSO-d_6 or D_2O) using either Bruker EMX400 MHz NMR spectrometer or a Bruker ADVANCE II 600 MHz spectrometer.

(f) Raman data was obtained using a Bruker Vertex 70-Ram II spectrometer equipped with a Nd:YAG laser that emit at 1064 nm and liquid nitrogen cooled germanium detector.

(g) Scanning electron microscope (SEM) images of electrospun polymer fibers were obtained using a JOEL JSM 840 scanning electron microscope and the average diameters obtained using Cell^D software from Olympus.

(h) Fluorescence images of electrospun fibers were taken with a DMLS fluorescence microscope. The excitation source was a high-voltage mercury lamp and light in the wavelength range of 550-730 nm.

(i) X-ray powder diffraction patterns were recorded on a Bruker D8 Discover equipped with a proportional counter, using Cu-K_α radiation (λ = 1.5405 Å, nickel filter). Data were collected at various 2θ ranges, scanning at 1^o min^{-1} with a filter time-constant of 2.5 s per step and a slit width of 6.0 mm. Samples were placed on a zero background silicon wafer slide. The X-ray diffraction (XRD) data were treated using Eva (evaluation curve fitting) software. Baseline correction was performed on each diffraction pattern by subtracting a spline fitted to the curved background and the full-width at half-maximum values used in this study were obtained from the fitted curves.

(j) Fluorescence emission and excitation spectra were obtained on a Varian Eclipse spectrofluorimeter.

(k) Fluorescence lifetimes were measured using a time correlated single photon counting setup (TCSPC), Fig. 2.1, (Fluo Time 200, Picoquant GMbH) with a diode laser as excitation source (LDH-P-670 driven by PDL 800-B, 670 nm, 20 MHz repetition rate, Picoquant GmbH). Fluorescence was detected under the magic angle with a peltier cooled photomultiplier tube (PMT) (PMA-C 192-N-M, Picoquant GmbH) and integrated electronics (PicoHarp 300E, Picoquant GmbH). A monochromator with a spectral width of about 4 nm was used to select the required measured emission wavelength. The response function of the system, which was with a scattering Ludox solution (DuPont), had a full width at half-maximum (FWHM) of about 300 ns. The ratio of stop to start pulses was kept low (below 0.05) to ensure good statistics. All luminescence decay curves were measured at the maximum of emission peak. The data were analyzed with the program FluoFit (Picoquant GmbH). The support plane approach [225] was used to estimate the errors of the decay times.

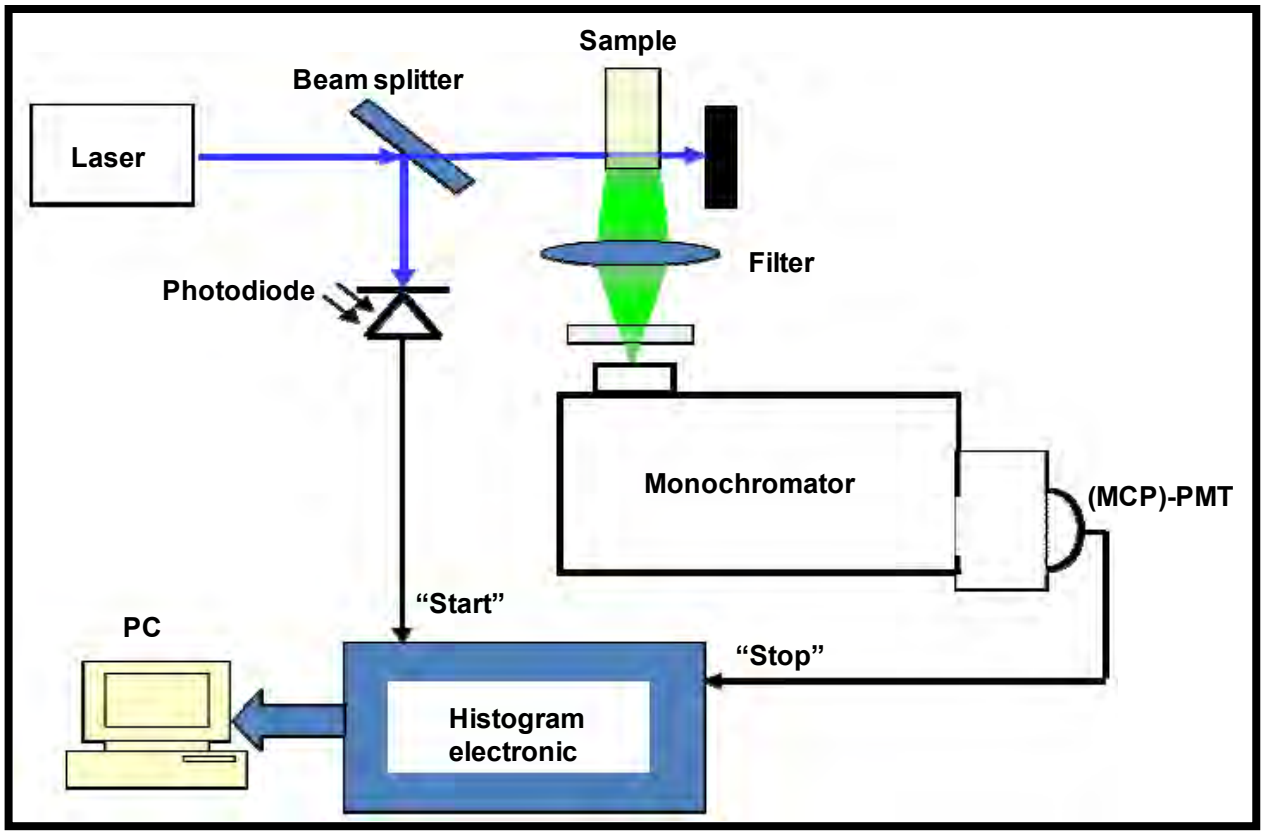

Figure 2.1: Schematic diagram of time-correlated single photon counting (TCSPC) setup. (MCP)-PMT = Monochromator photomultiplier tube, PC = Personal computer.

(l) The Guassian 03 programme [226] running on an Intel/Linux cluster was used to perform DFT calculations. The calculations were done at the B3LYP/6-31G(d) level for geometry optimization and excited energy calculations (TDDFT). All visualisation used the Gausview 4.1 program.

(m) Laser flash photolysis experiments, Fig. 2.2, were performed with light pulses produced by a Quanta-Ray Nd:YAG laser providing 400 mJ, 9 ns pulses of laser light at 10 Hz, pumping a Lambda-Physik FL3002 dye laser (Pyridin 1 dye in methanol). Single pulse energy ranged from 2 to 7 mJ. The analyzing beam source

was from a Thermo Oriel Xenon arc lamp, and photomultiplier tube (a Kratos Lis Projekte MLIS-X3) was used as a detector. Signals were recorded with a two-channel 300 MHz digital real time oscilloscope (Tektronix TDS 3032C); the kinetic curves were averaged over 256 laser pulses.

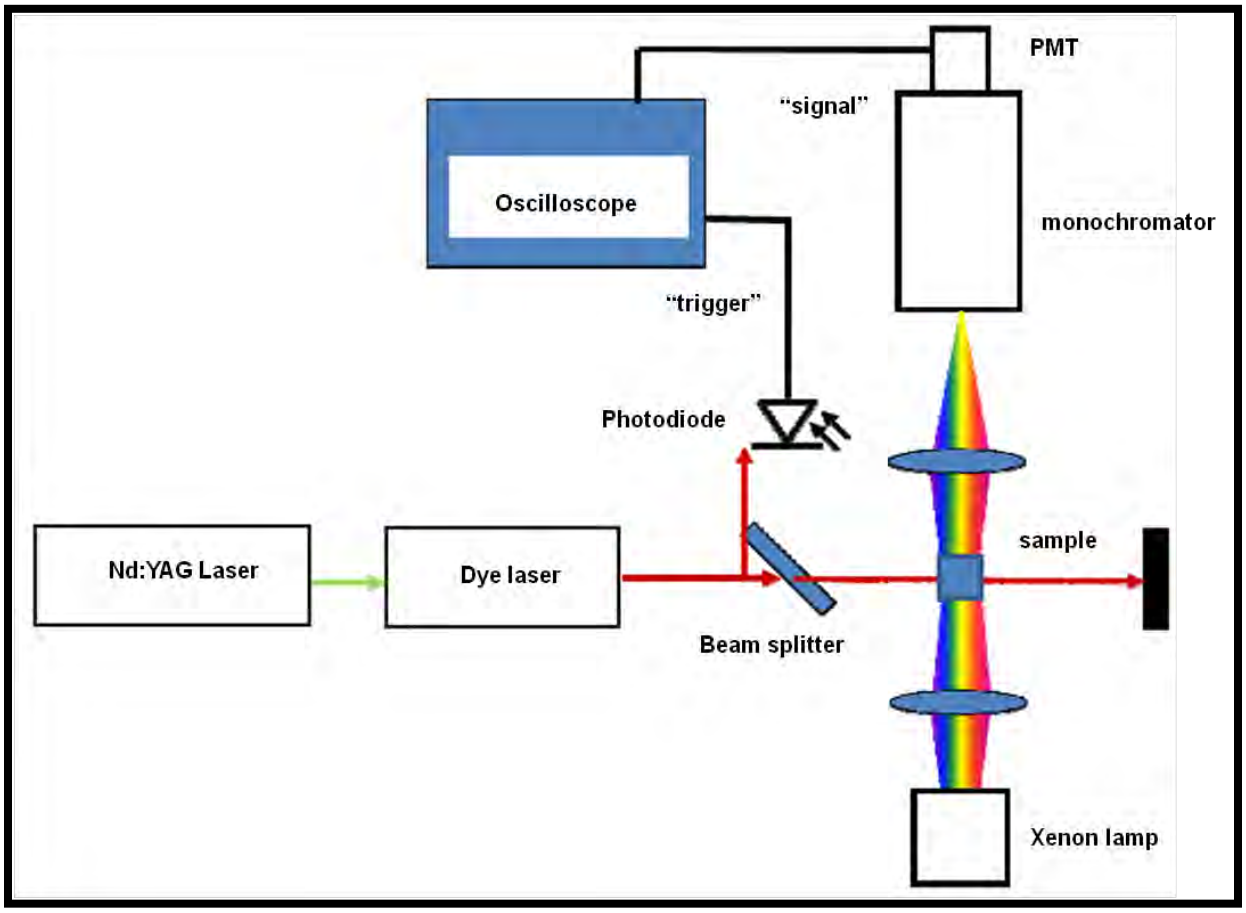

Figure 2.2: Schematic diagram for a laser flash photolysis setup.

PMT = Photomultiplier tube

(n) Determination of singlet oxygen and photodegradation quantum yields as well as photocatalytic conversion of environmental pollutants (4-chlorophenol, 4-nitrophenol and methyl orange) were done using General Electric Quartz lamp

(300 W) as irradiation source, Fig. 2.3. A 600 nm glass (Schott) and water filters were used to filter off ultra-violet and far infrared radiations respectively. An interference filter 670 nm with band of 40 nm was placed in the light path just before cell containing the sample. The intensity of the light reaching the reaction vessel, Fig. 2.3, was measured with a power meter (POWER MAX 5100, Molectron Detector Inc).

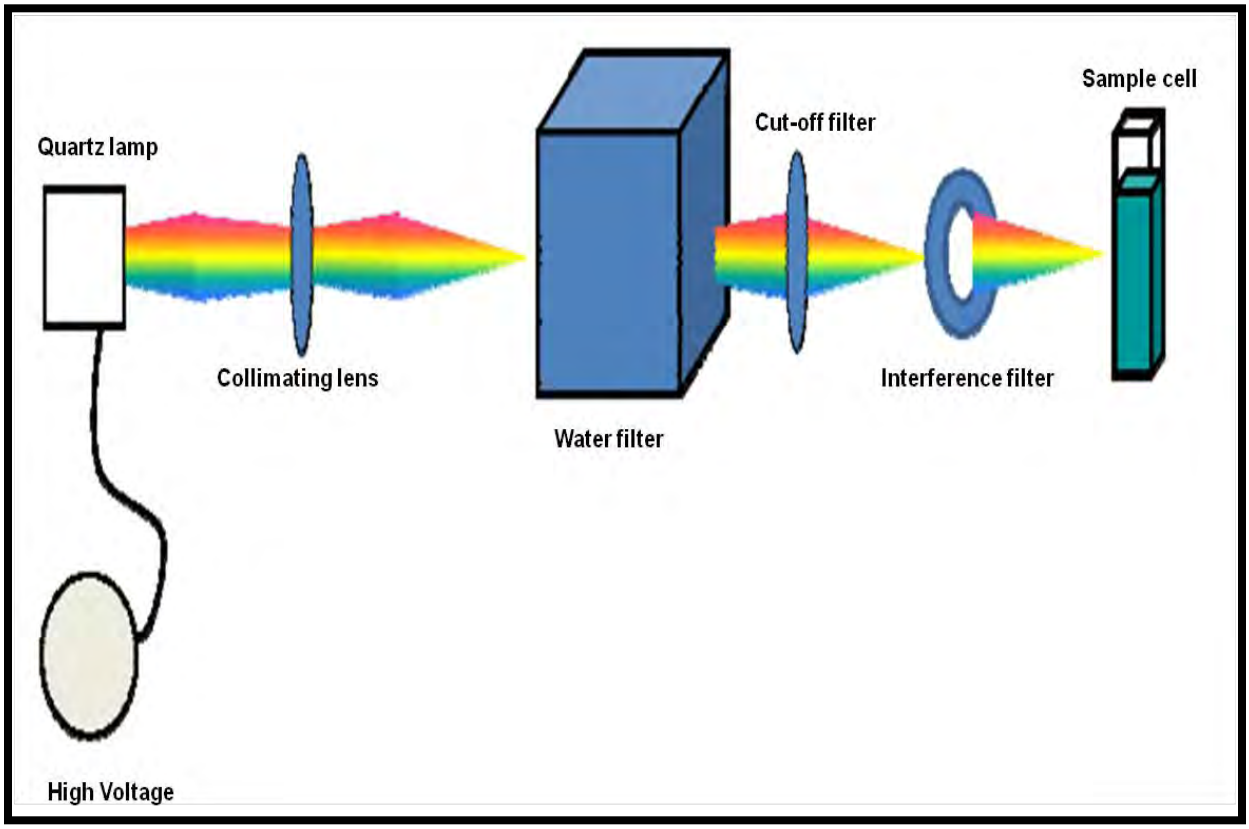

Figure 2.3: Schematic diagram of photolysis setup.

(o) The photolysis products of 4-chlorophenol and 4-nitrophenol were separated and analyzed using gas chromatography (GC), an Agilent Technologies 6820 GC system (fitted with a BD5-MS), using an Agilent J & W GC column.

(p) A Finnigan MAT LCQ ion trap mass spectrometer equipped with an electro-spray ionization (ESI) source was used for mass analysis of the chromatographic products. Spectra were acquired in the negative ion mode, with the capillary temperature set at 200 ^{o}C and sheath gas set at 80 arbitrary units, with the capillary and tube lens voltage set at -20 V and -5 V respectively.

(q) Time resolved phosphorescence decay of singlet oxygen at 1270 nm was used to determine singlet oxygen quantum yield in either DMF or THF. The dynamic phosphorescence decay of singlet oxygen **($O_2(^1\Delta_g)$)**, was demonstrated using time resolved phosphorescence of **$O_2(^1\Delta_g)$** at 1270 nm. For these studies an ultra sensitive germanium detector (Edinburgh Instruments, EI-P) combined with a 1000 nm long pass filter (Omega, RD 1000 CP) and a 1270 nm band-pass filter (Omega, C1275, BP50) was used to detect **$O_2(^1\Delta_g)$** phosphorescence under the excitation using Quanta-Ray Nd:YAG laser providing 400 mJ, 90 ns pulses of laser light at 10 Hz pumping a Lambda-Physik FL3002 dye laser (Pyridin 1 dye in methanol), with a pulse period of 7 ns and repetition rate of 10 Hz, Fig. 2.4. The near-infrared phosphorescence of the samples were focused onto the germanium detector by a lens (Edmund, NT 48-157) with detection direction perpendicular to the excitation laser beam. The detected signals were averaged with a digital oscilloscope (Tektronics, TDS 360) to show the dynamic decay of **$O_2(^1\Delta_g)$**.

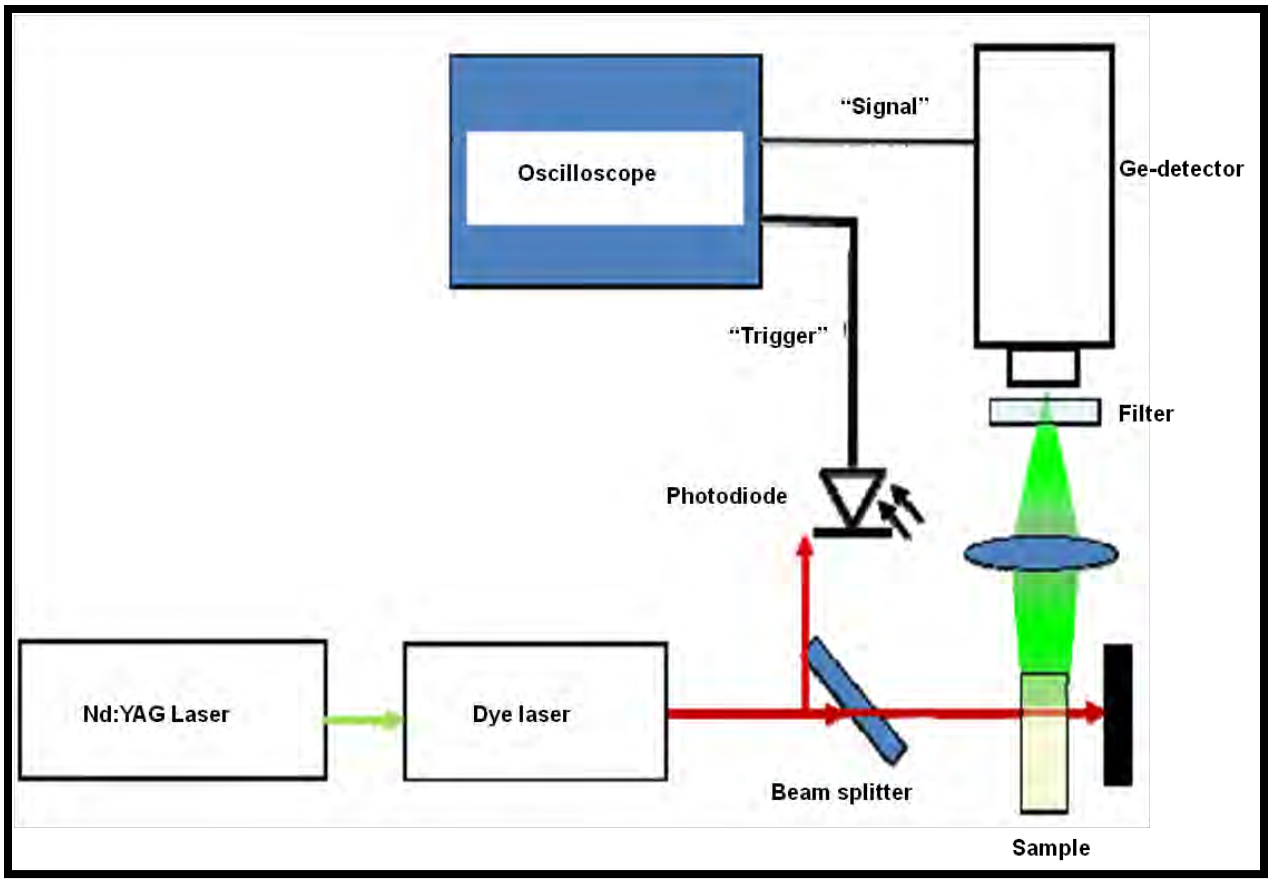

Figure 2.4: Schematic diagram for the singlet oxygen detection setup using its phosphorescence.

(r) Electrospun polymer fibers were obtained from a set up, Fig. 2.5, consisting of a high voltage source (Glassman High Voltage. Inc., EL series, 0-40 kV), a pump (Kd Scientific, KDS-100-CE), a glass syringe (Am Bildacker 3-7, D-97877 Wertheim, Poulten &Grat GmBh) connected to a steel needle of internal diameter of 0.584 mm and aluminum foil as collector.

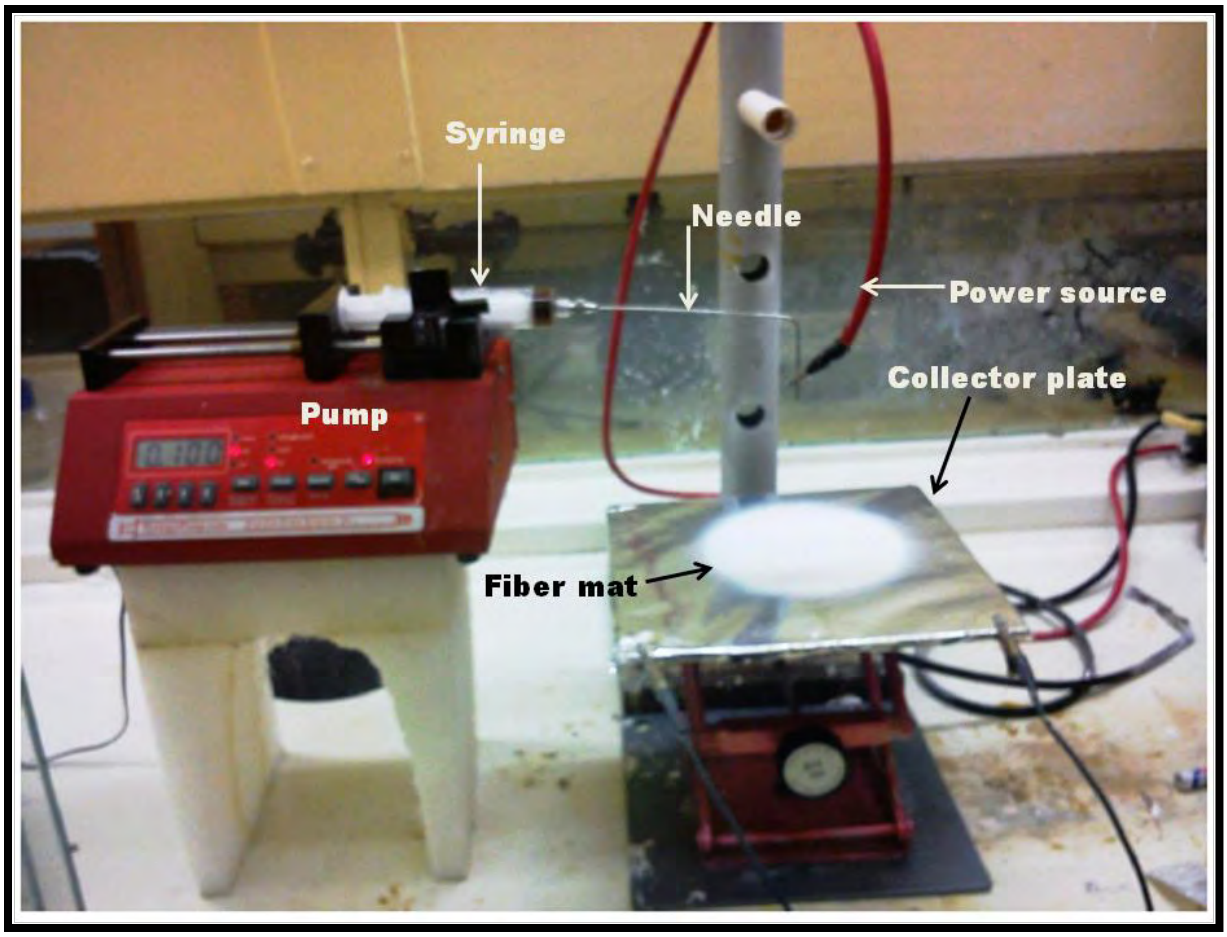

Figure 2.5: Electrospinning setup used in this work.

2.3 Synthesis of phthalocyanines

2.3.1 Synthesis of 1(4), 8(11), 15(18), 22(25)-(tetraphenoxyphthalocyaninato) lutetium(III) acetate (14), Scheme 3.1

A mixture of anhydrous lutetium(III) acetate (134 mg, 0.38 mmol) and 3-phenoxyphthalonitrile (**13**) (339 mg, 1.54 mmol) in 1-pentanol (2 mL) was refluxed for 7 h under nitrogen atmosphere with DBU as a catalyst. After cooling, the crude product was precipitated with n-hexane, filtered and washed with excess n-hexane and then

dried in air. Column chromatography (silica gel) was employed using THF:methanol (10:1) as the eluting solvent mixture. Complex (**14**) was obtained as the major product, which was recrystallized from hexane. Yield: 23%. IR [KBr, *v*, cm^{-1}] 748, 802, 862, 880, 969, 1024 (Pc skeleton), 1248, 1324, 1482 (C-O-C), 1727, 1771 (C=O, acetate), 2955 (C-H, aromatic), 3635 (CH_3). UV-vis (THF): λ_{max} nm (log ε) 321 (4.55) 430 (4.30) 627 (4.31), 690 (5.12). Anal. Calc. for $C_{58}H_{35}N_8O_6Lu$: C, 62.48; H, 3.16; N, 10.05. Found: C, 61.68; H, 3.32; N, 9.42%. ^1H NMR (DMSO-d_6): δ, ppm 7.76-7.86 (12-H, m, Pc-H), 6.58-6.87 (20-H, m, Phenyl-H), 2.09 (3-H, s, acetate-CH_3); MS (MALDI-TOF): (m/z); Calc. 1115; Found: 1119 [M+4H^+].

2.3.2 Synthesis of bis-{1(4), 8(11), 15(18), 22(25)-(tetraphenoxyphthalocyaninato)} dysprosium(III) complex (15), Scheme 3.1

A mixture of anhydrous dysprosium(III) acetate (129 mg, 0.38 mmol) and 3-phenoxyphthalonitrile (**13**) (339 mg, 1.54 mmol) in 1-pentanol (2 mL) was refluxed for 7 h under nitrogen atmosphere with DBU as a catalyst. After cooling, the crude product was precipitated with n-hexane, filtered and washed with excess n-hexane and then dried in air. The crude product was purified as explained above for **14** to give complex **15** which was recrystallized from hexane. Yield: 40%. IR [KBr, *v*, cm^{-1}] 751, 893 (Pc skeleton), 1090, 1220, 1246, 1360, 1433 (C-O-C), 2954 (C-H, aromatic). UV-vis (THF): λ_{max} nm (log ε), 430 (4.34), 625 (4.72), 690 (5.11). Anal. Calc. for $C_{112}H_{64}N_{16}O_8Dy$: C, 70.50; H, 3.91; N, 5.57. Found: C, 69.47; H, 4.86; N, 6.64%. MS (MALDI-TOF): (m/z); Calc. 1924; Found: 1926 [M+2H^+].

2.3.3 Synthesis of 1(4), 8(11), 15(18), 22(25)-(tetraphenoxyphthalocyaninato) erbium(III) chloride (17), Scheme 3.1

A mixture of 1(4), 8(11), 15(18), 22(25)-tetraphenoxyphthalocyanine (**16**) (500 mg, 0.56 mmol), synthesized and characterized as reported before [222], and erbium chloride (164 mg, 0.6 mmol) was heated in 1-pentanol (2 mL) under reflux for 2 h in the presence of DBU and under nitrogen gas. The product was precipitated with hexane filtered and air dried. The crude product was then purified on a column chromatography (silica gel) with THF:methanol (10:1) as eluting solvent mixture. Finally the product was recrystallized from hexanes. Yield: 17%. IR [KBr, υ, cm^{-1}] 784, 861, 886, 926, 1024 (Pc skeleton), 1120, 1201, 1249, 1363, 1474 (C-O-C), 2871, 2956 (aromatic C-H). UV-vis (THF): λ_{max} nm (log ε) 322 (4.64), 623 (4.38), 690 (5.03). Calcd. for $C_{56}H_{32}N_8O_4ClEr$: C, 62.07; H, 2.98; N, 10.34. Found: C, 62.04; H, 3.21; N, 10.10%. MS (MALDI-TOF): (m/z); Calc. 1084; Found: 1088 [$M+4H^+$].

2.3.4 Synthesis of 2,(3), 9(10), 16(17), 23(24)-(tetraphenoxyphthalocyaninato) lutetium(III) acetate (18a), Scheme 3.2

A mixture of anhydrous lutetium(III) acetate (134 mg, 0.38 mmol) and 4-phenoxyphthalonitrile (**10a**) (339 mg, 1.54 mmol) in 1-pentanol (2 mL) was refluxed for 7 h under nitrogen atmosphere with DBU as a catalyst. After cooling, the crude product was precipitated with n-hexane, filtered and washed with excess of n-hexane and then air dried. Column chromatography (silica gel) was employed using THF:methanol (10:1) as the eluting solvent mixture. Yield: 25%. IR [KBr, υ, cm^{-1}] 773, 824, 883, 938,

1039, 1067 (Pc skeleton), 1224, 1264, 1390, 1467, 1482 (C-O-C), 1606, 1714, 1770 (C=O), 2927, 2957 (C-H, aromatic), 3058 (CH_3). UV-vis (DMF): λ_{max} nm (log ε) 351 (4.51) 610 (5.11), 678 (5.78). Calcd. For $C_{58}H_{35}N_8O_6Lu$; C 62.48%, H 3.16%, N 10.05%. Found C 62.00%, H 3.32%, N 10.24%; ^{1}H NMR (DMSO-d_6): δ, ppm 7.79-7.91 (12-H, m, Pc-H), 6.88-6.97 (20-H, m, Phenyl-H), 1.99 (3-H, s, acetate CH_3); MS (MALDI-TOF): (m/z); Calc. 1115; Found: 1116 [M+H$^+$].

2.3.5 Synthesis of 2(3), 9(10), 16(17), 23(24)-(tetracarboxyphenoxyphthalocyaninato) lutetium(III) acetate (18b), Scheme 3.2

A mixture of anhydrous lutetium(III) acetate (134 mg, 0.38 mmol) and 4-(4-carboxyphenoxy)phthalonitrile (**10b**) (981 mg, 0.76 mmol) in 1-pentanol (2 mL) was refluxed for 7 h under a nitrogen atmosphere using DBU as a catalyst. After cooling, the crude product was precipitated with n-hexane, filtered and washed with excess n-hexane and then dried in air. Column chromatography (silica gel) was employed using DMF as the eluting solvent to purify the product. Yield: 10%. IR [KBr, υ, cm^{-1}] 748, 802, 862, 880, 969, 1024 (Pc skeleton), 1248, 1324, 1482 (C-O-C), 1656 (C=O), 2856, 2927 (C-H, aromatic), 3504 (O-H). UV-vis (DMF): λ_{max}/nm (log ε) 345 (5.02), 610 (4.61), 678 (5.31), calcd for $C_{62}H_{35}N_8O_{14}Lu$; C 57.68 H 2.73, N 8.68. Found C 57.23, H 3.10, N 9.04%; ^{1}H NMR (DMSO-d_6): δ, ppm 10.81 (4-H, s carboxylic acid), 8.00-8.10 (12-H, m, Pc-H), 6.58-7.87 (16-H, m, Phenyl-H), 2.09 (3-H, s, acetate CH_3). MS (MALDI-TOF): (m/z); calc. 1291; found: 1293 [M + 2H$^+$].

2.3.6 Synthesis of 2,(3), 9(10), 16(17), 23(24)-(tetra-2-pyridiloxyphthalocyaninato) lutetium(III) acetate (18c), Scheme 3.2

The synthesis of **18c** was as outlined for **18a** and **18b** except **10c** was employed as the phthalonitrile precursor. The amounts of the reagents and the purification procedures were similar to those of **18a**. Yield: 23%. IR [KBr, *v*, cm^{-1}] 837, 910, 1012, 1057, 1077, 1133 (Pc skeleton), 1269, 1355, 1384, 1489 (C-O-C), 1654, 1719, 1769 (C=O), 2927, 2957 (C-H, aromatic), 3053 (CH_3). UV-vis (DMF): λ_{max} nm (log ε) 337 (4.74) 613 (5.26), 678 (5.94). Calcd. for $C_{54}H_{31}N_{12}O_6Lu$; C 57.97%, H 2.79%, N 15.02%. Found C 58.14%, H 3.01%, N 14.89%; ^1H NMR (DMSO-d_6): δ, ppm 7.76-8.67 (12-H, m, Pc-H), 6.78-7.27 (16-H, m, Pyridyl-H), 2.11 (3-H, s, acetate CH_3); MS (MALDI-TOF): (m/z); Calc. 1119; Found: 1120 [$M+H^+$].

2.3.7 Synthesis of 2,(3), 9(10), 16(17), 23(24)-tetrakis[2-(N-methylpyridiloxy)-phthalocyaninato)] lutetium acetate (19), Scheme 3.2

This was synthesized following a reported procedure for forming quaternised phthalocyanines [227]. Complex **18c**, (Ac)LuTPyPcβ (100 mg, 0.09 mmol) was dissolved in freshly distilled DMF and the solution was heated under reflux. Dimethylsulphate (0.2 mL) was added drop-wise. The resulting mixture was then heated under reflux for 12 h after which the solution was cooled and the product precipitated with chloroform. The resulting solid product was purified by Soxhlet extraction with acetone. Yield: 21%, IR [KBr, *v*, cm^{-1}] 761, 857, 953, 1001, (Pc skeleton), 1042 (S=O), 1246, 1341, 1355 (C-O-C), 1482, 1472, (S=O), 1633, 1777 (acetate), 2795, 2957 (C-H aromatic), 3063 (acetate-CH_3),

3428 (H_2O); ^{1}HNMR (D_2O): δ, ppm 8.91-9.44 (28-H, m, Pc-H, and Pyridyl-H), 4.11-4.33 (12-H, m, Pyridyl-CH_3), 2.09 (3-H, s, acetate CH_3); Calcd for $C_{58}H_{43}N_{12}O_{22}S_4Lu \cdot 2(H_2O)$; C 43.56%, H 2.84%, N 10.51%, S 8.02%, Found C 43.63%, H 2.93%, N 10.35% S 8.51%; UV-vis (DMF): λ_{max} nm (log ε) 353 (4.55), 614 (4.41), 680 (5.68); MS (MALDI-TOF): (m/z); Calcd 1563; Found 1548 $[M\text{-}CH_3]^+$

2.3.8 Synthesis of 2,(3), 9(10), 16(17), 23(24)-tetraaminophthalocyanato lutetium(III) acetate (21), Scheme 3.3

Complex (**21**) was synthesized using the procedure reported for other tetraamino metallophthalocyanines complexes [223]. A mixture of anhydrous lutetium (III) acetate (134 mg, 0.38 mmol) and 4-nitrophthalonitile (**9**), (131 mg, 0.76 mmol) in quinoline (2.5 mL) was refluxed for 7 h under nitrogen atmosphere using DBU as catalyst. After cooling, the crude product was precipitated with n-hexane, filtered and dried. The crude product was purified using column chromatography on silica gel with DMF as eluting solvent. The solvent was evaporated to give product **20**. Product **20** was then stirred in 250 mL aqueous solution containing 10 g $NaS{\cdot}9H_20$ for 24 h. The solid product was separated in a centrifuge and treated with 500 mL of 1 M HCl. The residue was separated and treated with 500 mL of 1 M NaOH for 1 h, after which the solid product was separated in a centrifuge, washed several times with de-ionized water and dried in a vacuum. Yield 17% [KBr, υ, cm^{-1}] 3327 N-H stretching, 1623 N-H bending mode, 2846 and 2927 (C-H aromatic), 1570 C=O, 1443, 1434, 1347 and 1307 C-N vibrations due to the phthalocyanine ring. UV-vis (DMF): λ_{max}/nm (log ε) 350 (3.81), 704 (4.55), Calcd. for

$C_{34}H_{23}N_{12}O_2Lu$; C 50.63%, H 2.87%, N 20.81%. Found C 50.91%, H 3.00%, N 21.04%; ^{1}H-NMR (DMSO-d_6) δ, ppm: 2.12 (3-H, s, acetate CH_3), 4.02 (8-H, s, NH_2), 8.29 (4-H, s, Aromatic-H), 8.20 (4-H, d, Aromatic-H), 8.00 (4-H, d, Aromatic-H). MS (MALDI-TOF): (m/z); Calcd. 807; Found 807 [M+].

2.4 Preparation of functionalized electrospun polymer fibers

2.4.1 Preparation of electrospun fibers of polyamide 4.6 and polyamide 6.9

The fibers were obtained on a mono-nozzle electrospinning setup, Fig. 2.5, with a tip-to-collector distance of either 6 cm or 10 cm at a flow rate of 2 mL/h. The applied voltage was adjusted for each polymer solution under the prevailing humidity conditions to obtain a steady Taylor cone. To obtain 50% relative humidity, the setup was placed under the open laboratory conditions. For 10% and 70% relative humidity, a closed electrospinning chamber was used in which the air was dried using silica or wetted using a saturated solution of potassium nitrate. A humidity sensor, Vaila HMl 41 indicator was used to continuously monitor the humidity in the closed electrospinning chamber.

Various concentrations of polymer solutions ranging from 8%w/w to 20%w/w in different solvent ratios of formic acid (FA) and acetic acid (AA) were prepared and electrospun into fibers. SEM images of the fiber mats were taken and the fiber diameters measured from using Cell^D software from Olympus.

2.4.2 Preparation of functionalized polystyrene polymer fibers

The fibers were prepared by mixing the phthalocyanine with the polymer solution and the mixture electrospun into fibers. The same molar amount of the particular phthalocyanine was added in each polymer solution for easy comparison. Briefly, the following conditions were used: a solution containing 2.5 g (1.3×10^{-5} moles of polystyrene (PS) and the mass equivalent (mg) of 1.2×10^{-6} moles of the phthalocyanine in 10 mL DMF/THF (4:1) was stirred for 24 h to produce a homogeneous solution. The phthalocyanines which were employed for studies with this polymer are AcLuTPPc$^{\alpha}$ (**14**) (1.34 mg), AcLuTPPc$^{\beta}$ (**18a**) (1.34 mg), AcLuTPyPc$^{\beta}$ (**18c**) (1.34 mg), AcLuTmPyPc$^{\beta}$ (**19**) (1.87 mg) and ZnPc (0.70 mg). The phthalocyanines were employed for this polymer to enable electrostatic interaction between their aromatic systems that will prevent leaching of the phthalocyanines from the polymer fibers during application. They were also used in order to demonstrate the effect of the nature of the substituent and the position of the substitution on the phthalocyanine ring. The solution was then placed in a cylindrical glass tube fitted with a capillary needle. A potential difference of 20 kV was applied to provide charge for the electrospinning process. The distance between the cathode (static fiber collection point) and anode (tip of capillary needle) was 15 cm and pump rate of 0.02 mL/h. For electrospun polystyrene polymer fibers without the functional phthalocyanine molecules, all experimental conditions were maintained except the flow rate that was reduced to 0.01 mL/h.

2.4.3 Preparation of functionalized polysulfone (PSU) polymer fibers

The fibers were also prepared by mixing the phthalocyanine with the polymer solution and then electrospun under conditions as reported before [228] with modifications as follows: a solution containing 2.0 g of polysulfone (PSU) and AcLuTPyPc$^{\beta}$ (**18c**) (3.61 mg), ZnTPyPc$^{\beta}$ (**23**) (1.35 mg), ZnTmPyPc$^{\beta}$ (**24**) (2.2 mg) or ZnPc (0.70 mg) in 10 ml DMF/THF (4:1) was stirred for 24 h to produce a homogeneous solution. The choice of the phthalocyanines was also to enable electrostatic interaction between the aromatic systems of phthalocyanines and polymer. The solution was then placed in a cylindrical glass tube fitted with a capillary needle. A potential difference of 20 kV was applied to provide charge for the electrospinning process. The distance between the cathode (static fiber collection point) and anode (tip of capillary needle) was 10 cm and pump rate was 0.5 mL/h. Similar conditions were applied to obtain fiber of the polysulfone alone**.**

2.4.4 Preparation of functionalized polyurethane polymer fibers

The phthalocyanine employed here contained carboxy substituents to allow for the chemical linking with the amino group of the polymer. AcLuTCPPc$^{\beta}$ (**18b**) was employed for these studies. Experiments were also performed where AcLuTPPc$^{\alpha}$ (**14**), AcLuTPPc$^{\beta}$ (**18a**), AcLuTCPPc$^{\beta}$ (**18b**), AcLuTPyPc$^{\beta}$ (**18c**) or ZnPc were merely mixed with the polymer without the formation of a chemical bond. The chemical linking of phthalocyanine to polyurethane was done as follows. A solution of complex AcLuTCPPc$^{\beta}$ (**18b**) was prepared by dissolving 15.5 mg in 10 mL of DMF. Then 0.5 g of

dicyclohexylcarbodiimide (DCC) was added and the resulting solution stirred for four days. This was done to enhance the electrophilicity of the carbonyl in the carboxylic acid functional group for amide bond formation with the polyurethane polymer. In order to prepare 7.5% polymer solution, 0.75 g of polyurethane was then added to the solution containing AcLuTCPPcβ (**18b**) and stirred for a further four days and the resulting solution electrospun into fibers using the following conditions. The voltage was set at +20 kV and -10 kV with the flow rate of the solution set at 1 mL/h and the distance between the cathode (static fiber collection point) and anode (tip of capillary needle) was 15 cm.

2.4.5 Preparation of functionalized polyacrylic acid polymer fibers

The phthalocyanines employed here contained amino substituents to allow for the chemical linking with the carboxylic group of the polymer. The polyacrylic acid (PAA) functionalized fibers were prepared as follows. PAA (0.2 g) was dissolved in 100 mL of DMF. Dicyclohexylcarbodimide (DCC), 0.5 g was added and the solution stirred for four days. This is to activate the carbonyl of the carboxylic acid of PAA for covalent amide bond formation. A mass equivalent of 1.2 x 10^{-6} moles of LuTAPcβ (**21**) (1.0 mg) or ZnTAPcβ (**22**) (0.77 mg) was added to the resulting solution. Each mixture was stirred for several days while taking the IR spectra intermittently to monitor the amide bond formation, after which the composite was precipitated using diethyl ether and dried in a dessicator. For the conjugate of unsubstituted ZnPc with PAA, 10 mg (0.58 mmol) of ZnPc was mixed with 0.2 g (PAA) with no addition of DCC.

The solutions for electrospinning were prepared by dissolving 6.6 wt% of each composite in 1:4 (v/v) water/ethanol solvent mixture and stirred for 24 h. The following electrospinning conditions were used; 1 mL/h flow rate, 10 kV applied voltage and 15 cm collector distance. Similar conditions were used for PAA alone and PAA/ZnPc composite without a chemical bond.

2.5 Photophysical and photochemical conditions

2.5.1 Fluorescence quantum yields (Φ_F)

Fluorescence quantum yields (Φ_F) of the phthalocyanines were determined in either DMF or DMSO by a comparative method, Equation 1.3. The same solvent was used in each case for samples and standard. Unsubstituted ZnPc (DMF Φ_F^{Std} = 0.30 [228], DMSO Φ_F^{Std} = 0.2) [229]) was employed as the standard. Both the samples and standard were excited at the same wavelength. The absorbances of the solutions at the excitation wavelength were about 0.05 to avoid any inner filter effects.

2.5.2 Triplet quantum yields (Φ_T) and lifetimes (τ_T)

The decay kinetics of the triplet absorption of the phthalocyanines were recorded using laser flash photolysis setup, Fig. 2.2. The absorbance of sample solutions and that of the standard were adjusted to be approximately 1.5 at their Q-band maximum. After introducing the solution to a 1 cm quartz cell, argon was bubbled through the solution to remove dissolved oxygen before taking readings. The triplet quantum yields of the sample phthalocyanines were determined using Equation 1.1. Unsubstituted ZnPc

DMF $\boldsymbol{\Phi_T^{std}}$ = 0.68 [230] and DMSO $\boldsymbol{\Phi_T^{std}}$= 0.65 [231] was employed as the standard. Triplet lifetimes were determined from the kinetic data obtained, using ORIGIN Pro 8 software.

2.5.3 Singlet oxygen (Φ_Δ) and photodegradation (Φ_p) quantum yields

An optical method and a chemical method were employed in this work for Φ_Δ determination.

The optical method involves the monitoring of the fluorescence decay of the singlet oxygen generated at 1270 nm in air, Fig. 2.4. Sodium azide (NaN_3) was used as singlet oxygen quencher. The dynamic course of the singlet oxygen concentrations were clearly recorded following Equation 1.4. The Φ_Δ values were then determined using Equation 1.5, and employing ZnPc in DMF, Φ_Δ^{std} = 0.56 [232] or in THF, Φ_Δ^{std} = 0.53 [90] as a standard.

A chemical method was also used in the determination of Φ_Δ of the phthalocyanines in solution (DMF). The experiments were carried out in air with 1.5 mL of each phthalocyanine solution with approximate absorbance of 1 at its Q band mixed with equal volume of a solution of DPBF with approximate absorbance of 2 at 414 nm. The resulting solution was irradiated using the setup shown in Fig. 2.3 and the degradation of the DPBF monitored by recording the UV-vis spectra of the sample solution at 5 s time intervals. The singlet oxygen quantum yields of the standard ($\boldsymbol{\Phi_\Delta^{std}}$) were the same as used for the optical method. Equation 1.6 was employed.

The photodegradation quantum yield Φ_p of complex 24 was similarly determined but in this case DPBF was not added but the degradation of the Q band of the phthalocyanine was similarly monitored with time upon irradiation. Equation 1.7 was employed.

For the singlet quantum yield of the phthalocyanines within the fiber matrices, ADMA was used as the singlet oxygen quencher since the fabric materials are intended for use in aqueous media. In each case 10 mg of the modified fibers was suspended (as small pieces) in an aqueous solution of ADMA and similarly irradiated using the photolysis set-up, Fig. 2.3. The quantum yields (Φ_{ADMA}) were estimated using Equation 1.7, using the extinction coefficient of AMDA in water log (ε) = 4.1 [117] and using the absorbance of the phthalocyanine in the polymer fiber matrix. Equation 1.9 (the absolute method) was employed for $\mathbf{\Phi_\Delta}$ values. The $\mathbf{\Phi_\Delta}$ values are estimates due to light scattering and the intensity of light was the one reaching the spectrophotometer cell but not the fibers.

2.5.4 Fluorescence micrographs

Fluorescence micrographs of the functionalized fibers were taken by placing the fiber on a glass slide. This was then placed under the DMLS fluorescence microscope and the excitation source, a high-voltage mercury lamp, set at wavelength range of 550-730 nm to give the characteristic red fluorescence of phthalocyanines. Pictures of the micrographs were then taken using a digital camera.

2.5.5 Optical detection of nitrogen dioxide

Nitrogen dioxide (NO_2) gas was generated from a reaction of copper metal with dilute nitric acid. About 2 mL of the gas was then bubbled through a solution of the phthalocyanine and the fluorescence intensity of the solution recorded. This process was repeated for each spectrum recorded.

For the detection of the gas using the functionalized fibers, a small sample of each fiber mat was placed on a glass slide and placed on the sample holder of the DMLS fluorescence microscope. The sample was irradiated using a high-voltage mercury lamp as excitation source in the wavelength range of 550-730 nm. The initial micrograph was then taken and about 2 mL of the generated nitrogen dioxide gas sprayed into the air just above the sample. After a while a micrograph was taken and this process repeated several times for each sample. However the quantitative amount of nitrogen dioxide in each of 2 mL gas sample could not be determined as it contained air and not dried.

2.6 Photocatalysis and analysis of degradation products.

2.6.1 Photocatalytic reactions

Photocatalytic reactions were carried out in a magnetically stirred batch reactor (glass vial). The irradiation experiments were carried out using the photolysis setup described above for singlet oxygen determination, Fig 2.3. The intensity of the light reaching the reaction vessel was measured with a power meter (POWER MAX 5100, Molelectron Detector Inc) and found to be 3.52×10^{20} photons cm^{-2} s^{-1}. The transformations were

monitored by observing the absorption bands at 243 and 297 nm for 4-CP, 400 nm for 4-NP and 470 nm for methyl orange, after each photolysis cycle of thirty minutes, using a Shimadzu UV-2550 spectrophotometer. The experiments were carried out using a variety of concentrations of 4-chlorophenol (pH 11), 4-nitrophenol (pH 8.2) and methyl orange (pH 9.2) in aqueous buffer solutions. Each sample solution (4 mL) contained 20 mg of functionalized fiber, suspended in small pieces.

For the homogeneous catalytic conversion of methyl orange using complex **24**, all experimental conditions described above were maintained except the functionalized fibers were replaced with 1.5×10^{-5} mol L^{-1} of complex **24** in the sample solution.

2.6.2 Identification of photocatalytic products

The photolysis products were analyzed using gas chromatography (GC) and/or by direct injection into ion trap mass spectrometer fitted with an electrospray ionization (ESI-MS) mass source. The aqueous photocatalyzed sample solutions were extracted with dichloromethane in the case of 4-chlorophenol and 4-nitrophenol and then injected into the GC. The chromatographic peaks were identified by comparing with standards. Sample solutions of methyl orange were directly injected into the ion trap mass spectrometer.

Results and discussions

Chapter 3: Synthesis and characterization of phthalocyanines

Chapter 4: Characterization of fibers

Chapter 5: Detection and phototransformation of pollutants

Chapter 6: Conclusions and future prospects

Publications

The results presented in the next sections have been published in a patent and as articles published or submitted to peer-reviewed journals. The details of these publications are listed below and are not referred to in this thesis.

A. Patent

1. Ruphino Zugle, Godfred Darko, Nelson Torto, Christian Litwinski, Tebello Nyokong, **Polymer bound metallophthalocyanines**, 2012, PCT Int. Appl., WO2012023100 A1 20120223.

B. Peer-reviewed articles

1. Ruphino Zugle, Christian Litwinski, Tebello Nyokong, **Photophysical characterization of dysprosium, erbium and lutetium phthalocyanines tetrasubstituted with phenoxy groups at non-peripheral positions**, Polyhedron, 2011, 30, 1612-1619
2. Ruphino Zugle, Christian Litwinski, Nelson Torto, Tebello Nyokong, **Photophysical and photochemical behavior of electrospun fibers of a polyurethane polymer chemically linked to lutetium carboxyphenoxy phthalocyanine**, New Journal of Chemistry, 2011, 35, 1588-1595
3. Ruphino Zugle, Edith Antunes, Samson Khene, Tebello Nyokong, **Photooxidation of 4-chlorophenol sensitized by lutetium tetraphenoxy phthalocyanine anchored on electrospun polystyrene polymer fiber**, Polyhedron, 2012, 33, 74-81

4. Ruphino Zugle, Tebello Nyokong, **Electrospun Polyacrylic Acid Polymer Fibers Functionalized with Metallophthalocyanines for Photosensitizing and Gas Sensing Applications**, Journal of Macromolecular Science PartA: Pure and Applied Chemistry, 2012, 49, 279-287
5. Ruphino Zugle, Tebello Nyokong, **Physico-chemical properties of lutetium phthalocyanine complexes in solution and in solid polystyrene polymer fibers and their application in photoconversion of 4-nitrophenol**, Journal of Molecular Catalysis A: Chemical, 2012, 358, 49-57
6. Ruphino Zugle, Tebello Nyokong, **Comparative detection and phototransformation of environmental pollutants using metallophthalocyanines supported on electrospun polymer fibers**, Journal of Applied Polymer Science, 2012, DOI: 10.1002/app.38381
7. Ruphino Zugle, Tebello Nyokong, **Zinc(II) 2,9,16,23-tetrakis[4-(N-methylpyridyloxy)]-phthalocyanine anchored on an electrospun polysulfone polymer fiber: Application for photosensitized conversion of methyl orange**, Journal of Molecular Catalysis A: Chemical, 2012, doi.org/10.1016/j.molcata.2012.10.001

8. Bert De Schoenmaker, Lien Van der Schueren, Ruphino Zugle, Annelies Goethals, Westbroek Phillipe, Paul Kiekens, Nyokong Tebello, Karen De Clerck, **Effect of relative humidity on the fiber morphology of polyamide 4.6 and polyamide 6.9 nanofibers**, Journal of Material Science, 2012, DOI.10.1007/s10853-012-69349

C. Publication not related to this work

1. S. Adewuyi, D. A. Ondigo, R. Zugle, Z. Tshentu, T. Nyokong, N. Torto, **A highly selective and sensitive pyridylazo-2-naphthol-polyacrylic acid functionalized electrospun nanofiber fluorescence "turn-off" chemosensory system for Ni^{2+},** Analytical Methods, 2012, 4(6), 1729-1735

Chapter 3

3.1. Synthesis, characterization and physico-chemical properties of novel lanthanide phthalocyanines

3.1.1. Non-peripherally substituted phenoxy lutetium, dysprosium and erbium phthalocyanines (14, 15 and 17)

The dysprosium, erbium and lutetium phthalocyanines tetrasubstituted with phenoxy groups at non-peripheral positions were synthesized according to Scheme 3.1. Whereas dysprosium and lutetium phthalocyanines were obtained from the cyclotetramerization reaction from the substituted phthalonitrile **13**, erbium phthalocyanine was obtained from the unmetallated phthalocyanine, complex **16**.

MALDI-TOF method was employed for mass spectrometry study, using 2,5-dihydroxybenzoic acid as the matrix. Complex **14** showed a molecular ion peak corresponding to a protonated species $[M+4H]^+$ at 1119 amu which is consistent with the calculated values of 1115 amu. The matrix employed in this work (2,5-dihydroxybenzoic acid), which is known [233] to intensify the fragmentation process hence the observed mass spectral data. For complex **17**, the most intense ion peak at 1088 amu corresponding to a protonated species $[M+4H]^+$ is comparable to the calculated mass of 1084 amu. In the case of complex (**15**), a dysprosium bis-phthalocyanine, the molecular ion base peak occurred at 1926 amu, which compares well with the calculated value of 1924 amu and is consistent with the protonated species

$[M+2H]^+$, where M is -(Pc(-2)Dy^{III}Pc(-1) in this case, as will be proved by the near infra red spectra below.

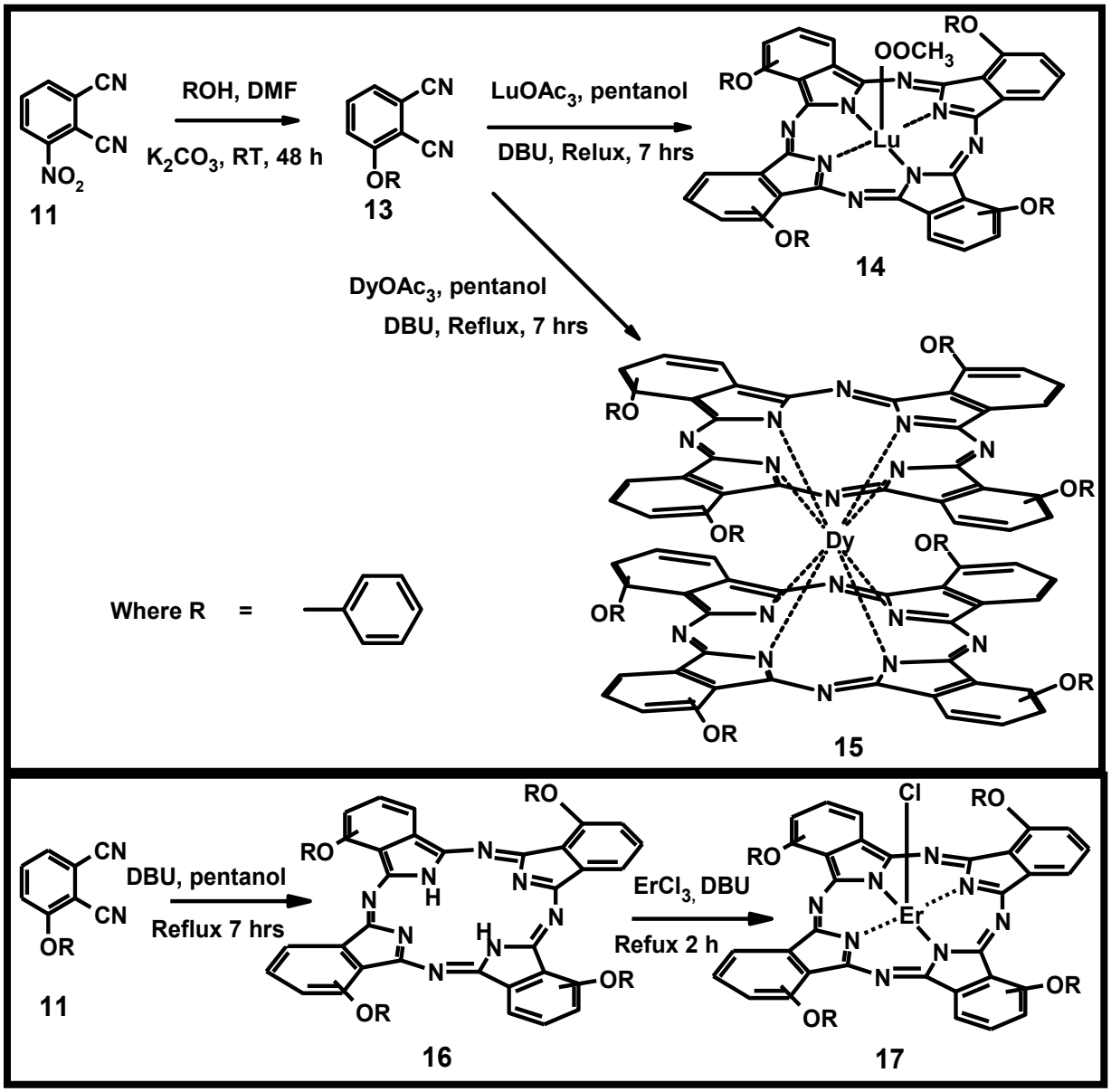

Scheme 3.1: Synthetic routes for non-peripherally substituted phthalocyanines (14, 15 and 17).

^{1}H NMR data was consistent with the structure for **14**. All the protons were observed in their respective regions. The phthalocyanine ring protons integrated for 12 and phenyl for 20 as expected. In addition, protons due to the acetate axial ligand were observed. The isomeric nature of the molecules results in the broadening of the ^{1}H NMR spectra, but the protons were observed in their respective positions. Complexes **15** and **17** are paramagnetic hence no NMR data was obtained. Elemental analysis results were in agreement with the proposed structure.

The fact that for Er and Lu, the main products were the monomeric phthalocyanine species while for Dy the main product was the dimer ($DyPc_2$) is consistent with the tendency of the lighter lanthanides to form complexes with higher coordination number than the heavier ones [43, 45]. The three lanthanide phthalocyanines are all soluble in polar organic solvents such as DMF, DMSO, THF and DCM. This is typical for phthalocyanines with alkyl and alkoxy substituent groups in either or both peripheral and non-peripheral positions of the phthalocyanine framework [234].

The UV–vis spectra of the three lanthanide phthalocyanines in THF are shown in Fig. 3.1. The spectra are typical of metallated phthalocyanines, with a similar Q-band

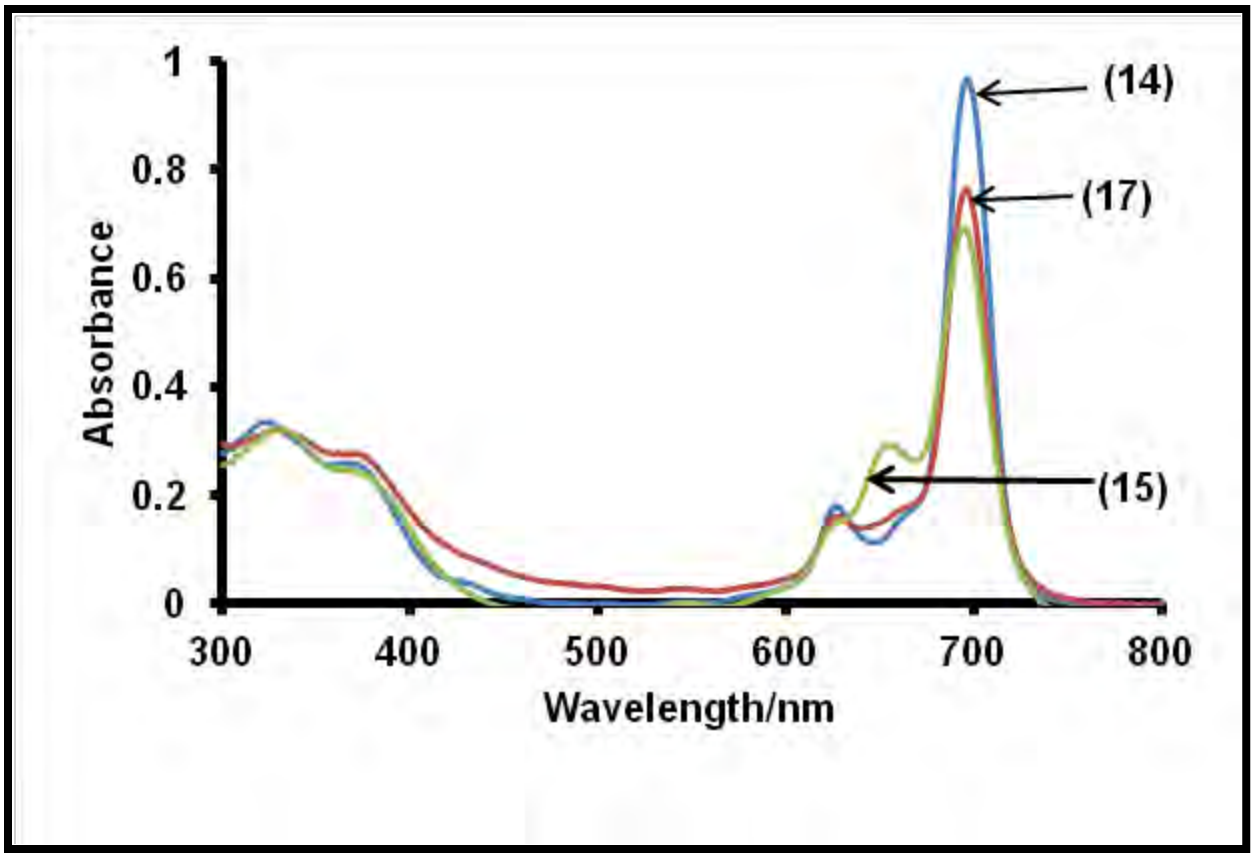

Figure 3.1: UV-vis spectra of complexes 14, 15 and 17 in THF, concentrations ~ 4 x 10^{-6} mol L^{-1}.

absorption maximum of 690 nm in THF, Table 3.1.

The introduction of the phenoxy substituents and the lanthanide central metals into the phthalocyanine macrocycle has led to appreciable red shift in the visible region compared to unsubstituted ZnPc (Q band maximum at 670 nm) [54]. Such a red shift in phenoxy substituted phthalocyanines has also been reported by Luk'yanets *et al*. [235]. The Q band maxima in THF and DMSO are listed in Table 3.1. In DMSO the peaks are more red-shifted than in THF. This is attributed to the fact that DMSO is more polar

than THF. A similar observation and explanation have been put forward for the changes in band positions of Ti(IV)Pc complexes with changes in polarity of the solvent [236].

Table 3.1: Q band maxima for complexes 14, 15, 17, and corresponding molar extinction coefficients as well as excitation and emission wavelengths.

Complex	Solvent	Q-band λ_{abs}/nm (log ε)	λ_{ex}	λ_{em}
AcLuTPPc$^{\alpha}$ (14)	**THF**	**690 (5.12)**	**690**	**699**
	DMSO	**697(5.16)**	**678**	**705**
DyPc$_2$ (15)	**THF**	**690 (4.87)**	**689**	**719**
	DMSO	**695 (5.04)**	**695**	**708**
ClErTPPc$^{\alpha}$ (17)	**THF**	**690 (5.03)**	**690**	**710**
	DMSO	**696 (5.11)**	**695**	**706**

Abs = absorption, ex = excitation and em = emission

In order to further ascertain whether these lanthanide phthalocyanines are monomeric or bis-phthalocyanines, the ground state electronic absorption spectra of the complexes were extended to 1600 nm, Fig. 3.2. It has been reported that a broad near-IR band near 900 nm is highly characteristic of lanthanide double deckers which contain a hole in one of the ligands [237].

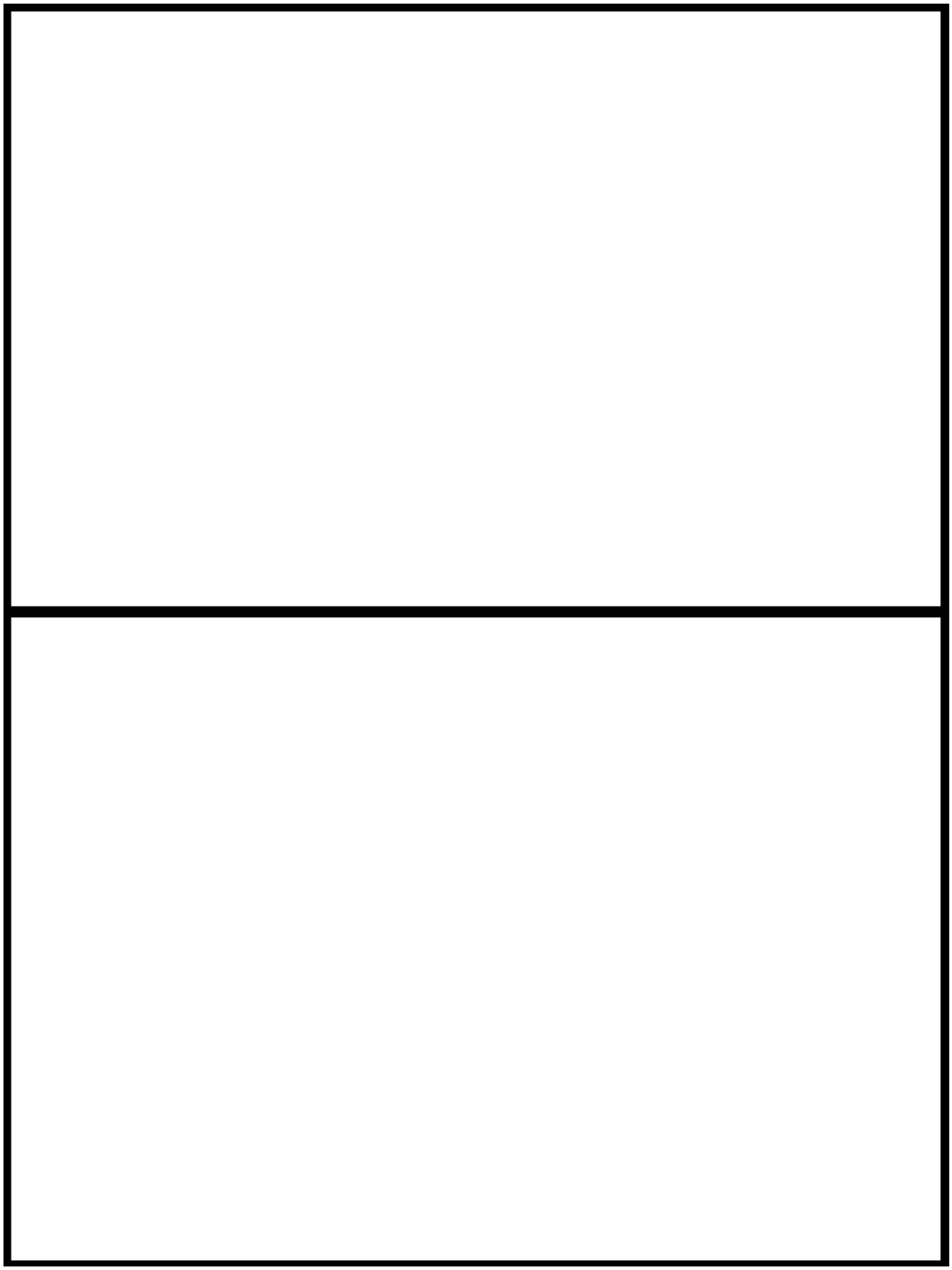

Figure 3.2: UV-vis-near IR spectra of complexes 14 (1.7 x 10^{-5} mol L^{-1}), 15 (1.5 x 10^{-5} mol L^{-1}) and 17 (8.2 x 10^{-6} mol L^{-1}) in THF.

As shown in Fig. 3.2, the spectrum of complex **15** (circled) has a weak near IR band near 920 nm, which is a diagnostic for the presence of an oxidized phthalocyanine ring in lanthanide bis-phthalocyanines. Thus complex **15** is the green neutral Pc(-2)DyPc(-1) complex. Chemical reduction of this complex resulted in the change of the colour from green to blue and the disappearance of the band at 920 nm, as is typical for reduction of Pc(-2)DyPc(-1) to $[Pc(-2)DyPc(-2)]^-$. The spectrum also confirms that the complex is a double decker phthalocyanine as indicated by its mass spectral data. On the other hand, the spectra of complexes **14** and **17** do not contain such near IR absorption bands, Fig. 3.2, which also confirms their monomeric nature. Fig. 3.3 shows the dependence of the

absorbance of complex **14** (as a representative of the other complexes) on concentration and the insert is a linear calibration plot at 690 nm, showing that the Beer–Lambert law is obeyed for concentrations ranging from 1.35 x 10^{-6} mol L^{-1} to 1.04 x 10^{-5} mol L^{-1}. All the complexes showed no aggregation in DMSO and THF at concentrations less than 1 x 10^{-5} mol L^{-1}.

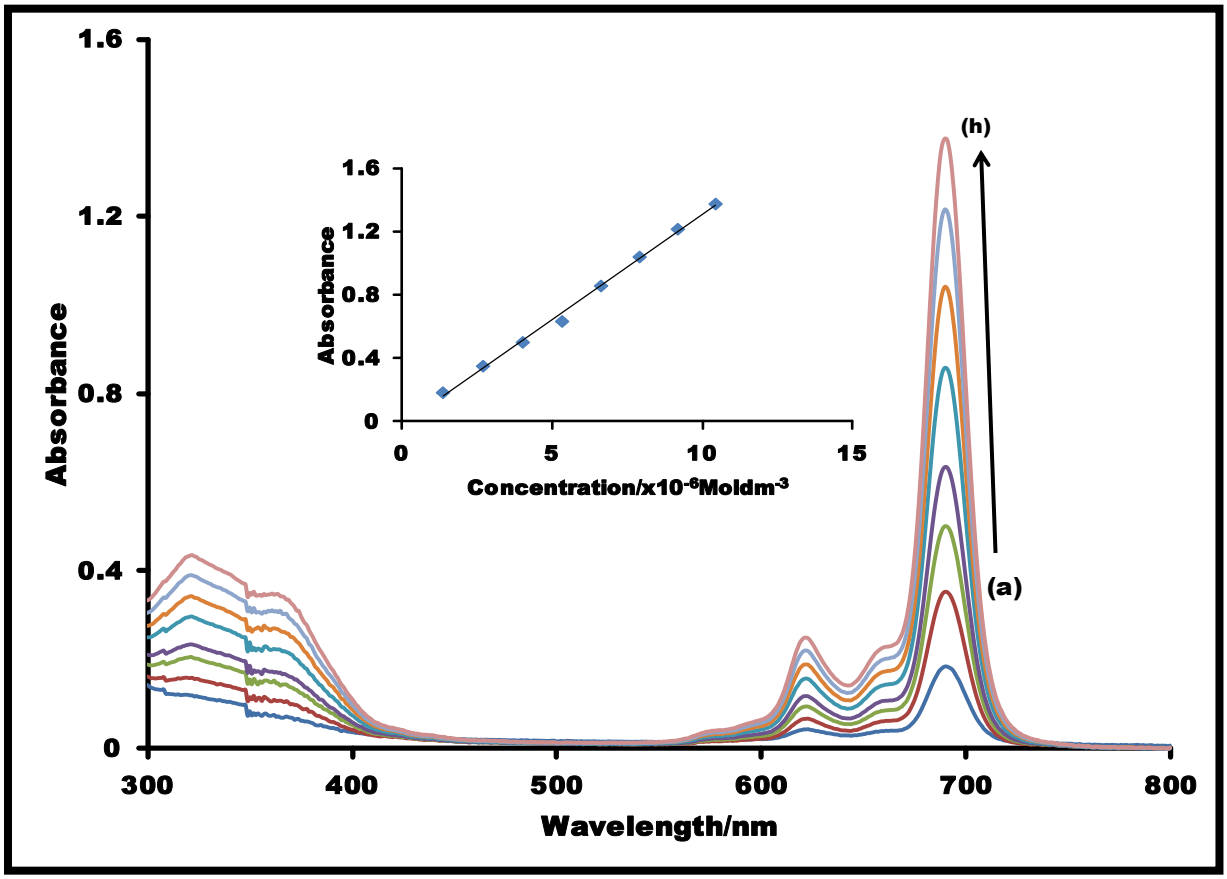

Figure 3.3: UV- visible spectra of complex 14 showing variation of absorbance with concentration in THF (a) minimum concentration: 1.35 x 10^{-6} mol L^{-1} and (h) maximum concentration 1.04 x 10^{-5} mol L^{-1}. Insert: Beer- Lambert law for concentration ranging from 1.35 x10^{-6} mol L^{-1} to 1.04 x 10^{-5} mol L^{-1}.

3.1.2. Lutetium phthalocyanines peripherally substituted with phenoxy, carboxyphenoxy, pyridiloxy, N-methylpyridiloxy and amino groups (18a-c, 19 and 21)

The monomeric lutetium phthalocyanines tetra-substituted with phenoxy (**18a**), phenoxycarboxy (**18b**) and pyridiloxy (**18c**) groups at the peripheral positions were synthesized from their corresponding substituted phthalonitriles (**10a, 10b** and **10c**) respectively, Scheme 3.2. Low phthalonitrile content was used in the cyclotetramerization reaction with the lutetium salt. The lutetium phthalocyanine tetra-substituted with N-methylpyridiloxy group (**19**) was obtained from quaternization of complex (**18c**), Scheme 3.2.

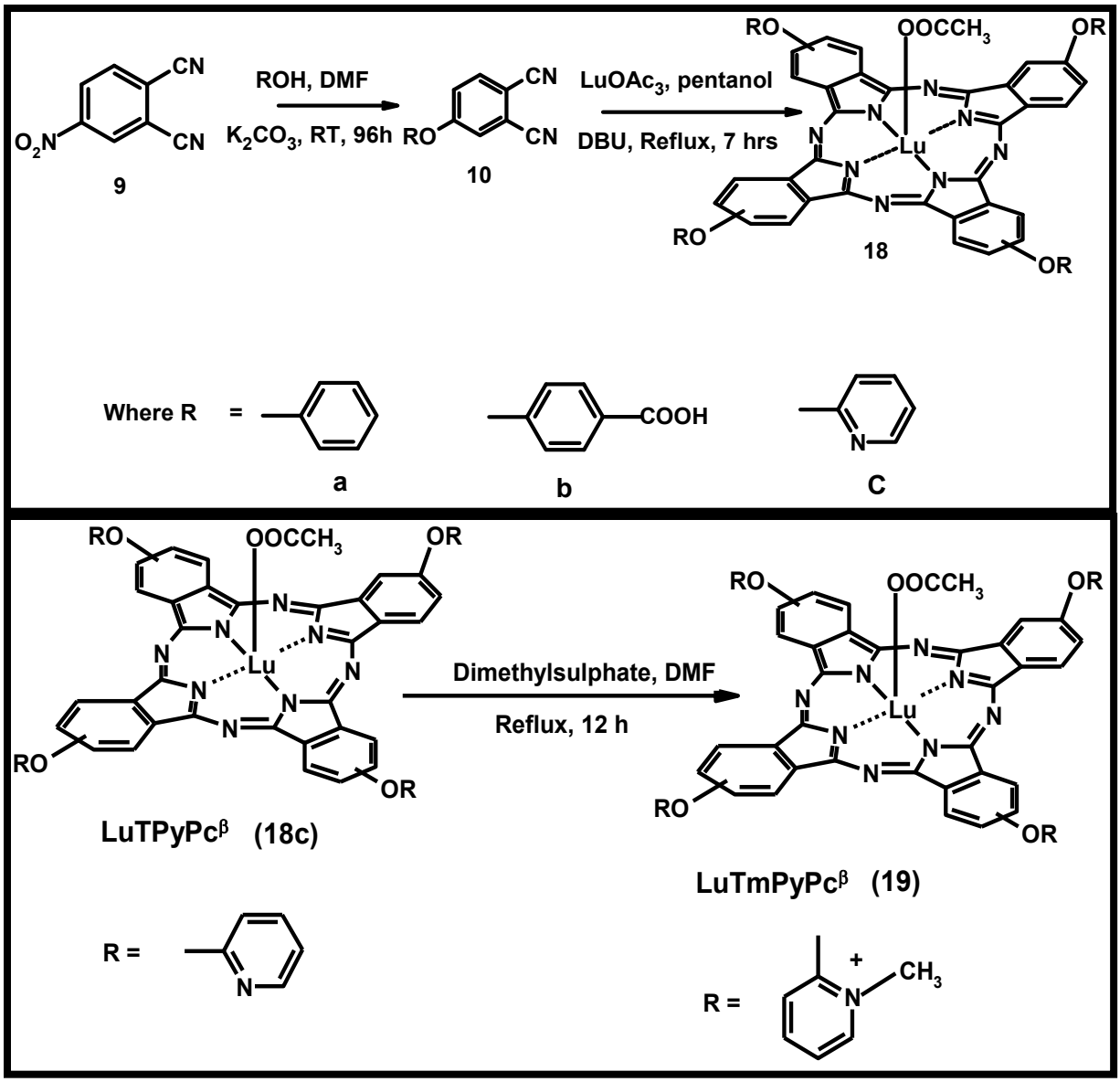

Scheme 3.2: Synthetic routes of peripherally substituted phthalocyanines (complexes 18a, 18b, 18c, and 19).

The complexes were characterized by several techniques including ^{1}H NMR, mass, IR and UV-vis spectroscopies as well as elemental analyses. For AcLuTCPPcβ **(18b),** a molecular ion peak corresponding to a protonated species $[M + 2H]^{+}$ at 1293 amu was obtained. The IR spectrum of AcLuTCPPcβ **(18b)** showed a broad peak around 3504

cm^{-1} due to the O–H stretch of the carboxylic acid functional group, the peaks at 2927 and 2856 cm^{-1} are due to C–H stretches, the sharp intense peak at 1656 cm^{-1} could be assigned to the C=O group of the carboxylic acid, the peaks at 1499, 1439, 1403 and 1383 cm^{-1} are due to phthalocyanine C–N vibrations, 1254 and 1221 cm^{-1} are due to the ether (C–O–C) bond while those at 1148, 1087 and 1060 cm^{-1} could be assigned to phenyl vibrations [238]. For AcLuTPPc$^{\beta}$ (**18a**), AcLuTPyPc$^{\beta}$ (**18c**) and AcLuTmPyPc$^{\beta}$ (**19**) molecular ion peaks corresponding to protonated species $[M+ H]^+$, $[M + 2H]^+$ and $[M-CH_3]^+$ respectively were obtained. Details of other spectroscopic and elemental characterization of the complexes are given in section 2.4.

The UV-vis spectra of all the complexes, Fig. 3.4, are typical of metallated phthalocyanines, with Q-band absorption maxima in DMF listed in Table 3.2. The Q band maxima of **14** (692 nm) is more red shifted compared to **18a** (678 nm), though they contain similar substituent but only differ in position. It is known that substitution at the α position leads to red shifting [239].

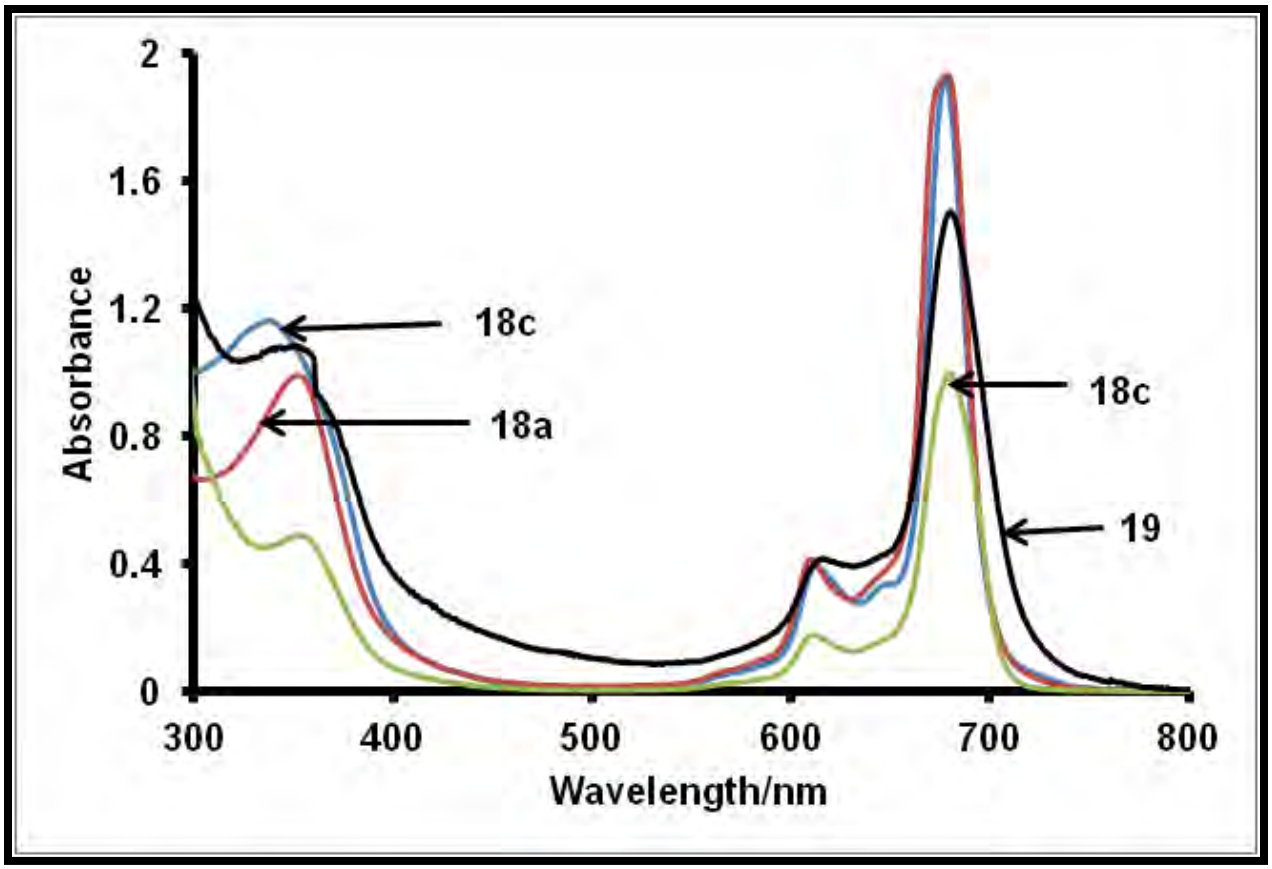

Figure 3.4: UV-vis spectra of complexes 18a (1.78 x10^{-6} mol L^{-1}), 18b (1.02 x 10^{-6} mol L^{-1}), 18c (1.78 x 10^{-6} mol L^{-1}) and 19 (1.46 x 10^{-6} mol L^{-1}).

Table 3.2: Spectral properties of complexes 18a, 18b, 18c and 19, Q-band maxima and corresponding molar extinction coefficients, solvent = DMF.

Complex	Q band λ_{abs} (log ε)	λ_{ex}	λ_{em}
AcLuTPPcβ (18a)	**678 (5.78)**	**677**	**692**
AcLuTCPPcβ (18b)	**678 (5.31)**	**679**	**689**
AcLuTPyPcβ (18c)	**678 (5.94)**	**681**	**689**
AcLuTmPyPcβ (19)	**680 (5.68)**	**680**	**705**
AcLuTAPc (21)	**701 (4.55)**	**--**	**--**

Abs = absorption, ex = excitation and em = emission

The synthesis of (Ac)LuTAPcβ (**21**), is reported here for the first time, Scheme 3.3 and was characterized by ^{1}H-NMR, mass and IR spectroscopy, as well as elemental analysis.

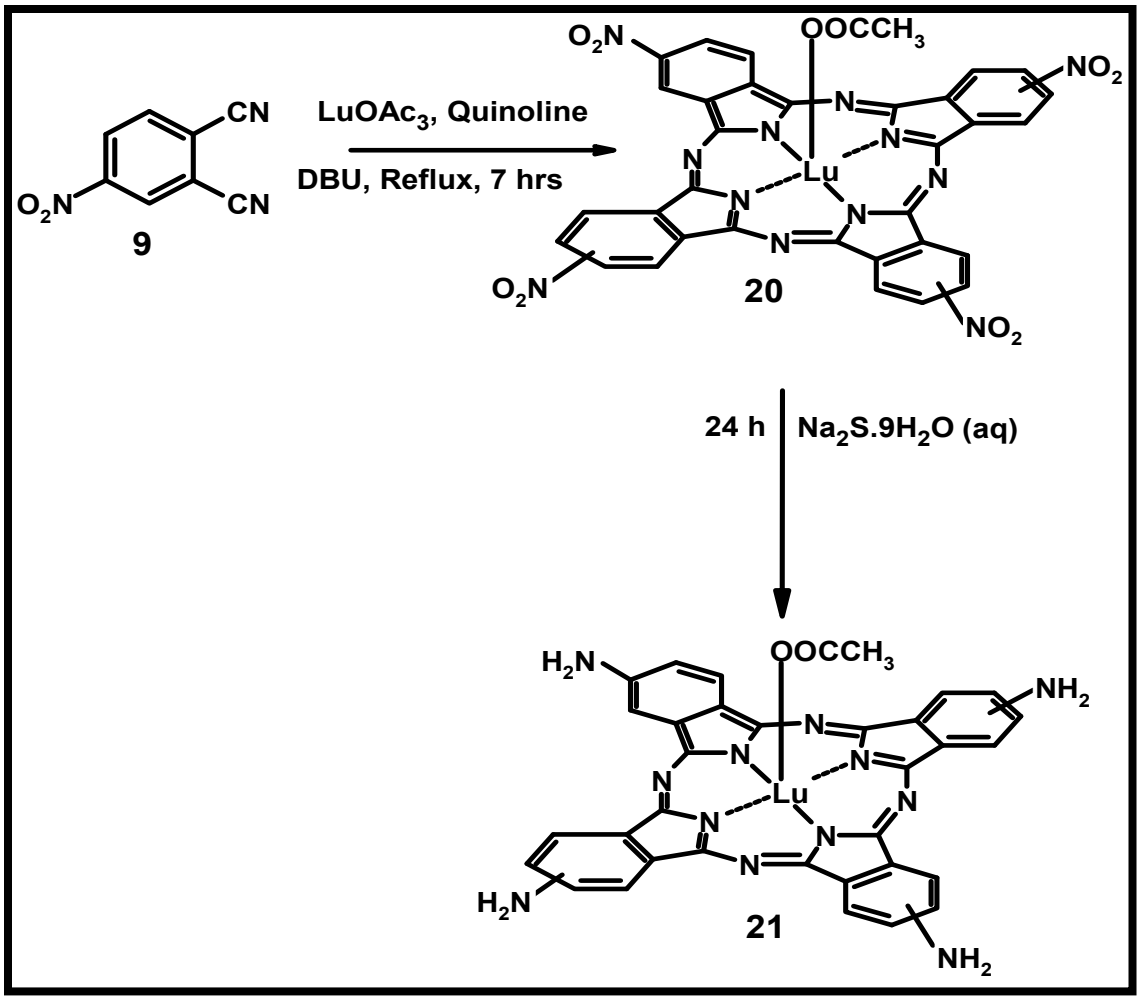

Scheme 3.3: Synthetic route for AcLuTAPc$^{\beta}$ (21).

A molecular ion peak corresponding to [M^+] at 807 amu was obtained. Infrared spectroscopic analysis of (Ac)LuTAPc$^{\beta}$ (**21**) showed a partially split peak around 3327 cm^{-1} which is characteristic of N-H stretching mode of a primary amine group [238]. This was supported by a corresponding N-H bending mode at 1623 cm^{-1}. The C-H stretchings were observed at 2846 and 2927 cm^{-1}. The peak at 1590 cm^{-1} is attributed to C=O bond from the axial acetate group, while the C-N vibrations due to the phthalocyanine ring were observed at 1443, 1434, 1347 and 1307 cm^{-1}. The UV-visible

spectral features of AcLuTAPcβ (**21**) in DMF was compared with that of ZnTAPcβ (**22**) which is well known [223, 240], Fig. 3.5.

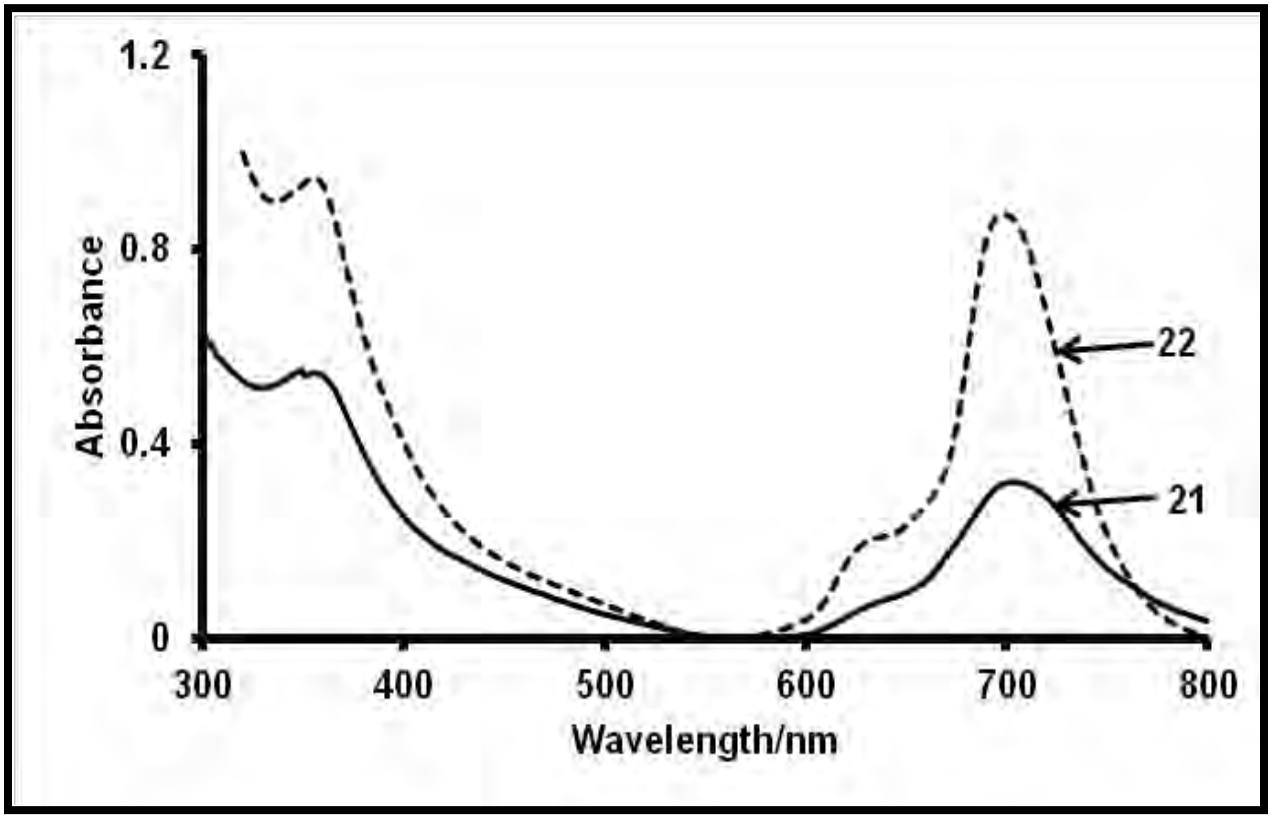

Figure 3.5: UV-visible spectra of 1 x 10^{-5} mol L^{-1} AcLuTAPcβ (21) and 1 x 10^{-4} mol L^{-1} ZnTAPcβ (22) in DMF.

The broad Q-band is characteristic of monomeric aminophthalocyanines. The Q band of AcLuTAPcβ (**21**), (701 nm), Table 3.2, is more red-shifted than the other β-substituted LuPc derivatives, Table 3.2, due to the electron donating ability of amino groups. The

Beer-Lambert law was obeyed for concentration below 1.42 x 10^{-5} mol L^{-1} for AcLuTAPc$^{\beta}$ (**21**).

3.2. Photophysical studies

3.2.1. Fluorescence quantum yields (Φ_F) and lifetimes (τ_F)

The fluorescence properties of the investigated complexes (**14, 15, 17, 18a-c, 19, 21**) were studied in either DMF or DMSO degassed with argon. The fluorescence spectra were mirror images of the excitation spectra for all the complexes, Fig. 3.6 for complex **18c**, used as an example. The proximity of the Q band maxima of the absorption and excitation spectra listed in Tables 3.1 and 3.2, for all complexes suggests that the nuclear configurations of the ground and excited states are similar and not affected by excitation in the various solvents.

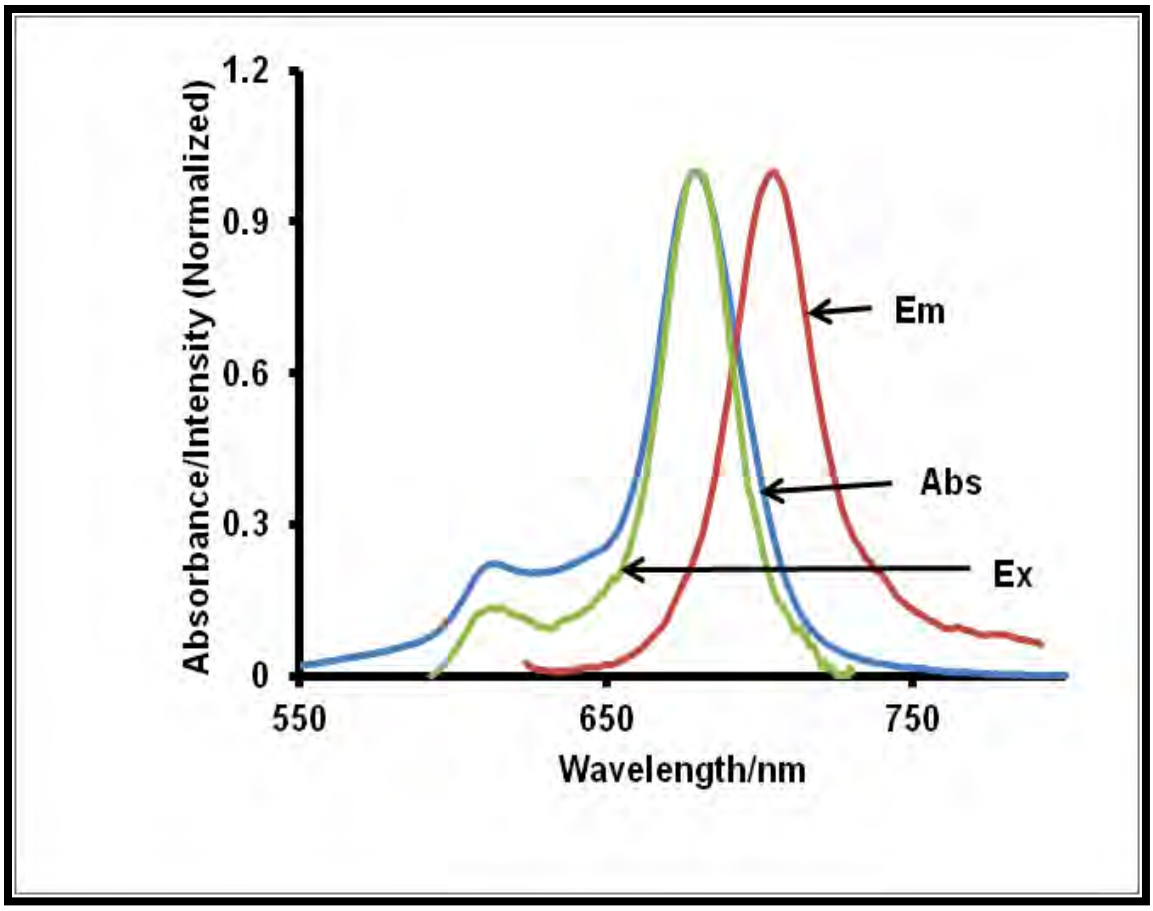

Figure 3.6: Fluorescence (Em), absorption (Abs), Excitation (Ex) spectra in DMF for complex 18c.

The Stokes shifts were typical for phthalocyanines [241], Tables 3.1 and 3.2. The fluorescence quantum yields (Φ_F) values were determined by the comparative method and the values were mostly lower than 0.01. These low Φ_F values, Table 3.3, could be attributed to the heavy atom effect of the central metals, which encourages intersystem crossing to the triplet state. A similar argument has also been suggested for hafnium phthalocyanines which do not fluoresce at all [242]. In the case of complexes **15** and **17,** the central metals are paramagnetic. Paramagnetic metal ions equally enhance the yield

of the triplet state, but only inevitably shorten the lifetime of the excited states, hence the low fluorescence quantum yields for the complexes [243].

For AcLuTAPc$^{\beta}$ (**21**) which contains large central metal and in addition to the quenching effect of the amino group, the lack of fluorescence is not surprising [223, 240, 242], Table 3.3.

Table 3.3: Fluorescence parameters.

complex	Φ_F	τ_F^1/ns (RA)	τ_F^2/ns (RA)	τ_F^3/ns (RA)
14	**< 0.01**	**0.09 ± 0.01 (0.96)**	**1.70 ± 0.60 (0.01)**	**4.70 ± 0.20 (0.03)**
15	**< 0.01**	**0.01 ± 0.05 (0.53)**	**2.20 ± 0.20 (0.17)**	**5.00 ± 0.10 (0.30)**
17	**< 0.01**	**0.08 ± 0.02 (0.96)**	**2.4 ± 0.50 (0.02)**	**4.60 ± 0.10 (0.02)**
18a	**< 0.01**	**0.01 ± 0.04 (0.91)**	**4.27 ± 0.31 (0.09)**	**----**
18b	**0.01**	**3.2 ± 0.05 (1.00)**	**----**	**----**
18c	**0.017**	**0.11 ± 0.04 (0.86)**	**4.60 ± 0.21 (0.14)**	**----**
19	**0.01**	**0.16 ± 0.04 (0.50)**	**4.23 ± 23 (0.95)**	**----**
21	**----**	**----**	**----**	**----**

RA = relative amplitude

The fluorescence decay profiles of complexes **18a, 18c** and **19** (Fig. 3.7, using complex **18c** as an example) are characterized by two exponential decay processes. The lifetimes of all the complexes are listed in Table 3.3. Biexponential fluorescence decay profiles of

phthalocyanines are attributed to the formation of ground-state dimers which can quench the monomer fluorescence, leading to a quenched and unquenched lifetimes [244].

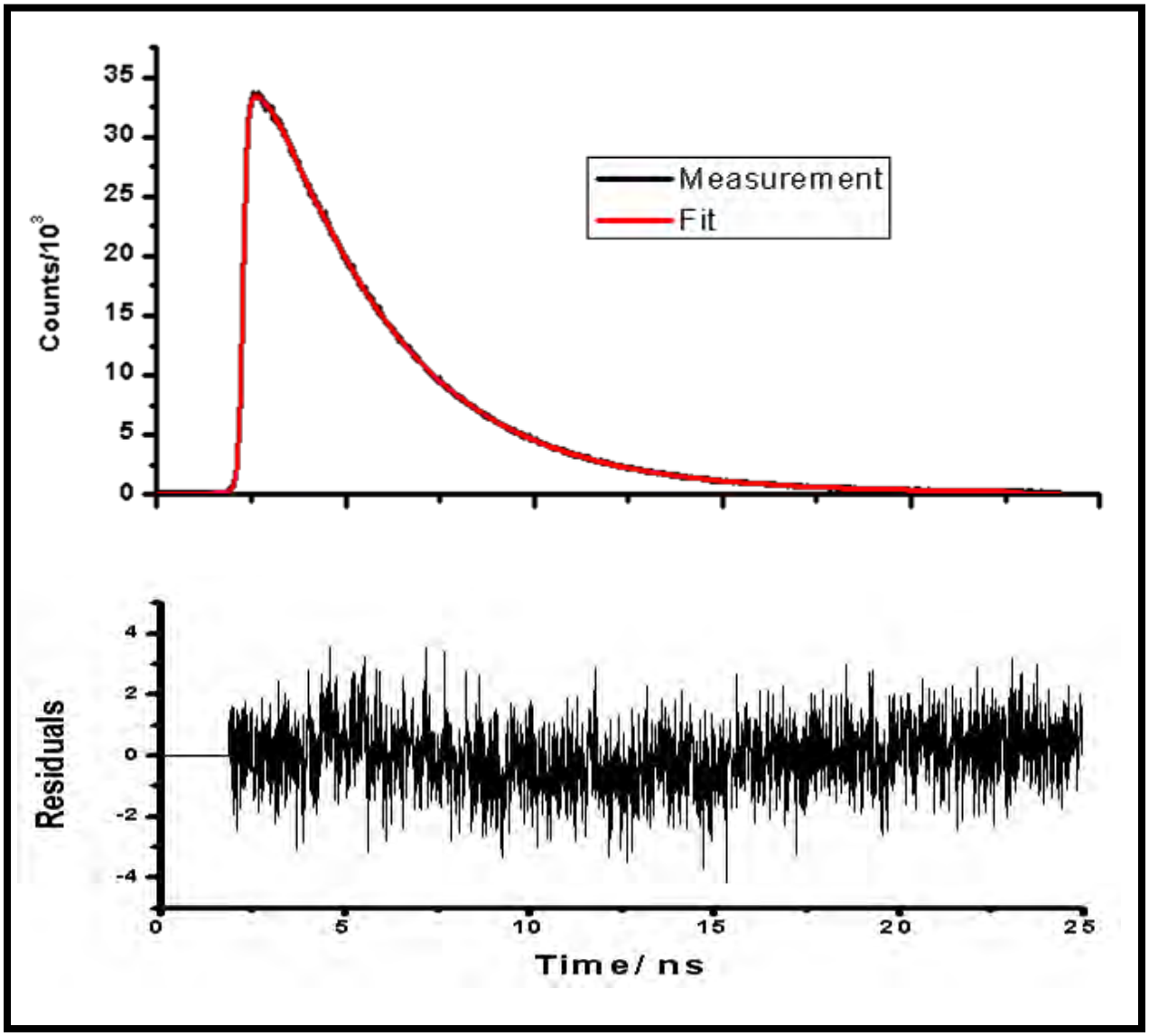

Figure 3.7: Fluorescence decay profile for complex 18c in DMF. Excitation wavelength 673 nm. X^2 = 1.06.

The longer (unquenched) lifetime is attributed to the monomer and the shorter lifetime is attributed to quenched lifetime of the dimer [244]. In this work three lifetimes were observed with some of the complexes (**14**, **15**, and **17**), Table 3.3. The short-lived component of the decay profile could then be attributed to the set of molecules in which the coordinating phthalocyanine ligand and the lanthanide ion behave as coordinating entities resulting in the observed fluorescence. This is a general characteristic feature in fluorescence of lanthanides phthalocyanines which due to their big mass, have shorter fluorescence lifetimes than the metal free phthalocyanines or porphyrins [52, 245]. The long lifetime (τ_F^3), Table 3.3, could then be attributed to some small amount of phthalocyanine molecules in which lanthanide ions seem to have been lost and the observed fluorescence attributed to the coordinating phthalocyanine without the central metal. The values for τ_F^3 are in the range observed for monomeric phthalocyanines [244]. The intermediate lifetime (τ_F^2) might be due to metal free phthalocyanine dimers or oligomers which are formed in the solution. The value of τ_F^2 lies in the range of the quenched lifetimes in metallophthalocyanines [244]. The estimated amplitudes of all three complexes confirmed the above assignments. In complexes **14** and **17** which are monomeric, the amplitude of τ_F^1 is about two to three orders of magnitude greater than the amplitudes of τ_F^2 and τ_F^3. Here only very small amounts of species without lanthanide central metal and dimers/oligomers are in the solution. In the case of complex **15** which is dysprosium bis-phthalocyanine the amplitudes of τ_F^1 is only about two times bigger than the amplitude of the other two lifetimes. The reason for this is the

lower stability of complex **15** which results in more phthalocyanine molecules which can lose their central metal (τ_F^3) or form dimers/oligomers (τ_F^2).

For complex **18b**, only one exponential decay process was observed with one lifetime. This suggests that one molecular species is present in solution. The value for the lifetime is in the range observed for monomeric phthalocyanines [244].

3.2.2. Triplet quantum yields (Φ_T) and lifetimes (τ_T)

Singlet oxygen which is mostly implicated in photosensitized reactions is produced through transfer of energy from the excited triplet state of the photosensitizer to ground state molecular oxygen [246]. Thus the ability of a sensitizer to undergo the spin forbidden transition from its excited singlet state to the triplet state is a fundamental requirement for photosensitization processes.

Dysprosium(III) and erbium(III) are open shell, paramagnetic metal ions which cause a short-lived excited triplet state [243, 239]. The lifetime of the excited triplet state seems to be faster than the resolution of the flash photolysis system used. Also for $DyPc_2$ (**15**), the strong intramolecular π-π interactions increase relaxation routes and therefore decreases the triple-state lifetime [241]. The triplet lifetime of phthalocyanines containing a central paramagnetic transition metal have been found to be very short (nanosecond scale), hence the lack of triplet decay curves for complexes **15** and **17**. The low triplet lifetimes impose a severe limitation on the use of phthalocyanines containing paramagnetic central metals as photosensitizers.

For the lutetium phthalocyanines (**14, 18a-c, 19 and 21**), there was evidence of population of their triplet states because lutetium is a large diamagnetic metal. This encourages intersystem crossing of the singlet excited states of the complexes to the triplet states. The triplet decay curves of all the complexes were consistent with first order kinetics. Fig. 3.8 shows the triplet decay profile of complex **14** in DMSO.

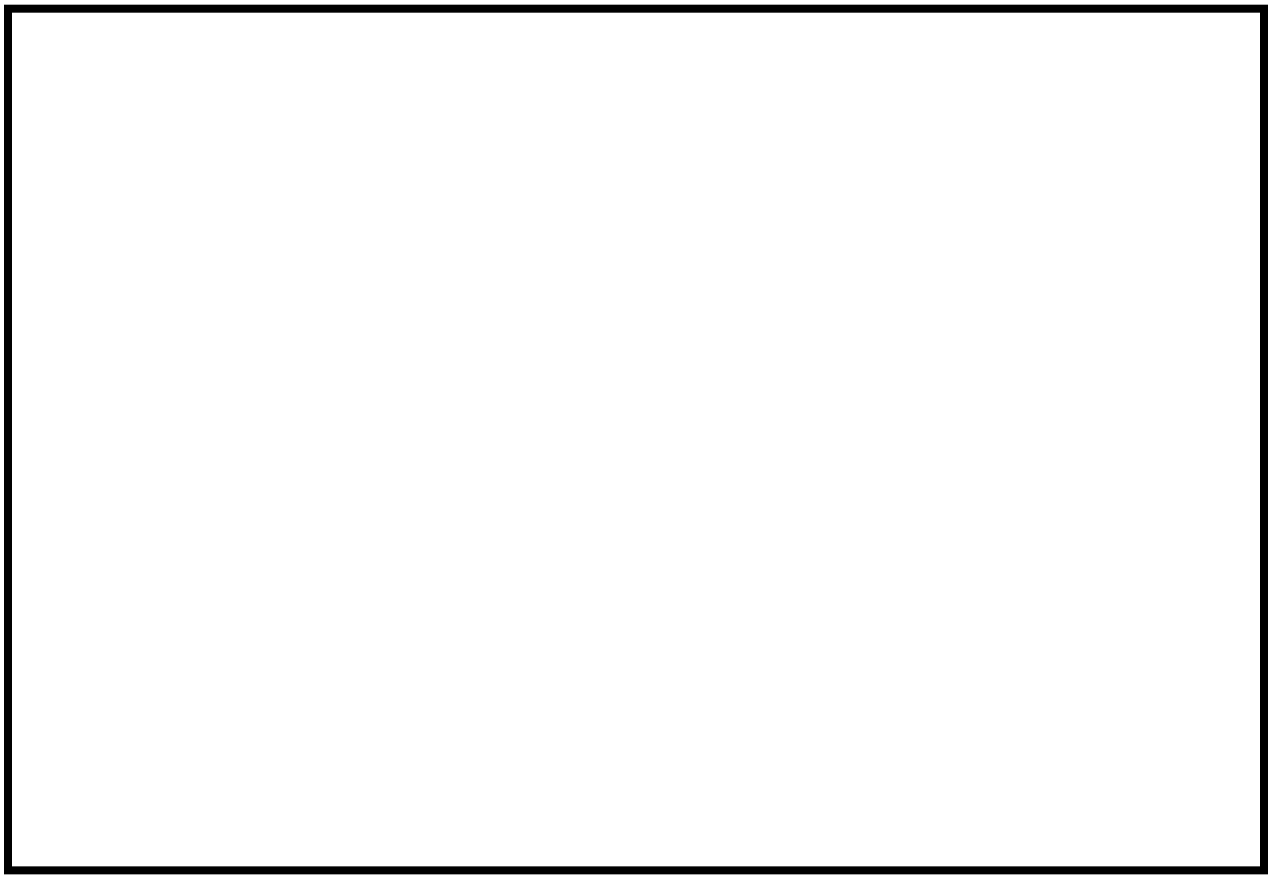

Figure 3.8: Triplet decay curve of complex 14 in DMSO at 490 nm. Excitation wavelength = 682 nm.

The triplet quantum yields and the corresponding lifetimes of the lutetium phthalocyanines are listed in Table 3.4. The triplet state quantum yields of the complexes presents a good possibility of them generating singlet oxygen. The lowest Φ_T

was for complex **21** due to the quenching of its singlet excited state by the amino groups. The largest Φ_T was observed for complexes **14**, **18a** and **19**. The Φ_T for complex **14** is higher than for **18a**, though both have the phenoxy group. This can be explained in the context of their symmetry. Low symmetry results in large intersystem crossing (ISC) to the triplet state. Phenoxy substituents results in lost of symmetry due to their bulky size. This is more pronounced when they are at the α position due to steric hinderance [247], hence the observed higher Φ_T for complex **14** compared to **18a**, **18b**, **18c** and **19**.

The triplet lifetimes of all the phthalocyanines were generally low due to the large central metal. The effect of solvent on the triplet lifetimes is shown using complex **14** as an example, Table 3.4. In DMSO its triplet lifetime is longer (25 ± 0.60 μs) than in DMF (3.10 ± 0.03 μs). Such an observation has also been made before [248].

Table 3.4: Triplet quantum yield (Φ_T), triplet lifetime (τ_T) and singlet oxygen quantum yield (Φ_Δ) of the lutetium complexes in DMF unless otherwise stated.

Complex	Triplet quantum yield (Φ_T)	Triplet lifetimes (τ_T)/μs	Singlet oxygen quantum yield (Φ_Δ)
14	0.83[a] 0.78	25.00 ± 0.60[a] 3.10 ± 0.03	0.71[b] (optical method) 0.63
18a	0.71	2.60 ± 0.01	0.68
18b	0.51	2.70 ± 0.01	0.33 (optical method)
18c	0.68	2.64 ± 0.01	0.62
19	0.73	3.21 ± 0.04	0.64
21	0.43	3.74 ± 0.01	0.29

[a] values in DMSO [b] values in THF

3.2.3. Singlet oxygen quantum yields (Φ_Δ)

Singlet oxygen quantum yield (Φ_Δ) values are expected to depend on the corresponding triplet quantum yield (Φ_T) values of the photosensitizer. That is if the triplet state of a photosensitizer is populated, it can then interact with ground state triplet molecular oxygen exciting it to its singlet excited state. In this work, the singlet oxygen quantum yields of the complexes were determined using either a chemical method or an optical method bases on time-resolved near-IR phosphorescence decay of singlet oxygen. Complexes $DyPc_2$ (**15**) and $ClErTPPc^{\alpha}$ (**17**) have no observed triplet state population as

stated above, due to the open-shell, paramagnetic nature of Dy^{3+} and Er^{3+}. Hence there was no singlet oxygen generation by these complexes. There were neither a signal corresponding to the phosphorescence decay of singlet oxygen upon irradiating them with laser light nor were there changes in the DPBF spectra even after long period of visible light exposure in the presence of these complexes in DMF solution.

The lutetium phthalocyanines AcLuTPPc$^{\alpha}$ (**14**), AcLuTPPc$^{\beta}$ (**18a**), AcLuTPyPc$^{\beta}$ (**18c**) and AcLuTmPyPc$^{\beta}$ (**19**) gave reasonably high singlet oxygen quantum yields, corresponding to high Φ_T, Table 3.4. For **18b** and **21**, low Φ_Δ values were obtained which also correspond to low Φ_T values. The singlet oxygen quantum yields for complexes AcLuTPPc$^{\alpha}$ (**14**) and AcLuTCPPc$^{\beta}$ (**18b**) were determined by the phosphorescence decay of singlet oxygen at 1270 nm in THF and DMF respectively. Fig. 3.9 shows the singlet oxygen decay profile for AcLuTPPc$^{\alpha}$ (**14**) in THF. The singlet oxygen quantum yield of AcLuTPPc$^{\alpha}$ (**14**) was also determined by the chemical method using DPBF as quencher, Table 3.4.

Figure 3.9: Singlet oxygen phosphorescence decay profile for AcLuTPPc$^{\alpha}$ (14) in THF.

For the other lutetium phthalocyanines, singlet oxygen quantum yields were determined in DMF using 1,3-diphenylisobenzofuran (DPBF) as quencher. Fig. 3.10 shows the UV-visible monitored decay profile of DPBF in DMF solution containing AcLuTmPyPc$^{\beta}$ (**19**) upon irradiation with visible light. The two methods have been compared and found to give quite similar results.

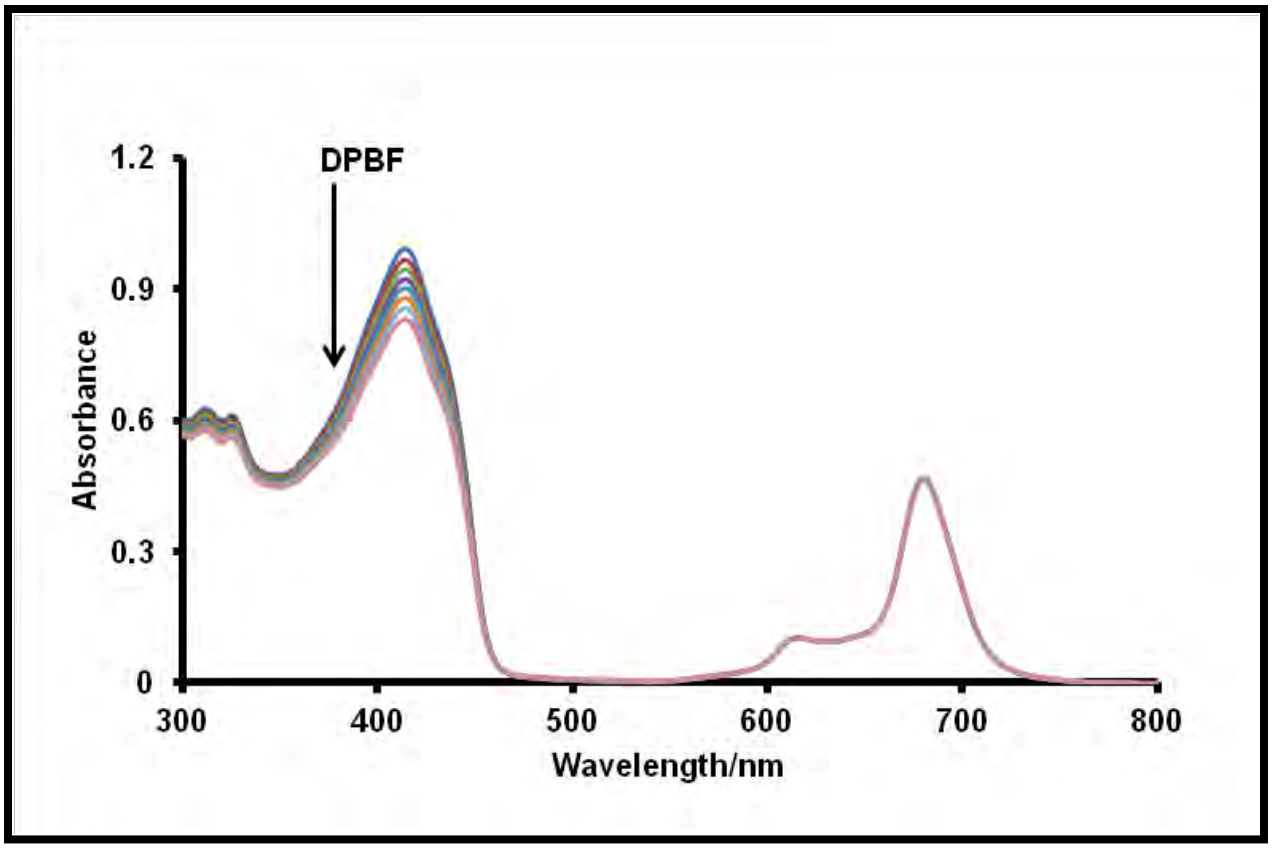

Figure 3.10: UV-visible spectral changes during degradation of 4.3 x 10^{-4} mol L^{-1} DPBF using AcLuTmPyPc$^{\beta}$ (19) in DMF. Time interval 5 sec.

There were no changes in the Q-band intensities during the process suggesting that the phthalocyanine was not degraded, but DPBF degraded due to singlet oxygen production by complex. The single oxygen quantum yields obtained for the lutetium phthalocyanines suggest that they are promising photosensitizing agents that could be applied for photoconversion of environmental pollutants such as phenols and azo dyes.

3.3. Remarks on chapter

Dysprosium bis-phthalocyanine and monomeric erbium phthalocyanines studied in this work did not show triplet state decay curves and their fluorescence quantum yields

Φ_F were found to be very low. Thus they can neither be applied in photoconversion of analytes where generation of singlet oxygen is required nor be applied in fluorimetric detection of analytes. On the hand the lutetium phthalocyanines were found to be photoactive and promising photosensitizers for the conversion of environmental pollutants such as phenols and dyes. However their low fluorescence limits them as fluorimetric agents for detection of analytes.

In further work therefore, zinc phthalocyanines, ZnTPyPc$^{\beta}$ (**23**) and ZnTmPyPc$^{\beta}$ (**24**) including the unsubstituted zinc phthalocyanine which are known photoactive and fluorescent agents were used alongside the lutetium phthalocyanines for detection and/or phototransformation of environmental pollutants. The phthalocyanines were first incorporated into electrospun polymer fibers and characterized as discussed in the next chapter.

Chapter 4

4. Electrospun polymer fibers

4.1. Influence of electrospinning conditions on morphorlogy of polymer fiber

Electrospun polymer fibers have a wide range of applications due to their porosity, small pore sizes and high surface area [249-252]. However, their uniformity and morphology during the production processes are heavily dependent on a number of factors. In this work, prior to functionalization of the electrospun polymer fibers with phthalocyanines for various applications, the effect of some of the electrospinning conditions (polymer concentration, relative humidity, tip-to-collector distance and solvent ratio) on the morphology of the fibers were investigated using polyamide 6.9 and polyamide 6.4 as model polymers. These are closely related polymers but differ significantly in some of their physical properties. Average fiber diameters and diameter of the circular deposition of fiber mats were used in this work to assess the effect of these electrospinning conditions. All electrospinning experiments were done at flow rate of 2 mL/h. This study will give a better understanding of how to generate electrospun fibers of other polymers incorporating functional molecules such as phthalocyanines as in this work.

4.1.1. Effect of polymer concentration at various humidity conditions on fiber morphology

The electrospinning processes of the two polymers were significantly affected by the polymer concentrations. It was quite impossible to obtained fibers at very low polymer concentration (6, 8 and 10 %w/w) at all humidity conditions studied as the polymer solutions formed drops. These drops appear significantly at higher humidity particularly for PA 4.6 which is known to be much more hydrophilic than PA 6.9 [253].
Table 4.1 gives the diameters of the circular deposition areas of the PA 4.6 and PA 6.9 solutions. The area of deposition of the fiber mat is particularly important where multi-nozzle jets are to be applied for large scale industrial production. The diameters are those of the fiber mats for each polyamide solutions that could be electrospun at steady state. The stable Taylor cone obtained resulted in uniform and reproducible electrospun fibrous structures with defined area of fiber mat for each polymer concentration.

The concentration of PA 4.6, did not really affect the area of deposition particularly at 50 and 70% relative humidity conditions. However the area was influenced by the relative humidity, decreasing with increasing humidity for all PA 4.6 concentrations. This may indicate that the water molecules adsorbed at the jet surface homogenize the charge density, which results in a steady Taylor cone with a smaller base area [253].
On the other hand, the area of deposition for fiber mats of PA 6.9 was less affected by both the relative humidity and polymer concentration, as no clear trends are noticeable. The reason may be found in the lower affinity of PA 6.9 to water. Electrospun fibers of

PA 6.9 have a significantly lower moisture absorption [253] and lower wicking rate [254] compared to PA 4.6.

Table 4.1: The diameters (cm) of the circular deposition as a function of the polyamide concentration and the relative humidity, solvent ratio was 50:50 of formic acid (FA)/acetic acid (AA).

Polymer conc./%w/w	P.A 4.6			P.A 6.9		
	10% RH	50% RH	70% RH	10% RH	50% RH	70% RH
12	3.3	2.8	2.4	2.2	2.8	2.8
14	3.7	3.0	2.5	2.2	2.8	2.8
16	3.1	3.1	2.3	2.4	2.6	2.6
18	2.8	2.8	2.3	2.4	2.6	2.4

The average fiber diameters of the electrospun fibers of both polymers were used also to assess the effect of polymer concentration and humidity. The fiber diameters generally increased with increasing polyamide concentration for both PA 4.6 and PA 6.9, at each relative humidity, Table 4.2. This is consistent with other works [255, 256]. The changes were much more dramatic for electrospun fibers of PA 4.6 than those of PA 6.9. Again the effect of relative humidity was very significant on the average fiber diameters of both polymers, generally decreasing with increasing humidity. Polymer solutions of

P.A 4.6 were virtually solidifying (drying up) especially at higher polymer concentrations resulting in very large fiber diameters.

Table 4.2: The average fiber diameter (nm) as a function of the polyamide concentration and the relative humidity. solvent ratio was 50:50 of FA/AA.

Polymer conc./%w/w	P.A 4.6			P.A 6.9		
	10% RH	50% RH	70% RH	10% RH	50% RH	70% RH
12	151 ± 27	83 ± 14	72 ± 10	209 ± 58	104 ± 32	93 ± 41
14	310 ± 30	167 ± 19	136 ± 24	214 ± 36	147 ± 40	128 ± 37
16	531 ± 62	198 ± 15	154 ± 14	353 ± 13	186 ± 43	171 ± 26
18	734 ± 122	250 ± 20	208 ± 18	413 ± 55	317 ±72	214 ± 35

4.1.2. Effect of tip-to-collector distance (TCD)

The distance between the tip of the capillary needle and the collector plate for the fiber mat also influences the morphology of the fibers. In this work collector distances (6 and 10 cm) were used at different relative humidity for the two polymers. Table 4.3 presents a typical data obtained in this work for P.A 4.6.

Table 4.3: Comparison of fiber diameters of P.A 4.6 at 6 and 10 cm tip to collector distance (TCD).

% FA solvent (FA:AA)	10% Humidity	50% Humidity	70% Humidity
	Ave fiber diameter/nm	Ave fiber diameter/nm	Ave fiber diameter/nm
30	321 ± 49[a] 315 ± 33 [b]	155 ± 19 [a] 134 ± 23 [b]	114 ± 21 [a] 116 ± 19 [b]
40	288 ± 30 [a] 256 ± 39 [b]	167 ± 22 [a] 139 ± 20 [b]	112 ± 25 [a] 130 ± 16 [b]
50	310 ± 35 [a] 309 ± 41 [b]	161 ± 19 [a] 141 ± 17 [b]	136 ± 24 [a] 160 ± 32 [b]

AA = acetic acid FA = formic acid TCD = tip-collector distance

[a] diameters at 6 cm TCD [b] diameters at 10 cm TCD

As indicated on Table 4.3, the fiber diameters were found to generally decrease with increasing tip-to-collector distance. This is expected since the polymer drop from the Taylor cone is stretched for a longer distance before being deposited as fiber mater under the same applied potential. However the area of fiber mat deposition was found to increase with the collector distance. This is not desirable as a uniform fiber mat with the same packing density cannot be obtained.

4.1.3. Effect of solvent ratios in polymer solutions and humidity conditions

The two polymers were dissolved in solvent mixtures of formic acid (FA) which acts a solvent for polymers and acetic acid (AA) which is a non-solvent but is required for the electrospinning to occur, with different ratios. As shown in Table 4.4, at 10% relative humidity, the fiber diameters of P.A 4.6 generally increased with decrease in the formic acid content. At the extreme content of 40% formic acid, the polymer solution dried up without fiber formation. However, for P.A 6.9, no clear pattern was obtained though the solution equally dried up at 40% formic acid content. As the relatve humidity was increased to 50 and 70%, a better pattern of increasing fiber diameters with decrease in formic acid content was observed in both cases. This can be attributed to the fact that formic acid is the solvent that dissolved the polymers. Reduction in its content in the solvent mixture results in an unforeseen high concentration of the polymers in solution leading to the larger fiber diameters observed. Also a steady state Taylor cone, from observation, could only be obtained at 50 and 60% formic acid content. This is a fundamental condition for producing electrospun polymer fibers which are expected to be uniform in diameter and other morphological characteristics.

Table 4.4: The average fiber diameters (nm) as a function of the percentage formic acid and the relative humidity, the polyamide concentration was 14 wt% PA.

Percentage FA/%v/v	P.A 4.6			P.A 6.9		
	10% RH	50% RH	70% RH	10% RH	50% RH	70% RH
90	144 ± 21	129 ± 17	80 ± 15	275 ± 25	135 ± 20	124 ± 20
80	251 ± 42	147 ± 18	130 ± 22	288 ± 19	158 ± 25	125 ± 16
70	321 ± 42	155 ± 19	114 ± 21	306 ± 35	187 ± 38	122 ± 14
60	288 ± 30	167 ± 22	112 ± 25	268 ± 21	170 ± 30	134 ± 27
50	310 ± 33	161 ± 19	136 ± 24	207 ± 41	149 ± 28	174 ± 28
40	--	231 ± 63	114 ± 25	--	152 ± 29	122 ± 42

Thus by optimizing all the above conditions, suitable electrospun polymer fibers functionalized with phthalocyanines possessing appropriate morphology can be obtained. Such functionalized fiber can then be applied in gas sensing and photodegradation of environmental pollutants which are core aims of this work.

4.2. Characterization of electrospun polymer fibers functionalized with lutetium and zinc phthalocyanines and their physico-chemical behavior

This section discusses the characterization of both covalently linked and physisorbed Pc/ polymer fibers. The choice of the polymers in this work was guided by their ability

to either covalently bind the phthalocyanine or interact strongly through their extensive aromatic systems.

For non-covalently linked functionalized fibers, the complexes used are **14**, **18a**, **18c**, **19**, **23** and **24** since they do not have functional groups for covalent linking. Polystyrene (PS) and polysulfone (PSU) do not also have appropriate functional groups. AcLuTCPPcβ (**18b**) and MTAPcβ (**21** and **22**) were employed for conjugation to polyurethane (PUR) and polyacrylic acid (PAA) respectively. Polyurethane (PUR) covalently binds to the carboxylic acid group of **18b** through an amide bond. Similarly polyacrylic acid binds to the amino groups of **21** and **22**. Though the covalent bond formation ensures that the phthalocyanine is tightly bound to the polymer, it limits the number of phthalocyanine molecules that can be held by the polymer. On the other hand, polystyrene (PS) and polysulfone (PSU) have extensive aromatic systems that can interact with that of the phthalocyanines. This might not bind the phthalocyanines molecules as tightly as with covalent bond formation. However, it has the advantage that different amounts of the phthalocyanines can be placed on the polymer until the onset of leaching of the phthalocyanine from the polymer.

4.2.1. Elemental analysis- Consistency of composition

This was done to assess the uniformity in composition of the functionalized fibers during production particularly for mixtures of the polymer and the phthalocyanine that are not covalently linked but are held together by sorption forces. This is important

because the phthalocyanines have relatively smaller sizes and are much more electrically conducting compared to the polymer, thus a separation of the composite during the electrospinning process similar to what has been observed in gel electrophoresis is possible [257]. This would result in fibers at different stages of the electrospinning process having different compositions, with fibers at the first stage of electrospinning having higher phthalocyanine content than those at later stages. In order to assess the uniformity in composition of the functionalized electrospun fibers during the different stages of their formation from the mixture of polymer and phthalocyanine, samples of the electropun fibers in each case were collected at different stages of the electrospinning process and analyzed using elemental analyses. Table 4.5 gives typical data of such elemental analysis involving electrospun polystyrene fiber functionalized with complex **14**.

Table 4.5: Elemental composition of samples of PS/AcLuTPPc$^{\alpha}$ (14) composite fiber.

SAMPLE	ELEMENT		
	C	H	N
PS/LuTPPc$^{\alpha}$ (14) 1	92.00	7.621	-
PS/LuTPPc$^{\alpha}$ (14) 2	92.39	7.533	-
PS/LuTPPc$^{\alpha}$ (14) 3	92.19	7.627	0.03

1 = fibers just at the start of formation, 2 and 3 = fibers after 5 and 10 mL of polymer solution has been electrospun respectively.

As indicated, the nitrogen content in the mixture was overshadowed by the high carbon and hydrogen content in the polystyrene and the phthalocyanine. However, the fibers have generally the same composition and are expected to show reproducible behavior in any application. Thus elemental analyses results confirm that there was no separation of the phthalocyanines from the polymers during the fiber formation. One important deduction from the elemental analysis is the fact that the molecules of the phthalocyanine and the polystyrene have interacted strongly through their π-π electrons of their aromatic systems. This was equally observed with other electrospun polymer fibers functionalized with phthalocyanines.

4.2.2. Microscopic characterization

Two geometric properties of the fibers (fiber diameter and morphology) were assessed using SEM technique. The average diameters of the electrospun fibers of each polymer alone and those when functionalized with phthalocyanine were determined using Cell^D software from Olympus.

For polystyrene (PS) polymer, the functionalized fibers contained complexes **14**, **18a**, **18c**, **19** and unsubstituted zinc phthalocyanine. The electrospun fibers of polystyrene alone and those functionalized with the phthalocyanines complexes did not form appreciable amount of beads under the experimental conditions and consist of mostly long unbranched strands of cylindrical fibers as shown in Fig. 4.1. for PS and PS/AcLuTPPc$^{\alpha}$ (**14**) fibers.

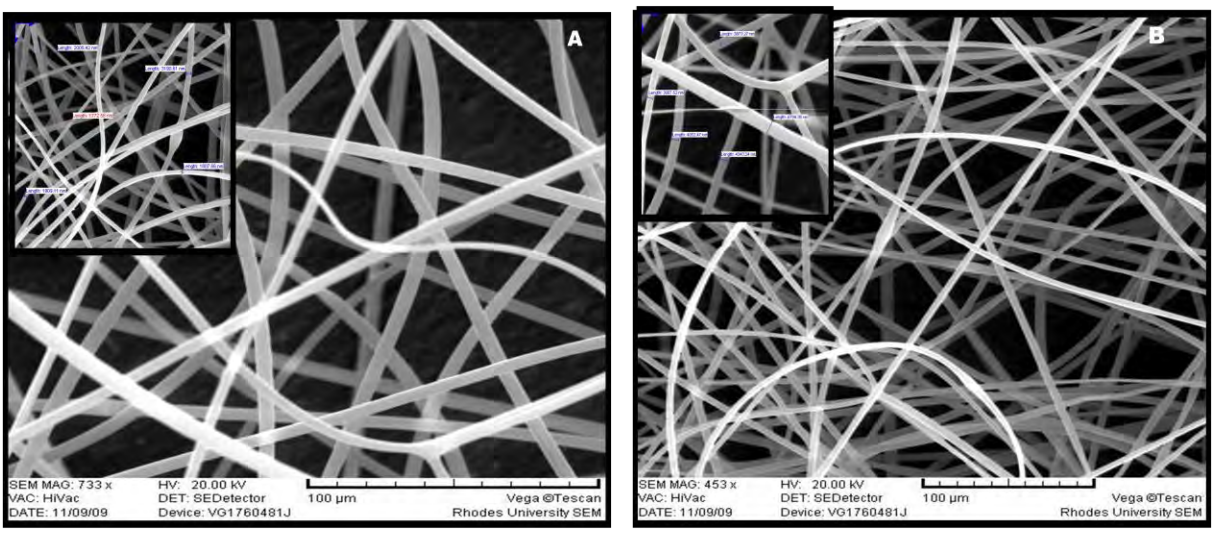

Figure 4.1: Fiber mat of (A) PS alone and (B) PS/AcLuTPPc$^{\alpha}$ (14) composite at 100 µm resolution and insert is 50 µm resolution.

The fiber diameters of the polystyrene alone ranged from 1800-3200 nm (1.8-3.2 µm). These fiber diameters were thinner than those obtained (3.52-4.09 µm) by Pai C.-L. *et al*. [258], using DMF alone as solvent, instead of THF:DMF solvent mixture used in this work. This is expected because higher concentration of the polymer in the solvent, 30%, was used in their case, while polymer concentration of 25% was used in the present work. This observation is consistent with theory which predicts that the fiber diameter depends allometrically on solution viscosity [255, 256]. Table 4.6 shows the average diameters of the other polystyrene polymer fibers functionalized phthalocyanines in this work.

Table 4.6: Average fiber diameters of electrospun polystyrene polymer fibers functionalized with phthalocyanines.

Electrospun fiber	Average diameter/ μm	Standard deviation
PS alone	**1.56**	**0.40**
PS/AcLuTPPc$^{\alpha}$ (14)	**1.73**	**0.51**
PS/AcLuTPPc$^{\beta}$ (18a)	**1.66**	**0.35**
PS/AcLuTPyPc$^{\beta}$ (18c)	**1.79**	**0.60**
PS/AcLuTmPyPc$^{\beta}$ (19)	**1.80**	**0.47**
PS/ZnPc	**1.63**	**0.32**

For electrospun fiber of polyacrylic acid functionalized with complexes **21** and **22** the conjugates were formed through an amide bond involving the NH_2 group of AcLuTAPc$^{\beta}$ (**21**) or ZnTAPc$^{\beta}$ (**22**) with the carboxylic acid groups of PAA. Their electrospun fibers were generally cylindrical and unbranched with relatively wide diameter range, Fig. 4.2. In the case of non functionalized PAA fibers, the diameters ranged from 124-930 nm, while the range for PAA/AcLuTAPc$^{\beta}$ (**21**) was 153-1356 nm and 130-1309 nm for PAA/ZnTAPc$^{\beta}$ (**22**). The fibers of PAA alone had a number of beads (circled), Fig. 4.2. However those of the functionalized AcLuTAPc$^{\beta}$ (**21**) and ZnTAPc$^{\beta}$ (**22**) fibers had virtually no beads. This could be accounted for by the fact that phthalocyanines are high charge density aromatic macromolecules. Thus their presence

in the functionalized polymer solution will lead to an increase in charge density. Such an increase in the net charge density of polymer solutions during electrospinning has been reported [259] to lead to elimination of beads similar to what has been observed in this work.

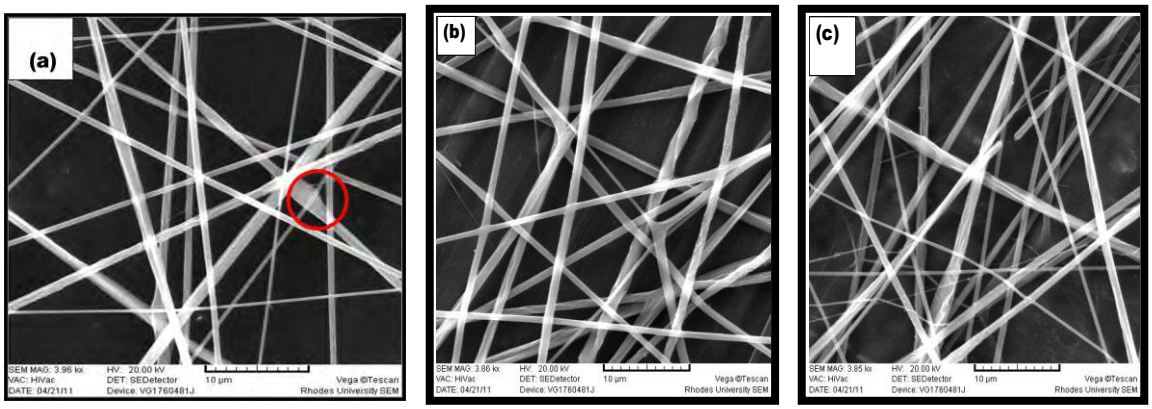

Figure 4.2: Fiber mats of (a) PAA alone, (b) PAA/AcLuTAPcβ (21) composite and (c) PAA/ZnTAPcβ (22) composite. Circle = bead.

The conjugate of polyurethane containing complex **18b** was formed through a covalent amide bond between the N-H group of PUR and the carboxylic group of the AcLuTCPPcβ (**18b**).

Fig. 4.3a shows the SEM image of the electrospun fiber mat of PUR/AcLuTCPPcβ (**18b**) hybrid. The fibers are randomly aligned and are more or less a network of random diameters ranging from 187-5734 nm under the operating conditions. The SEM of PUR alone shows more defined structure, Fig. 4.3b, than for the PUR/AcLuTCPPcβ (**18b**) hybrid**.**

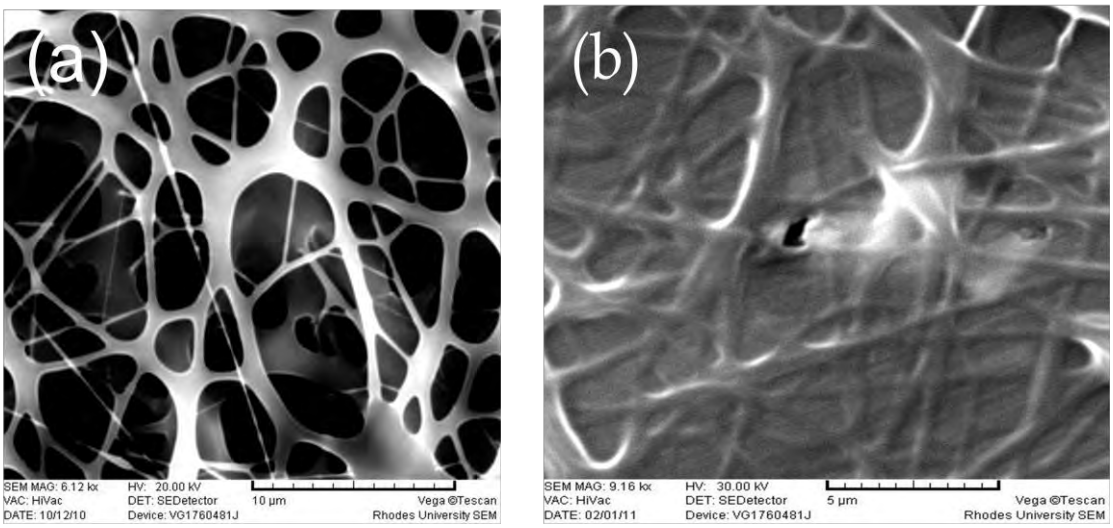

Figure 4.3: Fiber mat of (a) PUR/AcLuTCPPcβ (18b) composite and (b) PUR alone.

4.2.3. Spectroscopic characterization

The covalent attachment was done by first activating the COOH groups of 1**8b** for attachment to polyurethane (PUR) or polyacrylic acid (PAA) for attachment to **21** and **22**. Dicyclohexylcarbodiimide (DCC) was used as coupling agent.

4.2.3.1. FT-IR spectral characterization of covalently conjugated Pc-polymers

The attachment of AcLuTCPPcβ (**18b**) to polyurethane (PUR) is depicted in Scheme 4.1. The covalent attachment of AcLuTCPPcβ (**18b**) to the polyurethane polymer was first assessed using IR spectroscopy by observing changes of various functional groups of polyurethane and AcLuTCPPcβ (**18b**). Fig. 4.4 shows the FT-IR spectra of AcLuTCPPcβ (**18b**) powder (Fig. 4.4a) polyurethane fibers (Fig. 4.4b) and the AcLuTCPPcβ (**18b**) functionalized fiber (Fig. 4.4c) recorded from 4000 to 650 cm^{-1}.

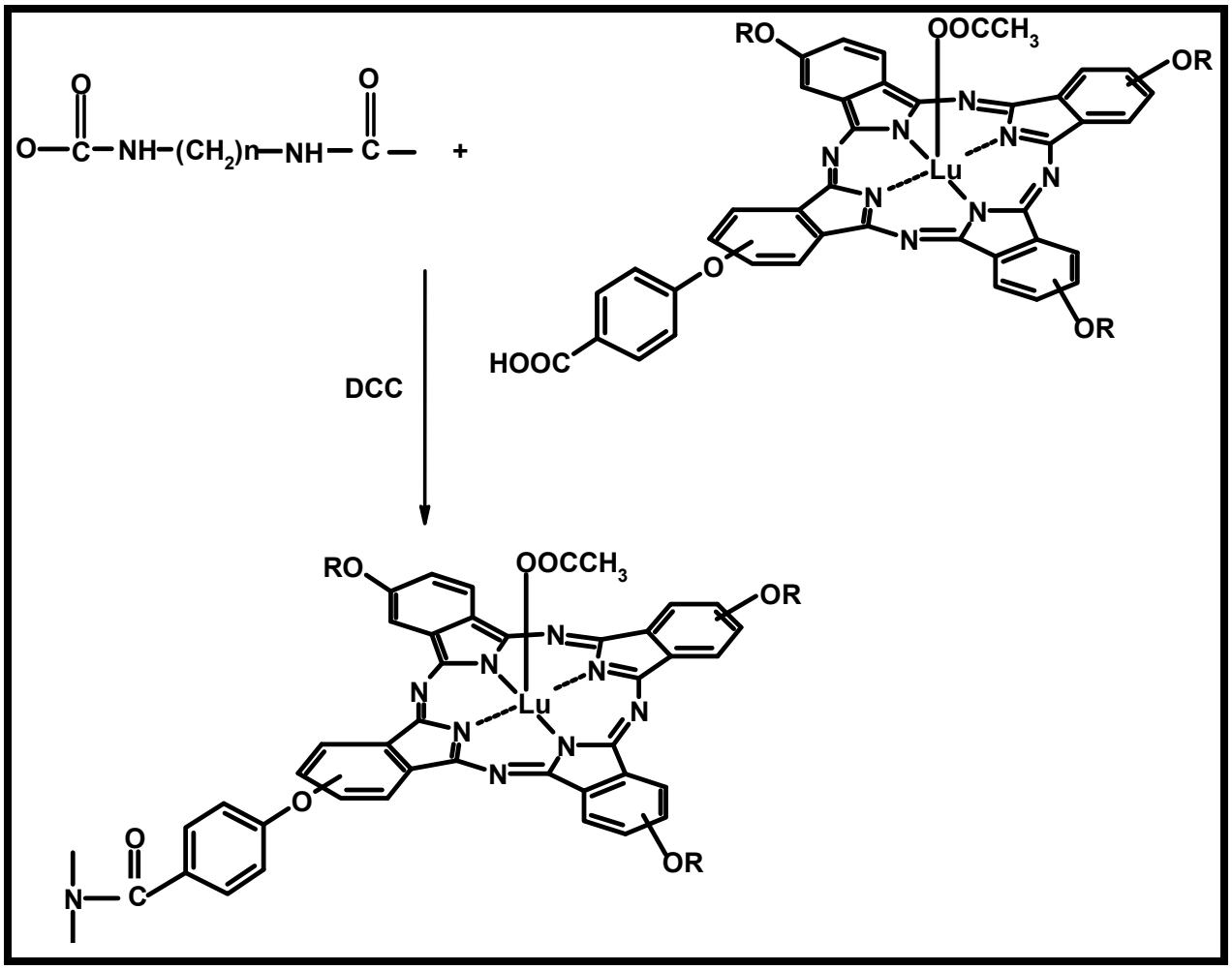

Scheme 4.1: Formation of amide bond between AcLuTCPPcβ (18b) and PUR.

The IR spectrum of PUR fiber (Fig. 4.4b), shows the following peaks: 3316 cm^{-1} is due to weak N-H stretching of a secondary amine; 2932, 2851 and 2790 cm^{-1} are due to C-H stretches, 1704 cm^{-1} is due to the C=O stretch of the amide; 1525 1444 and, 1365 cm^{-1} are due to C-N stretches; peak at 1224 cm^{-1} could be assigned to C-O-C stretching [238].

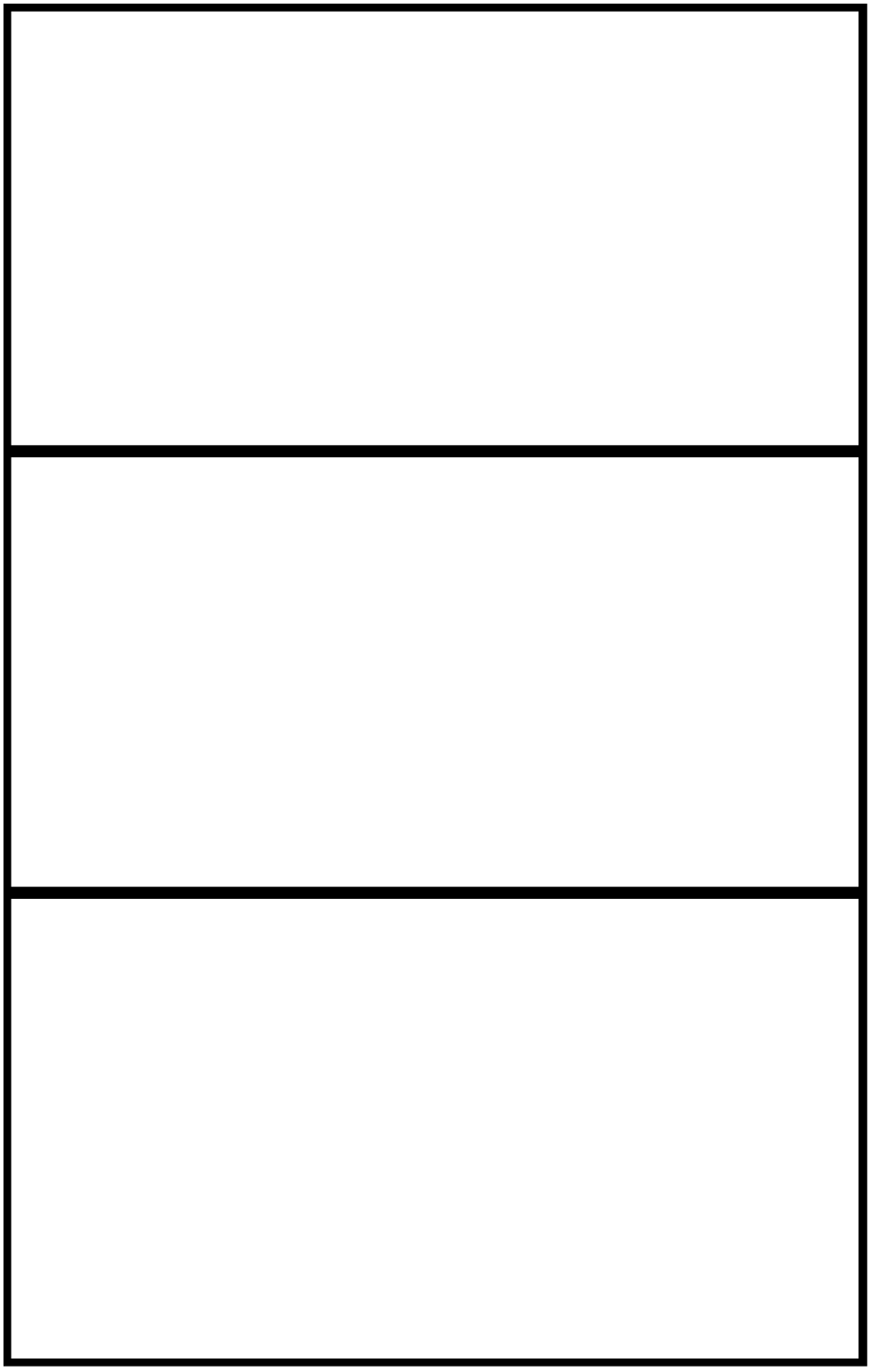

Figure 4.4: FT-IR spectra of (a) AcLuTCPPc$^{\beta}$ (18b) (b) PUR fiber (c) PUR/AcLuTCPPc$^{\beta}$ (18b) hybrid fiber.

In the case of the hybrid fiber (Fig. 4.4c), the disappearance of the broad band at about 3504 cm^{-1} in Fig. 4.4a (for AcLuTCPPcβ (**18b**) alone suggest the cleavage of the hydroxyl group of the acid functional group of AcLuTCPPcβ (**18b**) on covalent amide bond formation with some of the N-H groups of PUR. Also the shift of the carbonyl peak at 1656 cm^{-1} of AcLuTCPPcβ (**18b**) and 1704 cm^{-1} for PUR to 1699 cm^{-1} in the hybrid fiber suggest an electronic interaction involving the carbonyl group of AcLuTCPPcβ (**18b**) due to amide bond formation. This is supported by the shift of the N-H peak position from 3316 cm^{-1}, for PUR, to 3322 cm^{-1} for PUR/AcLuTCPPcβ (**18b**) hybrid. Equally the rest of the existing peaks in Fig. 4.4a and Fig. 4.4b especially those of the phenyl groups have their positions and intensities slightly changed in the hybrid fiber. These are indications that AcLuTCPPcβ (**18b**) molecules are embedded in the hybrid fiber and that there is electronic interaction between the two components. The strong new peak at 2116 cm^{-1} for the PUR/AcLuTCPPcβ (**18b**) fiber (Fig. 4.4c) is attributed to N=C=N stretch originating from some residual bound dicyclohexylcarbodiimide [260] in the hybrid fiber, which was used as a coupling agent .

In the case of polyacrylic acid functionalized with tetraaminophthalocyanines the conjugates were formed through an amide bond involving the NH_2 group of AcLuTAPcβ (**21**) and ZnTAPcβ (**22**) with the carboxylic acid groups of PAA as illustrated in Scheme 4.2 for AcLuTAPcβ (**21**)/PAA composite.

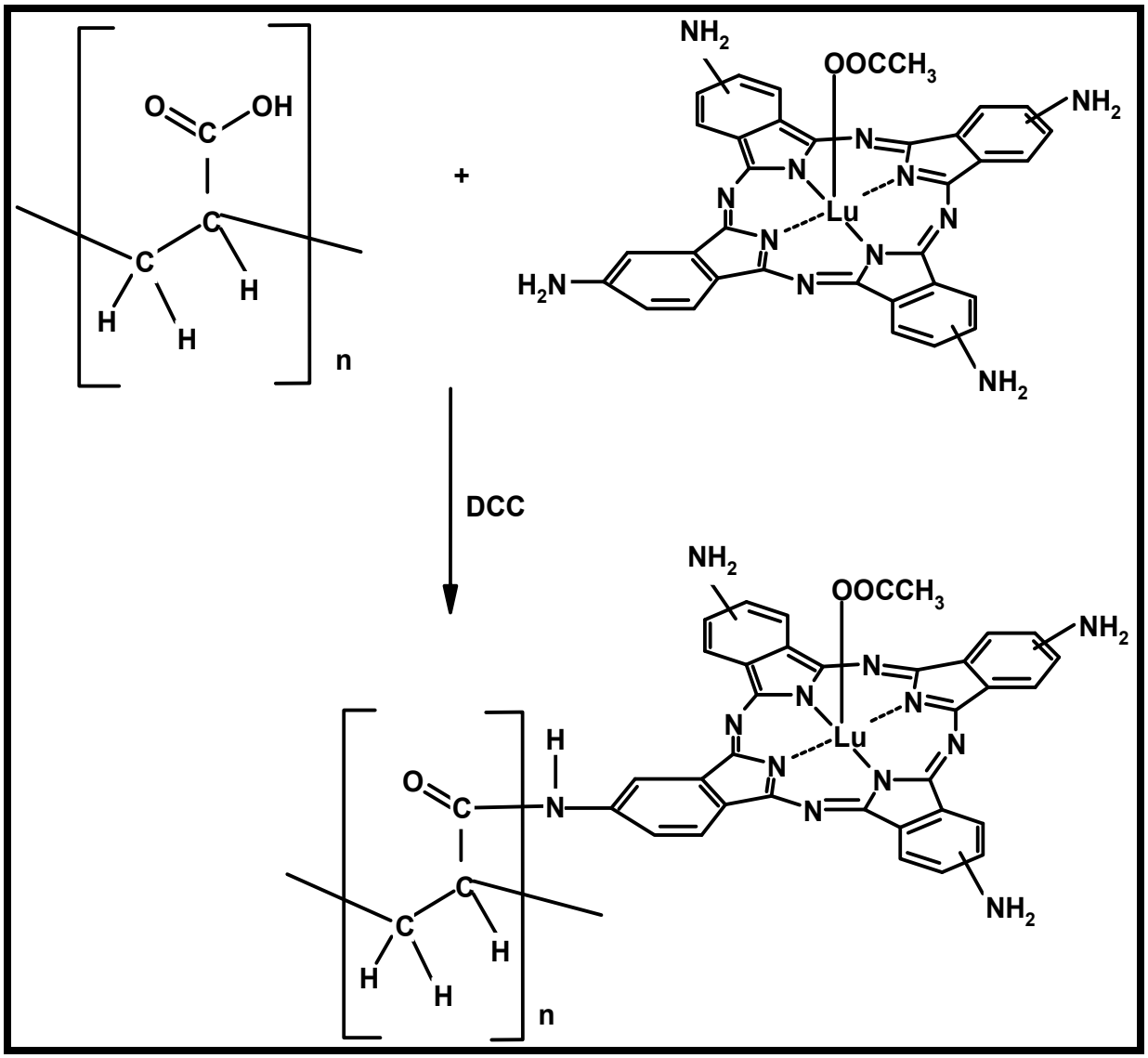

Scheme 4.2: Formation of amide bond between AcLuTAPc$^{\beta}$ (21) and PAA.

The FT-IR spectral features of polyacrylic acid, Fig. 4.5(b), include the broad O-H band around 3100-3600 cm^{-1} and the carbonyl stretching at 1699 cm^{-1}. In the case of AcLuTAPc$^{\beta}$ (**21**), Fig. 4.5(a), the partially split and broad band around 3270-3327 cm^{-1} may be assigned to asymmetric and symmetric stretching vibrations of the amino

groups of the phthalocyanine [223]. This is supported by the intense –NH_2 group in-plane bending vibration observed at 1623 cm^{-1}.

For PAA/ AcLuTAPcβ (**21**) composite, Fig. 4.5 (c), the N-H stretching vibration of the AcLuTAPcβ (**21**) has diminished in intensity, and the corresponding bending mode around 1623 cm^{-1} has almost disappeared. This suggests that the amino groups are engaged in amide bond formation with PAA. The incomplete disappearance of these two bands of the –NH_2 of the phthalocyanine could be due to the fact that not all four amino groups of any particular AcLuTAPcβ (**21**) molecule are engaged in the amide bond formation. There is slight shift of the carbonyl position indicating electronic interactions between the components. Similarly, the position and intensity of the aromatic C-H of AcLuTAPcβ (**21**) as well as it characteristic phthalocyanine C-N vibrations, have their positions slightly changed in the hybrid. These observations jointly suggest that the phthalocyanine molecules are bound within the polymer matrix through electronic interactions.

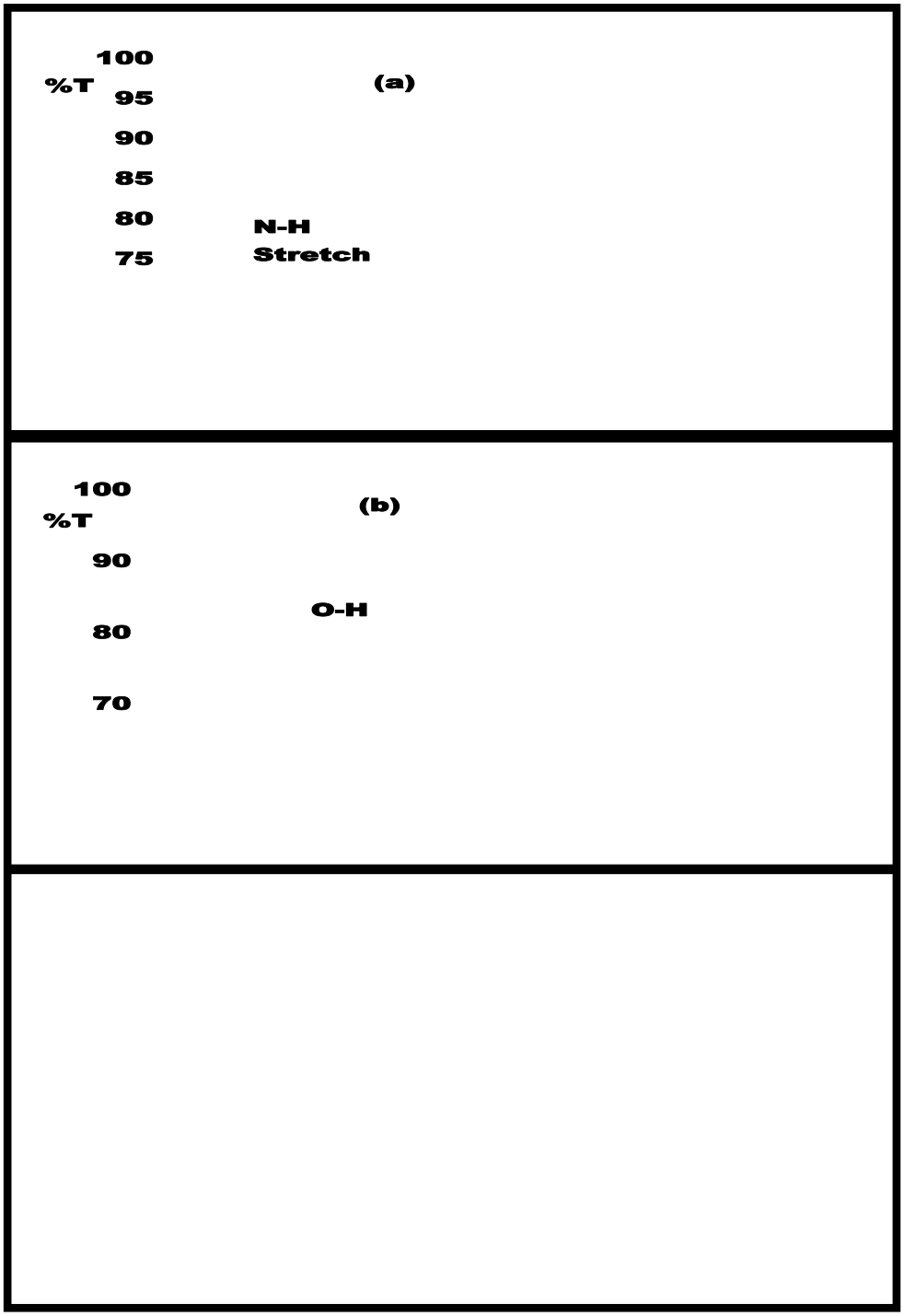

Figure 4.5: FT-IR spectra of fibers (a) AcLuTAPc$^{\beta}$ (21), (b) PAA and (c) PAA/ AcLuTAPc$^{\beta}$ (21) hybrid.

4.2.3.2.Raman spectral characterization

Non-covalently linked

The Raman spectral studies were done in order to ascertain the Van der Waal's electronic interactions between the polymers (PS and PSU) and the phthalocyanines where there is no covalent linkage between the two. Interpretation of these spectra was aided by the theoretical spectrum of the pure polymer obtained from density functional theory (DFT) calculations carried out on a subunit of the polymer. Fig. 4.6A shows the theoretical (a) and experimental (b) Raman spectra of the polystyrene alone.

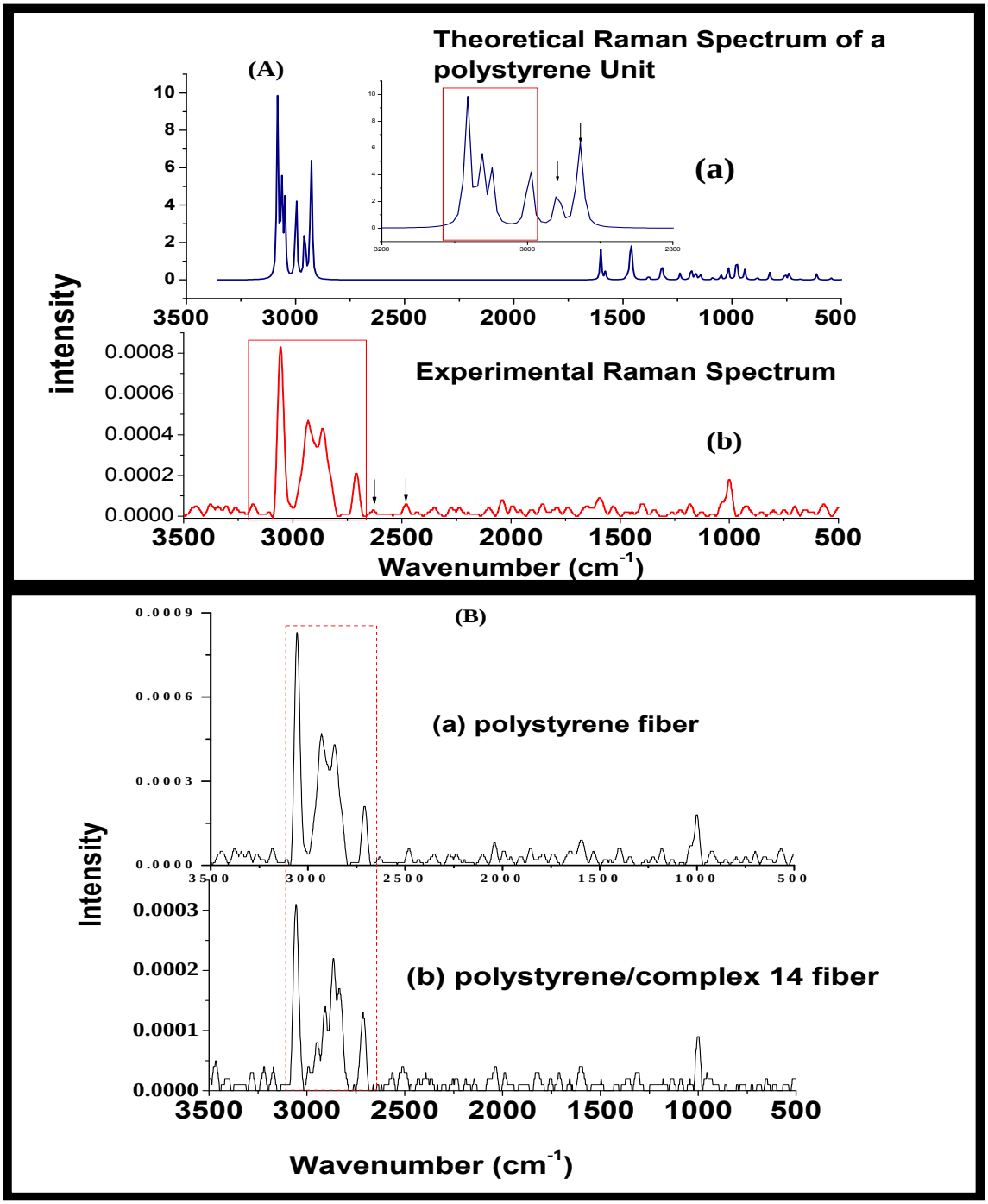

Figure 4.6: (A) Theoretical (a) and experimental (b) Raman spectra of PS and (B) Raman spectra of (a) PS and (b) PS/AcLuTPPc$^{\alpha}$ (14), composite fibers.

Polystyrene was used for these studies due to its extensive aromatic system capable of π-π interaction with the phthalocyanine.

As indicated in Fig. 4.6A, there is a good correlation between the theoretically obtained spectrum and the experimental one. The peaks between 2500 and 3000 cm^{-1} are attributed to stretches due to the aromatic ring of the polystyrene [261], and are consistent with the theoretical calculations. To determine any electronic interaction between the polystyrene and the phthalocyanine, the Raman spectrum of the composite fiber, PS/AcLuTPPc$^{\alpha}$ (**14**), was taken and compared with that of the polymer alone as depicted in Fig. 4.6B. The observed changes in the peak shapes of the PS/AcLuTPPc$^{\alpha}$ (**14**) composite, Fig. 4.6B (b) compared to PS alone, Fig. 4.6B (a) suggest that the phthalocyanine is interacting with the polystyrene aromatic system. This might be due to the strong π-π interactions of the phthalocyanine and polystyrene aromatic systems.

Similar changes in the aromatic region were also observed when AcLuTPPc$^{\beta}$ (**18a**), AcLuTPyPc$^{\beta}$ (**18c**) and AcLuTmPyPc$^{\beta}$ (**19**) were functionalized on the polystyrene polymer fibers. These phthalocyanines were used as examples for all Pcs in this work when non-covalently attached to polystyrene (PS).

Covalently linked

Apart from FT-IR spectroscopy, Raman spectroscopy was also used to establish the covalent linkage of AcLuTCPPc$^{\beta}$ (**18b**) to polyurethane fibers through covalent amide bond formation. As indicated in Fig. 4.7, the Raman spectra of PUR/AcLuTCPPc$^{\beta}$ (**18b**)

conjugate shows amide I, amide II and amide III bands at 1591, 1452 and 1294 cm^{-1} (low intensity) respectively, further confirming the linkage between the AcLuTCPPcβ (**18b**) and PUR. These amide bands are in agreement with what has been observed elsewhere for amides [262, 263]

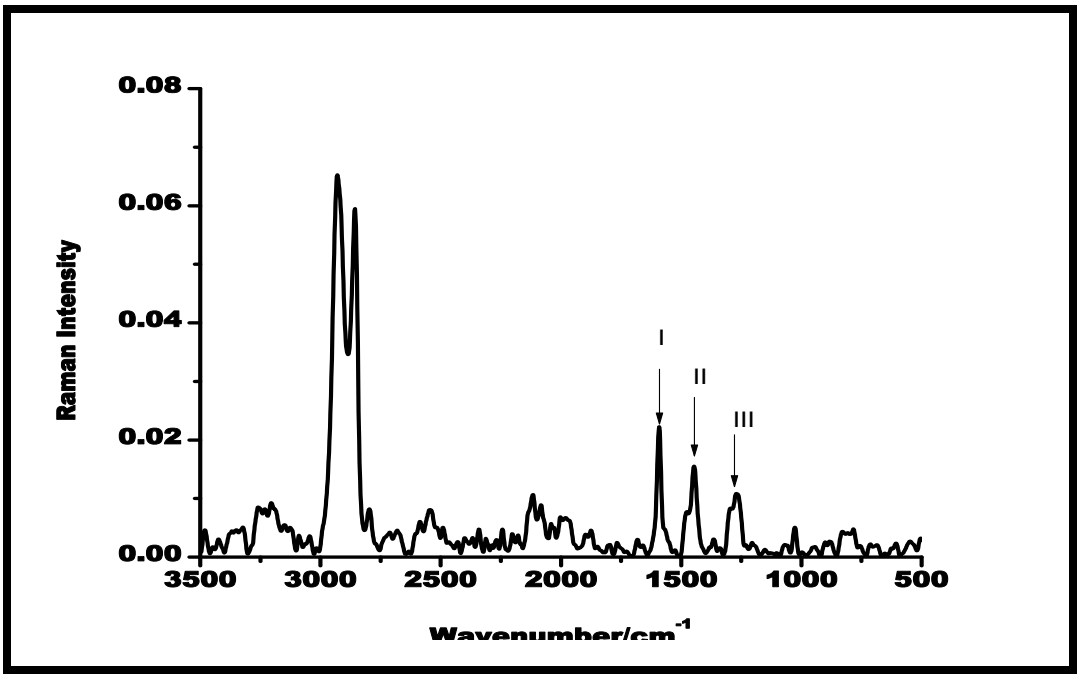

Figure 4.7: Raman spectrum of PUR/AcLuTCPPcβ (18b) composite fiber.

Similarly the covalent amide bond formation between tetraaminophthalocyanine complexes of lutetium and zinc and polyacrylic acid polymer were further established by identification the characteristic Raman bands. Fig. 4.8 shows the spectrum of PAA/AcLuTAPcβ (**21**) conjugate fiber. As shown in Fig. 4.8, the peaks at 1606 cm^{-1} (I), 1445 cm^{-1} (II) and 1298 cm^{-1} which are low in intensities, are the characteristic amide peaks [262, 263].

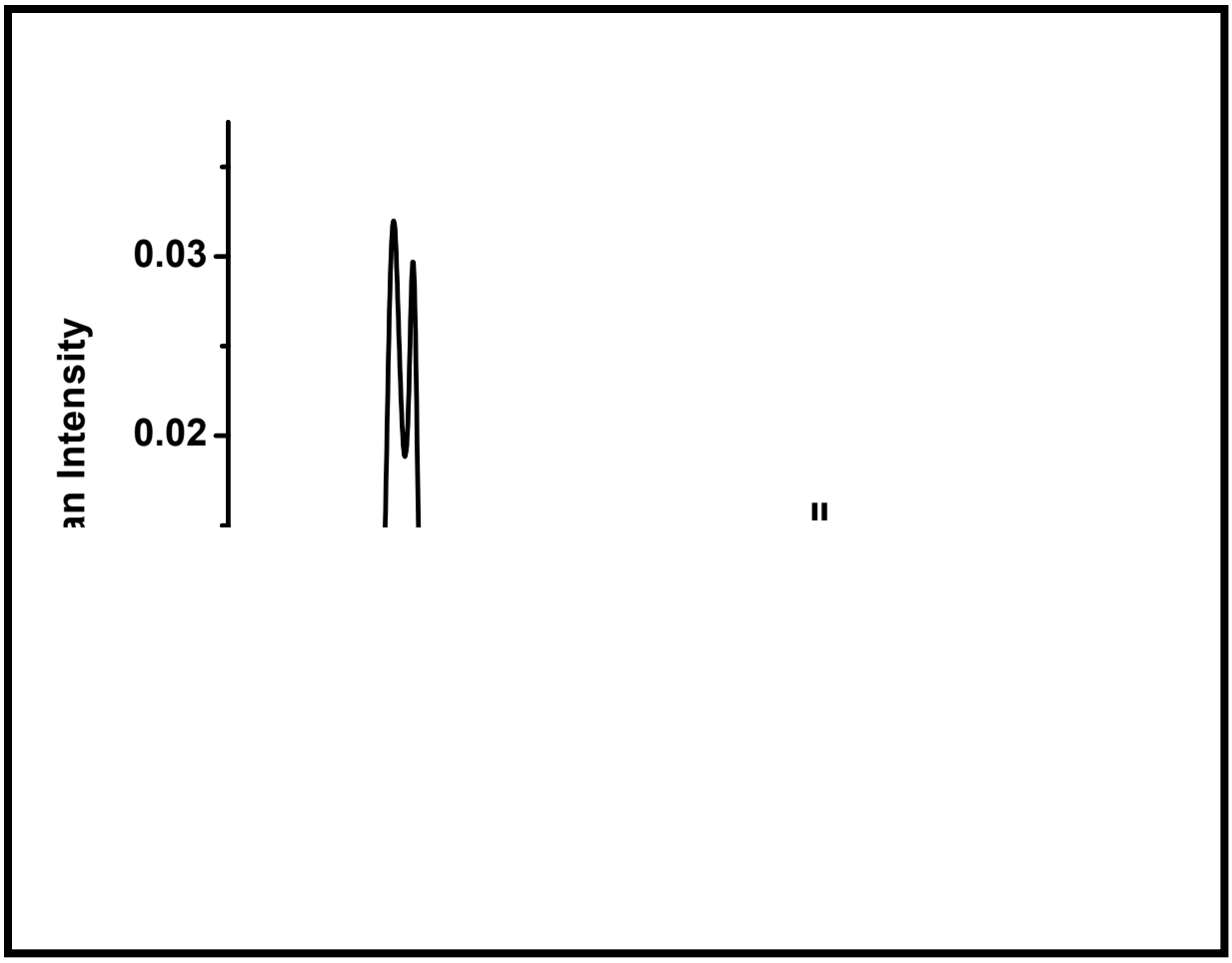

Figure 4.8: Raman spectrum of PAA/AcLuTAPcβ (21) fibers.

4.2.3.3. X-ray diffraction (XRD) spectral characterization

Non-covalently linked

ZnTmPyPcβ (**24**) was embedded in PSU polymer fiber matrix. PSU has aromatic systems and together with the sulphonate groups is capable of both electrostatic and ionc interaction with the complex **24** which ionic. X-ray diffraction was used to determine the presence of the phthalocyanine in the fiber. Figure 4.9 (a) shows the X-ray diffraction pattern of the phthalocyanine alone. The sharp peak around 28.6° is close to

the (002) reflection of carbon [264]. The sharp nature of this peak suggests that the phthalocyanine is quite crystalline which is characteristic of ionic compounds. The XRD pattern for PSU fiber Fig. 4.9 (b) shows a broad peak that suggests that it is not crystalline [265]. For the composite fiber Fig. 4.9 (c), the crystallinity of the ZnTmPyPc$^{\beta}$ (**24**) is lost as a result of the large polymer matrix. Nonetheless, the characteristic phthalocyanine peak clearly appears in the composite indicating the phthalocyanine is embedded within the polymer fiber matrix. Similar XRD patterns were obtained for the other non-covalently linked polymer/Pcs except the amorphous nature of the Pcs resulted in broader peaks for the Pc alone.

Similar X-ray diffraction patterns were obtained for polystyrene polymer fibers functionalized with phthalocyanines.

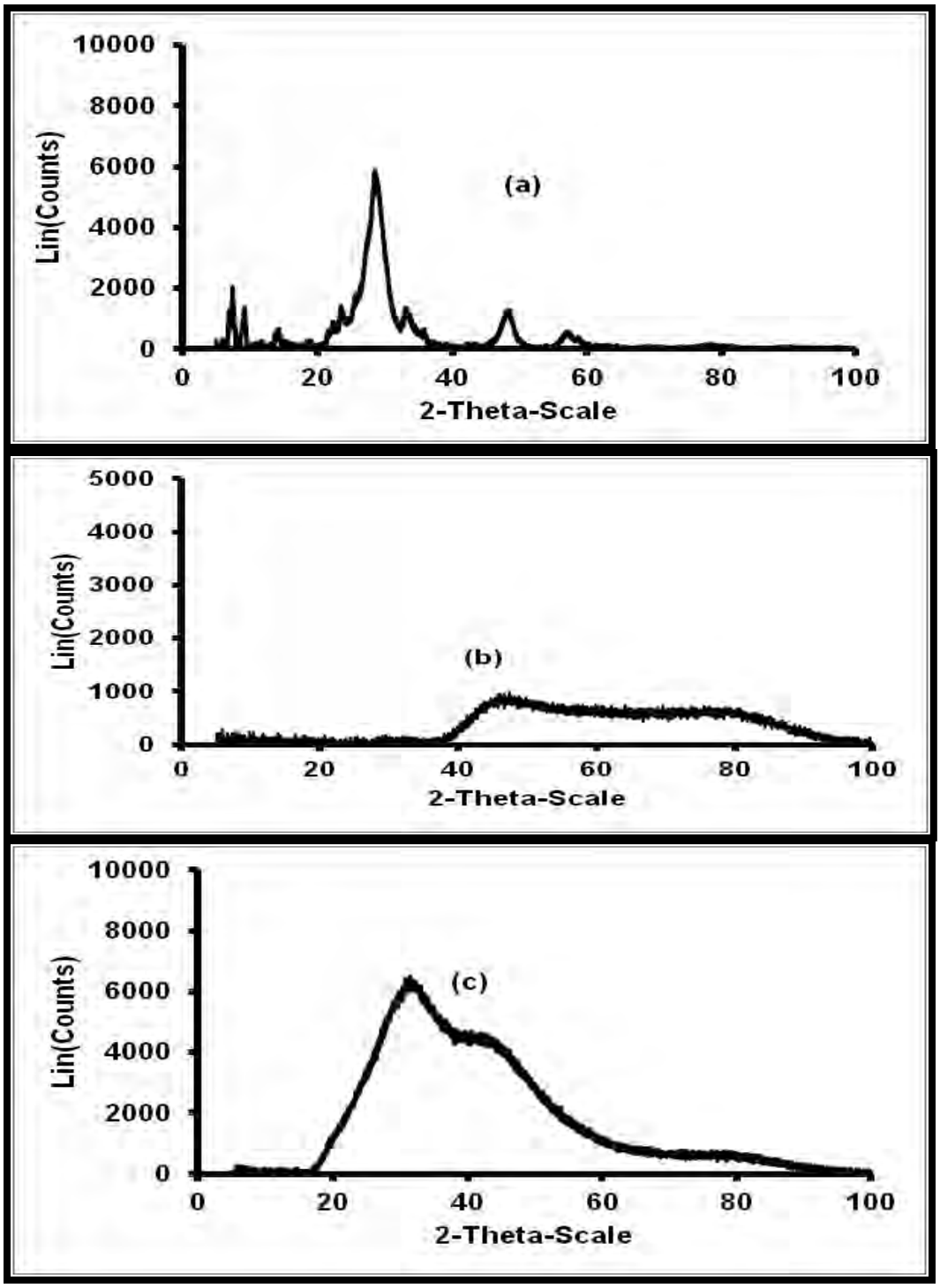

Figure 4.9: X-ray diffraction (XRD) patterns of (a) ZnTmPyPc$^{\beta}$ (24) alone (b) PSU fiber alone (c) PSU/ZnTmPyPc$^{\beta}$ (24) composite fiber.

Covalently linked

The XRD pattern of AcLuTAPcβ (**21**) Fig 4.10 (a) shows a pronounced broad peak covering 2θ = 15 - 30° with maximum occurring around 24°. The broad nature of this peak indicates that phthalocyanine is amorphous. The peak maximum around 24° is close to the (002) reflection plane of carbon [264]. In PAA alone the XRD pattern, Fig. 4.10 (b), shows two broad peaks. In the conjugate there is an overlap of PAA peaks with those of AcLuTAPcβ (**21**), Fig. 4.10 (c). The broadening in all peaks shows the low crystallinity of AcLuTAPcβ (**21**) in both the pure form and within the polymer fiber.

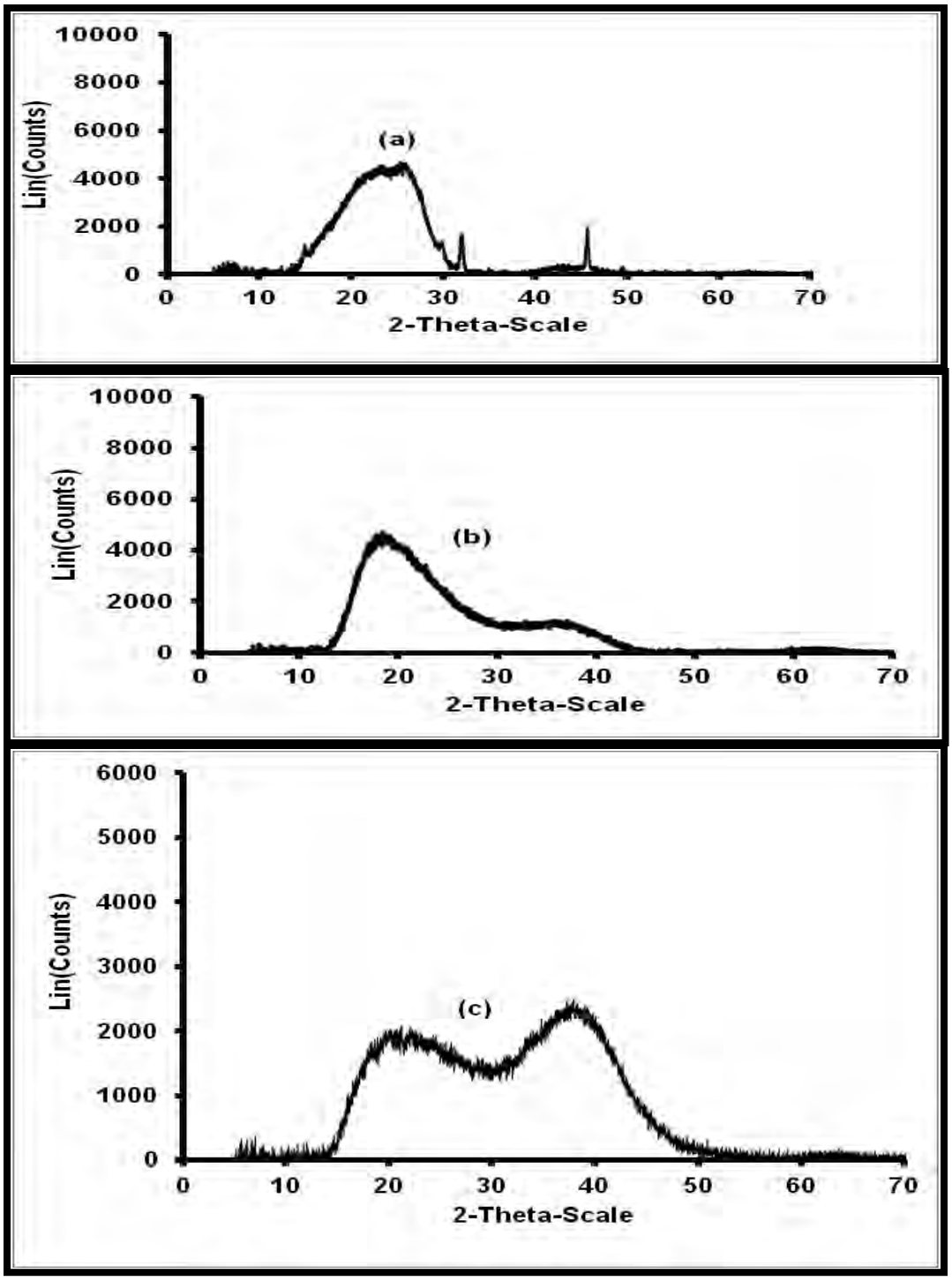

Figure 4.10: X-ray diffraction (XRD) patterns of (a) AcLuTAPc$^{\beta}$ (21) powder, (b) PAA fiber and (c) PAA/AcLuTAPc$^{\beta}$ (21) fiber.

4.2.3.4.UV-visible spectral characterization

Fig. 4.11 shows the electronic absorption spectrum of the AcLuTPPc$^{\alpha}$ (**14**), used as an example, in THF (both PS and the Pc are soluble in THF) together with the solid state electronic spectra of phthalocyanine, polystyrene fiber and that of the PS/AcLuTPPc$^{\alpha}$ (**14**) composite fiber. The spectra of the solid states of AcLuTPPc$^{\alpha}$ (**14**) power and fibers were recorded by placing them on a glass slide.

As shown in Fig. 4.11 (a), the electronic spectrum of AcLuTPPc$^{\alpha}$ (**14**) shows a sharp Q-band absorption maximum of 690 nm in THF. The solid state electronic spectrum of the phthalocyanine alone, Fig. 4.11 (b) shows broadening.

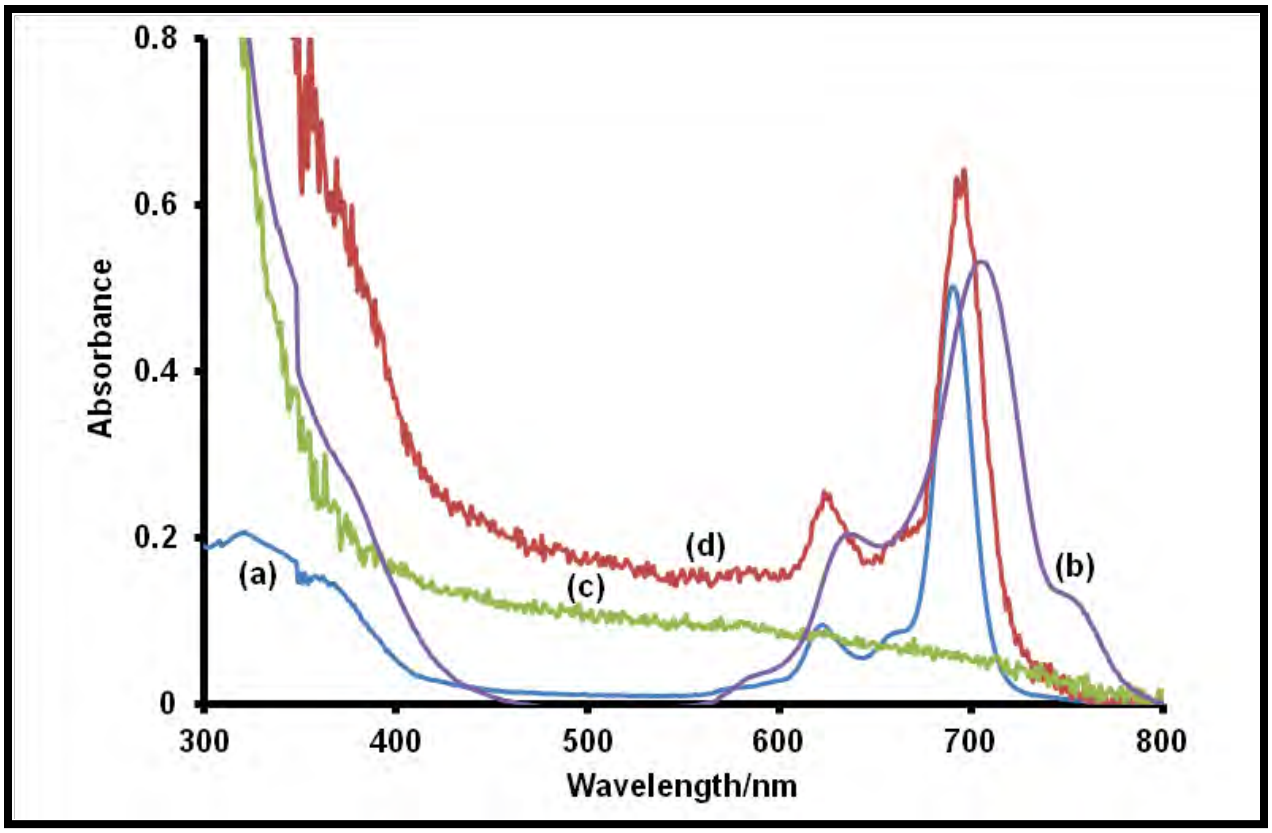

Figure. 4.11: UV-visible absorbance spectra of : (a) 3.8 x 10^{-6} mol L^{-1} AcLuTPPc$^{\alpha}$ (14) in THF solution (b) solid AcLuTPPc$^{\alpha}$ (14) (c) PS fiber (d) PS/AcLuTPPc$^{\alpha}$ (14) composite fiber.

For phthalocyanines in the solid state or on solid support systems, the theory of molecular exciton is usually used to rationalize the differences between the optical spectra in the liquid phase and those in the solid state [266-268].

When more than one phthalocyanine macrocycles are close to each other, whether they are chemically bonded or not, the transition diplole moments can couple (exciton coupling) to cause drastic spectral changes particularly in the Q-band region. Depending on the conformation between the chromophores, shifts of the Q-band

(generally to the blue, while to the red in less common cases), splitting and/or broadening can be observed [269]. The red-shifts of the Q-band have mostly been observed in the solid-state phase where the chromophores are aligned in a slipped-cofacial manner (the degeneracy of Q band is lifted in this arrangement) and can be rationalized in terms of exciton coupling. These differences in spectra of phthalocyanines in the solid state and solution have been reported by other workers [270]. Aggregation in the solid state however does not favor generation of singlet oxygen.

In Fig. 4.11 (c), the non-functionalized polystyrene fibers show no obvious absorption band. However for PS/AcLuTPPc$^{\alpha}$ (**14**), the Q-band absorption is relatively broader and more red-shifted (6 nm) compared to that of the phthalocyanine in THF solution, but less red shifted compared to solid AcLuTPPc$^{\alpha}$ (**14**), Fig. 4.11 (d). It could also be deduced from Fig. 4.11 (d), that the phthalocyanine is uniformly dispersed within the fiber matrix, since there is less broadening (hence less aggregation) compared to solid AcLuTPPc$^{\alpha}$ (**14**).

For further evidence of a uniform dispersal of the AcLuTPPc$^{\alpha}$ (**14**) on the fiber matrix and for possible quantitative applications of the functionalized polystyrene fiber, the electronic spectra of various packing of the fiber were obtained, Fig. 4.12. There is quantitative correlation between the amount of phthalocyanine on the fiber, since doubling the thickness of the fiber on the glass substrate, almost doubles the AcLuTPPc$^{\alpha}$ (**14**) absorbance. This observation also suggests that the composite fiber is

uniform in composition. Similar spectral features were observed for the other functionalized fibers.

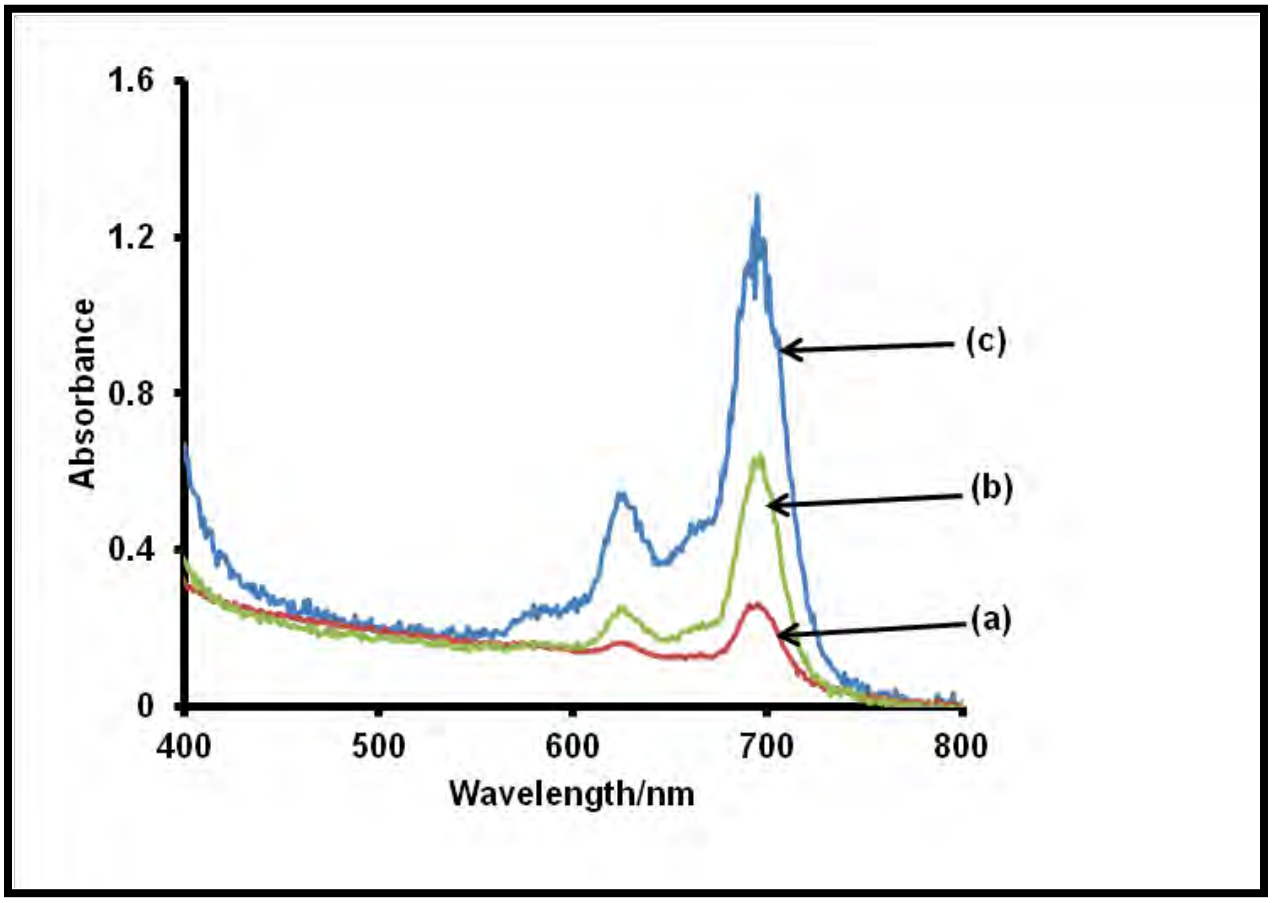

Figure 4.12: Variation of absorbance of the PS/ AcLuTPPc$^{\alpha}$ (14) composite fiber with fiber mat thickness r ≈ 0.1 cm placed on glass plate: (a) r (b) 2r (c) 4r.

4.3. Leaching studies

Leaching has been reported [271] to be a major problem associated with the application of these functionalized electrospun polymer fibers in various solvent media. In this

work, attempt was made to find a suitable solvent in which the functionalized polymer fibers could be applied with minimal or no leaching of the phthalocyanine from the fiber. It was observed that in purely hydrocarbon based solvents such as hexane; there was no leaching or very minimal leaching of the phthalocyanine molecules. Similarly there was no leakage in water for polystyrene, polysulfone and polyurethane electrospun fibers even when non-covalently attached. This suggests that the functionalized fiber can be applied in real-life environment especially in aquatic systems. However, in some organic solvents there is considerable leaching or even a complete dissolution of the fiber to liberate the phthalocyanine. A typical case involving THF, water and hexane as solvent media and complex (**14**) functionalized on polystyrene are shown in Fig. 4.13. As shown, even after 12 h in hexane and 18 h in water, there was no sign of the phthalocyanine in solution and thus hexane and water could serve as a solvent for a heterogeneous catalytic application of the functionalized fibers. Also Pcs do not dissolve in these solvents. However, even ZnTmPyPc$^{\beta}$ (**24**) and AcLuTmPyPc$^{\beta}$ (**19**) did not leach out of the polymers even though they are water soluble. This will be clearer in the photodegradation studies of methyl orange. The integrity of the phthalocyanine is also still maintained in the fiber as shown from the appearance of the Q-band region of spectrum (d) of Fig. 4.13.

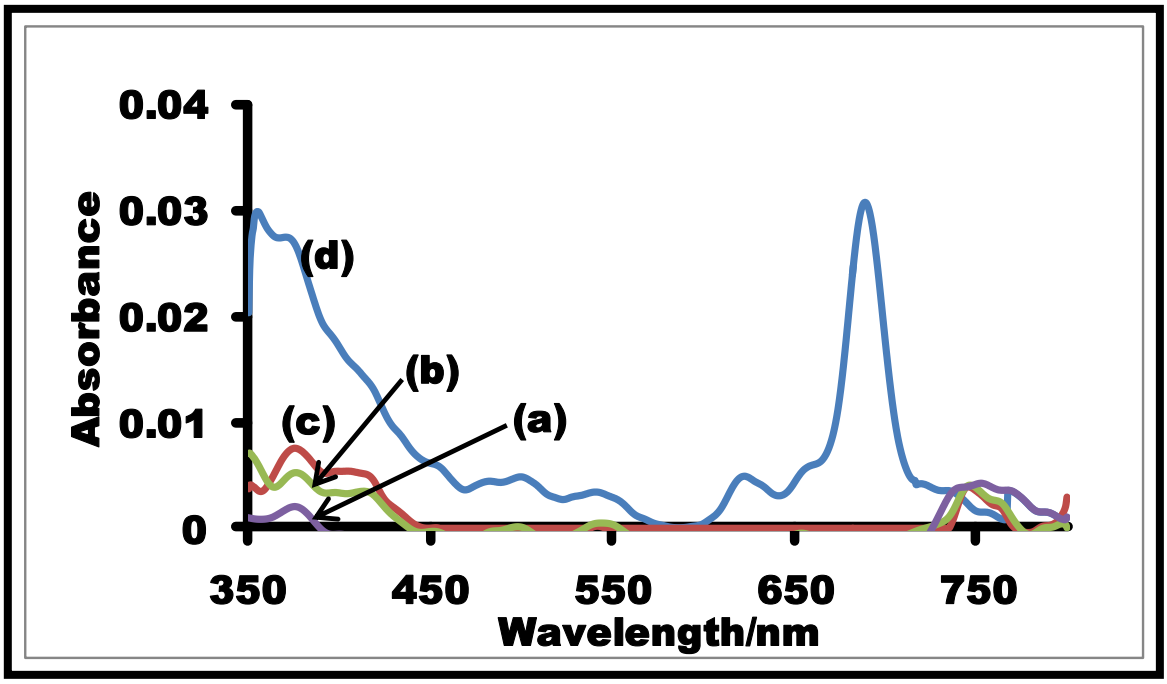

Figure 4.13: UV-visible spectra of PS/AcLuTPPc$^{\alpha}$ (14) functionalized fiber in water, THF and hexane after immersing it in (a) water, 18 h (b) hexane, (4 h) (c) hexane, 12 h (d) THF, momentarily.

4.4. Photophysical and photochemical behavior of the polymer fiber functionalized with metallophthalocyanines

The photophysical and photochemical properties of phthalocyanines functionalized on polymer fibers have been reported to be maintained within the solid polymeric matrix [267]. In this work, the fluorescence behavior of the electrospun polymer fibers functionalized with various phthalocyanines were assessed as well as their photoactivity with the view of possibly using these polymeric materials in gas sensing and/or for photocatalytic conversion of environmental pollutants. Table 4.7 gives fluorescence and singlet oxygen quantum yields of the phthalocyanines in solution as

well as their corresponding single quantum yields estimated within the fiber matrices. This helps in clearer understanding of their comparative behavior in solution and within the solid fiber supports. The Φ_Δ values for the fibers are estimates due to scattering of light discussed in chapter 2. For covalently linked PUR/AcLuTCPPc$^\beta$ (**18b**), Φ_Δ value is low since less Pc was contained in the fiber as the number of Pc molecules on the polymer is restricted by the number of functional groups available. The PSU functionalized fibers have higher singlet oxgen quantum yields than PS functionalized fibers. For instance PSU/ZnPc has a yield of 0.25 which higher than that of PS/ZnPc (0.13). A similar trend was observed for PSU/AcLuTPyPc$^\beta$ (**18c**) and PS/AcLuTPyPc$^\beta$ (**18c**). This could be due to the fact that polystyrene has more extensive aromatic system than polysulfone. Thus the phthalocyanine molecules are much more bound within the polystyrene fiber matrix resulting in decreased photochemical parameters [267].

Table 4.7: Fluorescence and singlet oxygen quantum yields of the phthalocyanines in DMF and within solid polymer fibers.

Complex	Φ_F (DMF)	Φ_Δ		Polymer
		Solution (DMF)	Fiber (water)	
ZnPc	0.30 [30]	0.56 [31,32]	0.25	PSU
			0.13	PS
(Ac)LuTPPc$^{\alpha}$ (14)	<0.01	0.71 (THF)	0.22	PS
(ac)LuTPPc$^{\beta}$ (18a)	<0.01	0.68	0.28	PS
(Ac)LuTCPPc$^{\beta}$ (18b)	0.01	0.33	0.11	PUR
(ac)LuTPyPc$^{\beta}$ (18c)	0.017	0.62	0.17	PS
			0.26	PSU
(ac)LuTmPyPc$^{\beta}$ (19)	0.01	0.64	0.15	PS
(ac)LuTAPc$^{\beta}$ (21)	a	0.29	B	PAA
ZnTAPc$^{\beta}$ (22)	<0.01	0.17	B	PAA
ZnTPyPc$^{\beta}$ (23)	0.23[224]	0.56	0.24	PSU
ZnTmPyPc$^{\beta}$ (24)	0.22[224]	0.59	0.21	PSU

[a]too low to be detected, [b] no value determined – polymer dissolves in water

4.4.1. Fluorescence behavior of the phthalocyanine with solid polymer fibers

The fluorescence behaviors of the phthalocyanines within the fiber were assessed by taking fluorescence micrographs by exciting the functionalized fibers in the Q band region with a high-voltage mercury lamp, Fig. 4.14. The fluorescence of unsubstituted zinc phthalocyanine, a known fluorophore, [84] functionalized on the various polymers was used as reference for the other phthalocyanine functionalized fibers. Fluorescence is judged by the red colour of the fiber under illumination. Electrospun polymer fibers functionalized with unsubstituted zinc phthalocyanine fluoresce, Fig. 4.14 (a-d) even though those of polyurethane fibers seem to be fused together, under excitation. This is consistent with the fluorescence behavior of the phthalocyanine in solution and suggests that the molecules are quite dispersed within the polymer matrices and not stacked together as in the solid state that are usually not emissive [272]. For ZnTAPc$^{\beta}$ (**22**) functionalized fibers, no (or very low) fluorescence has been reported due to the quenching effects of the amino group [223, 240, 273], hence no fluorescence is observed in Fig. 4.14 (a). The same explanation applies to (Ac)LuTAPc$^{\beta}$ (**21**) which is further affected by the heavy atom effect [117], Fig. 4.14 (a). For the other ZnPc derivativies, ZnTPyPc$^{\beta}$ (**23**) and ZnTmPPc$^{\beta}$ (**24**), fluorescence has been reported in solution [224]. Their fluorescence has been maintained in the functionalized fibers as shown in their fluorescence micrographs, Fig. 4.14 (c). The fluorescence intensities are not as strong as that for unsubstituted ZnPc, which is expected since this was also observed in solution.

The lutetium phthalocyanines are generally not emissive in solution due to the large size of lutetium atom which encourages intersystem crossing to the triplet state. Thus as shown in Fig. 4.14 (b and d), the fluorescence micrographs of the corresponding functionalized polymer fibers containing the various lutetium phthalocyanines do not show the red fluorescence exhibited by those containing the unsubstituted zinc phthalocyanine. Thus whether the phthalocyanine is embedded within the electrospun polymer fiber matrix through electrostatic or ionic attraction as well as being covalently linked, its fluorescence characteristics are quite similar to that in solution.

Polymer	MPc	Nature of composite	Fluorescence Micrograph
PAA	ZnTAPc$^{\beta}$	Covalently linked	
	LuTAPc$^{\beta}$	Covalently linked	
	ZnPc	Mixed	

(a)

Polymer	MPc	Nature of composite	Fluorescence Micrograph
PS	LuTPPc$^{\alpha}$	Mixed	
	LuTPPc$^{\beta}$	Mixed	
	LuTPyPc$^{\beta}$	Mixed	
	LuTmPyPc$^{\beta}$	Mixed	
	ZnPc	Mixed	

(b)

Polymer	MPc	Nature of composite	Fluorescence Micrograph
PSU	ZnTmPyPc^{II}	Mixed	
	ZnTPyPc$^{\beta}$	Mixed	
	ZnPc	Mixed	

(c)

Polymer	MPc	Nature of composite	Fluorescence Micrograph
PUR	LuTCPPc$^{\beta}$	Covalently linked	
	LuTCPPc$^{\beta}$	Mixed	
	ZnPc	Mixed	

(d)

Figure 4.14: Phthalocyanine functionalized fibers and their corresponding fluorescence micrographs with (a) PAA (b) PS (c) PSU and (d) PUR polymers.

4.4.2. Singlet oxygen generation behavior of functionalized fibers

Non-covalently linked

The ability of the functionalized fibers to generate single oxygen was demonstrated by monitoring the decay of 1,3-diphenylisobenzofuran (DPBF) a singlet oxygen quencher, using UV-visible spectroscopy. Fig. 4.15 shows spectral changes of the DPBF, monitored at 414 nm, in hexane on exposure to light in the presence of the functionalized fiber, PS/AcLuTPPc$^{\alpha}$ (**14**) as representative. There was degradation of the DPBF indicating that oxygen was generated.

Also it is apparent that the phthalocyanine could be regenerated after use as shown in Fig. 4.15, where the PS/AcLuTPPc$^{\alpha}$ (**14**) was re-dissolved in THF and the spectra recorded. When the PS/AcLuTPPc$^{\alpha}$ (**14**) modified fiber (which was used for DPBF studies) was re-dissolved, the peak due to DPBF was not evident on the UV-vis spectrum, Fig 4.15b. This confirmed that the decrease in absorbance of DPBF was not due to its adsorption onto the fiber, but was phototransformed in the presence of the Pc functionalized fiber which generates singlet oxygen.

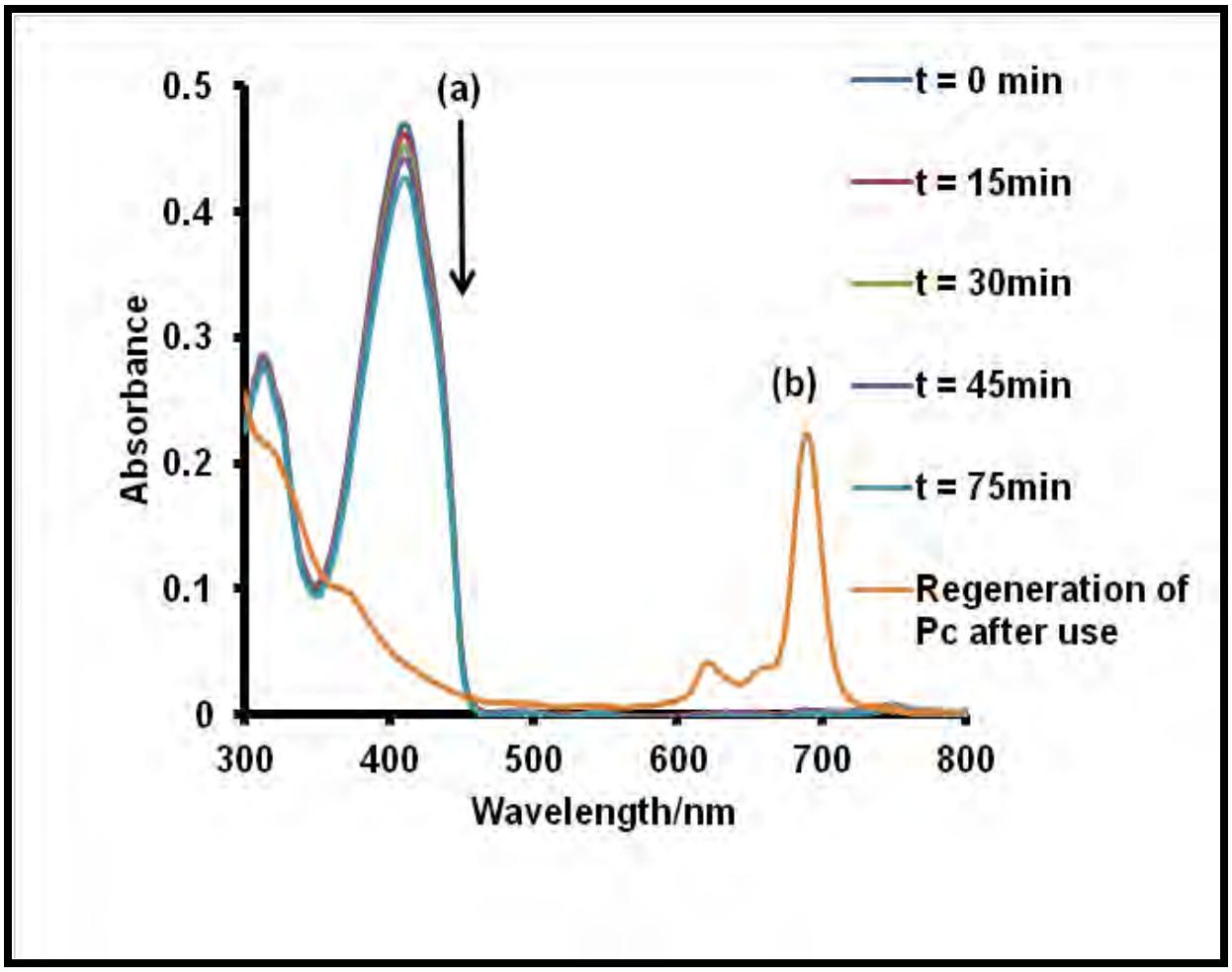

Figure 4.15: (a) Degradation of 2.10 x 10^{-4} mol L^{-1} DPBF in the presence of PS/AcLuTPPc$^{\alpha}$ (14) fiber in hexane at various photolysis times. (b) Regeneration of AcLuTPPc$^{\alpha}$ (14) from the fiber by dissolving the modified fiber in THF and recording the spectrum.

The singlet oxygen quantum yields of the phthalocyanines within the polymeric fibers were determined in water since the fibers were applied for the transformation of 4-chlorophenol, 4-nitrophenol and methyl orange in aqueous media. ADMA was used as

singlet oxygen quencher in aqueous media. Fig. 4.16 shows the degradation profile of ADMA in solutions containing PS/AcLuTPPc$^{\alpha}$ (**14**) fibers in water upon irradiation.

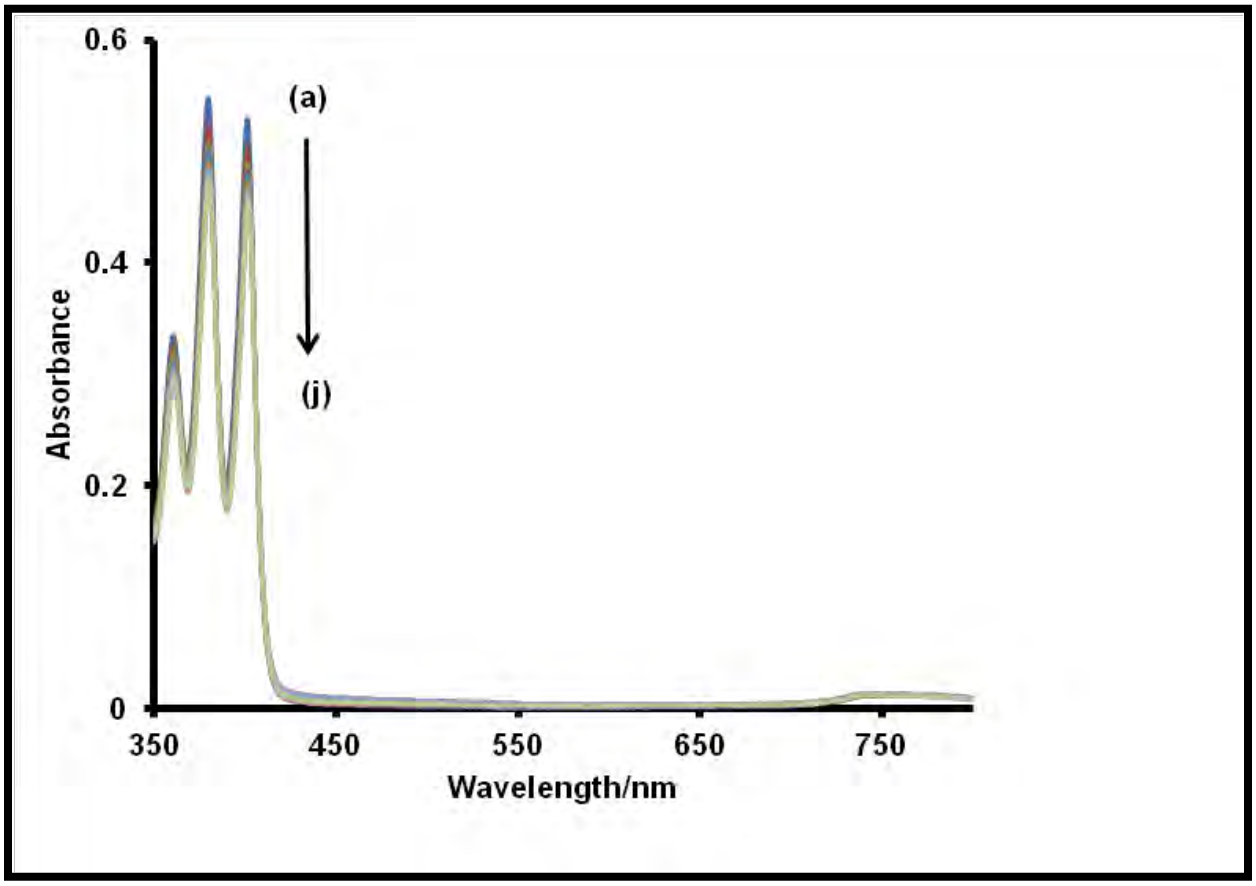

Figure 4.16: UV-vis spectral changes observed on photolysis of ADMA in water in the presence of 10 mg PS/AcLuTPPc$^{\alpha}$ (14) fiber. (a) starting spectrum of ADMA, (j) spectrum after 20 min of photolysis, starting ADMA concentration = 5.53 x 10^{-5} mol L^{-1}, irradiation interval = 2 min.

Similar spectral changes were observed for all other functionalized polymer fibers except those of polyacrylic acid which were soluble in water. The phthalocyanines did not leach out of solution, since they are bound within the fiber matrices as shown in Fig.

4.16. No degradation of ADMA was observed under similar conditions when fibers of the polymers were used alone without functionalization with phthalocyanines. The singlet oxygen quantum yields were estimated using Equation 1.9 and are listed in Table 4.7. These values are significantly lower than those obtained when the phthalocyanines were in DMF solution and can be explained in two contexts. First, it could be due to the fact that the photophysical and photochemical behavior of the phthalocyanine can be altered when constrained within the environment of a solid polymeric matrix. Thus a direct correlation between the phthalocyanine behavior in solution and in solid fiber matrix cannot be feasible. Such an assertion has been put forward by Lang K. *et al*. [267]. Secondly, equally important is the fact that such lowering of the singlet oxygen quantum yield of phthalocyanines in protic solvents such as water has been observed [229]. It is believed that such a decrease is due to interaction between the vibrational levels of the solvent molecules and the electronic or vibrational levels of singlet oxygen resulting in deactivation of the singlet oxygen in such solvents.

Nonetheless, the singlet oxygen quantum yields suggest that the functionalized fibers are promising photosensitizers that could be applied in the photo-conversion of various analytes. Thus as part of this work, an attempt was made to apply these fabric materials for conversion of environmental pollutants in aqueous media.

The photoactivity of the electrospun functionalized polymer fibers were also assessed using optical method based on time-resolved phosphorescence decay of singlet oxygen

using germanium detector at 1270 nm as described in Fig. 2.4, experimental section. Fig. 4.17 shows the decay curve for singlet oxygen phosphorescence irradiation of PS/AcLuTPPc$^{\alpha}$ (**14**) fiber with laser light.

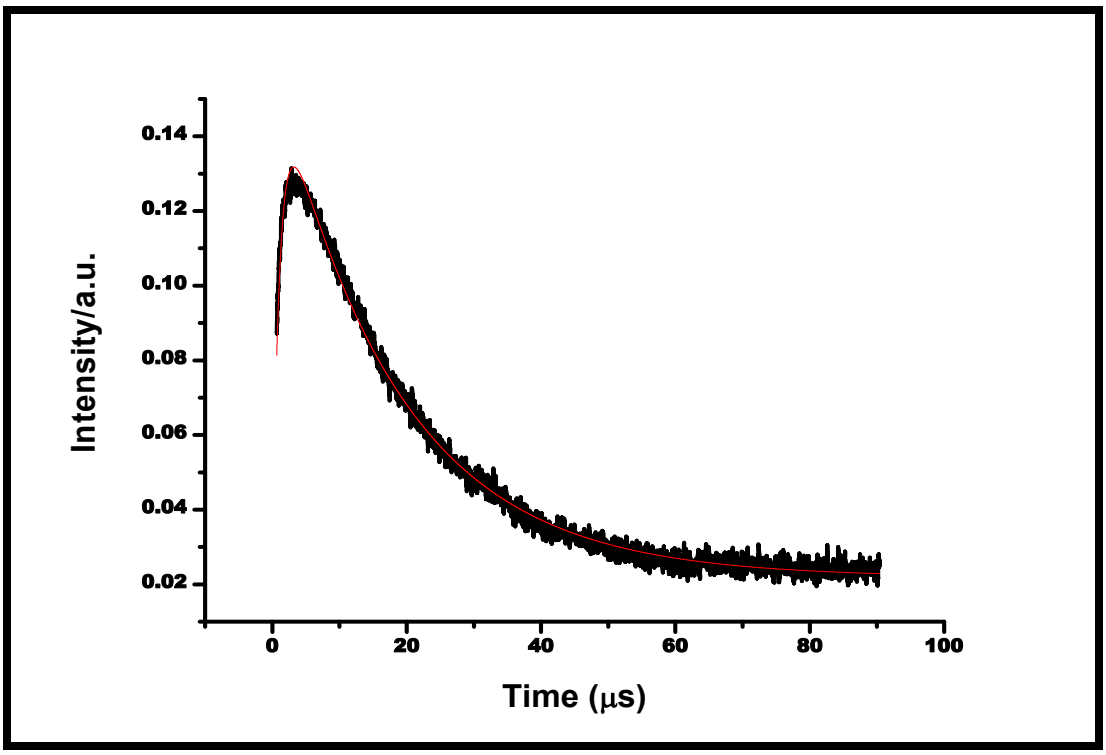

Figure 4.17: Singlet oxygen generation by PS/AcLuTPPc$^{\alpha}$ (14) fiber suspended in oxygen saturated water. λ_{exc} = 696 nm.

Fig. 4.17 clearly shows that PS/AcLuTPPc$^{\alpha}$ (**14**) is capable of generating singlet oxygen ($O_2(^1\Delta_g)$). The lifetime of the singlet oxygen generated was found to be 18 μs. The determination was done by exciting at the Q band of the PS/AcLuTPPc$^{\alpha}$ (**14**) fiber (696 nm). Similar decay profiles were obtained for the other functionalized fibers. This

further suggests that the properties of the phthalocyanines are maintained within the fiber matrix, especially their ability to generate singlet oxygen.

Covalently linked

The ability of the covalently linked functionalized fibers (PAA/AcLuTAPc$^{\beta}$ (**21**), PAA/ZnTAPc$^{\beta}$ (**22**) and PAA/ZnPc) to generate singlet oxygen within the polymeric fiber matrices were assessed using DPBF as singlet oxygen quencher in hexane as solvent. In water, the fibers gradually dissolved to form gelatinous solution and as such water was not a suitable medium. Pieces of the functional fibers were placed in solutions of DBPF in hexane and irradiated using the same photolysis setup as described in the experimental section and the degradation of DBPF monitored by UV-visible spectroscopy.

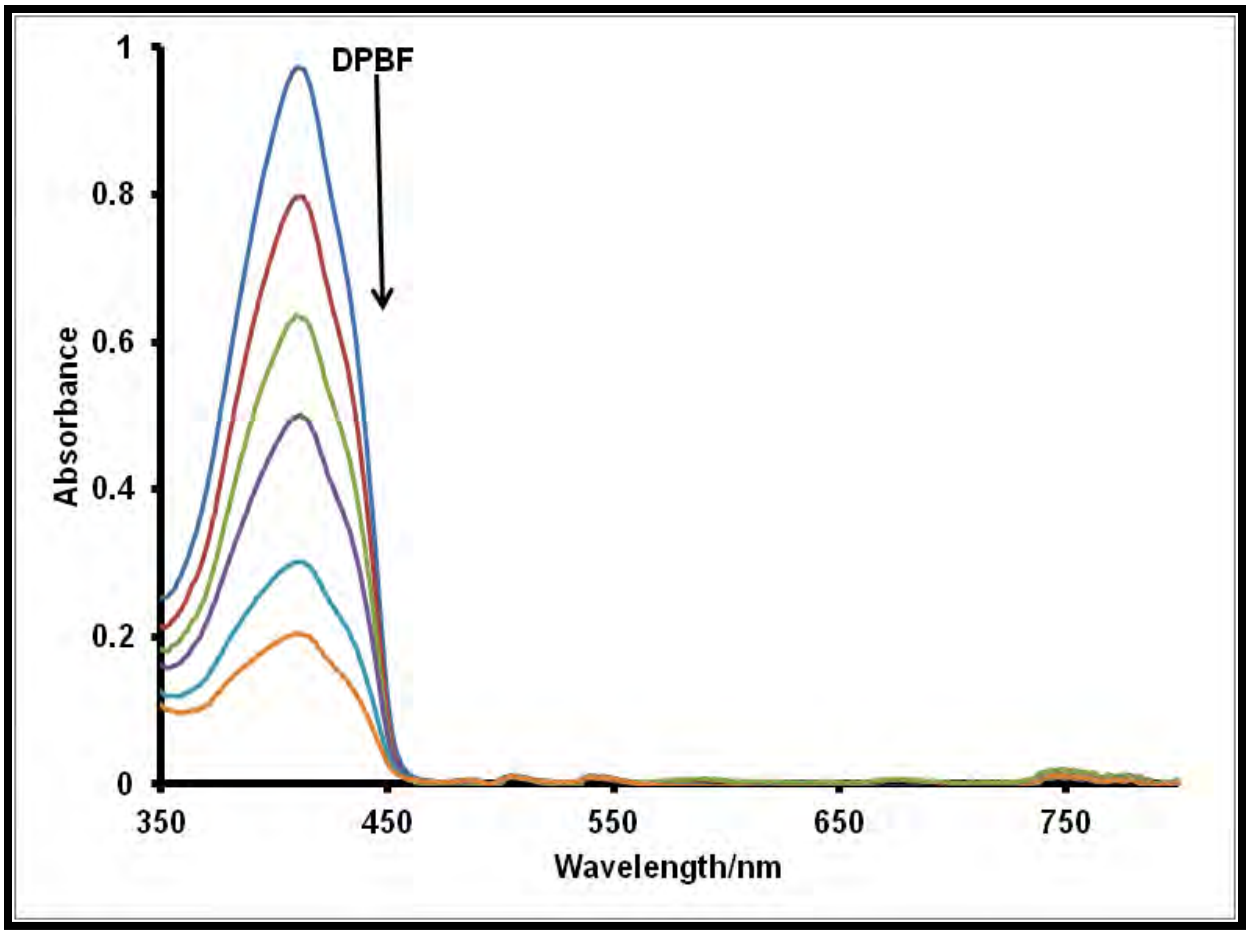

Figure 4.18: Spectral changes observed during degradation of DPBF using PAA/AcLuTAPcβ (21) composite fiber in hexane. Time interval 15 min.

Fig. 4.18 shows a typical degradation of DPBF when PAA/AcLuTAPcβ (**21**), composite fiber was used. This demonstrates that the phthalocyanines within the fiber matrix are still capable of generating singlet oxygen though a longer period of irradiation was required for a significant change of the absorbance of DPBF around 414 nm than in solution or when non-covalently linked. This could be due to the fact that the inherent photophysical and photochemical behavior of the phthalocyanine can be altered when constrained within the environment of a polymeric matrix. Thus a direct correlation

between the phthalocyanine behavior in solution and in solid fiber matrix cannot be feasible as suggested earlier [267]. Additionally, low amounts of the Pc molecules are within the fiber matrix due to the restriction on covalent bond formation. When PAA fiber alone was used no degradation of DPBF occurred suggesting that the phthalocyanine molecules within the fibers are the agents involved in the singlet oxygen generation. The fact the phthalocyanines showed photoactivity within the fiber matrix suggests that not all the molecules are completely encapsulated within the fiber but are found equally covalently bound around the large exposed surface area of the fiber because of the smaller fiber diameters. The phthalocyanines did not leach out of the fiber into solution as evidenced from the Q-band region of the sample solutions during photolysis. This confirms once again the bound nature of the phthalocyanines within the fiber matrix.

4.5. Remarks on chapter

The photophysical and photochemical properties of lutetium and zinc phthalocyanines incorporated into various polymer fiber matrices were studied. The fluorescence behaviors of the composite fibers were found to follow trends in solution. The zinc phthalocyanine composites showed the characteristic red fluorescence under irradiation. The fluorescence could possibly be quenched on interaction with gaseous nitrogen dioxide, a free radical and hence these functionalized fibers could serve as

promising fabric materials in developing optoelectronic devices that are responsive to the gas.

Also the singlet oxygen generating ability of the phthalocyanines were maintained in the solid fibers, thus these polymeric fiber materials incorporating the phthalocyanines could be promising materials for the photo-conversion of environmental pollutants such as 4-nitrophenol, 4-chlorophenol and methyl orange especially in aqueous media. These applications of the functional fabric materials are discussed in the next chapter.

Chapter 5

5. Detection and phototransformation of environmental pollutants

5.1 Optical detection of nitrogen dioxide gas ($NO_{2(g)}$)

Molecular orbital theory predicts nitrogen dioxide ($NO_{2(g)}$) gas to have an unpaired electron, thus it is a reactive radical and could quench fluorescence [274]. The electrospun polymer materials containing the fluorescent zinc phthalocyanines could therefore serve as promising sensing materials for fluorometric detection of $NO_{2(g)}$. As discussed above, Chapter 4, the functionalized polymer fibers containing lutetium phthalocyanines do not show fluorescence in the micrographs and therefore not suitable for detection of the gas.

Preliminary investigations were done by observing the fluorescence behavior of the zinc phthalocyanines in DMF solution in the presence of $NO_{2(g)}$. As shown in Fig. 5.1, for unsubstituted zinc phthalocyanine, a decrease in the fluorescence intensity was observed on exposure to $NO_{2(g)}$. The same was observed with the other zinc phthalocyanine derivatives (**23** and **24**). Though the amount of $NO_{2(g)}$ could not be quantified at each exposure, the changes in the emission spectra suggest that such chemical entities would be promising functional molecules for the detection of $NO_{2(g)}$. Thus the zinc phthalocyanines incorporated into various polymer fibers were applied for the detection of the gas.

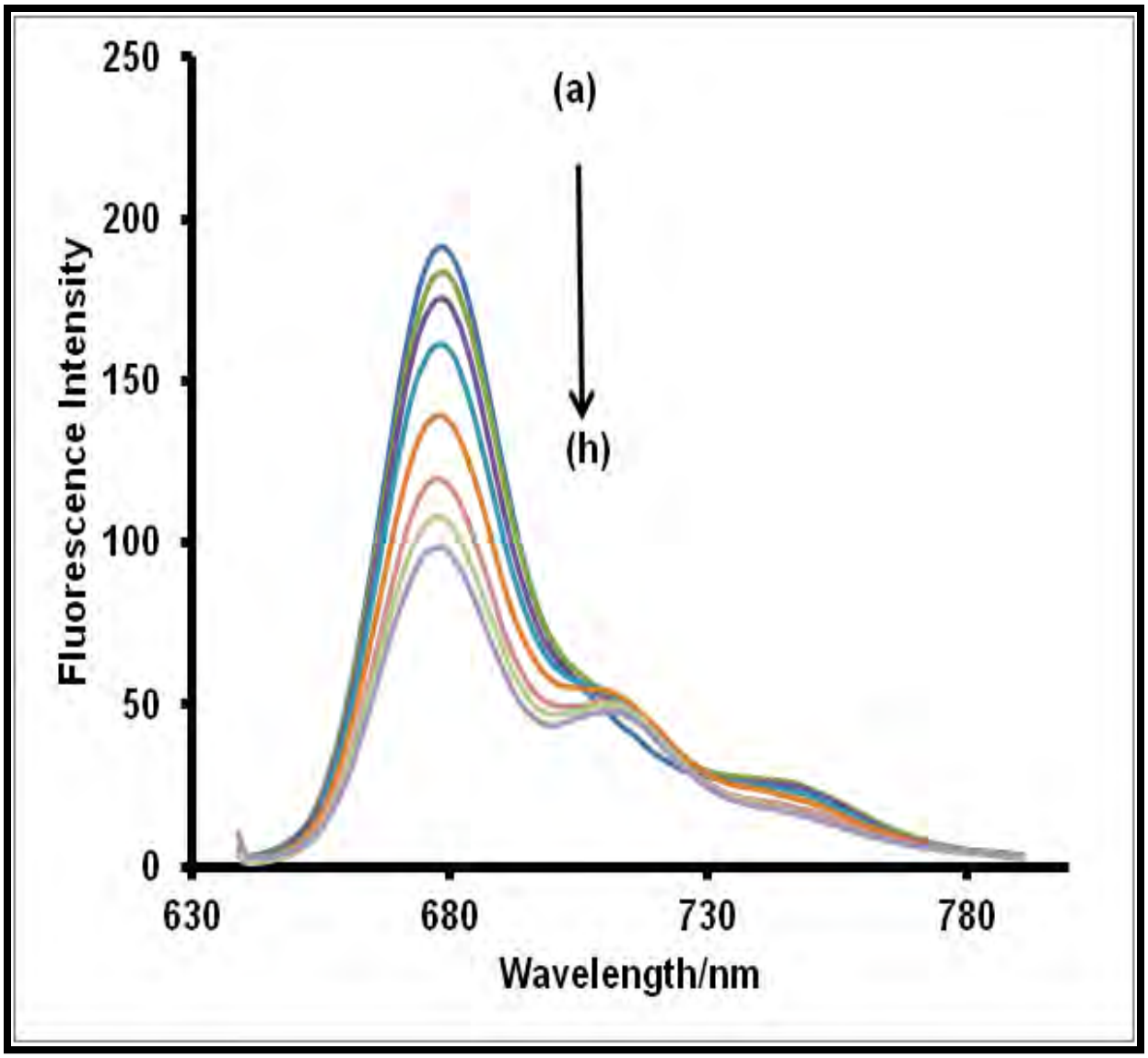

Figure 5.1: Decrease in the fluorescence intensity of ZnPc with introduction of $NO_{2(g)}$.

The functionalized fibers that were chosen for the detection were PS/ZnPc, PAA/ZnPc PSU/ZnPc, PSU/ZnTPyPc$^{\beta}$ (**23**) and PSU/ZnTmPyPc$^{\beta}$ (**24**) fiber mats, since they showed the fluorescence of the phthalocyanines in a dispersed solid state under irradiation, Chapter 4.

The emission intensity was observed to rapidly diminish on exposure of the fibers to $NO_{2(g)}$, Fig. 5.2 for PAA/ZnPc. Though the amount of $NO_{2(g)}$ could again not readily be quantified, the results suggest that the fabric materials are gas permeable and promising for qualitative detection of the gas in the natural environment. Other polymer support systems such as thin films have been reported for the detection of $NO_{2(g)}$ [275]. However, the use of electrospun fabric materials is still limited and remains much more promising for large scale application due to the ease of production of these electrospun fabrics materials.

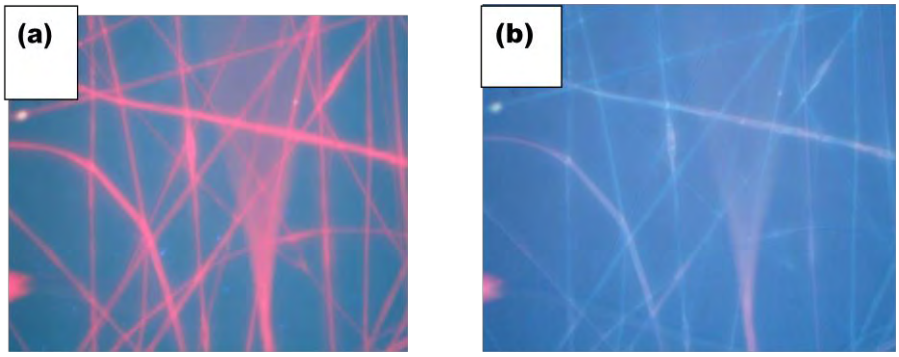

Figure 5.2: Detection of $NO_{2(g)}$ using PAA/ZnPc fiber mat: (a) before and (b) after exposure to $NO_{2(g)}$.

5.2 Photocatalytic applications of the functionalized fibers

Phthalocyanines can be employed as photocatalysts either in solution or in their solid state as well as when dispersed in solid support systems [85, 118, 276]. In this work the use of electrospun polymer fibers functionalized with lutetium and zinc phthalocyanines is explored for the degradation of environmental pollutants (4-chlorophenol, 4-nitrophenol and methyl orange) in aqueous media.

5.2.1 Suitability of the polymer fibers in photocatalytic application in aqueous solutions

The solvent compatibility of the functionalized electrospun polymer fibers is paramount in their applications. Thus the possibility of using the various functionalized fibers for photo-conversion of the environmental organic pollutants (4-chlorophenol, 4-nitrophenol and methyl orange) in aqueous media was first assessed.

Electrospun fibers from polyacrylic acid were found not to be suitable for application involving aquatic systems. This is because the functionalized electrospun polyacrylic acid fibers dissolved extensively in water to give a gelatinous solution. Thus the idea of holding the photoactive phthalocyanines on electrospun polyacrylic acid fibers as solid supports to mimic heterogeneous catalytic systems could not be achieved.

For electrospun polyurethane polymer fibers functionalized with phthalocyanines; AcLuTPPc$^{\alpha}$ (**14**), AcLuTPPc$^{\beta}$ (**18a**), AcLuTCPPc$^{\beta}$ (**18b**) and ZnPc as examples are photoactive as discussed in Chapter 4. However, these functionalized fibers could not degrade any of the pollutants to any detectable extent, even after 12 hours of irradiation. This was irrespective of whether the phthalocyanine and the polymer were merely mixed or covalently linked (for AcLuTCPPc$^{\beta}$ **18b**) and electrospun into fibers. This could be due primarily to the morphology and nature of the fiber mat which shows that the fibers are fused together as compared to those of polystyrene, Fig. 5.3. Thus

they are not porous enough for sufficient interaction of reacting species with the embedded photo-active phthalocyanines molecules within the fiber matrix.

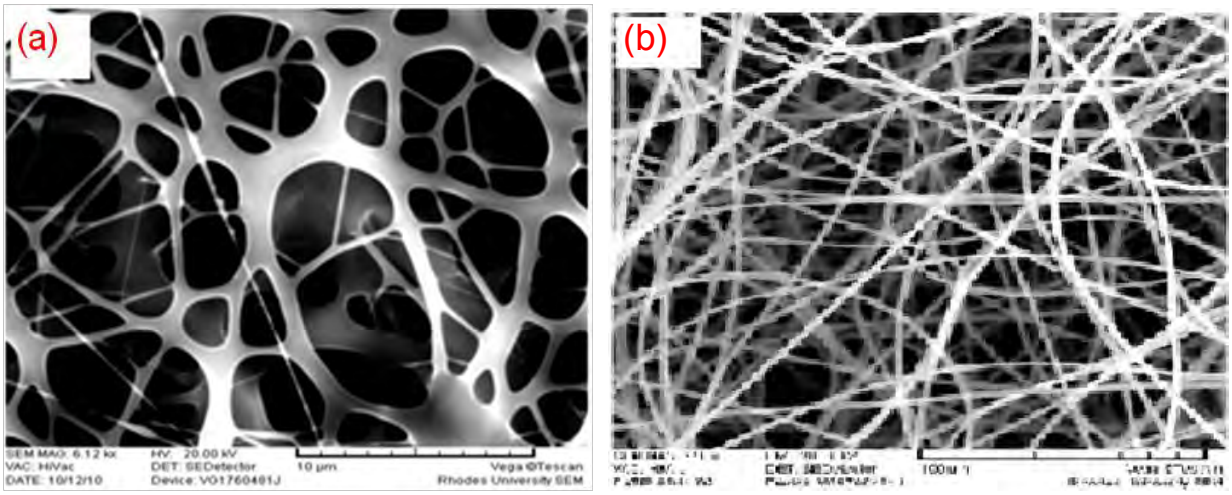

Figure 5.3: Fiber mats for (a) polyurethane polymer (b) polystyrene polymer.

On the other hand, functionalized electrospun fibers of polystyrene and polysulfone were found to be insoluble in water and cotton-like, being quite porous, thus more promising in the photocatalytic application in aqueous systems.

5.2.2 Photodegradation of 4-chlorophenol

Electrospun polystyrene polymer fibers functionalized with the phthalocyanines [ZnPc, AcLuTPPc$^{\alpha}$ (**14**), AcLuTPPc$^{\beta}$ (**18a**), AcLuTPyPc$^{\beta}$ (**18c**) and AcLuTmPyPc$^{\beta}$ (**19**)] and those of polysulfone functionalized with [AcLuTPyPc$^{\beta}$ (**18c**), ZnPc and ZnTPyPc$^{\beta}$ (**23**), ZnTmPyPc$^{\beta}$ (**24**)] were applied as examples for the photoconversion of 4-chlorophenol in aqueous media. Thus ZnPc and AcLuTPyPc$^{\beta}$ (**18c**) were studied with both polystyrene (PS) and polysulfone (PSU) as examples to compare the effect of the nature

of the polymer. The efficiency of the photoconversion of 4-CP was compared with that of other phthalocyanine support systems that have been applied in the photoconversion of 4-chlorophenol.

Studies of the photocatalyzed degradation of 4-chlorophenol (4-CP) were carried out at a pH of 11 to enhance the deprotonation of 4-chlorophenol, since its pKa value is 9.34. It has been reported that the deprotonated form of 4-chlorophenol, is more oxidizable by singlet oxygen than in its protonated or neutral forms [165, 210]. The progress of the reaction was monitored in each case by taking the UV-visible spectra of sample solutions at various time intervals during irradiation. Fig. 5.4 shows the electronic absorption spectral changes observed on photolysis of 4-chlorophenol using PS/ AcLuTPPc$^{\alpha}$ (**14**) fiber. The 4-chlorophenol peaks around 243 nm and 297 nm decrease in intensity during irradiation of the sample in the presence of the functionalized fiber. This suggests conversion of the 4-chlorophenol to photolysis products. This is supported by the emergence of two new absorbance bands, observed at 227 nm and 280 nm which increase in intensity with time, Fig 5.4 (insert). The increase is clearer for the peak at 227 nm since it is more resolved. These peaks are similar to what has been reported for the degradation of 4-chlorophenol in the presence of phthalocyanines and other photosensitizers [276]. The absorption peak at 227 nm could be assigned to benzoquinone while that at 280 nm to hydroquinone [162, 277, 278, 279]. When the pure polystyrene polymer fiber was used as control, no spectral changes of the aqueous 4-chlorophenol solution were observed. Thus suggesting that the phthalocyanines in the

functionalized fibers were the agents involved in the photo-conversion of the 4-chlorophenol. When PS/ZnPc fiber was employed, spectral changes similar to those in Fig. 5.4 were obtained though a longer time (30 min) was required for a significant change. This is due to lower singlet oxygen quantum yield for PS/ZnPc (0.13) compared to PS/AcLuTPPc$^{\alpha}$ (0.22) and the other fibers functionalized with LuPc and ZnPc derivatives.

There was no leaching of the phthalocyanines from the composite fiber into the aqueous solution of 4-chlorophenol. This was apparent from the fact that there was no Q-band absorption corresponding to the phthalocyanine in the UV-visible spectra of sample solution during photocatalysis, similar to what was observed with ADMA, Fig 4.16. Thus the polystyrene polymer fiber serves as a good support system.

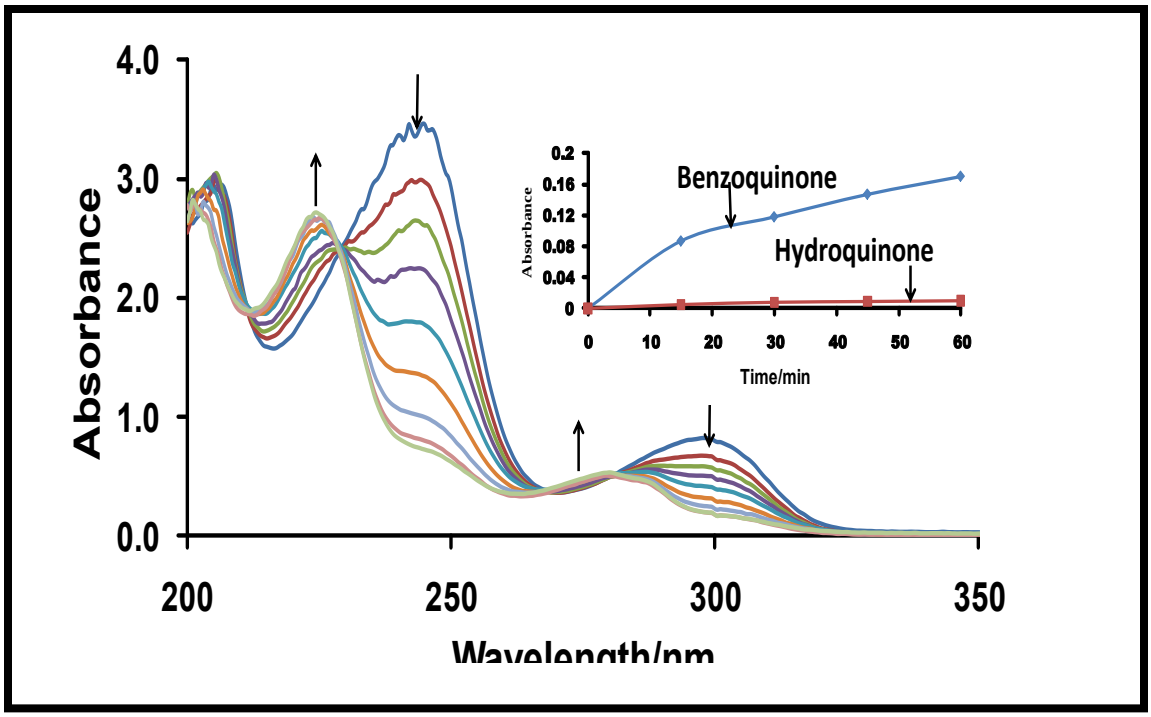

Figure 5.4: Electronic absorption spectral changes of 3.58 x 10^{-4} mol L^{-1} 4-CP during its visible light photocatalysis in the presence of PS/AcLuTPPc$^{\alpha}$ (14) functionalized fiber. The spectra were recorded 15 min intervals. Insert: plot of absorbance versus time for the two peaks.

It has been reported [162] that the formation of p-benzoquinone is mainly due to the reaction of singlet oxygen with 4-chlorophenol (Type II mechanism, Scheme 1.4), while the formation of hydroquinone and other dimeric products are explained by an electron transfer reactions involving the phthalocyanine, oxygen and 4-chlorophenol (Type I mechanism, Scheme 1.3). The type of mechanism involved was investigated by conducting the photolysis in an oxygen saturated solution and in a solution containing sodium azide, a singlet oxygen quencher. The production of p-benzoquinone at 227 nm

was quite enhanced in the oxygen saturated solution, while drastically reduced in the azide saturated solution, thus supporting the Type II mechanism proposed for its formation. Production of the hydroquinone, on the other hand under the above conditions was not affected all. Also when a free radical scavenger, tert-butyl alcohol, was used, hydroquinone was not produced. Thus the functionalized fibers are capable of degrading 4-chlorophenol via both the proposed Type II and Type I mechanisms, Scheme 5.1, which starts with the photogeneration of singlet oxygen and radicals, respectively, by the immobilized phthalocyanine. Such dual photodegradative routes have been reported for a sulphonated cobalt phthalocyanine anchored on MCM-41, a mesoporous molecular sieve, for the degradation of 2,4-dichlorophenol [167].

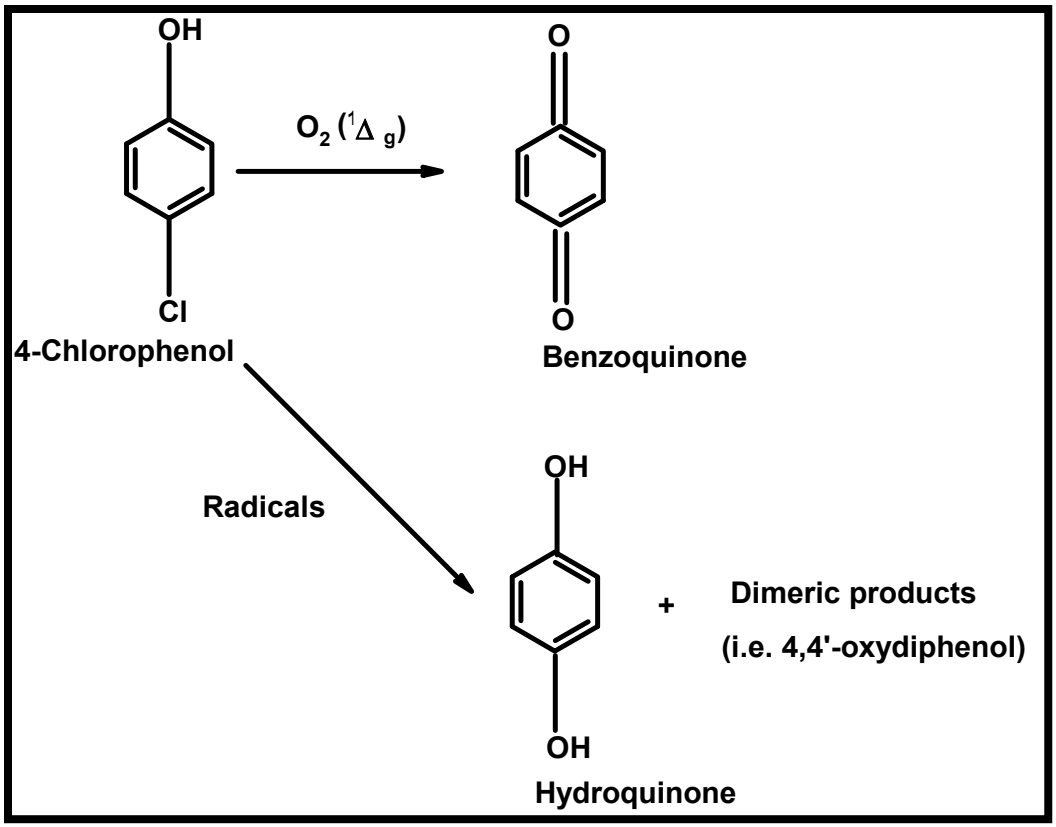

Scheme 5.1: Mechanism of photooxidation of 4-chlorophenol.

The reaction kinetics were also investigated since the initial concentration of the pollutant is of immense importance in any water treatment. First order kinetics were observed in all cases for the photodegradation of 4-chlorophenol as shown in Fig 5.5 for PS/AcLuTPPc$^{\alpha}$ (**14**). Similar kinetics were observed before for the photodegradation of 4-chlorophenol using sulphonated phthalocyanine complex of aluminum [280] and degradation of 2,4-dichlorophenol by sulphonated cobalt phthalocyanine immobilized on a mesoporous molecular sieves, (MCM-41) [167] as well as the heterogeneous photodegradation of 4-nitrophenol using suspension of TiO_2 [281].

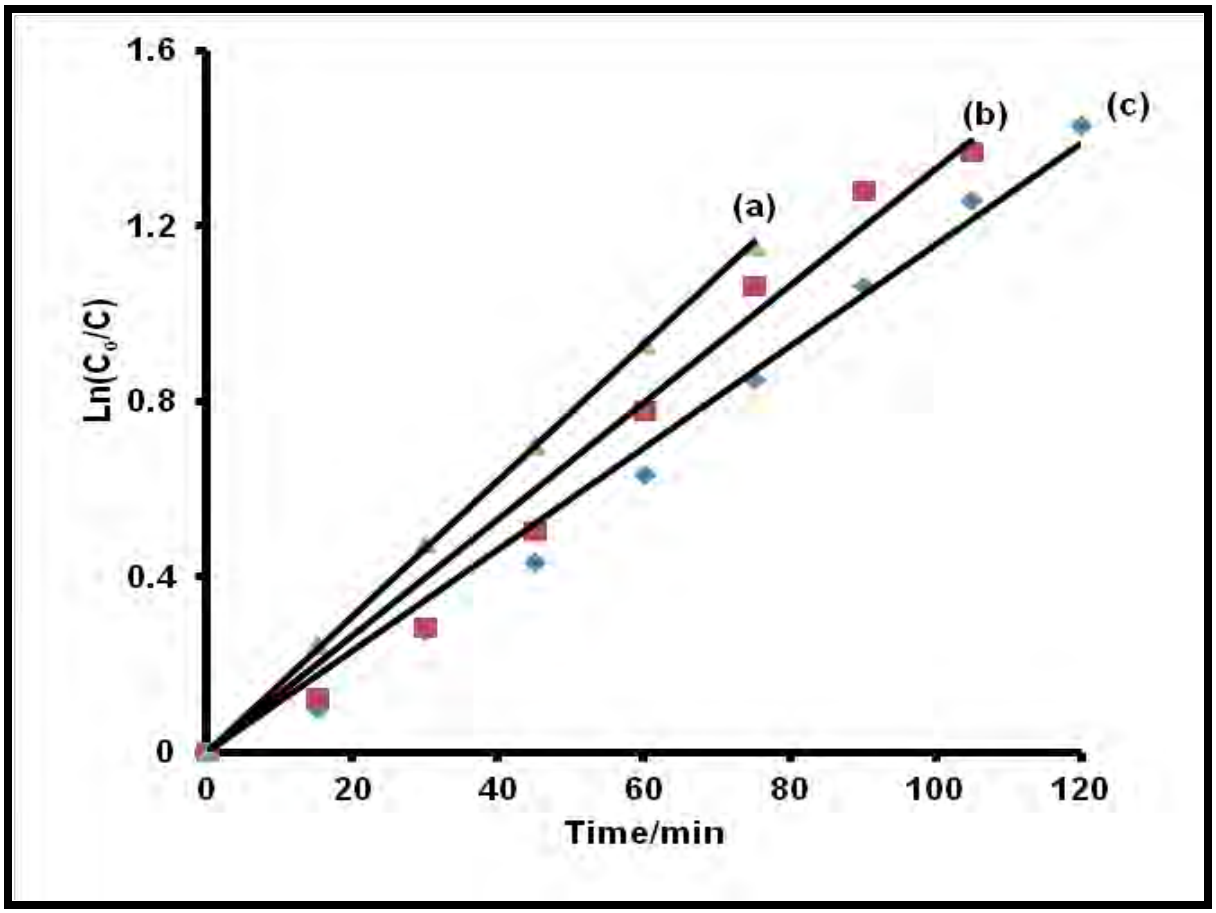

Figure 5.5: Effect of initial concentration of 4-chlorophenol on its rate of photodegradation: Concentrations were monitored at 243 nm. Starting concentrations (a) 2.72 x 10^{-4} mol L^{-1}, (b) 3.58 x 10^{-4} mol L^{-1} and (c) 4.36 x 10^{-4} mol L^{-1}. Amount of functionalized fiber 10 mg. Fiber = PS/AcLuTPPc$^{\alpha}$ (14).

The initial reaction rates (R) and half-lives ($t_{1/2}$) were evaluated from Equations 5.1 and 5.2 respectively, while the observed rate constants (k_{obs}) were evaluated from Fig. 5.5 and are listed Tables 5.1 and 5.2.

$$\text{Initial Rate } (R) = K_{obs}[4\text{-CP}]_0 \qquad 5.1$$

where $[4\text{-CP}]_0$ is the initial concentration 4-chlorophenol

$$t_{1/2} = \frac{\ln 2}{k_{obs}} \qquad 5.2$$

The observed rate constant (k_{obs}) decreased with an increase in concentration as expected, Table 5.1. The values of k_{obs} listed in Table 5.2 for all MPc derivatives are larger, (except ZnPc) than those reported using sulfonated phthalocyanines in aqueous media under homogeneous photocatalytic oxidation of 4-chlorophenol [280], which were of the order of 10^{-3} min^{-1} on average. The rate constants for LuPc derivatives and substituted ZnPc derivatives were larger than for PS/ZnPc used as standard. Thus the former showed faster photocatalytic behavior towards the oxidation of 4-chlorophenol than the later.

Table 5.1: The rate (R), rate constant (k_{obs}) and half-life ($t_{1/2}$) of various initial concentrations of 4-chlorophenol using PS/AcLuTPPc$^{\alpha}$ (14). Values in brackets are when PS/ZnPc fiber was employed.

Concentration/ x 10^{-4} mol L^{-1}	k_{obs}/min^{-1}	Initial Rate/x 10^{-6} mol L^{-1} min^{-1}	Half-life/min
1.56	0.0231 (0.006)	3.60 (0.94)	30.00 (116)
2.72	0.0155 (0.005)	4.22 (1.36)	44.72 (139)
3.58	0.0133 (0.0045)	4.76 (1.61)	52.12 (154)
4.04	0.0123 (0.0042)	4.97 (1.69)	55.45 (165)
4.36	0.0116 (0.0041)	5.06 (1.79)	59.75 (169)
5.06	0.0101 (0.0038)	5.11 (1.92)	68.63 (182)

From Table 5.2, the k_{obs} are highest for AcLuTPPc$^{\beta}$ (**18a**) which has the largest Φ_{Δ} in the fiber. AcLuTPPc$^{\alpha}$ (**14**) and ZnTPyPc$^{\beta}$ (**18c**) also have relatively large k_{obs} due to large Φ_{Δ}, Table 5.2. The nature of the polymer also has an effect with ZnPc in PSU having larger k_{obs} and Φ_{Δ} than in PS as discussed in Chapter 4. Polystyrene has much more extensive aromatic system than polysulfone. The ZnPc could therefore be more tightly bound within the PS polymer matrix than within the PSU resulting in decrese in singlet oxygen

quantum yield and hence k_{obs}. The same behaviour was observed for AcLuPyPc$^{\beta}$ (**18c**), where higher singlet oxygen quantum yield was obtained within the PSU fiber matrix (0.26) compared to that in PS in fiber matrix (0.17), Table 5.2. Comparing complexes AcLuTPPc$^{\beta}$ (**18a**) and AcLuTPPc$^{\alpha}$ (**14**), embedded in PS fiber, both contain the same substituent, but peripherally and non-peripherally substituted, respectively, PS/AcLuTPPc$^{\alpha}$ (**14**) functionalized fiber shows larger k_{obs} values for PS/AcLuTPPc$^{\beta}$ (**18a**) fiber with correspondingly smaller half-lives. The values correspond to the singlet oxygen quantum yields, Table 5.2. Thus factors which affect the production of singlet oxygen by the Pc within the fiber, will affect the effectiveness of the functionalized fibers for the phototransformation of pollutants.

The half-lives of the photo-degradation of 4-chlorophenol by the PS/AcLuTPPc or PSU/ZnPc substituted derivatives, within the experimental concentrations, are smaller than the values (three hours) reported for other higher substituted chlorinated phenols [167], Table 5.2. Equally encouraging is the fact that these half-lives are within half an hour of photo-irradiation for PS/LuPcs for concentration of 4-CP less than 2×10^{-4} M except unsubstituted ZnPc. Thus suggesting that the functionalized fibers are promising fabric materials that could be applied in real life removal of chlorophenols in aquatic systems since quite a short time is required for phototransformation.

Table 5.2: Kinetic data for phototransformation of 4-CP at initial concentration of 2 x 10^{-4} mol L^{-1} using different functional fibers.

Functionalized fiber	k_{obs}/x 10^{-2} min^{-1}	Initial reaction rate /x 10^{-6} mol L^{-1} min^{-1}	Half-life/min	Φ_Δ in fiber
PS/ZnPc	0.6	1.2	116	0.13
PSU/ZnPc	1.75	3.50	40	0.25
PS/LuTPPc$^{\alpha}$ (14)	1.98	3.95	35	0.22
PS/LuTPPc$^{\beta}$ (18a)	2.11	4.22	33	0.28
PS/LuTPyPc$^{\beta}$ (18c)	1.80	3.60	39	0.17
PSU/LuTPyPc$^{\beta}$ (18c)	2.07	4.14	34	0.26
PS/LuTmPyPc$^{\beta}$ (19)	1.77	3.55	39	0.15
PSU/ZnTPyPc$^{\beta}$ (23)	2.01	4.02	35	0.24
PSU/ZnTmPyPc$^{\beta}$ (24)	1.75	3.50	40	0.21

The Langmuir-Hinshelwood rate equation was also used to describe the relationship between the initial rate of degradation of 4-chlorophenol and the corresponding initial concentration. This model, equation 5.3, has successfully been applied to describe the kinetics of solid-liquid reactions. In particular, it has been applied in heterogeneous photocatalytic degradation reactions [282]. These studies were only carried out for PS/ZnPc and PS/AcLuTPPc$^{\alpha}$ (**14**) as examples. A linear relationship can conveniently be obtained by plotting the reciprocal of the initial rate against the reciprocal of the initial concentration, Equation 5.3.

$$\frac{1}{rate} = \frac{1}{k_a} + \frac{1}{k_a K C_o} \qquad 5.3$$

where k_a is the apparent reaction rate constant, K is the adsorption coefficient and C_o corresponds to the initial concentration of 4-chlorophenol.

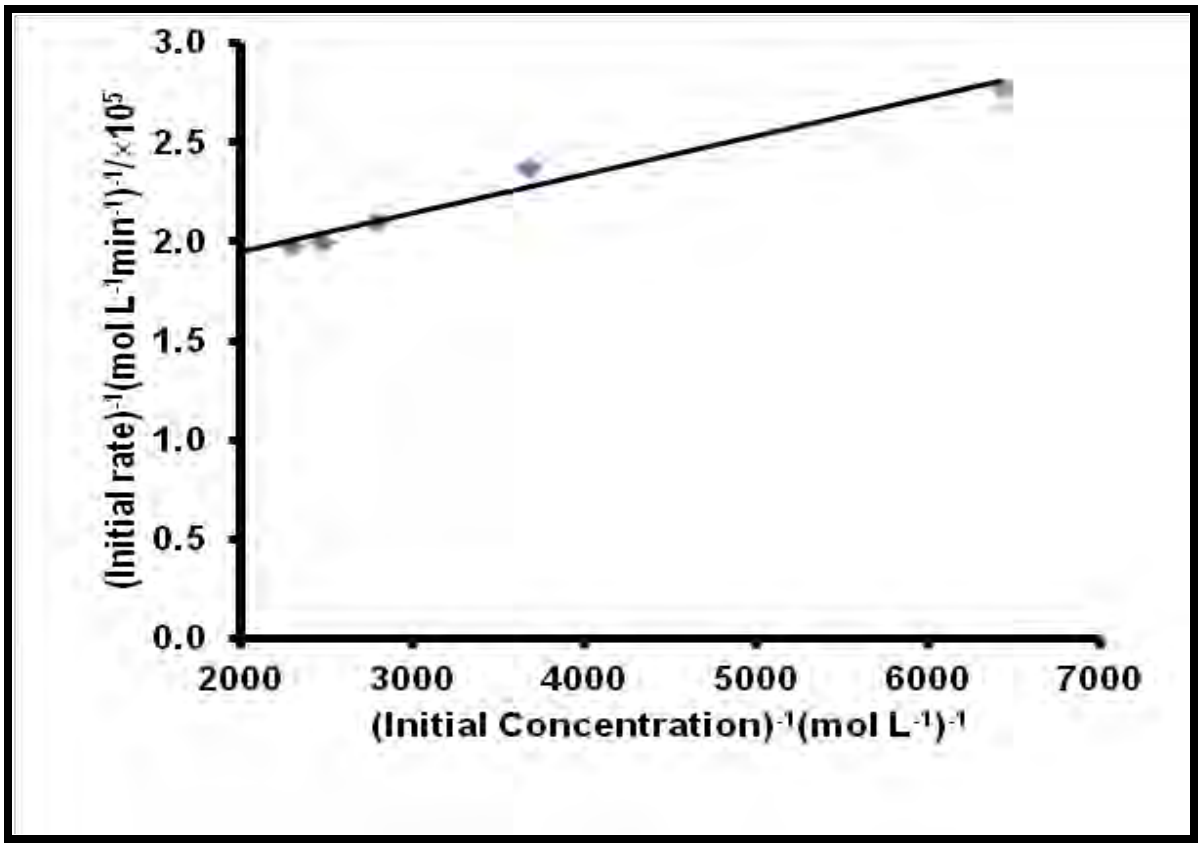

Figure 5.6: Plot of the inverse of initial reaction rate (rate^{-1}) versus the reciprocal of the initial concentration of 4-CP for photooxidation using 10 mg PS/AcLuTPPc$^{\alpha}$ (14) functionalized fiber.

In this work, a reasonable linear fit was obtained (for the plot of 1/rate versus $1/C_o$) with a non-zero intercept and a correlation coefficient of 0.98, Fig. 5.6. The results presented in Fig. 5.6 for PS/AcLuTPPc$^{\alpha}$ (**14**) give an indication that the Langmuir-Hinshelwood (L-H) kinetic model is an appropriate model in describing the kinetics of the photo-degradation of 4-chlorophenol by the heterogeneous catalytic system based on the phthalocyanines functionalized on polystyrene polymer fibers. A similar plot as

shown in Fig. 5.6 was also obtained for PS/ZnPc. Therefore it could be said that the catalysis occurs appreciably at the surface of the functionalized fiber.

From the intercept in Fig. 5.6, the apparent rate constants k_a were obtained. The adsorption coefficients, K were determined from Equation 5.3 and are listed in Table 5.3.

Table 5.3: Langmuir-Hinshelwood (L-H) parameters.

Functionalized fiber	**Analyte**	**k_a/mol L^{-1} min^{-1}**	**K/ mol^{-1}**
PS/ZnPc	**4-CP**	**3.30×10^{-7}**	**2.48×10^{3}**
PS/AcLuTPPc$^{\alpha}$ (14)		**6.39×10^{-3}**	**0.81**
PS/AcLuTPPc$^{\beta}$ (18a)	**4-NP**	**8.76×10^{-6}**	**1.50×10^{3}**
PS/AcLuTPyPc$^{\beta}$ (18c)		**8.48×10^{-6}**	**2.00×10^{3}**
PSU/ZnPc		**4.50×10^{-6}**	**5.80×10^{3}**
PSU/ZnTmPyPc$^{\beta}$ (24)	**MO**	**1.86×10^{-6}**	**0.03**

The apparent rate constant for PS/AcLuTPPc$^{\alpha}$ (**14**) (6.39×10^{-3} mol L^{-1} min^{-1}) is larger than that for PS/ZnPc (3.3×10^{-7}mol L^{-1} min^{-1}), Table 5.3. This again indicates faster reaction kinetics for the degradation of 4-chlorophenol with PS/AcLuTPPc$^{\alpha}$ (**14**) fiber than with PS/ZnPc fiber due to low Φ_{Δ} in the later. Additionally, the adsorption

coefficients, K, were found to be 0.81 mol^{-1} L for PS/AcLuTPPc$^{\alpha}$ (**14**) and 2.48 x 10^3 mol^{-1} L for PS/ZnPc. The value of adsorption coefficient is less than one ($K < 1$), in the case of PS/AcLuTPPc$^{\alpha}$ (**14**), suggesting that adsorption was less favored compared to desorption while the converse is true for PS/ZnPc fiber.

5.2.3 Photodegradation of 4-nitrophenol

In this work, 4-nitrophenol was used as a representative nitrophenol. The photocatalytic reaction was carried out in a buffer aqueous solution of pH 8.2 which is slightly higher than the pKa 7.15 of 4-nitrophenol [283], since the deprotonated forms of substituted phenols are much more easily oxidizable by singlet oxygen [165]. PS/AcLuTPPc$^{\beta}$ (**18a**), PS/AcLuTPyPc$^{\beta}$ (**18c**), PS/AcLuTmPyPc$^{\beta}$ (**19**) and PS/ZnPc fibers were used as examples.

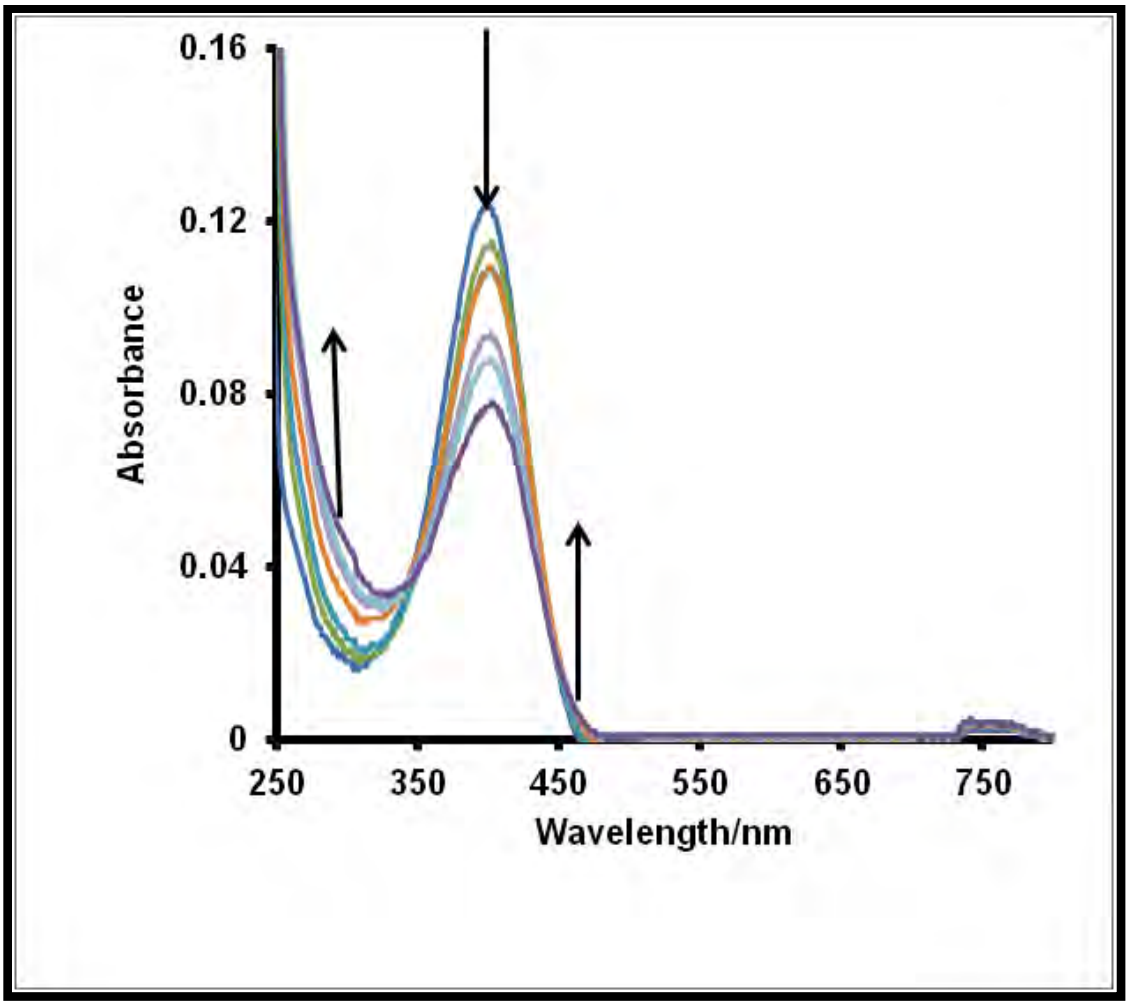

Figure 5.7: Electronic absorption spectral changes observed during photolysis of 2.72 x 10^{-4} mol L^{-1} 4-nitrophenol using 20 mg polystyrene fiber functionalized with PS/AcLuTPPc$^{\beta}$ (18a) in pH 8.2 buffer solution.

Fig. 5.7 shows the UV-visible spectral changes of 4-nitrophenol solution during the photolysis process using PS/AcLuTPPc$^{\beta}$ (**18a**). As shown, the peak around 400 nm corresponding to 4-nitrophenol decreases in intensity with irradiation in the presence of the functionalized fiber. There are corresponding increases in the absorbance around 280 and 455 nm, suggesting the formation of photodegradative products of 4-

nitrophenol. Similar spectral observations were made with the polystyrene fiber functionalized with complexes **18c**, **19** and ZnPc, though the changes were slightly less pronounced. This could possibly be due to higher singlet oxygen quantum yield of PS/AcLuTPPcβ (**18a**) (0.28) compared to PS/AcLuTPyPcβ (**18c**) (0.17), PS/AcLuTmPyPcβ (**19**) (0.15) and PS/ZnPc (0.13). However, when non functionalized polystyrene polymer fiber was used under similar conditions, no spectral changes of the aqueous 4-nitrophenol sample solutions were observed. This suggests that the phthalocyanines (AcLuTPPcβ (**18a**), AcLuTPPcβ (**18c**), AcLuTPyPcβ (**19**) and ZnPc) are the agents involved in the phototransformation process due to their ability to generate the reactive singlet oxygen. Similarly, when only the 4-nitrophenol sample solution was irradiated with the visible light no spectral changes were observed further suggesting that the catalysis can only occur in the presence of the sensitizer.

The supposed involvement of singlet oxygen in the conversion of 4-nitrophenol was assessed by conducting the photolysis reaction with and without sodium azide, a singlet oxygen quencher, in the sample solutions. Fig. 5.8 shows the kinetics of the various reaction conditions using first order kinetic model. There is generally a good fit with R^2 values above 0.96 in all cases. Fig 5.8 shows that the phototransformation reaction is slowed when sodium azide is added to 4-nitrophenol solution. This is an indication of the ability of PS/AcLuTPPcβ (**18a**), and PS/AcLuTPyPcβ (**18c**) to generate singlet oxygen which is a key factor in the phototransformation of 4-nitrophenol.

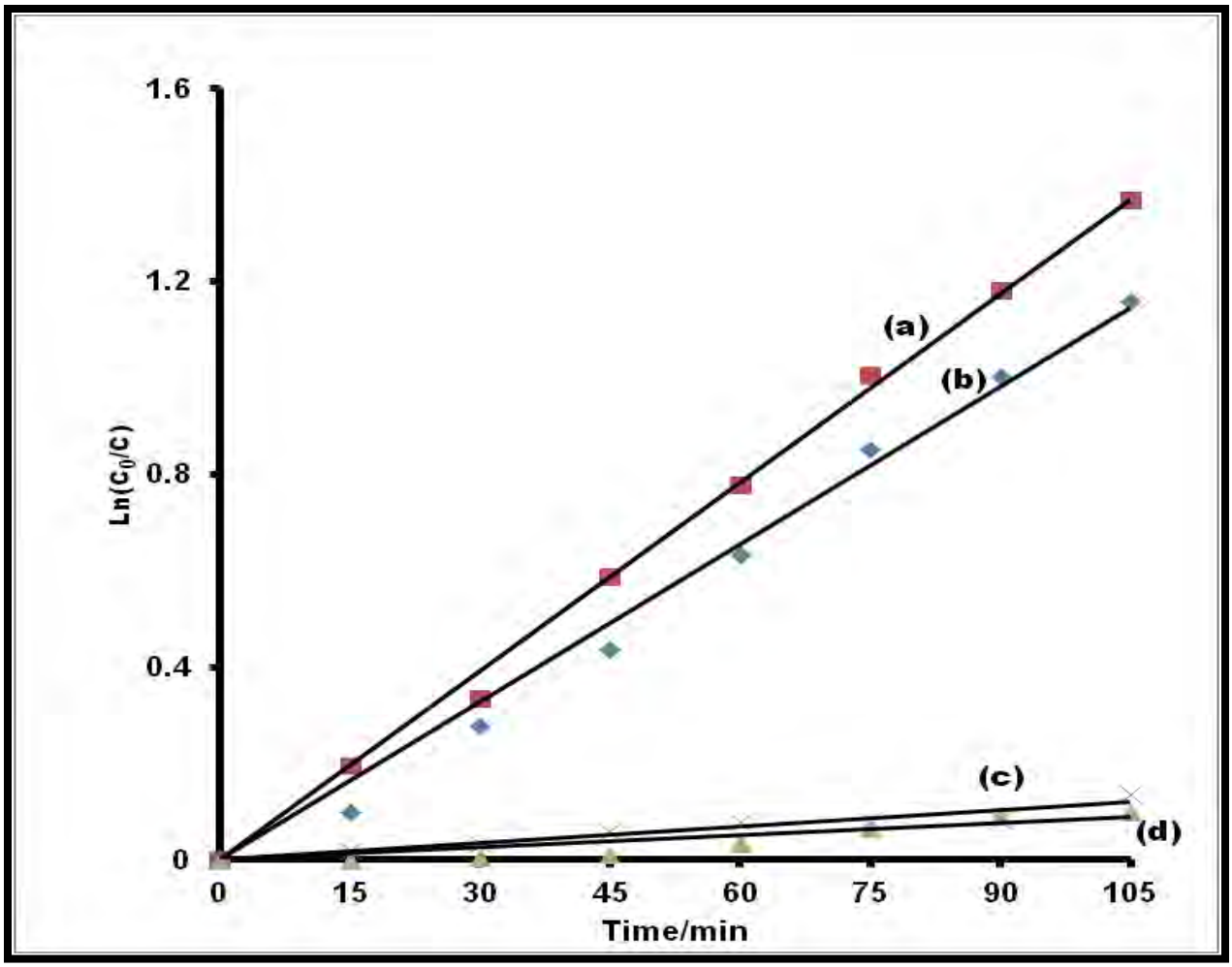

Figure 5.8: Effect of initial concentration of 4-NP on its transformation in air using (a) PS/AcLuTPPcβ (18a), (b) PS/AcLuTPyPcβ (18c). (c) PS/AcLuTPPcβ (18a) and (d) PS/AcLuTPyPcβ (18c) show fiber with sodium azide. An amount of 20 mg of the functionalized fibers used in all cases.

Kinetic parameters of the phototransformation of 4-nitrophenol at different initial concentrations using the functionalized fibers (PS/AcLuTPPcβ (**18a**), PS/AcLuTPyPcβ (**18c**), PS/AcLuTmPyPcβ (**19**) and PS/ZnPc) are given in Tables 5.4 and 5.5. Again lower k_{obs} values for PS/ZnPc were obtained compared to PS/AcLuTPPcβ (**18a**),

PS/AcLuTPyPcβ (**18c**) and PS/AcLuTmPyPcβ (**19**) due to lower Φ_Δ for the former. The half-lives for PS/ZnPc are slightly higher than for the other complexes but not as high as using PS/ZnPc for the transformation of 4-CP due to the differences in reactivity of these substituted phenols.

Table 5.4: Rates, rate constants (k_{obs}) and half-lifes ($t_{1/2}$) of various initial concentrations of 4-nitrophenol.

4-NP Concentration/ x 10^{-4} mol L^{-1}	Complex	k_{obs}/min^{-1} x 10^{-2}	Initial Rate/x 10^{-6} $molL^{-1}min^{-1}$	Half-life/min
0.9	PS/18a	1.46	1.31	47
	PS/18c	1.12	1.01	61
	PS/ZnPc	1.00	0.90	69
1.2	PS/18a	1.38	1.66	50
	PS/18c	1.07	1.26	64
	PS/ZnPc	1.02	1.22	68
2.0	PS/18a	1.22	2.44	56
	PS/18c	1.05	2.14	66
	PS/19	0.97	1.94	71
	PS/ZnPc	0.85	1.69	81
2.5	PS/18a	1.11	2.78	61
	PS/18c	0.95	2.38	72
	PS/ZnPc	0.74	1.86	93

Comparing all complexes at the same concentration of 4-NP, Table 5.5, shows that the largest k_{obs} occur where Φ_Δ is large. The half-life for PS/ZnPc is comparable to the rest of the lutetium phthalocyanines though slightly higher, Table 5.5.

Table 5.5: Kinetic data for phototransformation of 4-NP at initial concentration of 2×10^{-4} mol L^{-1} using different functional fibers.

Functionalized fiber	$k_{obs}/x\ 10^{-2}$ min^{-1}	Initial reaction rate/x 10^{-6} mol L^{-1} min^{-1}	Half-life/min	Φ_Δ in fiber
PS/ZnPc	0.85	1.69	82	0.13
PS/AcLuTPPc$^{\alpha}$ (14)	1.03	2.06	67	0.22
PS/AcLuTPPc$^{\beta}$ (18a)	1.22	2.44	57	0.28
PS/AcLuTPyPc$^{\beta}$ (18c)	1.05	2.14	66	0.17
PS/AcLuTmPyPc$^{\beta}$ (19)	0.97	1.94	71	0.15

The Langmuir-Hinshelwood rate expression, Equation 5.1, was also used to describe the relationship between the initial rate of degradation of 4-nitrophenol and the corresponding initial concentration. Complexes **18a**, **18c** and unsubstituted ZnPc were used as examples. Plots of the inverse of initial reaction rate $(rate)^{-1}$ versus the reciprocal of the initial concentration of 4-nitrophenol $(C_0)^{-1}$ were found to be linear with non zero

intercepts for the functionalized fibers, Fig. 5.9. The apparent rate constants k_a and the adsorption coefficients, K, are listed in Table 5.3.

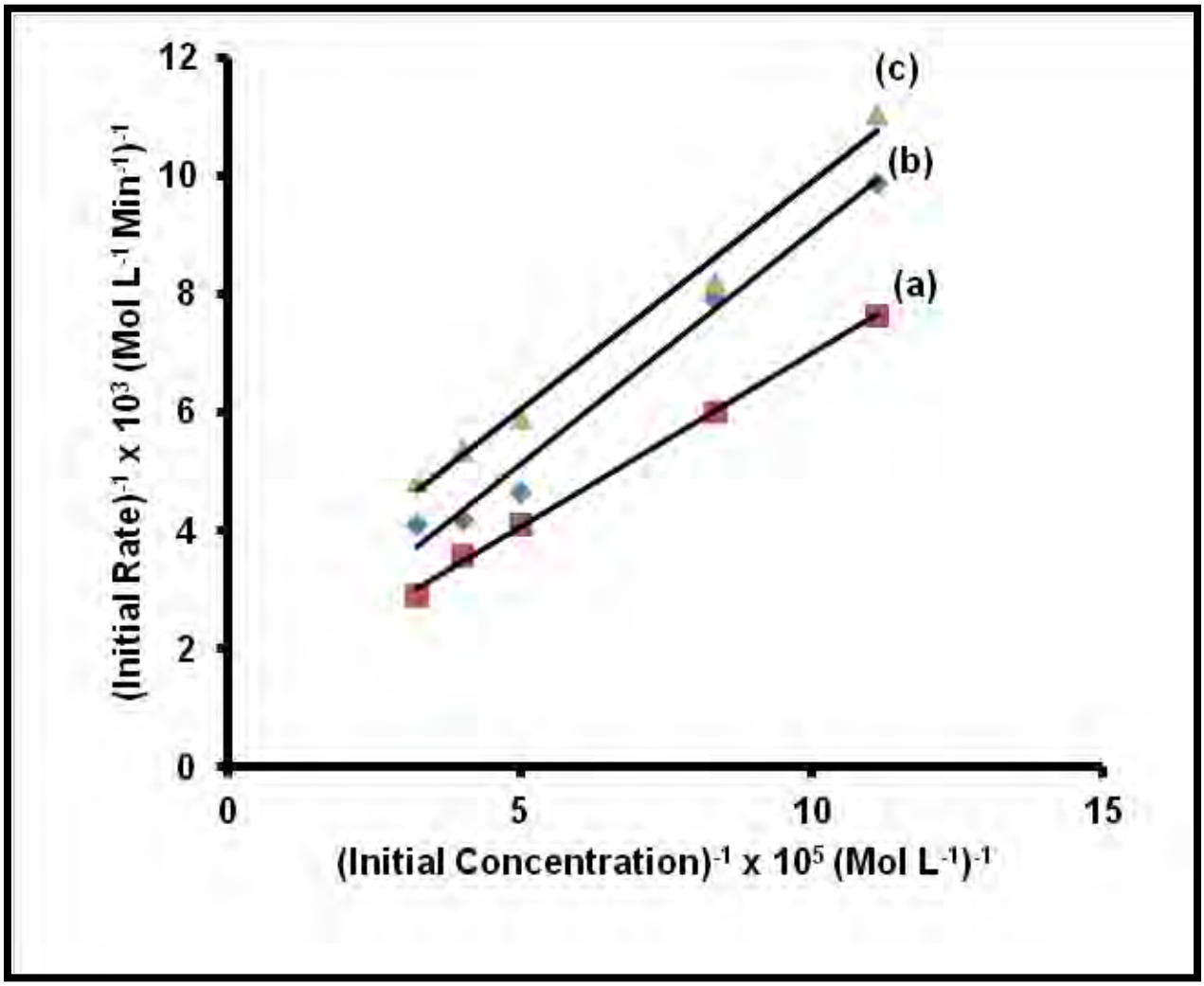

Figure 5.9: Plot of the inverse of initial reaction rate (rate^{-1}) versus the reciprocal of the initial concentration of 4-nitrophenol for photooxidation using 20 mg (a) PS/AcLuTPPc$^{\beta}$ (18a) (b) PS/AcLuTPyPc$^{\beta}$ (18c) (c) PS/ZnPc functionalized fiber.

The apparent rate constant for PS/AcLuTPPcβ (**18a**) (8.76 x 10^{-6} mol L^{-1} min^{-1}) is larger than for both PS/AcLuTPyPcβ (**18c**) (8.48 x 10^{-6} mol L^{-1} min^{-1}) and PS/ZnPc (4.5 x 10^{-6} mol L^{-1} min^{-1}). This also indicates a slightly faster reaction kinetics for the degradation of 4-nitrophenol with PS/AcLuTPPcβ (**18a**) fiber than with both PS/AcLuTPyPcβ (**18c**) and PS/ZnPc fibers. This is a reflection of the slightly higher singlet oxygen quantum yields of the former. The absorption coefficient, K of PS/AcLuTPPcβ (**18a**) (1.5 x 10^3 mol^{-1}) is slightly lower than those of PS/AcLuTPyPcβ (**18c**) (2 x 10^3 mol^{-1}) and PS/ZnPc (5.8 x 10^3 mol^{-1}) but all greater than 1. This suggests that adsorption was favored than desorption.

5.2.4 Photodegradation of methyl orange

The double bond in azo dyes determines the colour of the dyes and is very reactive usually undergoing oxidation leading to fading of the color of its solution [213]. In this work methyl orange was used as representative azo dye. The catalysis of methyl orange was carried out at pH of 9.2 in an aqueous buffer solution. Preliminary work was done on homogeneous catalysis using ZnTmPyPcβ (**24**) and when ZnTmPyPcβ (**24**) was functionalized on polysulfone (PSU) electropun fiber. It has been reported that azo dyes with the sulphonic groups, such as methyl orange, tend to adsorb onto the surface of a positively charged catalyst at low pH and thus are merely being transferred from solution to solid and no degradation occurs [284, 285]. In this work the functionalized fiber, PSU/ZnTmPyPcβ (**24**) has such positive units, hence the choice of basic (pH 9.2) instead of acidic pH. The change in the absorption spectra of aqueous solutions of

methyl orange, an azo dye, during the photocatalytic processes at different irradiation times are shown in Fig 5.10. As shown in both cases, the band around 470 nm that corresponds to azo dye decreases in intensity during irradiation of methyl orange in the presence of the ZnTmPyPc$^{\beta}$ (**24**) in solution or in the functionalized fiber. The band in the UV portion (around 330 nm) could be attributed to the benzene rings of methyl orange [155, 286]. This band did not decrease in intensity but rather showed a slight increase in both cases. This suggests that the benzene rings were not degraded during the catalysis. Thus products of substituted benzene are expected in the reaction mixture and not products resulting from ring opening. When methyl orange solution alone as well as the solution in the presence of the non-functionalized fiber, were irradiated, no visible decrease in the azo band absorption was observed.

This suggests that the phthalocyanine is the agent involved in the photo-transformation of the dye.

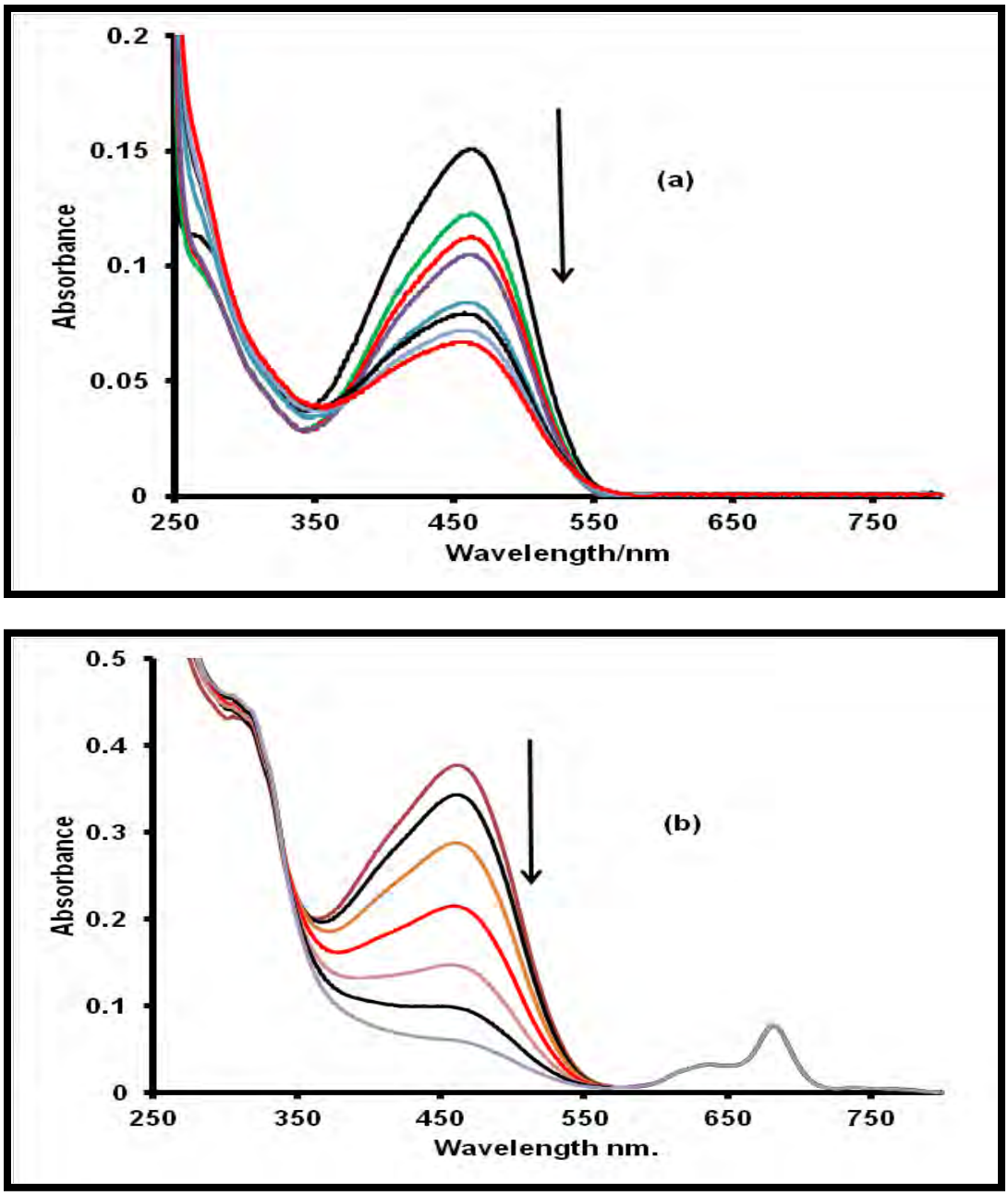

Figure 5.10: UV-visible spectral changes of an aqueous solution of methyl orange containing (a) 20 mg PSU/ZnTmPyPc$^{\beta}$ (24) and (b) 1.5 x 10^{-5} mol L^{-1} ZnTmPyPc$^{\beta}$ (24).

The plots of $\ln(C_0/C_t)$ versus irradiation time, Fig. 5.11, in both cases were linear and this suggests that the photodegradation reactions follows first order reaction kinetics.

The observed rate constant at various initial concentrations and other kinetic parameters are listed in Table 5.6. The reaction rates are faster for the photo-conversion of the dye occuring in aqueous solution of ZnTmPyPc$^{\beta}$ (**24**). This is expected since generally in homogeneous systems there is better and more effective interaction between the reactants. Also the singlet oxygen oxygen quantum yield of the ZnTmPyPc$^{\beta}$ (**24**) is higher in water (0.43) than when it is constrained within the solid fiber matrix (0.21). Singlet oxygen is implicated in photocatalysed reactions and hence the above observed differences in the reaction rates.

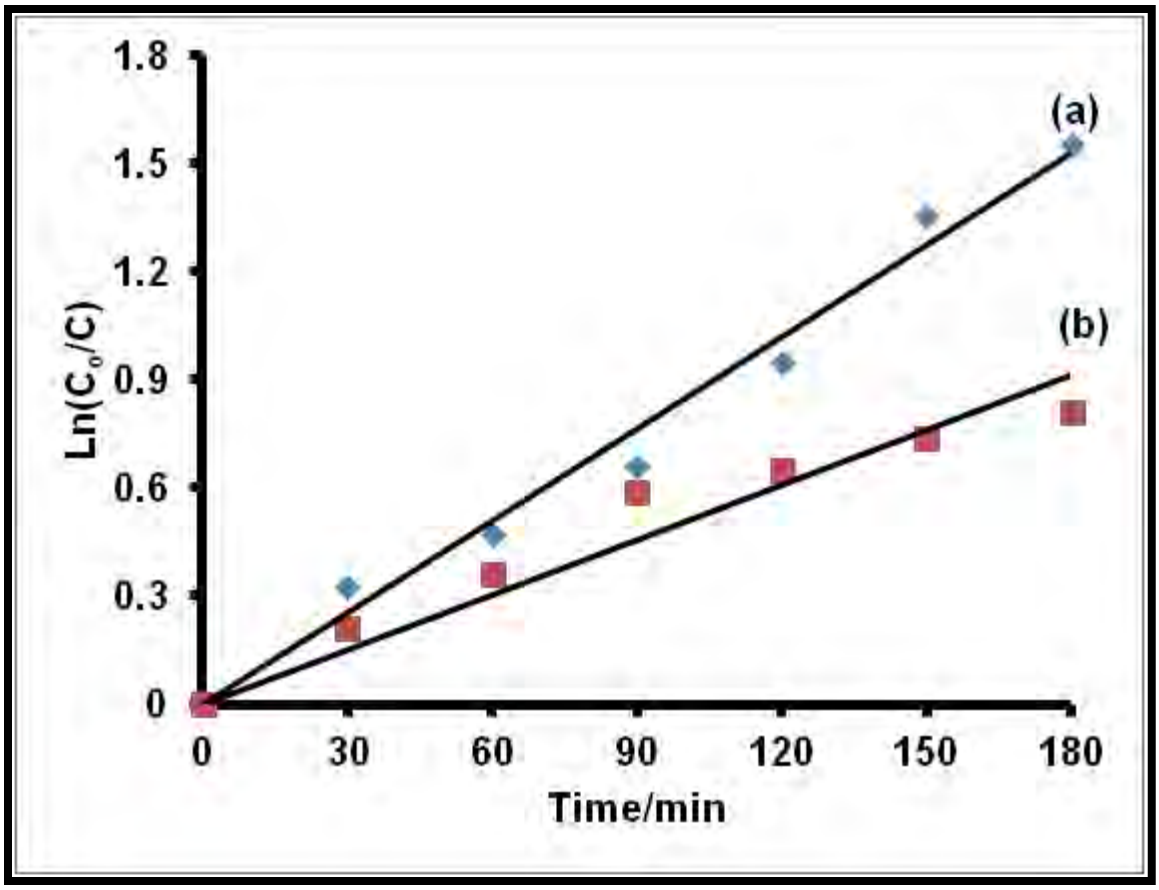

Figure 5.11: First order kinetics plots for degradation of 1.5 x 10^{-4} mol L^{-1} of methyl orange using ZnTmPyPc$^{\beta}$ (24), (a) in solution (b) in fiber.

Table 5.6: The kinetic data of various initial concentrations of methyl orange using ZnTmPyPc$^{\beta}$ (24) in aqueous solution and PSU fiber.

Concentration/ x 10^{-4} mol L^{-1}	Medium of the ZnTmPyPc$^{\beta}$ (19)	k_{obs}/ x 10^{-3} min^{-1}	Initial Rate/x 10^{-6}mol L^{-1} min^{-1}	Half-life /min
1.5	Solution	8.5	1.28	81.55
	Fiber	5.1	0.77	135.91
2.5	Solution	5.6	1.40	123.78
	Fiber	3.7	0.93	187.34
3.1	Solution	4.8	1.49	144.41
	Fiber	3.3	1.02	210.04
4.0	Solution	4.2	1.68	165.04
	Fiber	2.9	1.16	239.04

Kinetic studies were also conducted for complexes **14**, **18a**, **18c**, and **19** using PS fiber in addition to PSU/ZnTmPyPc$^{\beta}$ (**24**) fiber. Table 5.7 compares the kinetics of the phototransformation of methyl orange using PS or PSU functionalized fibers. As shown, the reaction rates are again dependent on Φ_{Δ} values for Pc complexes, with AcLuTPPc$^{\beta}$ (**18a**) with high Φ_{Δ} value giving the largest k_{obs}, and AcLuTmPyPc$^{\beta}$ (**19**) with a low Φ_{Δ} giving the lowest k_{obs}. The half-lives are largest for lowest Φ_{Δ} as was the case for 4-CP and 4-NP.

Table 5.7: Kinetic data for phototransformation of methyl orange at initial concentration of 2.5 x 10^{-4} mol L^{-1} using different functional fibers.

Functionalized fiber	k_{obs}/x 10^{-2} min^{-1}	Initial reaction rate/x 10^{-6} mol L^{-1} min^{-1}	Half-life/min	Φ_Δ in fiber
PS/AcLuTPPc$^{\beta}$ (18a)	0.40	1.0	173	0.28
PS/AcLuTPPc$^{\alpha}$ (14)	0.36	0.91	192	0.22
PS/AcLuTPyPc$^{\beta}$ (18c)	0.34	0.85	204	0.17
PS/AcLuTmPyPc$^{\beta}$ (19)	0.32	0.80	216	0.15
PSU/ZnTmPyPc$^{\beta}$ (24)	0.37	0.93	187	0.21

In the case of the photocatalysis involving the functionalized fiber, the Langmuir-Hinshelwood (L-H) expression was also used to assess the extent of adsorption of methyl orange onto the functionalized fiber. The apparent rate constant was found to be 1.86 x 10^{-6} mol L^{-1} min^{-1} and the adsorption coefficient of methyl orange onto the functionalized fiber surface was found to be 0.025 mol^{-1} . The adsorption coeffient is less

than one (K < 1), suggesting that adsorption of the methyl orange is less favourable than desorption at pH 9.2.

5.3 Summary of the degradation of 4-chlorophenol, 4-nitrophenol and methyl orange

5.3.1 Polystyrene PS/phthalocyanine functionalized fibers

The reactivity of phenolic compounds can be drastically affected by the electronic nature of substituents and by their positions in the aromatic ring [287, 288]. Thus the extent to which each of these phenolic pollutants can be removed from the environment by any particular catalytic system is greatly influenced by their reactivity. In this work the ease of photodegradation of the two substituted phenolic compounds (4-CP and 4-NP) was assessed using the polystyrene functionalized fibers PS/(Ac)LuTPPc$^{\alpha}$ (**14**), PS/(Ac)LuTPPc$^{\beta}$ (**18a**), PS/(Ac)LuTPyPc$^{\beta}$ (**18c**) and PS/(Ac)LuTmPyPc$^{\beta}$ (**19**), these are photoactive with Φ_{Δ} = 0.22, 0.28, 0.17 and 0.15, respectively, Table 5.8.

Table 5.8: Kinetic data using PS fibers for photodegradation of the pollutants.

Functionalized fiber	Φ_Δ	Pollutant	Initial conc. /x 10^{-4} mol L^{-1}	k_{obs}/ x 10^{-2} min^{-1}	Initial rate/x 10^{-6} mol L^{-1} min^{-1}	Half-life /min
PS/(Ac)LuTPPc$^{\beta}$ (18a)	0.28	4CP	1.2	3.00	3.60	23
		4NP		1.38	1.66	50
		MO		0.61	0.73	114
		4CP	2.0	2.11	4.22	33
		4NP		1.22	2.44	57
		MO		0.46	0.91	151
		4CP	2.5	1.90	4.76	36
		4NP		1.11	2.78	62
		MO		0.40	1.00	173
PS/(Ac)LuTPPc$^{\alpha}$ (14)	0.22	4CP	1.2	2.62	3.14	26
		4NP		1.09	1.31	64
		MO		0.53	0.64	131
		4CP	2.0	1.98	3.95	35
		4NP		1.03	2.06	67
		MO		0.38	0.76	182
		4CP	2.5	1.71	4.27	41
		4NP		1.01	2.53	69
		MO		0.36	0.91	193
PS/(Ac)LuTPyPc$^{\beta}$ (18c)	0.17	4CP	1.2	1.93	2.31	36
		4NP		1.07	1.26	65
		MO		0.38	0.45	182
		4CP	2.0	1.80	3.60	39
		4NP		1.05	2.14	66
		MO		0.36	0.72	193
		4CP	2.5	1.58	3.95	44
		4NP		0.95	2.38	73
		MO		0.34	0.85	204

PS/(Ac)LuTmPyPcβ (19)	**0.15**	**4CP**	**1.2**	**1.83**	**2.20**	**38**
		4NP		**0.98**	**1.17**	**71**
		MO		**0.38**	**0.45**	**182**
		4CP	**2.0**	**1.77**	**3.55**	**39**
		4NP		**0.97**	**1.94**	**71**
		MO		**0.34**	**0.68**	**204**
		4CP	**2.5**	**1.58**	**3.95**	**44**
		4NP		**0.92**	**2.31**	**75**
		MO		**0.32**	**0.80**	**217**

In general, it was observed that photodegradation of 4-chlorophenol occurs faster than for 4-nitrophenol, with higher k_{obs} values for similar initial concentrations, Table 5.8. This is consistent with reported studies using other sensitizers [287]. The reported studies showed that the kinetics of the photocatalytic degradation of phenolic pollutants is faster for those containing electron-donating substituents. The –Cl group in this case is more electron donating than the $-NO_2$ group which accounts for the observed trend.

Furthermore, as illustrated in Fig. 5.12, a solution of 2.72×10^{-4} mol L^{-1} 4-chlorophenol could be degraded completely within two and half hours of irradiation with PS/(Ac)LuTPPcβ (**18a**) fiber, while sample solution of 4-nitrophenol of the same concentration and under similar experimental condition was not completely degraded.

The use of these functionalized fibers for the photoconversion of methyl orange, an azo dye, showed much slower reaction kinetics than those of the phenolic compounds, Table 5.8. Such slow photoconversion has been reported before for methyl orange [289,

290]. In all cases it was observed that the initial reaction rates increases with the initial concentration of the analyte. This is consistent with basic reaction kinetics laws.

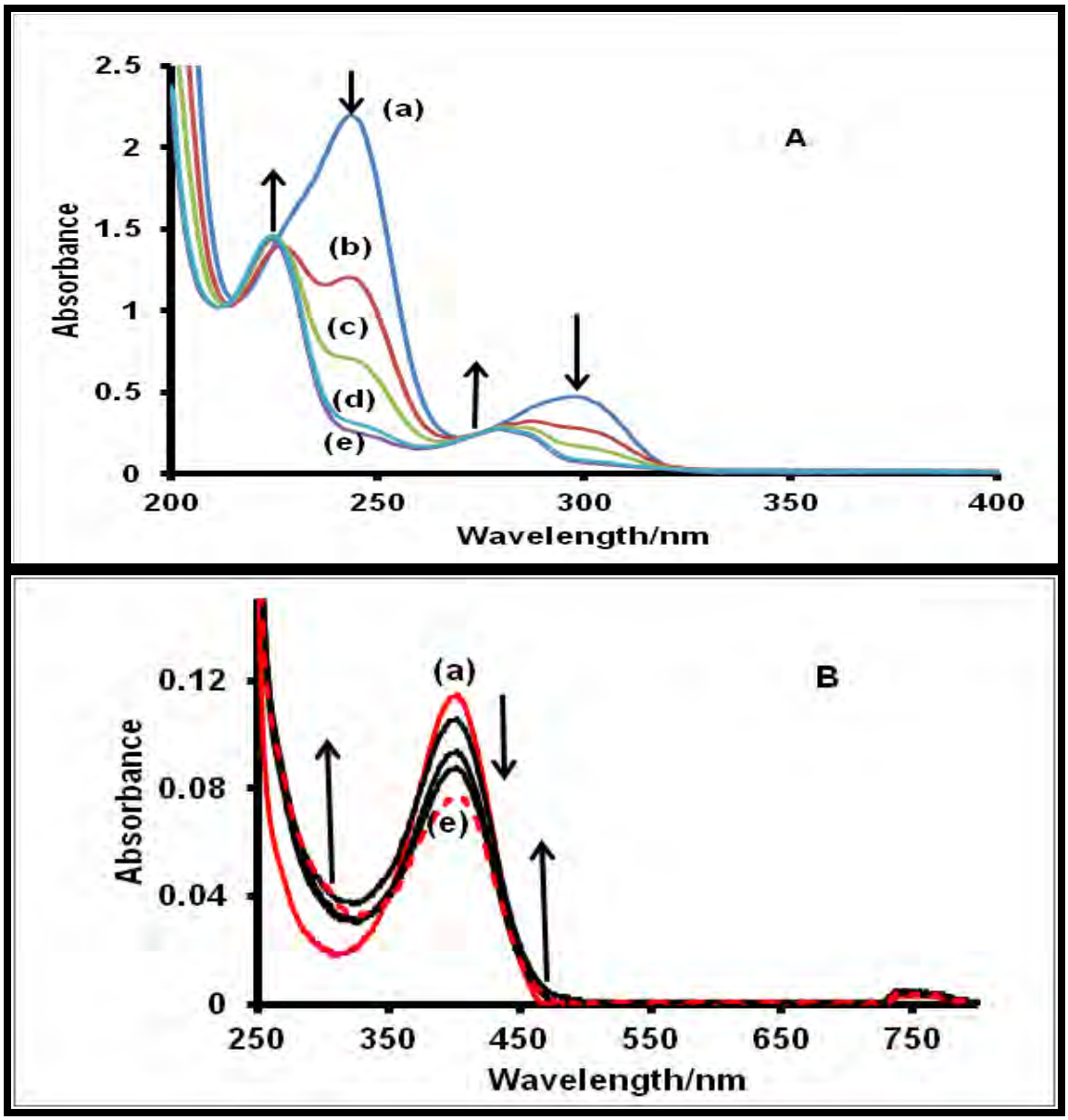

Figure 5.12: Electronic spectral changes of 2.72 x 10^{-4} mol L^{-1} of (A) 4-chlorophenol showing complete and (B) 4-nitrophenol incomplete degradation during its visible light photocatalysis in the presence of PS/(Ac)LuTPPc$^{\beta}$ (18a) fiber at times: (a) 0 (b) 1 h (c) 1.5 h (d) 2 h (e) 2.5 h.

5.3.2 Polysulfone PSU/phthalocyanine functionalized fibers

Zinc pthalocyanines complexes ZnPc, ZnTPyPcβ (**23**) and ZnTmPyPcβ (**24**), as examples, were used to functionalize polysulfone polymer fibers for the photoconversion of 4-chlorophenol, 4-nitrophenol and methyl orange. The fibers were generally insoluble in water and quite porous cotton-like in morphology and thus promising materials for photocatalytic application in aquatic systems.

ZnTPyPcβ (**23**) and ZnTmPyPcβ (**24**) have been reported to be photoactive with the quantum yield of singlet oxygen production 0.56 and 0.59 respectively in DMF [224], which are quite reasonable values for zinc phthalocyanines in DMF [212, 291].

The singlet oxygen yields in water were estimated to be 0.24 for PSU/ZnTPyPcβ (**23**), 0.21 for PSU/ZnTmPyPcβ (**24**) and 0.25 for PSU/ZnPc fibers, Table 5.9. The lower singlet oxygen quantum yield for ZnTPyPcβ (**23**), ZnTmPyPcβ (**24**) and ZnPc within the solid fiber matrices and in water compared to those in DMF (at Φ_{Δ} = 0.56, 0.59 and 0.56, respectively) could be due the reasons given above for polystyrene functionalized fibers. The efficiency of the photoconversion of 4-chlorophenol, 4-nitrophenol and methyl orange using PSU/ZnTPyPcβ (**23**), PSU/ZnTmPyPcβ (**24**) and PSU/ZnPc fibers follow similar trends as those of polystyrene functionalized fibers Table 5.9. Again 4-chlorophenol proved to be much more susceptible to photodegradation than 4-nitrophenol with methyl orange been quite difficult to photodegrade.

Table 5.9: Kinetic data for PSU functionalized electrospun fibers with various initial concentrations of the pollutants. Values in brackets for DMF solution.

Functionalized fiber	Φ_Δ fiber	Pollutant	Initial conc. /x 10^{-4}mol L^{-1}	k_{obs}/ x 10^{-2} min^{-1}	Initial rate/x 10^{-6} mol L^{-1} min^{-1}	Half-life /min
PSU/ZnTPyPc$^{\beta}$ (23)	0.24 (0.56)	4CP	1.2	2.83	3.39	24
		4NP		1.21	1.45	57
		MO		0.62	0.74	112
		4CP	2.0	2.01	4.02	34
		4NP		1.19	2.37	58
		MO		0.45	0.89	154
		4CP	2.5	1.68	4.21	41
		4NP		1.05	2.63	66
		MO		0.38	0.94	182
PSU/ZnTmPyPc$^{\beta}$ (24)	0.21 (0.59)	4CP	1.2	2.24	2.69	31
		4NP		1.09	1.31	64
		MO		0.50	0.60	139
		4CP	2.0	1.75	3.50	40
		4NP		0.99	1.98	70
		MO		0.41	0.82	169
		4CP	2.5	1.64	4.10	42
		4NP		0.81	2.02	86
		MO		0.37	0.93	187
PSU/ZnPc	0.25 (0.56)	4CP	1.2	2.34	2.81	30
		4NP		1.13	1.36	61
		MO		0.50	0.60	139
		4CP	2.0	1.75	3.50	40
		4NP		1.02	2.03	68
		MO		0.42	0.83	165
		4CP	2.5	1.64	4.11	42
		4NP		0.85	2.13	82
		MO		0.37	0.93	187

The PSU/ZnPc and PSU/ZnTPyPc$^{\beta}$ (**23**) fibers are more promising photo-sensitising material than PSU/ZnTmPyPc$^{\beta}$ (**24**) fibers possibly due to their difference in singlet oxygen quantum yields.

5.4 Product analysis

The catalytic products of 4-chlorophenol and 4-nitrophenol were identified with gas chromatography using standards. Also samples solutions were injected directly into ion trap mass spectrometer to further ascertain the identity of the products.

In the case of 4-chlorophenol, three degradation products were obtained, benzoquinone, hydroquinone and 4,4'-oxydiphenol, Fig. 5.13 (a). The benzoquinone and hydroquinone photoproducts are consistent with what was suggested from the UV-visible spectral changes of the sample solutions, Section 5.2.2, while 4,4'-oxydiphenol, a dimeric product originate from electron transfer reactions (Type I mechanism) as been reported [162], Scheme 5.1.

In the case of 4-nitrophenol, benzoquinone, hydroquinone and 4-nitrocatechol (Fig. 5.13 (b)) were the products also suggesting the involvement of both Type I and Type II photodegradation mechanisms involving the sensitizers, Scheme 5.2.

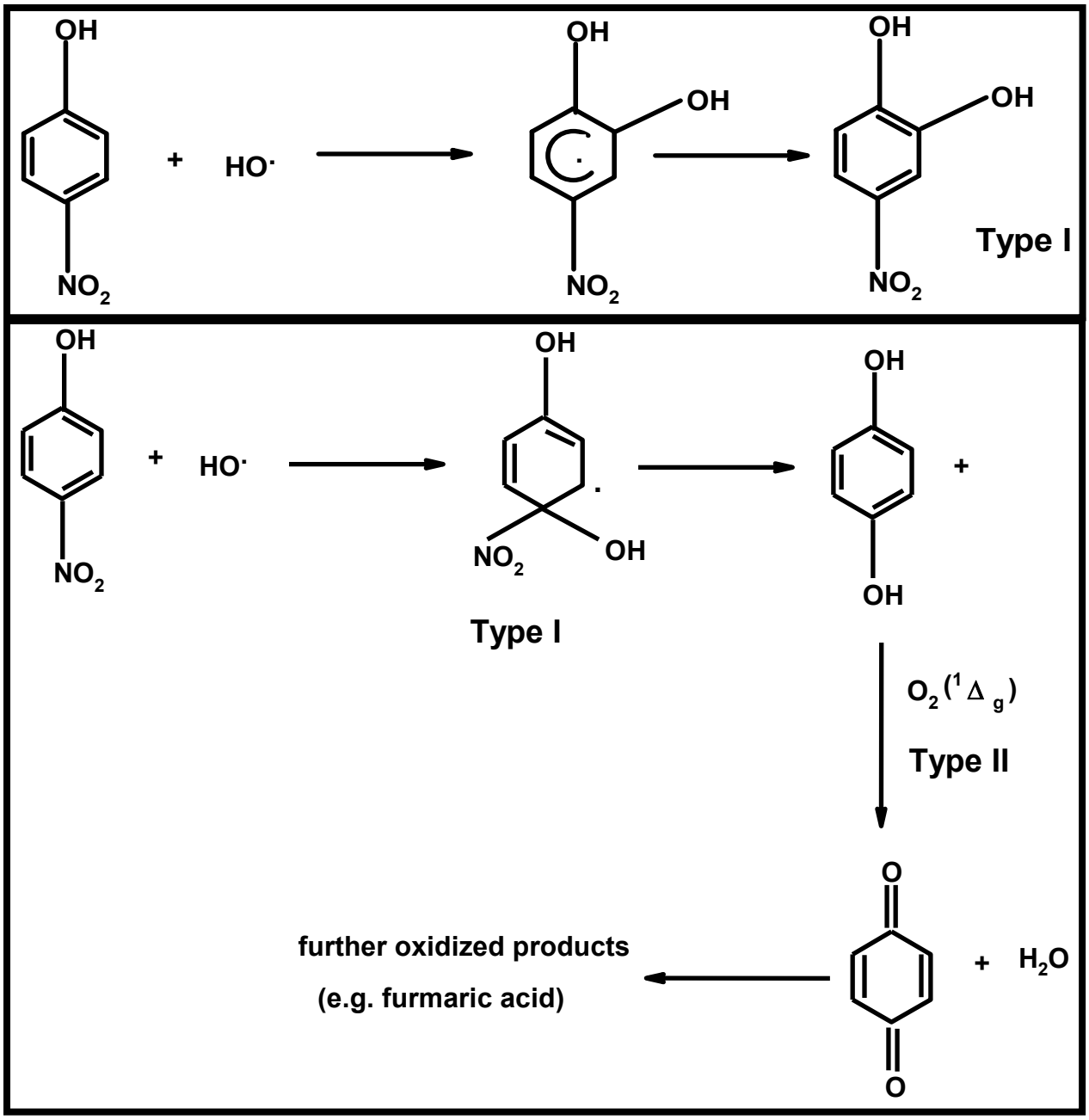

Scheme 5.2: Mechanisms of photooxidation of 4-NP to form benzoquinone, 4-nitrocatecol and hydroquinone.

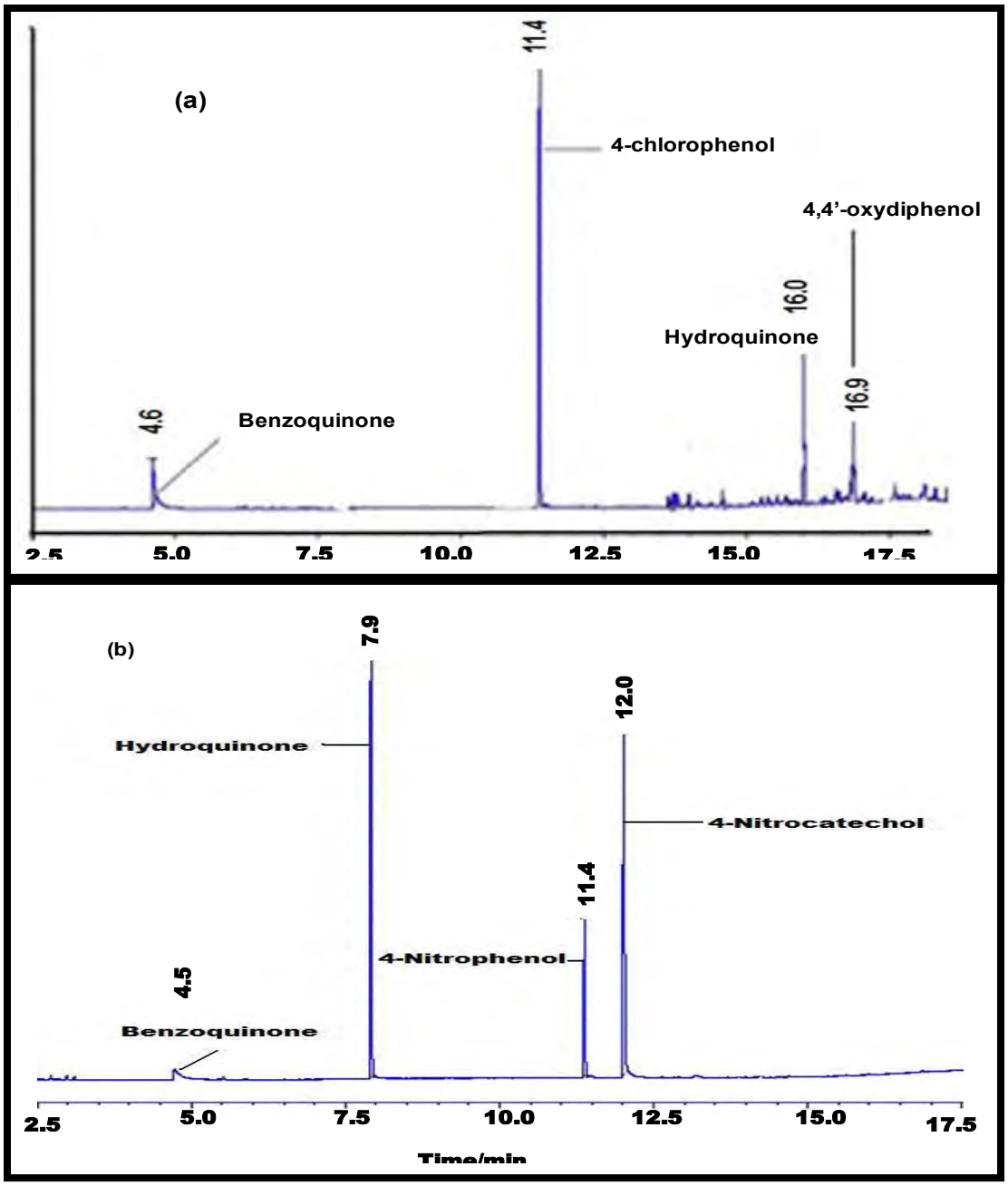

Figure 5.13 : Gas chromatographic traces of photolysis products of (a) 4-chlorophenol (b) 4-nitrophenol in dichloromethane after extraction from aqueous sample solutions.

Mass spectral analysis of the photodegradation products of methyl orange showed the presence in the solution of a coupling product at m/z = 293 amu as well as a series of oligopolymeric products (m/z = 324, 325, 397, 398 amu). Similar degradation products have been reported for oxidative degradation of methyl orange, and the coupling product was identified as 2-amino-5-(3-hydroxy-4-oxo-cyclohexa-2,5-dienylideneamino)-benzene sulphonic acid (m/z = 293 amu) and the oligopolymeric product (m/z = 325 amu) was identified as poly(catechol) [292].

5.5 Stability and re-usability of fibers

The photostability of imbedded sensitizer is an important factor for the application of such fabric materials for photocatalysis. Therefore the photostability of phthalocyanines within the fiber matrices were assessed by observing the Q-band absorption spectrum of an equivalent amount (10 mg) of the fibers before and after catalysis, both dissolved in equal volume of THF (4 mL), Fig 5.14, for (Ac)LuTPPc$^{\alpha}$ (**14**)/PS fiber. As indicated, the decrease in the absorption band after the photolysis suggests that the

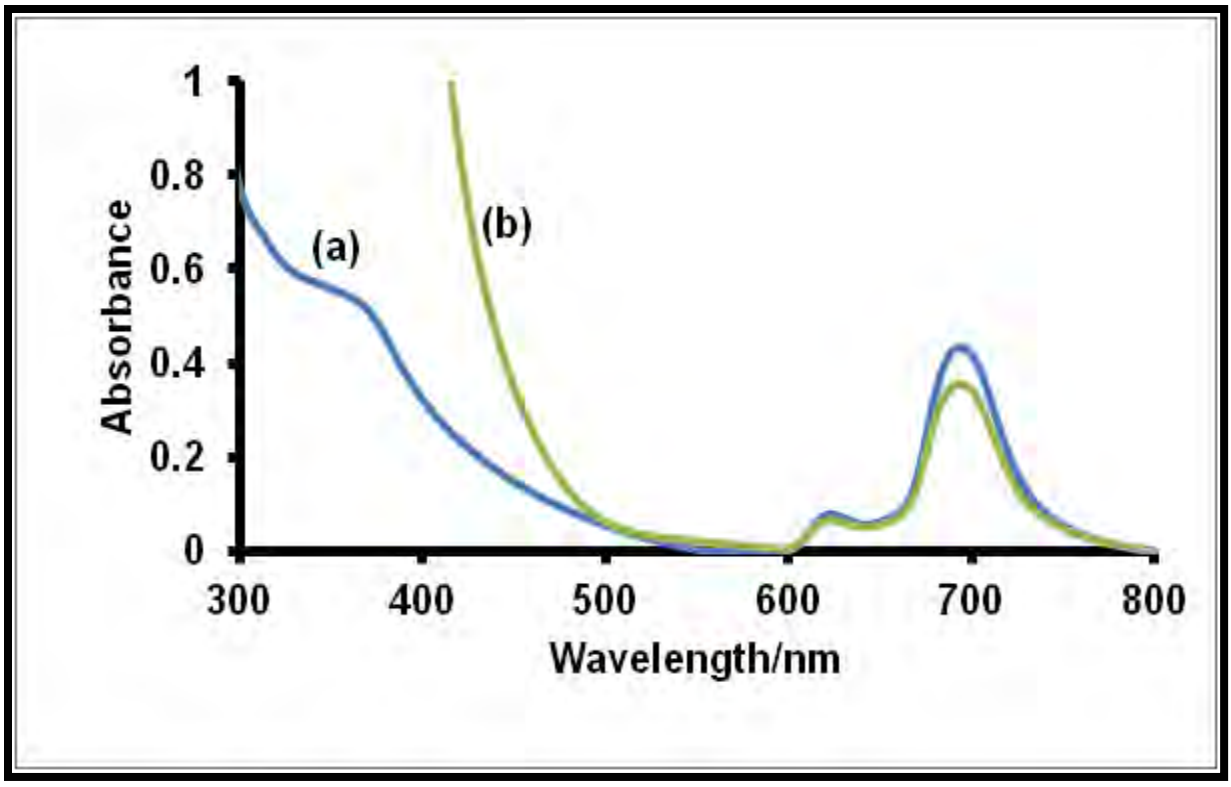

Figure 5.14: UV-Vis spectra of 10 mg of PS/(Ac)LuTPPC$^{\alpha}$ (14) functionalized fiber (a) not used in catalysis and (b) used in catalysis (Time 12 h), each dissolved in 4 mL of THF.

phthalocyanine photodegrades slightly upon continuous irradiation for 12 h. This could account for the decrease in the reaction rates when the functionalized fibers were used for repetitive conversion of the the pollutants. Nonetheless, the fiber could be re-used for at least three cycles of degradation. FT-IR analysis of the fibers before and after irradiation showed no apparent structural changes in the components. Also scanning electron microscopic (SEM) images of all the functionalized electrospun polystyrene polymer fibers after use indicate that their average diameters remained virtually the

same. However the strands of fibers became more closely compressed than before use. Thus there was reduced porosity in the fiber mats and this could also account for the reduced degradation rate of the analytes during re-use of the fibers.

In the case of the polysulfone functionalized fiber, the zinc phthalocyanines were quite stable under the applied irradiation light intensity. However, the functionalized fibers folded up into a hard lump when they dried after the first cycle of catalysis and could not be applied again.

For ZnTmPyPc$^{\beta}$ (**24**), its stability was assessed as an example, by irradiating an aqueous solution of it with visible light. This was done since this complex was employed to phototransform methyl orange in solution. It is known that phthalocyacines oxidatively decompose with time in the presence of singlet oxygen upon irradiation with visible light. Fig 5.15 shows the degradation profile of the phthalocyanine which occurred at an elevated light intensity of 3.52×10^{20} photons $cm^{-2}\ s^{-1}$. A very slow decrease in both the Q and B bands were observed. The decomposition follows first order kinetics and the rate constant which is a quantitative index of the stability of the phthalocyanine was found to be $8.0 \times 10^{-4}\ min^{-1}$. This is far smaller than the rate constants reported for other alkoxy and arloxy substituted phthalocyanines [85]. The difference in the rate constants could be attributed to the different solvent media, as stated before since water quenches singlet oxygen. Nonetheless the small value of rate constants obtained suggests that the phthalocyanine is photostable and could be applied for catalysis involving long periods of irradiation. The corresponding photodegradation quantum yield (Φ_P) was found to

be 1.9 x 10^{-4} quantum cm^{-2} s^{-1} which is comparable to those of alkoxy-substituted phthalocyanine complexes reported [85], which have been described as stable complexes.

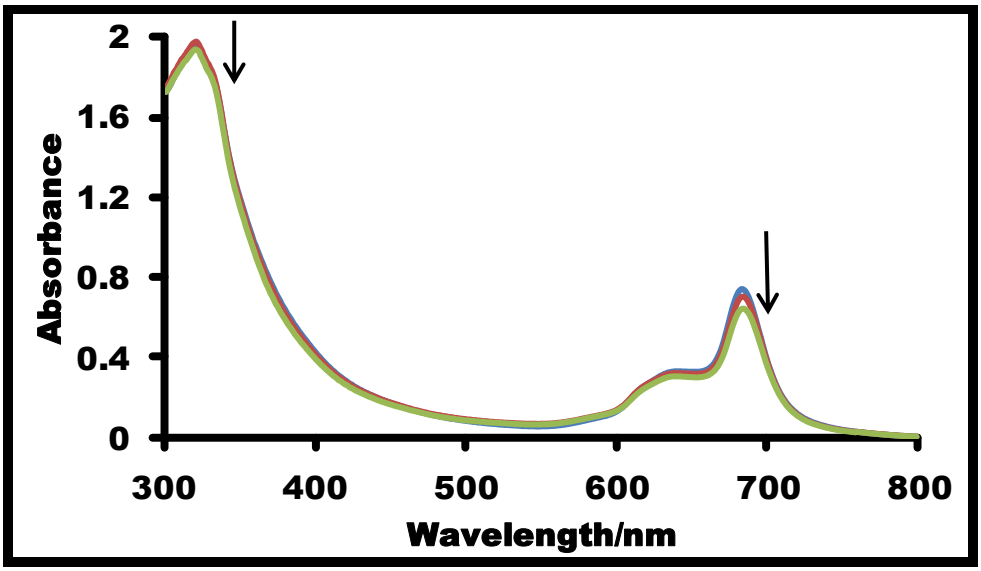

Figure 5.15: Photodegradation profile of ZnTmPyPc$^{\beta}$ (24) in DMF, light intensity: 3.52 x 10^{20} photons cm^{-2} s^{-1}, time interval 1 h.

5.6 Remarks on chapter

In this work various polymers incorporating a series of zinc and lutetium phthalocyanine complexes were electrospun into fibers and used for either the detection of nitrogen dioxide or the photo-conversion of azo dye and phenolic compounds in aqueous media. Polystyrene and polysulfone functionalized fibers were found to be promising fabric materials for the photodegradation of 4-chlorophenol, 4-nitrophenol and the methyl orange with the ease of conversion generally in the order 4-chlorophenol > 4-nitrophenol > methyl orange. Polystyrene fibers were found to be re-

usable for at least three times. Electrospun polymer fibers incorporating the fluorescent zinc phthalocyanine derivatives were found to be promising materials for the detection of nitrogen dioxide gas in the environment.

Chapter 6

6. Conclusions and suggestions

6.1. Conclusions

In this work, syntheses and spectroscopic characterization of lanthanide phthalocyanines containing dysprosium, erbium and lutetium as central metals were carried out. It was intended to synthesize the monomers of these lanthanide phthalocyanines. However under the synthetic conditions employed, a dimeric dysprosium bis-phthalocyanine was obtained, while those of erbium and lutetium were the monomers. The dysprosium bis-phthalocyanine and monomeric erbium phthalocyanines did not show photoactivity and their fluorescence was found to be very low. Thus they could neither be applied in photoconversion of analytes where generation of singlet oxygen is required nor be applied in fluorimetric detection of analytes. On the other hand the lutetium phthalocyanines were found to be photoactive and promising photosensitizers for the conversion of environmental pollutants such as phenols and dyes. However their low fluorescence limited them as fluorimetric agents for detection of analytes.

Zinc phthalocyanines, zinc(II) 2(3), 9(10), 16(17), 23(24)-(tetrapyridyloxy)]-phthalocyanine and zinc(II) 2(3), 9(10), 16(17), 23(24)- tetrakis[4-(N-methylpyridyloxy)]-phthalocyanine including the unsubstituted zinc phthalocyanine which are known photoactive and fluorescent agents were used alongside the lutetium phthalocyanines

for detection and phototransformation of environmental pollutants. The phthalocyanines were first incorporated into electrospun polymer fibers and characterized using various spectroscopic and microscopic techniques. Results suggested that the phthalocyanines were embedded and uniformly disperse within the fiber matrices.

The photophysical and photochemical properties of the lutetium and zinc phthalocyanines incorporated into various electrospun polymer fiber matrices were also assessed. The fluorescence behaviors of the composite electrospun fibers were found to parallel those in solution. The zinc phthalocyanines composite electrospun fibers showed the characteristic red fluorescence under irradiation, while those of lutetium did not fluoresce which was similar to studies in solution. Also the singlet oxygen generating ability of each of the phthalocyanines was maintained in the solid fibers. These polymeric fiber materials incorporating the phthalocyanines were thus promising fabric materials in developing optoelectronic devices that are responsive free radical especially nitrogen dioxide gas as well as promising materials for the photo-conversion of environmental pollutants such as 4-nitrophenol, 4-chlorophenol and methyl orange especially in aqueous media.

The electrospun polymer fibers containing the zinc phthalocyanines could detect qualitatively nitrogen dioxide within the environment by fluorescence quenching, while those containing lutetium phthalocyanine were not suitable.

All the functionalized electrospun fibers containing both lutetium and zinc phthalocyanines were found to be promising fabric materials for the photodegradation of 4-chlorophenol, 4-nitrophenol and the methyl orange. The ease of photo-transformation of these environmental pollutants was found to follow generally the order: 4-chlorophenol > 4-nitrophenol > methyl orange except a small difference in the trend with PS/ZnPc.

Electrospun fibers of polyacrylic acid and polyurethane were found not to be suitable in the photocatalytic applications while those of polystyrene could be applied and re-used for at least three times. Those of polysulfone could be applied once.

6.2. Future Prospects

The use of electropun fibers functionalized with phthalocyanines for solving environmental problems is quite promising. However, the porosity of these electrospun fibers and catalyst loading could be studied alongside the efficiency (mol of pollutant substrate transformed by mol of the catalyst) of the photocatalytic reaction as well as all other conditions that affect the quality of the fibers. Also a mixture of the pollutants to mimic a real-life environment should be photocatalyzed for a comparative study of the ease of phototransformation.

It will be of interest if these photoactive fabric materials could be applied in photodynamic anti-fungal and anti-bacterial studies possibly to use them as fabric materials for wound dressing.

References

1. N. B. Mckeown, Phthalocyanine Materials: Synthesis, Structure, Functions Cambridge Univ. Press, Cambridge, UK, 1998, 30
2. F. H. Moser, A. L. Thomas Eds), The Phthalocyanines, 2nd ed, CRC Press, Boca Raton, FL, 1983, vol 2
3. A. Braun, J. Tscherniac, Chem. Ber., 1907, 40, 2709
4. H. De Diesbach, E. von der Weid, Helv. Chem. Acta, 1927, 10, 886
5. A. G. Dandridge, H. A. Drescher, J. Thomas, GB patent, 3221691928
6. R. P. Linstead, J. Chem. Soc., 1934, 1022
7. C. E. Dent, R. P. Linstead, A. R. Lowe, J. Chem. Soc., 1934, 1033
8. J. M. Robertson, J. Chem. Soc., 1935, 615
9. J. M. Robertson, R. P. Linstead, C. E. Dent, Nature, 1935, 135, 506
10. J. M. Robertson, J. Chem. Soc., 1936, 1195
11. J. M. Robertson, I. Woodard, J. Chem. Soc., 1937, 219
12. J. M. Robertson, I. Woodard, J. Chem. Soc., 1940, 36
13. H. Zollinger, Color Chemistry, 2nd ed., VCH verlaggesellschaft, Weinheim, Germany, 1991
14. C. C. Leznoff, A. B. P. Lever (eds) Phthalocyanines, Properties and Applications, VCH, New York, 1989
15. H. A. Lubbs (eds) The Chemistry of Synthetic Dyes and Pigments, Reinhold Publishing, New York, 1955
16. G. E. Buono-Core, H. Li, B. Marciniak, Coord. Chem. Rev., 1990, 90, 87
17. W-N . Wu, N. Tang, L. Yan, J. Mater. Chem., 2008, 14, 2450

18. A. Edward, T. Y. Chu, C. Claude, I. Sokolik, Y. Okamoto, R. Dorisinville, Synth. Met., 1997, 84, 433

19. C. F. Meares, T. G. Wensel, Acc. Chem. Res., 1984, 17, 202

20. A. Kukhta, E. Kolesnik, I. Grabchev, S. Sali, J. Fluoresc., 2006, 16, 375

21. F. B. Wu, C. Zhang, Anal. Biochem., 2002, 311, 57

22. T. N. Sokolova, T. N. Lomova, V. V. Morozov, B. D. Berezin, Koord. Khlim., 1994, 20, 637

23. I. P. Kalashnikova, S. E. Nefedov, L. G. Tomilova, N. S. Zefirov, Russ. Chem. Bull., Int. Ed., 2007, 56, 2427

24. L. G. Tomilova, E. V. Chernykh, N. T. Ioffe, E. A. Luk'yanets, Zh. Obshch. Khim., 1983, 53, 2594

25. I. S. Kirin, P. N. Moskalev, Y. A. Makashev, Russ. J. Inorg. Chem., 1965, 10, 1065

26. I. S. Kirin, P. N. Moskalev, Russ. J. Phys. Chem., 1972, 46, 1019

27. P. N. Moskalev, A. I. Almova, Russ. J. Inorg. Chem., 1975, 20, 474

28. N. Nensala, T. Nyokong, Polyhedron, 1997, 16, 2971

29. K. M. Kadish, R. Guilard, K.M. Smith, the porphyrin handbook, Eds., phthalocyanines: synthesis vols 11-12, 1998, 63

30. A. Louati, M. E. I. Meray, J. J. Andre, J. Simon, K. M. Kadish, M. Gross, A. Giraurdeau, Inorg. Chem., 1985, 24, 1175

31. N. B. Mckeown, J. Painter, J. Mater, Chem., 1994, 4, 1153

32. L. F. Levey, H. Stephen, J. Chem. Soc., 1931, 79-82

33. J. G. Young, W. Onyebuagu, J. Org. Chem., 1990, 55, 2155-2159

34. R. D. George, A. W. Snow, J. Heterocyclic Chem., 1995, 32, 495

35. A. Tomoda, S. Saito, S. Ogawa, S. Shiraishi, Chem. Lett., 1980, 1277

36. P. A. Barret, D. A. Frye, R. P. Linstead, J. Chem. Soc., 1938, 1157

37. M. Hanack, D. Meng, A. Beck, M. Sommerauer, L. R. Subramanain, J. Chem. Soc. Chem. Comm., 1953, 58

38. G. Schmid, M. Sommerauer, M. Hanack, Angew Chem. Int. Ed. Engl., 1993, 32, 1422

39. M. Sommerauer, C. Rager, M. Hanack, J. Am. Chem. Soc., 1996, 118, 10085

40. S. Bayer, H. A. Dinçer, E. Gonca, Dyes and Pigmen., 2009, 80, 156

41. B. I. Kharisov, L. M. Blanco-Jerez, A. Garcia-Luna, Revista de la Sociedad Quimica de México, 1999, 43, 50

42. K. S. Jung, J. H. Kwon, S. M. Shon, J. P. Ko, J. S. Shin, S. S. Park, J. Mater. Sci., 2004, 39, 723

43. A. L. Thomas, Phthalocyanine Research and Application. CRC Press, 1990, F. H. Moser: A. L. Thomas Phthalocyanine Properties 1 CRC Press 1983

44. C. C. Lenznoff, A. B. P. Lever (eds), Phthalocyanines, Properties and Applications, VCH Publ. Inc., 1993

45. V. E. Prushkarev, L. G. Tomilova, Yu. V. Tomilov, Russ. Chem. Rev., 2008, 77, 875

46. M. M'Sadac, J. Ronclay, F, Garrier, J. Chim. Phys. Phys-Chim. Biol., 1986, 83, 211

47. V. N. Nemykin, N. A. Kostromina, N. B. Subbotin, S. V. Volkov, Russ. Chem. Bull., 1996, 45, 89

48. V. N. Nemykin, V. Y. Chernii, S. V. Volkov, J. Chem. Soc., Dalton Trans., 1998, 2995

49. G. Clarisse, M. T. Riou, Inorganic Chimica Acta, 1987, 130, 139

50. S. Bo, D. Tang, X. Liu, Z. Zhen, Dyes and Pigmen., 2008, 76, 35

51. A. V. Ziminov, T. A. Yurre, S. M. Ramsh, M. M. Mezdrogha, Phys. Solid state, 2010, 52, 1915

52. M. Durmuş, S. Yeşilot, B. Coşut, A. G. Gürek, A. Kilic, V. Ahsen, Syn. Met., 2010, 160, 436

53. F. H. Moser, Phthalocyanine Research and Applications, CRC Press, Boca Raton, 1990

54. M. J. Stillman, T. Nyokong, in C. C. Leznoff and A. B. P. Lever (eds), Phthalocyanines: Properties and Applications, vol 1, V. C. H., New York, 1989, 133

55. N. S. Hush, I. S. Woolsey, Mol. Phys. 1971, 21, 465

56. I. Renge, J. Phys. Chem., 1993, 97, 6583

57. E. Orti, J. L. Bredas, C. Clarisse, J. Chem. Phys., 1990, 92, 1228

58. N. Ishikawa, O. Ohno, Y. Kaizu, H. Kobayashi, J. Chem. Phys., 1992, 96, 8832

59. A. Ghosh, P. G. Gassman, J. Almlof, J. Am. Chem. Soc., 1994, 116, 1932

60. T. G. Gantchev, F. Beaudry, J. E. Van Lier, A. G. Michel, Int. J. Quantum Chem. 1993, 46, 191

61. C. Fierro, A. B. Anderson, D. A. Scherson, J. Phys. Chem., 1988, 92, 6902

62. M. Gouterman, in The Porphyrins, Part A. Physical Chemistry, D. Dolphin (Ed), Academic Press, New York, Vol 3, 1978, 1-165

63. J. Mack, M. J. Stilman, J. Am. Chem. Soc., 1994, 116, 1292

64. T. Kobayashi, T. Ashida, N. Uyeda, E. Surro, M. Kakuda, Bull. Chem. Soc. Jpn., 1971, 44, 2095

65. K. Ukei, Acta. Cryst., 1973, B29, 2290

66. M. J. Stillman, A. J. Thomson, J. Chem. Soc. Faraday Trans. II, 1974, 70, 790

67. A. B. P. Lever, Adv. Inorg. Radiochem., 1965, 7, 27

68. W. J. Schutte, M. Sluyters-Rehbach, J. H. Sluyters, J. Phys. Chem., 1993, 97, 6069

69. N. Kobayashi, S. Nakajima, H. Ogata, T. Fukuda, Chem. Eur. J., 2004, 10, 6294

70. N. Kobayashi, Coord. Chem. Rev., 2002, 227, 129

71. S. Makarov, Ch. Litwinski, E. A. Ermilov, O. Sovorova, B. Röder, D. Wöhrle, Chem. Eur. J., 2006, 12, 1468

72. E. S. Dodsworth, A. B. P. Lever, P. Seymour, C. C. Leznoff, J. Phys.Chem., 1985, 89, 5698

73. N. Kobayashi H. Lam, W. A. Nevin, P. Janda, C. C. Leznoff, A. B. P. Lever, Inorg. Chem., 1990, 29, 3415

74. Y. Asano, N. Kobayashi, Tetrahedron Lett., 2004, 45, 9577

75. K. Ishii, S. Abiko, M. Fujitsuka, O. Ito, N. Kobayashi, J. Chem. Soc. Dalton Trans., 2002, 1735

76. N. Kobayashi, A. B. P. Lever, J. Am. Chem. Soc., 1987, 109, 7433

77. D. Wöhhrle, L. Kreienhoop, D. Schletttwein, in Phthalocyanines. Properties and Applications, C. C. Leznoff, A. B. P. Lever, VCH Publishers, New York, 1996, 4, 219

78. H. M. Safarpour, H. Homborg, Z. Naturforsch., 1991, 46B, 1641

79. H. Konami, M. Hatano, A. Tajiri, Chem. Phys. Lett., 1989, 160, 163

80. N. Koike, H. Uekusa, Y. Ohashi, C. Harnoode, F. Kitamura, T. Ohsaka, K. Tokuda, Inorg. Chem., 1996, 35, 5798

81. H. Konami, M. Hatano, A. Tajiri, Chem. Phys. Lett., 1990, 166, 605

82. S. Abdurrahmanoğlu, A. R. Özkaya, M. Bulut, Ö. Bekaroğlu, Dalton Trans., 2004. 4022-4029

83. P. Suppan, Chemistry and light, Royal society, Cambridge, 1st ed., 1994

84. T. Shen, Z-I. Yuan, H-J. Xu, Dyes Pigm., 1989, 11, 77

85. P. Tau, T. Nyokong, J. Mol. Catal. A: Chem., 2007, 273, 149

86. A. Jablonski, Z. Phys. 1935, 94, 38

87. P. W. Atkins, in Physical Chemistry, P.W. Atkins (Ed.), Oxford University Press, Oxford, 6th Edition, 1998, Chapter 17

88. K Ishii, N. Kobayashi, in The Porphyrin Handbook, K. M. Kadish, K. M. Smith, R. Guilard, (Eds.)Elsevier Science, New York, 2003, Vol 16, Chapter 102

89. D. R. Arnold, N. C. Baird, J. R. Bolton, J. C. D. Brand, P. W. M. Jacobs, P. de Mayo, W. R. Ware, Photochemistry: An Introduction, Academic Press, New York, 1974

90. L. Kaestner, M. Cesson, K. Kassab, T. Christensen, P. D. Edminson, M. J. Cook, T. Chambrier, G. Jori, Photochem. Photobiol. Sci., 2003, 2, 660

91. B. Agboola, K. I. Ozoemena, T. Nyokong, J. Mol. Catal. A: Chem., 2006, 248, 84

92. P. Kubat, J. Mosinger, J. Photochem. Photobiol. A: Chem., 1993, 96, 93

93. S. Fery-Forgues, D. Lavabre, J. Chem. Educ., 1999, 76, 1260–1264.

94. S. E. Maree, D. Phillips, T. Nyokong, J. Porphyrins Phthalocyanines, 2002, 6, 17

95. X. F. Wang, T. Uchida, S. Minami, Appl. Spectrosc., 1991, 45, 560

96. G. J. Brakenhoff, M. Müller, R. I. Ghauharali, K. Visscher, Proc. SPIE, 1995, 2412, 115

97. H. C. Gerritse, R. Sanders, A. Draaijer, Proc. SPIE, 1994, 2329, 260

98. A. G. Ryder, S. Power, T. J. Glynn, J. J. Morrison, Proc. SPIE, 2001, 4529, 102

99. J. D. Spikes, J. Photochem. Photobiol. B. Biol. 1990, 6, 259

100. J. M Wessels, W. Strauβ, H. K. Seidlitz, A. Rück, H. Schneckberger, J. Photochem. Photobiol. B: Biol., 1992, 12, 275

101. I. Rosenthal, Photochem. Photobiol., 1991, 53, 859

102. T. J. Dougherty, Adv. Photochem., 1992, 17, 275

103. D. Wöhrle, W. Spiller, G. Schneider, G. Schulz-Ekloff, J. Stark, J. Inf. Rec. Mats., 1994, 21, 1

104. D. Wöhrle, G. Schneider, J. Stark, G. Schulz -Ekloff, J. Mol. Catal., 1992, 75, L39

105. M. C. Palumbo, N. A. Garcia, Toxicol. Environ. Chem., 1988, 17, 103

106. J. R. Wagner, H. Ali, R. Langlois, N. Brasseur, J. E. Lier, Photochem Photobiol., 1987, 45, 587

107. J. Davila, A. Harriman, Photochem. Photobiol., 1989, 50, 29

108. J. D Spikes, J. E. van Lier, J. C. Bommer, J. Photochem. Photobiol. A: Biol., 1995, 91, 193

109. J. R. Darwent, P. Douglas, A. Harriman, G. Porter, M. C. Richoux, Coord, Chem. Rev., 1982, 44, 83

110. M. Niedre, M. S. Patteerson, B. C. Wilson, Photochem. Photobiol., 2003, 75, 382

111. M. S. Patterson, S. J. Madsen, R. Wilson, J. Photochem. Photobiol. B: 1990, 5, 69

112. C. S. Foote, SPIE Institute Series, 1990, 6, 115

113. F. Wilkinson, W. P. Helman and A. B. Ross, J. Phys. Ref. Data., 1993, 22, 113

114. I. B. C. Matheson, Photochem. Photobiol., 1979, 29, 875

115. M. Jirsa, M. Jirsa Jr and P. Kuba´t, Sbornik le´karsky, 1995, 96, 1

116. C. S. Foote, In singlet oxygen (eds H. H. Wasserman and R. W. Murray) Academic Press, New York, San Francisco, London, 1979, 139

117. A. Ogunsipe, T. Nyokong, J. Photochem. Photobiol. A: Chem., 2005, 173, 211

118. D. Gu, Q. Chen, X. Tang, F. Gan, S. Shen, K. Liu, H. Xu, Opt. Comm., 1995, 121, 125

119. R. L. Milgrom, The colours of life, Oxford University Press, Oxford, 1997

120. M. I. Stilman, Immobilisation on polymers, VSP, Utrecht-Tokyo, 1991

121. N. V. Konovalova, R. P. Evstigneeva, V. N. Luzgina, Usp. Khim., 2001, 70, 1059

122. F. P. Montforts, B. Gerlach, F. Hoper, Chem. Rev., 1994, 94, 327

123. R. P. Linsted, M. J. Whalley, J. Chem. Soc., 1952, 4893

124. O. I. Koifman, T. A. Ageeva, Porphyrin Polymers, Izd.-Mat. Liter., Moscow, 2006

125. D. Wöhrle, J. Porphyrin Phthalocyanine, 2000, 4, 418

126. F. R. Hartley, Supported metal complexes, Reidel, Dordrecht, 1985

127. F. P. Sidel'kovskaya, Chemistry of N-vinylpyrrolidone and its polymers, Nuaka, Moscow, 1970

128. Yu. E. Kirsh, Poly-N-vinylpyrrolidone and other ploy-N-vinylamides: synthesis and physicochemical properties, Nauka, Moscow, 1998

129. V. V. Lopatin, Askadskii, Polyacrylamide, Hydrogels in Medicine, Nauchnyi Mir, Moscow, 2004

130. AI. Berlin, S. A. Vol'fson, V. G. Oshmyan, Principles of creation of polymer composite materials, Khimiya, Moscow, 1990

131. J. Simon, J. J. Andre, Molecular semiconductors, Springer, Berlin, 1985

132. H. Shirai, S. Higaki, J. Polym. Sci. Lett. Ed., 1984, 22, 1309

133. I. Yu. Denisyuk, N. V. Kamanina, opt. Spektrosk., 2004, 96, 269

134. J. H. Schutten, , J. Zwart., Mol. Catal., 1979, 5, 109

135. M. Sanchez, N. Chap, Eur. J. Inorg. Chem., 2001, 1775

136. H. Tsuiki, E. Masuda, Polymer, 1996, 37, 3637

137. A. K. Amanbaeva, Candidates Dissertation, Karaganda University, 2000

138. R. Zhou, L. Tang, Makromol. Chem. Phys., 1994, 795, 2409

139. D. Li, Y. N. Xia, Adv. Mater, Electrospinning of Nanofibers: Reinventing the Wheel?, 2004, 16, 1151

140. A. Frenot, I. S. Chronakis, Curr. Opin. Colloid interface Sci., 2003, 8, 64

141. A. Koski, K. Yim S. Shivkumar, Mater. Lett., 2004, 58, 493

142. B. Carlberg, M. Z. Axell, U. Nannmark, J. Liu, H. G. Kuhn, Biomed. Mater., 2009, 4, 045004

143. S-H. Tan, R. Inai, M. Kotaki, S. Ramakrishna, Polymer, 2005, 46, 6128

144. X. H. Zong, K. Kim, D. Fang, S. F. Ran, B. S. Hsiao, B. Chu, Polymer, 2002, 43, 4403-4412

145. S. Tombe, W. Chidawanyika, E. Antunes, G. Priniotakis, P. Westbroek, T. Nyokong, J. Photochem. Photobiol. A: Chem., 2012, 240, 50-58

146. M. M. Demir, I. Yilgor, E. Yilgor, B. Erman, Polymer, 2002, 43, 3303

147. V. N Morozov, T. Y. Morozova, N. R. Kallenbach, Int. J. Mass Spectrom., 1998, 178, 143

148. M. Y. Li, Y. Guo, Y. Wei, A. G. MacDiarmid, P. I. Lelkes, 2006, Biomaterials, 27, 2705

149. E. D. Boland, G. E. Wnek, D. G. Simpson, K. J. Pawlowski, G. L. Bowlin, J. Macromol. Sci. Pure Appl. Chem., 2001, 38, 1231

150. X. F. Wang, I. C. Um, D. F. Fang, A. Okamoto, B. S. Hsiao, B. Chu, Polymer, 2005, 46, 4853

151. M. Bognitzki, W. Czado, T. Frese, A. Schaper, M. Hellwig, M. Steinhart, A. Greiner, J. H. Wendorff, Adv. Mater., 2001, 13, 70-72

152. G. Verreck, I. Chun, J. Rosenblatt, J. Peeters, A. Van Dijck, J. Mensch, M. Noppe, M. E. Brewster, J. Control Release, 2003, 92, 439-360

153. S. Tang, C. Shao, Y. Li, R. Mu, J. Phys. Chem. Solids, 2007, 68, 2337

154. J. Mosinger, K. Lang, P. Kubát, J. Sýkora, M. Hof, L. Píštil, B. Mosinger Jr., J. Fluorec., 2009, 19, 709

155. S-L. Cheng, X-J. Huang, Z-K. Xu, Cellulose, 2011, 18, 1295

156. Z. Guo, B. Chen, J. Mu, M. Zhang, P. Zhang, Z. Zhang, J. wang, X. Zhang, Y. Sun, C. Shao, Y. Liu, J. Hazard. Mater., 2012, 219-220, 156-163

157. M. Karaskova, J. Rakusan, O. Jirsak, P. Jilek, NANCON 2010, Olomouc, Czech Republic, EU.

158. M. Alvaro, E. Carbonell, M. Esplá, H. Garcia, Appl. Catal. B, 2005, 57, 37

159. O. Legrini, E. Oliveiris, A. M. Braun, Chem. Rev. 1993, 93, 671

160. H. Ali, J. E. van Lier, Chem. Rev., 1999, 99, 2379

161. R. P. S. Suri, J. Liu, D. W. Hand, J. C. Crittenden, D. L. Perram, M. E. Mullins, Water Environ. Res., 1993, 65, 665

162. E. Silva, M. M. Pereira, H. D. Burrows, M. E. Azenha, M. Sarakha, M. Bolte, Photochem. Photobiol. Sci., 2004, 3, 200

163. J. G. Calvert, J. N. Pitts, Photochemistry, New York, John Wiley, 1967, 258

164. R. Bonnet, Chemical aspect of Photodynamic therapy S.1, Gordon and Breach, London, 2000, 70

165. R. Gerdes, D. Wöhrle, W. Spiller, G. Schneider, G. Schulz-Ekloff, J. Photochem. Photobiol. A, 1997, 111, 65

166. A. Gilbert, J. E. Baggott, Essentials of Molecular Photochemistry, Backwell Scientific, Oxford, 1991, 8-100

167. M. A. Zanjanchi, A. Ebrahimian, M. Arvand, J. Hazard. Mat., 2010, 175, 992

168. B. Agboola, K. I. Ozoemena, T. Nyokong, J. Mol. Catal. A Chem., 2006, 248, 84

169. L. Wu, A. Li, G. Gao, Z. Fei, S. Xu, Q. Zhang, J. Mol. Catal. A Chem., 2007, 269, 183

170. V. Iliev, D. Tomova, Catal. Comm., 2002, 3, 287

171. P. Kluson, M. Drobek, A. Zsigmond, J. Baranyi, P. Bata, S. Zarubova, A. Kalaji, Appl. Catal. B Envron., 2009, 91, 605

172. S-L. Wang, Y-F. Fang, Y. Yang, J-Z. Liu, A-P. Deng, X-R. Zhao, Y-P. Huang, Chinese Sci. Bull., 2011, 56, 969

173. R. Słota, G. Dyrda, K. Szczegot, G. Mele, I. Pio, Photochem. Photobiol. Sci., 2011, 10, 361

174. V. Iliev, D. Tomova, L. Bilyarska, L. Prahov, L. Petrov, J. Photochem. Photobiol. A Chem., 2003, 59, 281

175. Ma. I. Coahuila Hernandez, M. A. Garc´ıa Sanchez, A. M. Soto Estrada. A. Camp, J. Sol-Gel Sci. Techn., 2006, 37, 117

176. O. K. Varghese, A. A. Grimes, J. Nanosci. Nanotech., 2004, 3, 277

177. S. Dogo, J. P. Germain, C. Maleysson, A. Pauly, Thin Solid Films, 1992, 219, 251-256

178. J. D. Wright, P. Roisin, G. P. Rigby, Sens. Actuators B, 1993, 13-14, 276-280

179. J. C. Hsieh, C. J. Liu, Y. H. Ju, Thin Solid Films, 1998, 322, 98-103

180. A. Krier, A. K. Abass, R. A. Collins, Adv. Mater. Opt. Electron., 1993, 2, 289-293

181. J. Mortesson, H. Arwin, I. Lundström, Sens. Actuators B, 1990, 1, 134-137

182. J. F. Fernández-Sánchez, T. Nezel, R. Steiger, U. E. Spichiger-Keller, Sens. Actuators B, 2006, 113, 630-638

183. A. Fontijin, A. J. Sabadell, R. J. Ronco, Anal. Chem., 1970, 42, 575

184. X. Y. Tang, Atmosphere Environmental Science, High Education Press, Beijing, 1990

185. T. Nezel, U. E. Spichiger-Keller, C. Ludin, A. Hensel, Chimia, 2001, 55,725

186. T. Nezel, PhD Thesis, ETH Nr., 2002, 14602

187. K. Morishige, S. Tomoyasu, G. Iwano, Langmuir, 1997, 13, 5184

188. B. Yuliarto, H. Zhou, T. Yamada, I. Honma, Y. Katsumura, M. Ichihara, Anal. Chem., 2004, 76, 6719-6726

189. Z. Ling, C. leach, Sens. Actuators B, 2004, 102, 102-106

190. P. K. Dasgupta, Z. Genfa, S. K. Poruthoor, S. Caldwell, S. Dong, Anal. Chem., 1998, 70, 4661-4669

191. S. Chakane, A. Gokarna, S. V. Bhoraskar, Sens. Actuators B, 2003,92, 1- 5

192. J. W. Fleeger, K. R. Carman, R. M. Nisbet, Sci. Total Environ., 2003, 317, 207

193. D. Mukherjee, S. Bhttacharya, V. Kumar, J. Moitra, Biomed. Environ. Sci. 1990, 3, 337

194. D. Mukherjee, D. Guha, V. Kumar, S. Chakrabarty, Aquat. Toxicol., 1991, 21, 29

195. A. M. Shalaby, M. A. Mousa, H. A. Tag Elden, Egypt. J. Aquatic Biol. Fisheries, 2007, 11, 145

196. G. C. Jagetia, R. Aruna, Toxicology, 1997, 39, 205

197. T. Tsutsui, N. Hayashi, H. Maizumi, J. Huff, J. Burret, Mutat Res., 1997, 373, 112

198. T. S. Hori, L. M. Avilez, K. L. Inoue, G. Moraes, Biochemical Physiol., 2006, 143, 67

199. S. Koh, M. V. Mccullar, D. D. Focht, Appl. Environ. Microbiol., 1997, 63, 2054

200. G. W. Kohring, J. E. Rogers, J. Wiegel, Appl. Environ. Microbiol., 1989, 55, 348

201. F. Al-Momani, Environ. Eng. Sci., 2006, 23, 722

202. W. Z. Tang, C. P. Huang, Water Res., 1995, 29, 745

203. I. F. Cheng, Q. Fernando, N. Korte, Environ. Sci. Technol., 1997, 31, 1074

204. M. S. Ureta-Zanartu, P. Bustos. C. Berros, M. C. Diez, Electrochim. Acta, 2002, 47, 2399

205. T. A. Albanis, T. G. Danis, M. G. Kourgia, Environ. Technol. 1998, 19, 25

206. J. W. Lee, W. G. Shim, J. Y. Ko, H. Moon, Sep. Sci. Technol., 2004, 39, 2041

207. Y. Ku, C. B. Hsieh, Ind. Eng. Res., 1992, 31, 1823

208. J. Giménez, D. Curcó, M. A. Queral, Catal. Today, 1999, 54, 229

209. M. P. Ormada, J. L. Ovelleiro, J. Kiwi, Appl. Catal. B: Environ., 2001, 32, 157

210. K. Ozoemena, N. Kuznetsoval, T. Nyokong, J. Photochem. Photobiol. A: Chem., 2001, 139, 217

211. M. C. DeRosa, J. R. Crutchley, Coord. Chem. Rev., 2002, 233, 351

212. A. Ogunsipe, D. Maree, T. Nyokong, J. Mol. Struct., 2003, 650, 131

213. C. Zhu, L. Wang, L. Kong, X. Yang, L. Wang, S. Zheng, F. Chen, F. Maizhi, H. Zong, Chemosphere, 2000, 41, 303

214. F. Sosath, Biologisch-chemische Behandlung von Abwässern der Textilveredelung mit ReaKtivfarbstoffen, VDI Fortschrittsberichte, Reihe Umweltverfahrenstechnik, 1999, 209

215. J. Chang, C. Chou, Y. Lin, P. Lin, J. Ho, T. L. Hu, Water Res., 2001, 35, 2841

216. U. Pagga, D. Brown, Chemosphere, 1986, 15, 479

217. D. Brown, B. Humberger, Chemosphere, 1987, 16, 1539

218. N. Daneshvar, H. Ashassi-Sorkhabi, A. Tizpar, Sep. Purif. Technol., 2003, 31, 153

219. Y. M. Slokar, A. M. L. MareChal, Dyes Pigm., 1998, 37, 335

220. C. Galindo, P. Jacques, A. Kalt, Chemosphere, 2002, 48, 1047

221. N. Daneshvar, D. Salari, A. R. Khataee, J. Photochem. Photobio. A: Chem., 2004, 162, 317

222. M. Idowu, T. Nyokong, J. Photochem. Photobiol. A, 2008, 199, 282

223. B. N. Achar, G. M. M. Fohlen, J. A. Parker, J. Keshavayya, Polyhedron 1987, 6, 1463-1467

224. I. Scalise, E. N. Durantini, Bioorg. med. Chem., 2005, 13, 3037-3045

225. J. R. Lakowicz, Principles of Fluorescence Spectroscopy, 2nd ed., Kluwer Academic/Plenum Publishers, New York, 1999, p35

226. Gaussian 03, Revision E.01, M. J. Frisch, G. W. Trucks, H. B. Schlegel, G. E. Scuseria, M. A. Robb, J. R. Cheeseman, J. A. Montgomery, Jr., T. Vreven, K. N. Kudin, J. C. Burant, J. M. Millam, S. S. Iyengar, J. Tomasi, V. Barone, B. Mennucci, M. Cossi, G. Scalmani, N. Rega, G. A. Petersson, H. Nakatsuji, M. Hada, M. Ehara, K. Toyota, R. Fukuda, J. Hasegawa, M. Ishida, T. Nakajima, Y. Honda, O. Kitao, H. Nakai, M. Klene, X. Li, J. E. Knox, H. P. Hratchian, J. B. Cross, V. Bakken, C. Adamo, J. Jaramillo, R. Gomperts, R. E. Stratmann, O. Yazyev, A. J. Austin, R. Cammi, C. Pomelli, J. W. Ochterski, P. Y. Ayala, K. Morokuma, G. A. Voth, P. Salvador, J. J. Dannenberg, V. G. Zakrzewski, S. Dapprich, A. D. Daniels, M. C. Strain, O. Farkas, D. K. Malick, A. D. Rabuck, K. Raghavachari, J. B. Foresman, J. V. Ortiz, Q. Cui, A. G. Baboul, S. Clifford, J. Cioslowski, B. B. Stefanov, G. Liu, A. Liashenko, P. Piskorz, I. Komaromi, R. L. Martin, D. J. Fox, T. Keith, M. A. Al-Laham, C. Y. Peng, A. Nanayakkara, M. Challacombe, P. M. W. Gill, B. Johnson, W. Chen, M. W. Wong, C. Gonzalez, and J. A. Pople, Gaussian, Inc., Wallingford CT, 2004.

227. T. D. Smith, J. Livorness, H. Taylor, J. Chem. Soc. Dalton Trans, 1983, 1391-1400

228. X. Yuan, Y. Zhang, C. Dong, J. Sheng, Polym. Int., 2004, 53, 1704-1710

229. A. Ogunsipe, J-Y. Chen, T. Nyokong, New J. Chem., 2004, 28, 822

230. J. Kossanyi, D. Chachraroui, Int. J. Photoenergy, 2000, 2, 9-15

231. T. H. Tran-Thi, C. Desforge, C. Thiec, J. Phys. Chem., 1989, 93, 1226

232. N. Kuznetsova, E. Makarova, S. Dashkevich, N. Gretsova, E. Kalmykova, V. Negrimovsky, O. Kaliya, E. Luk'yanets, Obshch. Khim., 2000, 70, 140-148

233. A. Y. Tolbin, V. E. Pushkarev, G. F. Nikitin, L. G. Tomilova, Tetrahedron Lett., 2009, 69, 4848

234. A. Beck, K. M. Mangold, M. Hanack, Chem. Ber., 124, 1991, 2321

235. E. A. Luk'yanets, V. M. Derkacheva, J. Gen. Chem. USSR, 50, 1980, 1874

236. P. D. Hale, W. J. Pietro, M. A. Ratner, D. E. Ellis, T. J. Marks, J. Am. Chem. Soc., 109, 1987, 5943

237. Y. Brien, R. Wang, D. Wang, P. Zhu, R. Li, J. Dou, Helv. Chim. Acta, 2004, 87, 2581

238. R. M. Silverstein, G. C. Bassler and T. C. Morrill, Spectrometric Identification of Organic Compounds, 4th edn, John Wiley and Sons, New York, 1981

239. T. Nyokong, Coord. Chem. Rev., 2007, 251, 1707

240. X. F. Zhang, H. J. Xu, J. Chem. Soc. Faraday Trans., 1993, 89, 3347–3351.

241. M. O. Liu, C. H. Tai, A. T. Hu, T. H. Wei, J. Organomet. Chem., 2004, 689, 2138

242. L. A. Tomachynski, I. N. Tretyakova, V. Ya. Chernii, S. V. Volkov, M. Kowalska, J. Legendziewicz, Y. S. Gerasymchuk, S. Radzki, Inorg. Chim. Acta, 2008, 361

243. J. R. Darwent, P. Douglas, A. Harriman, G. Poter, M. C. Richoux, Coord. Chem. Rev., 44, 1982, 83

244. J. A. Lacey, D. Phillips, Photochem. Photobiol. Sci., 2002, 1, 378

245. M. P. Tsvirko, G. F. Stelmakh, V. E. Pyatosin, K.N. Solovyov, T. F. Kachura, A. S. Piskarskas, R. A. Gadonas, Chem. Phys., 1986, 106, 467

246. V. Duarte, D. Gasparutto, L. F. Yamaguchi, J. L. Ravanat, G. R. Martinez, M. H. G. Medeiros, P. D. Mascio, J. Cadet, J. Am Chem. Soc., 2000, 122, 12622-12628

247. N. Kobayashi, H. Ogata, N. Nonaka, E. A. Luk'yanets, Chem. Eur. J., 2003, 9, 5123-5134

248. W. Chidawanyika, E. Antunes, T. Nyokong, J. Photochem. Photobiol. A, 2008, 195, 183-190

249. B. Decostere, N. Daels, S. De Vrieze, P. Dejans, T. Van Camp, W. Audenaert, J. Hogie, P. Westbroek, K. De Clerck, S. W. H. Van Hull, Desalination, 2009, 249, 942-948

250. M. M. Bergahoef, G. J. Vansco, Adv. Mater., 1999, 11, 1362-1365

251. S. Honarbakhsh, B. Pourdeyhimi, J. Mater. Sci., 2011, 46, 2874-2881

252. C. Xu, F. Xu, B. Wang, T. J. Lu, J. Nanomater., 2011, 2011, 201834

253. P. Adriaensens, A. Pollaris, R. Carleer, D. Vanderzande, J. Gelan, V. M. Litvinov, J. Tijssen Polymer, 2001, 42, 7943–7952

254. B. De Schoenmaker, L. De Van Schueren, S. De Vrieze, P. Westbroek, K. De Clerck, J. Appl. Polym. Sci., 2011, 120, 305-310

255. J. M. Deitzel, J. Kleinmeyer, D. Harris, N. C. Beck Tan, Polymer, 2001, 42, 261-271

256. X. H. Qin, Y. Q. Wan, J. H. He, J. Zhang, J. Y. Yu, and S. Y. Wang, Polymer, 2004, 45, 6409-6413

257. J. M. Berg, J. L. Tymoczko, L. Stryer, Biochemistry, 5thed, WH Freeman, 2002, Chapter 4

258. C. L. Pai, M. C. Boyce, G. C. Rutledge, Macromolecules, 2009, 42, 2102-2114

259. H. Fong, I. Chun, D. H. Reneker, Polymer, 1999, 40, 4585-4592

260. J. Tang, T. Mohan and J. G. Verkade, *J. Org. Chem*., 1994, **59**, 4931-4938

261. D. W. Mayo, F. A. Miller, R. W. Hannah, Course notes on the interpretation of Infrared and Raman spectra, John Wily and Sons, Inc, New Jersey, 2004, chapter 5

262. N. E. Triggs, J. J. Valentini, J. Phys. Chem., 1992, **96**, 6922-6931

263. D. Gani, P. J. Hendra, W.F. Maddams, C. Passingham, I. A. M. Royaud, H. A. Willis, V. Zichy, M. E. A. Cudby, Analyst, 1990, 115, 1313-1318

264. B. N. Achar, K. S. Lokesh, J. organomet. Chem., 2004, 689, 2601-2605

265. F. Meng, R. Zhao, M. Xu, Y. Zhang, Y. Lei, J. Zhong, X. Liu, Colloids surf. *A*, 2011, 375, 245-251

266. N. Kobayashi, in: C. C. Leznoff, A. B. P. Lever (Eds.), Phathalocyanines—Properties and Applications, vol. 2, VCH Publishers Inc., New York, 1993, p. 97

267. K. Lang, J. Mosinger, D. M. Wagnerova, Coord. Chem. Rev., 2004, 248, 321–350

268. L. Alagna, A. Capobianchi, M. P. Casaletto, G. Mattogna, A. M. Paoletti, G. Pennesi, G. Rossi, J. Mater. Chem. 11 (2001) 1928–1935

269. T. Nyokong, H. Isago, J. Porphyrins Phthalocyanines, 2004, 8, 1083-1090

270. N. Peltekis, B. N. Holland, S. Krishnamurty, I. T. McGovern, N. R. J. Poolton, S. Patel, C. McGuiness, J. Am. Chem. Soc., 2008, 132, 13008-13012

271. O. Nestler, K. Severin, Org. Lett., 2001, 3, 3907

272. T. Ngai, G. Zhang, X. Li, D. K. P Ng, C. Wu, Langmuir, 2001, 17, 1381-1383

273. X. F. Zhang, X. Li, L. Niu, L. Sun, L. Liu, J. Fluoresc., 2009, 19, 947–954

274. K. Ishii, K. Kubo, T. Sakurada, K. Komori, Y. Sakai, Chem. Commun., 2011, 47, 4932-4934

275. N. Inagaki, S. Tasaka, Y. Sei, Polym Bull, 1996, 36, 601-607

276. M. Hu, Y. Xu, J. Zhao, Langmuir, 2004, 20, 6302–6307

277. K. Lang, D. M. Wagnerová, J. Brodilova, J. Photochem. Photobiol. A: Chem., 1993, 72, 9-14

278. M. Sarakha, M. Bolte, H. D. Burrows, J. Phys. Chem., A, 2000, 104, 3142-3149

279. T. Nyokong, V. Ashen (Eds), Photosensitizers in Medicine, Environment and Security, Springer, Dordrecht, 2012, pp 433-467

280. P. Kluson, M. Drobek, T. Strasak, J. Krysa, M. Karaskova, J. Rakusan, J. Mol. Catal. A: Chem., 2007, 272, 213-219

281. D. Chen, A. K. Ray, Water Res., 1998, 32, 3223

282. D. D. Dionysiou, A. P. Khodadoust, A. M. Kern, M. T. Suidan, I. Baudin, J. M. Laîné, Appl. Catal. B: Environ., 2000, 24, 139–155

283. M. M. Fickling, A. Fischer, B. R. Mann, J. Packer, J. Vaughan, J. Am. Chem. Soc., 1959, 81, 4226423

284. H. Lachheb, E. Puzenat, A. Houas, M. Ksibi, E. Elaoui, C. Guillard, J. M. Herrmann, Appl. Cat. B: Environ., 2002, 39, 75-90

285. J. Moon, C. Y. Yun, K. Chung, M. Kang, J. Yi, Catal. Today, 2003, 87, 77-86

286. S. L. Chen, X. J. Huang, Z. K. Xu, Cellulose, 2011, 18, 1295-1303

287. S. Parra, J. Olivero, L. Pacheco, C. Pulgarin, Appl Catal B Environ, 2003, 43, 293-301

288. J. C. D'Oliveira, C. Minero, E. Pelizzetti, P. Pichat, J. Photochem. Photodiol. Chem. A, 1993, 72, 261-267

289. M. Abdullah, G. K. C. Low, R. W. Mathews, J. Phys. Chem., 1990, 94, 6820-6825

290. M. Hou, F. Li, X. Liu, X. Wang, H. Wan, J. Hazard. Mater., 2007, 145, 305-314

291. R. W. Redmond, J. N. Gamlin, Photochem. Photobiol., 1999, 70, 391-475

292. A. Zille, B. Górnacka, A. Rehorek, A. Cavaco-Paula, Appl. Environ. Microbiol., 2005, 71, 6711-6718